SECONDARY ORGANIC AEROSOL (SOA) FORMATION FROM AQUEOUS OH RADICAL OXIDATION OF DICARBONYL COMPOUNDS IN THE ATMOSPHERE

by

YI TAN

A Dissertation submitted to the

Graduate School-New Brunswick

Rutgers, The State University of New Jersey

in partial fulfillment of the requirements

for the degree of

Doctor of Philosophy

Graduate Program in Environmental Sciences

written under the direction of

Barbara Turpin

and approved by

_____

_____

_____

_____

New Brunswick, New Jersey

October 2010

ABSTRACT OF THE DISSERTATION

SECONDARY ORGANIC AEROSOL (SOA) FORMATION FROM AQUEOUS OH RADICAL OXIDATION OF DICARBONYL COMPOUNDS IN THE ATMOSPHERE

By YI TAN

Dissertation Director:
Barbara Turpin

Secondary organic aerosols (SOA) affect visibility, health and global climate. Current chemical transport models cannot represent SOA in the free troposphere. Fog/cloud processing, which is the dominant source of atmospheric sulfate, has been recognized as a missing source of SOA globally. Aqueous photooxidation of water-soluble products (e.g., glyoxal and methylglyoxal) of gas-phase photochemistry yields low-volatility compounds including oxalic acid. When this chemistry takes place in clouds and fogs followed by droplet evaporation (or if this chemistry occurs in aerosol water) then products remain in part in the particle phase, forming SOA. However, current aqueous SOA formation mechanism has not shown how the starting concentrations of precursors and presence of acidic sulfate affect product formation.

Aqueous phase photochemical batch reactions were conducted with glyoxal and methylglyoxal at cloud relevant concentrations, using hydrogen peroxide photolysis as the hydroxyl radical (·OH) source. Experiments were repeated at higher concentrations and with/without sulfuric acid. Precursors and products were investigated using ion chromatography (IC), electrospray ionization mass spectrometry (ESI-MS), and

IC-ESI-MS. Products included carboxylic acids and higher molecular weight compounds, which are major constituents of aerosols. Sulfuric acid shows little effect on product formation. Dilute aqueous chemistry models successfully reproduced product formation for glyoxal and methylglyoxal at cloud relevant conditions, but measurements deviated from predictions from predictions at elevated concentrations. Higher molecular weight products become increasingly important as precursor concentration increases. Aqueous radical-radical reactions provide explanations for observed higher molecular weight products. Additionally, acetic acid is identified as an SOA precursor for the first time.

This work provides an improved understanding of aqueous phase dicarbonyl oxidation mechanism and the overall significance of aqueous SOA formation. Kinetic data are made available to regional and global atmospheric models, and the mechanism described in this work will help people to mitigate adverse aerosol effects.

Acknowledgement

The past five years have been scientifically and personally rewarding to me. I owe my sincerest gratitude to so many people who have been influential in my development as an environmental scientist. During my years in Rutgers, Dr. Barbara Turpin has inspired me with her erudition and enthusiasm; has trusted and thrust me to conduct independent research; has provided sagacious advice, generous support and resources; and at the same time has created a comfortable environment in which I can pursue my hobbies besides scholarly dedication and hard work. Her elegant manners have really influenced me to become a better scientist and person. Dr. Sybil Seitzinger has involved in every aspect of my research since the very beginning although she is not my official advisor, and our collaboration was amazingly fruitful. As a friend and my committee member, Dr. Ann Marie Carlton oriented me to the lab in my first year and provided resourceful advices thereafter. Appendix B12 of this dissertation is generously provided by Dr. Carlton. Dr. John Reinfelder has made insightful comments and provided crucial assistance for the completion of this dissertation.

Many colleagues in Rutgers have been instrumental in various aspects. Thanks to all the members in Dr. Turpin's lab, present and past, for their lab assistance. Drs. Mark Perri and Katye Altieri analyzed some samples in Woods Hole Organic Mass Spectrometry Facility for me and helped me with mass spectrometry techniques. Dr. Yong Bin Lim is talented at radical chemistry and helped me with development of chemical mechanisms. Ron Lauck helped me with total organic carbon analysis, and he also has the talent to fix anything "demolished" by me and my lovely labmates. Thanks to Diana Ortiz for the delicious Puerto Rican food and all sorts of events organized by her. Jeffrey Kirkland, the

singing graduate student, has made my time in the lab incredibly entertaining. Anjuli Ramos worked with me as an undergraduate student and now she readily takes my role as the “lab destroyer”. All of the Environmental Sciences graduate students, among whom the big “Chinese mafia” exists, have shown their sincere friendship and support for the past five years.

Finally, the love and support of my parents underlies anything I have ever accomplished. And of course my fiancée, Changqing Zhang. I can’t fully express how important she meant to me.

Table of Contents

Lists of tables

List of illustrations

Chapter 1. Introduction

1.1 Effects and Sources of Atmospheric Aerosols

Atmospheric aerosols are particles suspended in air; they have diameters in the range of 10^{-9} – 10^{-4} m [1]. Aerosols modify the Earth's radiative balance by scattering and absorbing solar and terrestrial radiation, by influencing formation and properties of clouds, and by affecting the abundance and distribution of atmospheric trace gases through heterogeneous chemical reactions and other multiphase processes in the atmosphere [2]. At elevated concentrations they are linked to adverse human health effects and inhibit visibility degradation [3]. However, incomplete knowledge of aerosol sources, composition, properties and formation mechanisms lead to significant uncertainties in the impact of control strategies on aerosol concentrations and the impact of atmospheric aerosols on environmental processes [4-5].

Organic aerosol (OA) is a major component of the aerosol mass in the atmosphere, typically 20–60% in the continental mid-latitudes and up to 90% in tropical forested areas [6-9]. Despite the abundance of organic aerosol, one of the main barriers to a complete understanding of its effects is the chemical complexity of organic aerosol [4, 10]. A substantial fraction of the OA consists of water-soluble multifunctional compounds (e.g. dicarboxylic acids, functionalized acids, polyols, and amino acids) [5, 11], but information about the thousands of individual compounds is particularly sparse [1]. The situation is further complicated by large uncertainties in OA sources and precursors [8, 12-14]. OA has been implicated in a growing number of respiratory and cardiovascular system health studies [3, 15-18]. Like sulfate, organics degrade visibility in urban and remote continental locations [3, 19-20]. Organics are sometimes responsible

for as much as 60% of aerosol scattering, especially in the urban areas of the western United States [21]. A limited number of studies have investigated the direct radiative forcing resulting from OA (IPCC 2007 and references therein). One explicitly predicted the globally averaged annual radiative forcing of OA (-0.18 W m^{-2}) [22]. A large uncertainty in the prediction of indirect aerosol effects on climate is associated with uncertainty in the properties of OA; because most OA mass remains unidentified, OA sources are not fully understood, and because of the wide range of chemical and physical properties of OA [5, 23]. Without proper representation of OA in atmospheric models, our ability to address the numerous public health, climate, and environmental issues surrounding atmospheric aerosols remains seriously hindered.

Organic aerosols originate from a wide variety of natural and anthropogenic sources. Organic compounds that are emitted directly in particulate form from sources such as biomass burning, incomplete combustion of fossil fuel and wind-driven suspension of organic materials are referred to as primary organic aerosol (POA). Secondary organic aerosol (SOA) forms when gas phase organic compounds undergo atmospheric oxidation to yield semi- or non- volatile products that partition into the aerosol phase. Previous studies indicate that 20 – 80% of continental organic aerosol can be of secondary origin [24-28], and the chemical formation of SOA could be at least 50% of POA emissions at the global scale [5]. In the atmosphere, POA and SOA components are mixed with each other, with black carbon (BC), and with inorganic aerosol components (externally and internally) [29]. Moreover, both POA and SOA components are semi-volatile; their partitioning changes with temperature and dilution, and they can be efficiently transformed upon interaction with reactive trace gases and solar radiation

(chemical aging) [30-32]. Quantifying the SOA mass separately from the POA mass is difficult [4]. Generally, SOA is considerably more oxygenated, polar, and hygroscopic than POA [7-8, 12-13]. The contribution of SOA to aerosol optical depth (AOD) is also estimated to be larger than that of POA, partly because of the larger water content associated with SOA [33]. Understanding the contributions of primary and secondary organic aerosol is essential to the development of effective air pollution control strategies since POA is emitted directly and SOA is formed from emission of volatile organic compounds (VOCs). A comprehensive mechanistic understanding of SOA formation is needed for global and regional atmospheric models to accurately predict the effects of various emission changes.

1.2 Secondary Organic Aerosol Formation

Recent analyses suggest that the global SOA budget is 25 to 210 TgC/yr with a best estimate of 115 TgC/yr [4]. Generally, semi-volatile products are produced via gas-phase photochemical oxidation of anthropogenic and biogenic reactive organic compounds by oxidants present in trace amounts in the atmosphere (e.g. hydroxyl radical (OH), ozone (O_3), and nitrate radical (NO_3)). These semi-volatile products then form SOA through nucleation or condensation. Since the l970s, this pathway has been demonstrated by numerous smog chamber experiments [34-39]. The gas phase degradation chemistry of a number of VOCs, including selected terpenes and aromatic hydrocarbons, has been studied. Laboratory data indicate that SOA yields (defined as $\Delta M/\Delta HC$, the mass of aerosol formed per mass of hydrocarbon reacted) are dependent on the concentration of absorbing organic material, temperature, and VOC/NOx ratio [4, 40]. Observed SOA yields are modeled by using two lumped semivolatile products, each

of which partitions between the gas phase and particle phase [41]. Simplified chemistry models generally represent smog chamber experimental data well, and have been incorporated in air quality and climate models to represent SOA formation (e.g. [22, 42-44]).

Gas phase oxidation of VOCs introduces additional oxygenated functional groups, such as carbonyl, hydroxyl and peroxyl groups, which make products less volatile and more water soluble than precursors. However, gas phase oxidation also leads to the fragmentation of precursors; when this occurs the products are more volatile. SOA formation from VOCs with more than seven carbons (e.g. cycloalkenes, aromatics and terpenes) has been traditionally accepted; while smaller VOCs, such as acetylene, glyoxal and isoprene, have not traditionally been considered SOA precursors due to the high volatility of their oxidation products [45]. When compared to field measurements, models based on this traditional understanding of SOA often underpredict ambient SOA concentrations. For example, de Gouw et al. [28] indicated that SOA formation in the New England Air Quality Study cannot be explained by the oxidation of traditionally recognized SOA precursors. Similarly, models underpredicted SOA in the Mexico City Metropolitan Area by one to two orders of magnitude [46-47]. Moreover, Heald et al. found that the GEOS-Chem global 3-D chemical transport model underestimated free tropospheric SOA concentrations observed in the ACE-Asia campaign by a factor of 10 – 100 [48]. In contrast, the same model generally reproduced sulfate and elemental carbon aerosols well. Even the most complex explicit model with around 14000 reactions (from the Master Chemical Mechanism V3.1) had to increase all partitioning coefficients by a factor of 500 to capture observed OA concentrations [49].

Potential factors causing the underestimation of SOA include the large uncertainty in precursor emissions, different aerosol yields between chamber experiments and the atmosphere, inaccurate treatment of SOA chemistry in models, missing precursors, and missing physical and chemical processes that contribute to SOA in models [50-51]. For example, over the last 5 – 10 years, both field [52-54] and laboratory studies [39, 55-57] indicate that isoprene (2-methyl-1,3-butadiene, C_5H_8), which is the most abundant non-methane volatile organic compound [58] and was not traditionally considered as a SOA precursor [59], could contribute SOA through gas-phase oxidation. Additionally, higher molecular weight compounds, including humic-like substances (HULIS) and oligomers, were identified in the oxidation of a wide range of organics in chamber experiments, including acetylene (C_2H_2), glyoxal (CHOCHO), isoprene, α-pinene, cycloalkenes, and aromatic compounds [34, 60-68]. These compounds were produced from previously unrecognized heterogeneous and condensed phase reactions. They could have vapor pressures several orders of magnitude lower than precursors and substantially enhance SOA formation. This work suggests that the contribution of smaller VOCs (e.g. isoprene, acetylene and glyoxal) to the SOA budget should not be neglected.

Chemical and photochemical oxidation in the atmospheric aqueous phase (i.e., rain, clouds, fogs and aerosol water), which is the dominant source of particulate sulfate in the atmosphere [69-70], has been hypothesized to be an important source of OA not included in traditional SOA models [51, 71-72]. Briefly, reactive organic precursors (i.e., isoprene, acetylene, acetone, and xylenes) are oxidized in the interstitial spaces of clouds [73] to form water soluble products, such as aldehydes, ketones, and alcohols [74]. These products readily partition into cloud droplets [75-76] and react further with aqueous

oxidants to form lower volatility compounds than those produced in analogous gas phase reactions. Upon cloud droplet evaporation these products remain, at least in part, in the particle phase (e.g. 90% for oxalic acid; [77]), forming SOA. Similar reactions in aerosol water also produce SOA. During the summer in Atlanta, particle-phase water soluble organic carbon (WSOC) is predominantly secondary and biogenic [78]. Hennigan et al. [79-80] observed a significant increase in WSOC partitioning to the particle phase when relative humidity is higher than 70%, due to the increase of liquid water content. The increase was not explained by simple Henry's law-type partitioning or gas-organic phase partitioning, because the liquid water content was too small to dissolve the observed WSOC mass partitioned to the particle phase. The high effective Henry's law constant for the total WSOC ($\sim 2\times10^{9}$ M atm^{-1}) suggested that aqueous phase reactions after partitioning played an important role in SOA formation in Atlanta during the summer [80]. SOA formation through aqueous reactions has only recently been recognized.

1.2.1 Evidence for Aqueous SOA Formation

Growing evidence suggests that SOA formation through processing of organic compounds in atmospheric waters is sbustantial. Several chemical and air parcel models predict formation of dicarboxylic acids (e.g. oxalic, malonic and succinic acids) and functionalized acids (e.g. glycolic, glyoxylic, and pyruvic acids) from cloud processing of water soluble organic compounds, and indicate that considerable additional SOA could form after cloud droplet evaporation [81-85]. For example, Lim et al. [84] studied cloud processing of isoprene in a photochemical box model. The simulated air parcel transported for 5 days over the tropical Amazon followed by 5 days over the Atlantic Ocean with a daily cloud period. By taking into account a global emission flux of 500 Tg

yr^{-1}, this work conclude that cloud processing of isoprene could yield substantial amount of SOA (1.6 Tg yr^{-1}). Ervens et al. [85] developed a cloud parcel model with a more detailed multiphase chemical mechanism and showed that more SOA formed from isoprene through cloud processing than from gas phase pathways. This work concluded that cloud processing might contribute substantially to the SOA budget in regions with high NOx and isoprene emissions, together with abundant clouds (e.g. Northeastern US or Southeast Asia). In addition, Heald et al. [86] presented indirect evidence for in-cloud SOA formation from biogenic VOC precursors by using GEOS-Chem model. This study showed that free tropospheric water-soluble organic carbon (WSOC) aerosol in the ACE-Asia data strongly correlated with methanol and sulfate. Methanol can be regarded as a tracer of biogenic emissions, and sulfate can be regarded as a tracer of aqueous phase oxidation.

More recently, in-cloud SOA formation has been incorporated to 3-D chemical transport models. Carlton et al. [87] found improved agreement between organic carbon predicted by Community Multiscale Air Quality (CMAQ) model and aircraft measurements of WSOC by incorporating in-cloud SOA production from glyoxal and methylglyoxal. This study demonstrated that cloud-produced SOA could account for around 50% of the total SOA under particular conditions. Similarly, reactive uptake of glyoxal and methylglyoxal by clouds and aqueous aerosols was included in the GEOS-Chem model [88-89]. Results suggested that inclusion of dicarbonyl SOA (glyoxal and methylglyoxal) improved the representation of OC and WSOC aerosol. The global SOA source from glyoxal and methylglyoxal is 2.6 and 8 TgC a^{-1}, respectively; and 90% of this source takes place in clouds [89]. Uncertainties associated with these predictions

were large, partly because Carlton et al. [87] and Fu et al. [88-89] used simplified SOA yields and reactive uptake coefficients from laboratory experiments to represent aqueous SOA formation. Detailed aqueous oxidation mechanisms were not implemented by both studies, since current mechanistic understanding is limited.

Rate constants of the aqueous phase oxidation of a few organic compounds by different oxidants have been studied for the purpose of tropospheric chemistry or wastewater treatment (e.g. [90-92]). Product identification has been more limited. Several laboratory studies have taken place in the past decade, as summarized in Table 1-1. However, the mechanisms, kinetics, products and total aerosol yields central to SOA formation via atmospheric aqueous chemistry remain very sparsely characterized.

1.2.2 Oxalic Acid: A Particulate Product of Aqueous Phase Reactions

Dicarboxylic acids (DCAs) are ubiquitous in atmospheric aerosols [93-98], in cloud and fog water [99-103], and in snow and ice [104-105]. Dicarboxylic acids and their salts have received attention in part because of their potential to alter the hygroscopic properties of aerosols, and their recognized roles in influencing aerosols to act as cloud condensation nuclei (CCN) which affect cloud formation and the earth's radiation balance [5, 106-107]. Among these DCAs, oxalate (C_2) is the most abundant in the atmosphere, followed by malonate (C_3) and succinate (C_4) [4-5, 108-109].

The sources of atmospheric oxalate are still not well understood. Oxalate can be directly emitted from automobiles [110] and biomass burning [109], though vehicle exhaust as a significant primary source has been challenged [111]. Observed diurnal and seasonal cycles of oxalate in both urban and remote areas are also consistent with secondary photochemical production of oxalate [108, 112-114]. Growing evidence

suggests that a large fraction of oxalate is produced from heterogeneous and aqueous photochemistry of volatile organic precursors. Field studies revealed a peak in the size distribution of oxalate in the droplet mode (0.56 – 1.0 μm), similar to sulfate [98, 100, 115-116]. It has been established that the droplet mode sulfate is from cloud processing of condensation mode particles [117-118]. Therefore, cloud processing could be the common source of both sulfate and oxalate. Haze layers above cloud with elevated organic acid levels have also been observed, and in-cloud production of oxalate was proposed as an important source [100, 119-120].

As shown in Table 1-1, experimental studies have shown that the aqueous oxidation of aldehydes, ketones, and carboxylic acids can produce oxalate under atmospherically relevant conditions. The dynamics of oxalate production have been measured in the OH oxidation of pyruvic acid [121], glyoxal [122], and methacrolein [123], but only Carlton et al. [124] compared experiment observations with aqueous chemistry predictions. Carlton et al. [124] found that oxalic acid concentrations in the aqueous oxidation of glyoxal were considerably lower than predictions based on recognized mechanisms. Although a revised mechanism was proposed to reproduce the observed oxalic acid time profiles, application of the revised mechanism to different conditions was not tested. The very limited information about oxalic acid yields in aqueous oxidation of organic compounds under atmospherically relevant conditions introduces large uncertainties regarding the importance of cloud processing to the atmospheric abundance of oxalate.

1.2.3 Higher Molecular Weight Compounds from Aqueous Phase Reactions

Higher molecular weight compounds are often detected in ambient atmospheric aerosols, cloud and fog droplets, and rainwater [64, 125-129]. Together these compounds constitute a complex mixture of multifunctional compounds, including oligomers, organosulfates and nitrooxy organosulfates, with molecular weights between 150 – 500 amu [4]. Based on the microphysical properties of higher molecular weight compounds extracted from real aerosol samples, it has been suggested that these species can affect the hygroscopicity, CCN activity, surface tension and optical properties of atmospheric aerosols [130-134].

Higher molecular weight compounds are associated with both primary (e.g. biomass combustion) and secondary sources (e.g., condensed phase reactions). Laboratory studies have indicated that aqueous phase reactions might help to explain the formation of this class of organic molecules, especially oligomers [122-123, 135-140] (Table 1-1). Higher molecular weight products are commonly observed products in the aqueous OH oxidation of $\geq C_2$ multifunctional compounds and have been observed to form through photolysis of aqueous pyruvic acid solutions (without OH) [135].

In general, acid/base catalyzed reactions and radical reactions have been proposed to explain oligomer formation in atmospheric aqueous phase reactions. Altieri et al. [137] determined the elemental composition and structures of products in methylglyoxal + OH reactions by ultra-high resolution mass spectrometry and tandem mass spectrometry [137]. Nine oligomers series showed repetitive addition of a subunit $C_3H_4O_2$. The oligomer structures were consistent with formation by acid catalyzed esterification with hydracrylic acid ($C_3H_6O_3$), which would add $C_3H_4O_2$ subunits to parent compounds. Similarly, oligomers observed in OH oxidation of levoglucosan were attributed to acid

catalyzed hemiacetal/acetal formation [141]. Alternatively, dimers and trimers formed during the photolysis of pyruvic acid were attributed to the recombination of organic radicals [135]. Guzman et al. [135] reported that dissolved oxygen cannot efficiently scavenge radical precursors even in aerated solutions when the pyruvic acid concentration is higher than 5 mM, thus pyruvic acid was capable to produce multifunctional compounds in atmospheric waters under solar irradiation. El Haddad et al. [140] also suggested that oligomers produced during the OH oxidation of methacrolein were better explained by the combination of first generation radicals [140]. The structures of oligomers and the possible mechanisms explaining their formation in atmospheric aqueous phase reactions is still quite limited and needs further investigation.

1.2.4 Precursors

A large number of organic compounds have been identified in atmospheric water samples, including aldehydes, ketones, carboxylic acids, alcohols and organic peroxides [142]. And many of these compounds (e.g. acetaldehyde, propionaldehyde, glyoxal, methylglyoxal, acetone, methyl ethyl ketone, acetic acid, propionic acid, pyruvic acid, 1-propanol, and 1-butanol) are predicted to produce oxalic acid via aqueous phase oxidation (CAPRAM 3.0) [143]. Therefore, these compounds are potential precursors of SOA formation through aqueous phase reactions.

Focus of this work is glyoxal (CHOCHO) and methylglyoxal ($CH_3C(O)CHO$), the two smallest α-dicarbonyls compounds. Glyoxal and methylglyoxal are produced in the atmospheric oxidation of both biogenic and anthropogenic precursors [89], and their precursors include isoprene, acetone, acetylene, isoalkanes, alkenes, monoterpenes, aromatics, methylbutenol (2-methyl-3-buten-2-ol) [144-145]. Glyoxal and methylglyoxal

are also emitted directly from biofuel use and biomass burning [146-147]. The estimated global sources of glyoxal and methylglyoxal are 45 Tg a^{-1} and 140 Tg a^{-1} [89]. UV photolysis and reaction with hydroxyl radical (·OH) are primary gas phase loss processes for glyoxal and methylglyoxal, and these processes are unlikely to produce oxalic acid [148-149]. Glyoxal was found to be at a significantly lower concentration than predicted in the atmosphere of Mexico City, suggesting the existence of unidentified sinks. Reative uptake by aerosols was put forth as a possible explanation, although the chemical processes responsible were not identified [150].

Glyoxal and methylglyoxal can enter the aqueous phase readily due to high effective Henry's law constants ($H_{eff} > 3\times10^5$ M atm^{-1} and $H_{eff} = 3.71\times10^3$ M atm^{-1} at 25°C, respectively) [75-76, 151]. Irreversible uptake of glyoxal by aqueous inorganic particles [152] and cloud droplets/ice crystals [153] have been measured in chamber experiments, with effective uptake coefficients (γ) around 10^{-3}. Reactive uptake of methylglyoxal by liquid sulfuric acid has also been measured [154]. Typical concentrations of glyoxal and methylglyoxal vary from a few μM in rain water to >100 μM in fog water [155]. Once in the aqueous phase, both glyoxal and methylglyoxal hydrate [156-157]. Aqueous phase oxidation of glyoxal forms low volatility compounds including glyoxylic acid, oxalic acid and larger multifunctional products [124]. The major oxidation products of methylglyoxal are pyruvic acid, acetic acid, glyoxylic acid, oxalic acid, and oligomers (Table 1-1). In the absence of oxidants, glyoxal and methylglyoxal can still form oligomers via hemiacetal/acetal formation and aldol condensation reactions during simulated droplet evaporation. Unlike oligomers formed by oxidation reactions, these oligomers are reversible. There is some indication that the

amount of SOA produced via these self-reactions may be smaller than the amount of SOA from oxidation reactions [158].

1.2.5 OH Radical in Atmospheric Waters

Cloud/fog processing of organic compounds can be initiated by numerous oxidants, including radicals (e.g. OH, NO_3, and HO_2), radical anions (e.g. O_2^-, Cl_2^-, Br_2^-, SO_4^-, and CO_3^-), O_3, and H_2O_2. Under atmospheric conditions (i.e., at pH $\leq$ 7, O_2 saturated), the OH radical is the most efficient oxidant [159-161]. OH radical can be scavenged from the gas phase by cloud droplets (Henry's law constant at 298K, H = 25 M atm^{-1}) or produced in the aqueous phase. Photolysis of H_2O_2, NO_3^-, NO_2^-, and Fe(III) complexes, as well as Fenton chemistry can form OH radical in the aqueous phase [159]. For clouds in the free troposphere, Arakaki and Faust [162] showed that gas-to-droplet partitioning is the most important OH radical source, but aqueous phase photoformation is also important. H_2O_2 can be the dominant aqueous phase OH radical source via both direct photolysis and Fenton chemistry. Cloud and rainwater samples showed a wide range of H_2O_2 concentrations (from less than 0.1 μM to over 200 μM) [163-166], which can be several orders of magnitude higher than the concentration of dissolved ozone [160]. In the experiments herein, photolysis of H_2O_2 is used as the source of OH radical.

In general, model predicted OH radical concentrations in cloud droplets vary over two orders of magnitude as a result of different assumptions [167-169]. According to Jacob [167], the predicted chemical lifetime of OH radical in cloud droplets is 6.7×10^{-5} s under tropical spring conditions. Because of this short lifetime, OH radical is poorly mixed within droplets. The surface concentration (1.8×10^{-12} M), which is affected by gas-to-droplet partitioning, is much higher than bulk concentration (2.3×10^{-13} M).

Monod and Carlier [169] followed the same assumptions made by Jacob [167], but more reactions of soluble organic compounds were considered. They found that organic compounds could be important aqueous OH radical sinks. The concentration of OH could reach 2×10^{-13} M – 1.7×10^{-12} M when organics are mostly consumed. Warneck [168] considered the effect of transition metals on the steady state aqueous OH radical concentrations in a simple box model of a sunlit small cumulus cloud. The predicted OH radical concentration is $2.6 – 5.0 \times 10^{-14}$ M in a typical continental fair weather cloud. Although OH radical concentrations in cloud/fog droplets have not been measured directly in field studies, photochemical formation of OH radical in atmospheric waters has been confirmed in several studies [162, 170-172]. For example, Anastasio and McGregor [171] illuminated winter fog waters collected in Davis, California with simulated sunlight and found that the characterized steady-state OH radical concentrations from aqueous production alone were $3.4 – 6.6 \times 10^{-16}$ M through aqueous reactions. As a result of its high reactivity towards organic compounds, OH radical is an important day-time oxidant in atmospheric waters [160].

1.2.6 Acidic Sulfate in the Aqueous Phase

Sulfur-containing compounds are present in the Earth's atmosphere at a total volume mixing ratio of less than 1 ppm. Because the atmosphere is a potent oxidizing medium, a large fraction of atmospheric reduced sulfur compounds are ultimately oxidized to sulfate. For example, reactions in cloud water effectively convert dissolved sulfite to sulfate. Sulfate is a prevalent species found in aerosols and atmospheric water samples [5, 160]. Collett et al. [173] reviewed field measurements of the chemical compositions of fogs and intercepted clouds in the United States. Fog and cloud sulfate

concentrations vary considerably between regions, from ~35 μM at the Oregon coast to over 1 mM at Mt. Mitchell. Average cloud/fog pH values observed in these field studies are usually below 7.0, largely because of acidic sulfate [160]. The most acidic regions were Mt. Mitchell (average cloud pH = 2.8, minimum pH = 2.45), southern California coastal sites (average pH = 3.3, minimum pH = 2.83), and Whiteface Mountain (average pH = 3.5, minimum pH = 2.77).

Interaction between organic compounds and acidic sulfate has been investigated in a number of laboratory studies. Several studies observed enhanced particle growth from gas phase oxidation of isoprene, terpenes, and aromatic compounds in the presence of acidic sulfate seed aerosol [60, 67, 174]. In contrast, other similar experiments suggested that negligible enhancement in SOA yields was observed from the oxidation of toluene and m-xylene [175]. Reactive uptake of carbonyls by acidic sulfate aerosols has also been studied extensively [68, 154, 176]. For example, Kroll et al. [68] investigated the reactive uptake of several small carbonyls (formaldehyde, octanal, trans,trans-2,4-hexadienal, glyoxal, methylglyoxal, 2,3-butanedione, 2,4-pentanedione, glutaraldehyde, and hydroxyacetone) onto aqueous seed particles (ammonium sulfate or mixed ammonium sulfate/sulfuric acid). Substantial uptake was only observed for glyoxal. Particle growth was not greater for the acidic seed than for the neutral seed, and Kroll et al. [68] concluded that the reactive uptake of glyoxal was more likely driven by ionic strength of the seed rather than the particle acidity. Zhao et al. [154] measured the heterogeneous reaction of methylglyoxal and aqueous sulfuric acid solutions (55 – 85 wt %). The uptake of gaseous methylglyoxal on sulfuric acid decreased with increasing acidity, thus this study does not support the acid-catalyzed uptake of methylglyoxal.

Organosulfate compounds, specifically sulfate esters, were observed in smog chamber experiments involving reactions of carbonyls on acidic sulfate aerosols [64, 125, 152, 176]. Recently, organosulfate products have been identified in the laboratory aqueous phase OH radical oxidation of glycolaldehyde in the presence of sulfuric acid [177]. This result suggests that sulfuric acid might affect the oxidation of organic compounds in atmospheric waters.

1.3 Critical Knowledge Gaps

Despite large uncertainties, growing evidence indicates that aqueous phase processing of organic compounds could considerably contribute to the global SOA budget [81-89, 121-123, 135-141, 178-181]. However, knowledge about photochemical processing of organics in the atmospheric aqueous phase is still quite limited and needs further investigation. In particular, aqueous chemical mechanisms are largely unverified.

Effect of precursor concentrations. Previous aqueous-phase kinetic studies were conducted with precursor concentrations 1 – 3 orders of magnitude higher than typical cloud/fog conditions in order to generate enough products for analysis. However, it is well known that properties of SOA produced in "traditional" high concentration smog chamber experiments are different from those of ambient aerosols [4]. SOA yields are higher in high concentration smog chamber experiments than in chamber experiments conducted at ambient concentrations [4]. The properties of the SOA might also be different [182]. Similarly, concentration-dependant differences might also exist for "aqueous" SOA formation. The effect of precursor concentrations in the aqueous phase photochemistry has not been explored previously. It is evident that laboratory data should

preferably reflect conditions which allow confident extrapolation to ambient environment.

Effect of acidic sulfate. Acidic sulfate, a major constituent of aerosols and cloud water, is generally recognized to be a catalyst for heterogeneous reactions of gaseous compounds on/in particles [60, 67-68, 154, 174, 176]. The role of acidic sulfate in aqueous phase oxidation of glyoxal and methylglyoxal is not well understood.

Characterization of higher molecular weight compounds. Higher molecular weight products have been detected in atmospherically relevant lab studies of aqueous phase reactions and in field measurements of aerosols and clouds [64, 122-123, 125-129, 135-140]. While generally recognized that these humic-like substances form in atmospheric condensed phase reactions, they remain poorly characterized and their identity, concentration, and formation pathways remain largely unknown.

A foundation for the incorporation of aqueous-phase SOA formation into models. Aqueous chemical modeling has made use of measured rate constants, but little has been done to validate product formation. Product formation simulated by models need to be tested against experimental observations.

1.4 Objectives of Dissertation

The hypothesis of this dissertation is that cloud processing of dicarbonyl compounds (i.e. glyoxal and methylglyoxal) by hydroxyl radical is a substantial source of secondary organic aerosol (SOA). To test this hypothesis, the following specific aims are addressed:

1. Conduct batch photochemical experiments to further investigate the aqueous-phase oxidation of glyoxal and methylglyoxal by OH radical. Investigate how the starting concentrations of precursors and the addition of acidic sulfate affect product formation.

2. Model the concentration dynamics in these experiments to validate and refine the dilute aqueous chemistry model for OH radical oxidation of glyoxal and methylglyoxal.

3. Resolve the discrepancy in the literature regarding the fate of acetic acid during aqueous-phase oxidation. Explore the role of formaldehyde and of organic radical reactions in oligomer formation in wet aerosols.

1.4.1 Dissertation Overview

This dissertation verifies for the first time that organic species found predominantly in the particle phase in the atmosphere are formed from hydroxyl radical oxidation of atmospheric water-soluble gases (e.g. glyoxal and methylglyoxal) at cloud relevant concentrations. When this chemistry takes place in atmospheric aqueous phase (i.e., clouds, fogs, and aerosol water) then low-volatility products such as oxalate and oligomers are expected to remain predominantly in the particle phase, forming SOA.

Chapter 2 [183] describes the effect of starting concentrations of glyoxal (30 – 3000 μM) on product formation in the aqueous reaction between glyoxal and OH radical in the presence and absence of acidic sulfate (0 – 840 μM). Samples were analyzed by electrospray ionization mass spectrometry (ESI-MS), Fourier transform ion cyclotron resonance (FT-ICR) ESI-MS and ion chromatography (IC) to identify and quantify reaction products. A dilute aqueous chemistry model [84] was used to predict the concentration dynamics of precursors and products in the reaction vessel. The addition of

sulfuric acid had little effect on oxalic acid concentrations. The dilute aqueous chemistry model successfully reproduced oxalic acid and total organic carbon concentrations when the experiment was performed at cloud relevant concentrations (glyoxal < 300 μM). However, higher molecular weight products formed at higher concentrations, which caused predictions to deviate from measurements. As organic concentrations in aerosol water could exceed those covered by this work, it is likely that aqueous glyoxal chemistry in wet aerosols produces more complex higher molecular weight products than the simple chemistry in dilute cloud droplets. These results suggest that the aqueous phase processing of glyoxal could be an important source of SOA.

Chapter 3 describes the aqueous OH radical oxidation of methylglyoxal [184]. This effort is the first time that quantification of products of the aqueous reaction of methylglyoxal (30 – 3000 μM) and OH radical (approx. 4×10^{-12} M) are reported in the peer reviewed literature. Product formation in the reaction vessel was modeled using a dilute aqueous chemistry model [84]. The effect of starting concentrations of precursors and the presence of acidic sulfate (0 – 840 μM) on product formation were also investigated. An analytical technique (IC-ESI-MS) added to the Turpin laboratory was used for the first time in this work. The ESI-MS spectra can identify different masses of coeluting acids and also confirm the masses of those organic acids that were already identified by IC alone. In addition, compounds with low signal strength in IC can be detected with a high signal-to-noise ratio by IC-ESI-MS. Organic acids predicted by the model were observed. The dilute aqueous chemistry model successfully predicted oxalic acid and total organic carbon at cloud relevant concentrations (30 μM), suggesting that methylglyoxal cloud chemistry is valid for use in chemical transport models. However,

predictions deviate from observations at higher concentrations (300 and 3000 μM). The addition of sulfuric acid at cloud relevant concentrations had little effect on oxalic acid yields. Products not predicted by the model were also identified. At aerosol water relevant concentrations (3000 μM), larger carboxylic acids ($\geq C_4$) and other high molecular weight products become important. Small carboxylic acids are the major products of OH radical oxidation in clouds while larger carboxylic acids and oligomers could be important in wet aerosols.

Chapter 4 makes use of experiments conducted with acetic and pyruvic acids to obtain a better understanding of the formation of higher molecular weight products from methylglyoxal in conditions relevant to wet aerosols. Possible structures of selected higher molecular weight products from methylglyoxal oxidation were proposed based on FT-ICR MS analysis, and radical-radical reactions successfully explained the formation of those products. SOA formation from acetic acid via aqueous OH radical oxidation at atmospherically relevant conditions was explicitly verified. Future directions, conclusions, and atmospheric implications for research concerning "aqueous" SOA formation are discussed in Chapter 5.

1.5 References

1. Poschl, U., Atmospheric Aerosols: Composition, Transformation, Climate and Health Effects. *Angewandte Chemie International Edition* **2005,** *44*, (46), 7520-7540.

2. IPCC, *Intergovernmental Panel on Climate Change (IPCC): Climate Change 2007: The Physical Science Basis*. Cambridge University Press: Cambridge, UK, 2007.

3. USEPA, *Air Quality Criteria for Particulate Matter*. U.S. Environmental Protection Agency: Research Triangle Park, 2004.

4. Hallquist, M.; Wenger, J. C.; Baltensperger, U.; Rudich, Y.; Simpson, D.; Claeys, M.; Dommen, J.; Donahue, N. M.; George, C.; Goldstein, A. H.; Hamilton, J. F.; Herrmann, H.; Hoffmann, T.; Iinuma, Y.; Jang, M.; Jenkin, M. E.; Jimenez, J. L.; Kiendler-Scharr, A.; Maenhaut, W.; McFiggans, G.; Mentel, T. F.; Monod, A.; Prévôt, A. S. H.; Seinfeld, J. H.; Surratt, J. D.; Szmigielski, R.; Wildt, J., The formation, properties and impact of secondary organic aerosol: current and emerging issues. *Atmos. Chem. Phys.* **2009,** *9*, (14), 5155-5236.

5. Kanakidou, M.; Seinfeld, J. H.; Pandis, S. N.; Barnes, I.; Dentener, F. J.; Facchini, M. C.; Van Dingenen, R.; Ervens, B.; Nenes, A.; Nielsen, C. J.; Swietlicki, E.; Putaud, J. P.; Balkanski, Y.; Fuzzi, S.; Horth, J.; Moortgat, G. K.; Winterhalter, R.; Myhre, C. E. L.; Tsigaridis, K.; Vignati, E.; Stephanou, E. G.; Wilson, J., Organic aerosol and global climate modelling: a review. *Atmos. Chem. Phys.* **2005,** *5*, 1053-1123.

6. Zhang, Q.; Jimenez, J. L.; Canagaratna, M. R.; Allan, J. D.; Coe, H.; Ulbrich, I.; Alfarra, M. R.; Takami, A.; Middlebrook, A. M.; Sun, Y. L.; Dzepina, K.; Dunlea, E.; Docherty, K.; DeCarlo, P. F.; Salcedo, D.; Onasch, T.; Jayne, J. T.; Miyoshi, T.; Shimono, A.; Hatakeyama, S.; Takegawa, N.; Kondo, Y.; Schneider, J.; Drewnick, F.; Borrmann, S.; Weimer, S.; Demerjian, K.; Williams, P.; Bower, K.; Bahreini, R.; Cottrell, L.; Griffin, R. J.; Rautiainen, J.; Sun, J. Y.; Zhang, Y. M.; Worsnop, D. R., Ubiquity and dominance of oxygenated species in organic aerosols in anthropogenically-influenced Northern Hemisphere midlatitudes. *Geophys. Res. Lett.* **2007,** *34*, L13801, doi:10.1029/2007GL029979.

7. Kanakidou, M.; Seinfeld, J. H.; Pandis, S. N.; Barnes, I.; Dentener, F. J.; Facchini, M. C.; Van Dingenen, R.; Ervens, B.; Nenes, A.; Nielsen, C. J.; Swietlicki, E.; Putaud, J. P.; Balkanski, Y.; Fuzzi, S.; Horth, J.; Moortgat, G. K.; Winterhalter, R.; Myhre, C. E. L.; Tsigaridis, K.; Vignati, E.; Stephanou, E. G.; Wilson, J., Organic aerosol and global climate modelling: a review. *Atmospheric Chemistry and Physics* **2005,** *5*, 1053-1123.

8. Turpin, B. J.; Saxena, P.; Andrews, E., Measuring and simulating particulate organics in the atmosphere: Problems and prospects. *Atmos. Environ.* **2000,** *34*, 2983-3013.

9. Yu, S.; Bhave, P. V.; Dennis, R. L.; Mathur, R., Seasonal and Regional Variations of Primary and Secondary Organic Aerosols over the Continental United States: Semi-Empirical Estimates and Model Evaluation. *Environmental Science & Technology* **2007,** *41*, (13), 4690-4697.

10. Goldstein, A. H.; Galbally, I. E., Known and Unexplored Organic Constituents in the Earth's Atmosphere. *Environmental Science & Technology* **2007,** *41*, (5), 1514-1521.

11. Saxena, P.; Hildemann, L. M., Water-Soluble Organics in Atmospheric Particles: A Critical Review of the Literature and Application of Thermodynamics to Identify Candidate Compounds. *Journal of Atmospheric Chemistry* **1996,** *24*, 57-109.

12. Turpin, B. J.; Lim, H. J., Species contributions to PM2.5 mass concentrations: Revisiting common assumptions for estimating organic mass. *Aerosol Science and Technology* **2001,** *35*, 602-610.

13. Pang, Y.; Turpin, B. J.; Gundel, L. A., On the importance of organic oxygen for understanding organic aerosol particles. *Aerosol Sci. Technol.* **2006,** *40*, 128-133.

14. Turpin, B. J., Options for Characterizing Organic Particulate Matter. **1999,** *33*, 76A-79A.

15. Nawrot, T. S.; Torfs, R.; Fierens, F.; De Henauw, S.; Hoet, P. H.; Van Kersschaever, G.; De Backer, G.; Nemery, B., Stronger associations between daily mortality and fine particulate air pollution in summer than in winter: evidence from a heavily polluted region in western Europe. *Journal of Epidemiology and Community Health* **2007,** *61*, (2), 146-149.

16. Nel, A., Air pollution-related illness: effects of particles. *Science* **2005,** *309*, 1326-1326.

17. Davidson, C.; Phalen, R.; Solomon, P., Airborne Particulate Matter and Human Health: A Review. *Aerosol Science and Technology* **2005,** *39*, 737-749.

18. Pope III, C. A.; Dockery, D. W., Health Effects of Fine Particulate Air Pollution: Lines that Connect. In *Journal of the Air & Waste Management Association (1995)*, Air & Waste Management Association: 2006; Vol. 56, pp 709-742.

19. Cabada, J. C., *Sources and Physical Characteristics of Atmospheric Carbonaceous Aerosols*. Ph.D. dissertation, Carnegie Mellon University, Department of Chemical Engineering: Pittsburgh, PA., 2003.

20. Vasconcelos, L. A.; Macias, E. S.; White, W. H., Aerosol composition as a function of haze and humidity levels in the southwestern U.S. *Atmos. Environ.* **1994,** *28*, 3679-3691.

21. Jacobson, M. C.; Hansson, H. C.; Noone, K. J.; Charlson, R. J., Organic Atmospheric Aerosols: Review and State of the Science. *Rev. Geophys.* **2000,** *38*, 267–294, doi:10.1029/1998RG000045.

22. Chung, S. H.; Seinfeld, J. H., Global distribution and climate forcing of carbonaceous aerosols. *J. Geophys. Res.* **2002,** *107*, 4407, doi:10.1029/2001JD001397.

23. Lohmann, U.; Feichter, J., Global indirect aerosol effects: a review. *Atmos. Chem. Phys.* **2005,** *5*, (3), 715-737.

24. Turpin, B. J.; Huntzicker, J. J., Identification of secondary organic aerosol episodes and quantitation of primary and secondary organic aerosol concentrations during SCAQS. *Atmos. Environ.* **1995,** *29*, 3527-3544.

25. Lim, H.-J.; Turpin, B. J., Origins of primary and secondary organic aerosol in Atlanta: Results of time-resolved measurements during the Atlanta supersite experiment. *Environmental Science and Technology* **2002,** *36*, (21), 4489-4496.

26. Dechapanya, W.; Russell, L. M.; Allen, D. T., Estimates of anthropogenic secondary organic aerosol formation in Houston, Texas. *Aerosol Sci. Technol.* **2004,** *38*, (S1), 156-166.

27. Strader, R. L.; Lurmann, F.; Pandis, S. N., Evaluation of secondary organic aerosol formation in winter. *Atmos. Environ.* **1999,** *33*, 4849-4863.

28. de Gouw, J. A., et al., Budget of organic carbon in a polluted atmosphere:Results from the New England Air Quality Study in 2002. *J. Geophys. Res.* **2005,** *110*, D16305, doi:10.1029/2004JD005623.

29. Marcolli, C.; Luo, B. P.; Peter, T.; Wienhold, F. G., Internal mixing of the organic aerosol by gas phase diffusion of semivolatile organic compounds. *Atmos. Chem. Phys.* **2004,** *4*, (11/12), 2593-2599.

30. Rudich, Y.; Donahue, N. M.; Mentel, T. F., Aging of Organic Aerosol: Bridging the Gap Between Laboratory and Field Studies. *Annual Review of Physical Chemistry* **2007,** *58*, (1), 321-352.

31. Robinson, A. L.; Donahue, N. M.; Shrivastava, M. K.; Weitkamp, E. A.; Sage, A. M.; Grieshop, A. P.; Lane, T. E.; Pierce, J. R.; Pandis, S. N., Rethinking Organic

Aerosols: Semivolatile Emissions and Photochemical Aging. *Science* **2007,** *315*, (5816), 1259-1262.

32. Chan, A. W. H.; Kautzman, K. E.; Chhabra, P. S.; Surratt, J. D.; Chan, M. N.; Crounse, J. D.; Kürten, A.; Wennberg, P. O.; Flagan, R. C.; Seinfeld, J. H., Secondary organic aerosol formation from photooxidation of naphthalene and alkylnaphthalenes: implications for oxidation of intermediate volatility organic compounds (IVOCs). *Atmos. Chem. Phys.* **2009,** *9*, (9), 3049-3060.

33. Tsigaridis, K.; Krol, M.; Dentener, F. J.; Balkanski, Y.; Lathiere, J.; Metzger, S.; Hauglustaine, D. A.; Kanakidou, M., Change in global aerosol composition since preindustrial times. *Atmos. Chem. Phys.* **2006,** *6*, (12), 5143-5162.

34. Volkamer, R.; Ziemann, P. J.; Molina, M. J., Secondary Organic Aerosol Formation from Acetylene (C2H2): seed effect on SOA yields due to organic photochemistry in the aerosol aqueous phase. *Atmos. Chem. Phys.* **2009,** *9*, (6), 1907-1928.

35. Heisler, S. L.; Friedlander, S. K., Gas-to-particle conversion in photochemical smog: aerosol growth laws and mechanisms for organics. *Atmos. Environ.* **1977,** *11*, 157-168.

36. McMurry, P. H.; Grosjean, D., Photochemical formation of organic aerosols: growth laws and mechanisms. *Atmos. Environ.* **1985,** *19*, 1445-1451.

37. Pandis, S. N. P., S.E.;Seinfeld,J.H.;Flagan,R.C., Aerosol formation in the photooxidation of isoprene and β-pinene. *Atmos. Environ.* **1991,** *25*, (Part A), 997-1008.

38. Odum, J. R.; Jungkamp, T. P. W.; Griffin, R. J.; Flagan, R. C.; Seinfeld, J. H., The atmospheric aerosol-forming potential of whole gasoline vapor. *Science* **1997,** *226*, 96-99.

39. Kroll, J. H.; Ng, N. L.; Murphy, S. M.; Flagan, R. C.; Seinfeld, J. H., Secondary organic aerosol formation from isoprene photooxidatin under high-NOx conditions. *Geophys. Res. Letts.* **2005,** *32*, (18), L18808, doi:10.1029/2005GL023637.

40. Seinfeld, J. H.; Pankow, J. F., Organic Atmospheric Particulate Material. *Annual Review of Physical Chemistry* **2003,** *54*, (1), 121-140.

41. Odum, J. R.; Hoffmann, T.; Bowman, F.; Collins, D.; Flagan, R. C.; Seinfeld, J. H., Gas/Particle Partitioning and Secondary Organic Aerosol Yields. *Environmental Science & Technology* **1996,** *30*, (8), 2580-2585.

42. Henze, D. K.; Seinfeld, J. H., Global secondary organic aerosol from isoprene oxidation. *Geophys. Res. Lett.* **2006,** *33*, (9), L09812, doi:10.1029/2006GL025976.

43. Tsigaridis, K.; Kanakidou, M., Global modelling of secondary organic aerosol in the troposphere: a sensitivity analysis. *Atmos. Chem. Phys.* **2003,** *3*, (5), 1849-1869.

44. Henze, D. K.; Seinfeld, J. H.; Ng, N. L.; Kroll, J. H.; Fu, T. M.; Jacob, D. J.; Heald, C. L., Global modeling of secondary organic aerosol formation from aromatic hydrocarbons: high- vs. low-yield pathways. *Atmos. Chem. Phys.* **2008,** *8*, (9), 2405-2420.

45. Pandis, S. N.; Harley, R. A.; Cass, G. R.; Seinfeld, J. H., Secondary organic aerosol formation and transport. *Atmospheric Environment. Part A. General Topics* **1992,** *26*, (13), 2269-2282.

46. Volkamer, R.; Jimenez, J. L.; San Martini, F.; Dzepina, K.; Zhang, Q.; Salcedo, D.; Molina, L. T.; Worsnop, D. R.; Molina, M. J., Secondary organic aerosol formation from anthropogenic air pollution: Rapid and higher than expected. *Geophys. Res. Lett.* **2006,** *33*, (17), L17811, doi:10.1029/2006GL026899.

47. Kleinman, L. I.; Springston, S. R.; Daum, P. H.; Lee, Y. N.; Nunnermacker, L. J.; Senum, G. I.; Wang, J.; Weinstein-Lloyd, J.; Alexander, M. L.; Hubbe, J.; Ortega, J.; Canagaratna, M. R.; Jayne, J., The time evolution of aerosol composition over the Mexico City plateau. *Atmos. Chem. Phys.* **2008,** *8*, (6), 1559-1575.

48. Heald, C. L.; Jacob, D. J.; Park, R. J.; Russell, L. M.; Huebert, B. J.; Seinfeld, J. H.; Liao, H.; Weber, R. J., A large organic aerosol source in the free troposphere missing from current models. *Geophys. Res. Lett.* **2005,** *32*, L18809, doi:10.1029/2005GL023831.

49. Johnson, D.; Utembe, S. R.; Jenkin, M. E., Simulating the detailed chemical composition of secondary organic aerosol formed on a regional scale during the TORCH 2003 campaign in the southern UK. *Atmos. Chem. Phys.* **2006,** *6*, (2), 419-431.

50. Kroll, J. H.; Seinfeld, J. H., Chemistry of secondary organic aerosol: Formation and evolution of low-volatility organics in the atmosphere. *Atmospheric Environment* **2008,** *42*, (16), 3593-3624.

51. Carlton, A. G.; Wiedinmyer, C.; Kroll, J. H., A review of Secondary Organic Aerosol (SOA) formation from isoprene. *Atmos. Chem. Phys.* **2009,** *9*, (14), 4987-5005.

52. Claeys, M.; Graham, B.; Vas, G.; Wang, W.; Vermeylen, R.; Pashynska, V.; Cafmeyer, J.; Guyon, P.; Andreae, M. O.; Artaxo, P.; Maenhaut, W., Formation of Secondary Organic Aerosols Through Photooxidation of Isoprene. *Science* **2004,** *303*, (5661), 1173-1176.

53. Edney, E. O.; Kleindienst, T. E.; Jaoui, M.; Lewandowski, M.; Offenberg, J. H.; Wang, W.; Claeys, M., Formation of 2-methyl tetrols and 2-methylglyceric acid in secondary organic aerosol from laboratory irradiated isoprene/NOX/SO2/air mixtures and their detection in ambient PM2.5 samples collected in the eastern United States. *Atmospheric Environment* **2005,** *39*, (29), 5281-5289.

54. Kleindienst, T. E.; Lewandowski, M.; Offenberg, J. H.; Jaoui, M.; Edney, E. O., Ozone-isoprene reaction: Re-examination of the formation of secondary organic aerosol. *Geophys. Res. Lett.* **2007,** *34*, (1), L01805, doi:10.1029/2006GL027485.

55. Kroll, J. H.; Ng, N. L.; Murphy, S. M.; Flagan, R. C.; Seinfeld, J. H., Secondary Organic Aerosol Formation from Isoprene Photooxidation. *Environmental Science & Technology* **2006,** *40*, (6), 1869-1877.

56. Kleindienst, T. E.; Edney, E. O.; Lewandowski, M.; Offenberg, J. H.; Jaoui, M., Secondary Organic Carbon and Aerosol Yields from the Irradiations of Isoprene and α-Pinene in the Presence of NOx and SO2. *Environmental Science & Technology* **2006,** *40*, (12), 3807-3812.

57. Ng, N. L.; Kwan, A. J.; Surratt, J. D.; Chan, A. W. H.; Chhabra, P. S.; Sorooshian, A.; Pye, H. O. T.; Crounse, J. D.; Wennberg, P. O.; Flagan, R. C.; Seinfeld, J. H., Secondary organic aerosol (SOA) formation from reaction of isoprene with nitrate radicals (NO3). *Atmos. Chem. Phys.* **2008,** *8*, (14), 4117-4140.

58. Guenther, A.; Karl, T.; Harley, P.; Wiedinmyer, C.; Palmer, P. I.; Geron, C., Estimates of global terrestrial isoprene emissions using MEGAN (Model of Emissions of Gases and Aerosols from Nature). *Atmos. Chem. Phys.* **2006,** *6*, (11), 3181-3210.

59. Pandis, S. N.; Paulson, S. E.; Seinfeld, J. H.; Flagan, R. C., Aerosol formation in the photooxidation of isoprene and β-pinene. *Atmospheric Environment. Part A. General Topics* **1991,** *25*, (5-6), 997-1008.

60. Jang, M.; Czoschke, N. M.; Lee, S.; Kamens, R. M., Heterogeneous Atmospheric Aerosol Production by Acid-Catalyzed Particle-Phase Reactions. *Science* **2002,** *298*, (5594), 814-817.

61. Gao, S.; Keywood, M.; Ng, N. L.; Surratt, J.; Varutbangkul, V.; Bahreini, R.; Flagan, R. C.; Seinfeld, J. H., Low-Molecular-Weight and Oligomeric Components in Secondary Organic Aerosol from the Ozonolysis of Cycloalkenes and α-Pinene. *The Journal of Physical Chemistry A* **2004,** *108*, (46), 10147-10164.

62. Kalberer, M.; Paulsen, D.; Sax, M.; Steinbacher, M.; Dommen, J.; Prevot, A. S. H.; Fisseha, R.; Weingartner, E.; Frankevich, V.; Zenobi, R.; Baltensperger, U., Identification of polymers as major components of atmospheric aerosols. *Science* **2004,** *303*, 1659-1662.

63. Surratt, J. D.; Murphy, S. M.; Kroll, J. H.; Ng, N. L.; Hildebrandt, L.; Sorooshian, A.; Szmigielski, R.; Vermeylen, R.; Maenhaut, W.; Claeys, M.; Flagan, R. C.; Seinfeld, J. H., Chemical Composition of Secondary Organic Aerosol Formed from the Photooxidation of Isoprene. *The Journal of Physical Chemistry A* **2006,** *110*, (31), 9665-9690.

64. Surratt, J. D.; Gómez-González, Y.; Chan, A. W. H.; Vermeylen, R.; Shahgholi, M.; Kleindienst, T. E.; Edney, E. O.; Offenberg, J. H.; Lewandowski, M.; Jaoui, M.; Maenhaut, W.; Claeys, M.; Flagan, R. C.; Seinfeld, J. H., Organosulfate Formation in Biogenic Secondary Organic Aerosol. *The Journal of Physical Chemistry A* **2008,** *112*, (36), 8345-8378.

65. Iinuma, Y.; Boge, O.; Gnauk, T.; Herrman, H., Aerosol-chamber study of the a-pinene/O3 reaction: Influence of particle acidity on aerosol yields and products. *Atmos. Environ.* **2004,** *38*, 761-773.

66. Tolocka, M. P.; Jang, M.; Ginter, J. M.; Cox, F. J.; Kamens, R. M.; Johnston, M. V., Formation of oligomers in secondary organic aerosol. *Environmental Science and Technology* **2004,** *38*, 1428-1434.

67. Surratt, J. D.; Lewandowski, M.; Offenberg, J. H.; Jaoui, M.; Kleindienst, T. E.; Edney, E. O.; Seinfeld, J. H., Effect of Acidity on Secondary Organic Aerosol Formation from Isoprene. *Environmental Science & Technology* **2007,** *41*, (15), 5363-5369.

68. Kroll, J. H.; Ng, N. L.; Murphy, S. M.; Varutbangkul, V.; Flagan, R. C.; Seinfeld, J. H., Chamber studies of secondary organic aerosol growth by reactive uptake of simple

carbonyl compounds. *J. Geophys. Res.* **2005,** *110*, (D23), D23207, doi:10.1029/2005JD006004.

69. Hegg, D. A., The importance of liquid-phase oxidation of SO_2 in the troposphere. *J. Geophys. Res.* **1985,** *90*, 3773-3779.

70. Feichter, J.; E. Kjellstrom; H. Rodhe; F. Dentener; J. Lelieveld; Reolofs, G., Simulation of the tropospheric sulfur cycle in a global climate model. *Atmos. Environ.* **1996,** *30*, 1693-1707.

71. Blando, J. D.; Turpin, B. J., Secondary organic aerosol formation in cloud and fog droplets: a literature evaluation of plausibility. *Atmospheric Environment* **2000,** *34*, (10), 1623-1632.

72. Gelencser, A.; Varga, Z., Evaluation of the atmospheric significance of multiphase reactions in atmospheric secondary organic aerosol formation. *Atmos. Chem. Phys.* **2005,** *5*, 2823-2831.

73. Mauldin, R. L. I.; Madronich, S.; Flocke, S. J.; Eisele, F. L.; Frost, G. J.; Prevot, A. S. H., New insights on OH: Measurements around and in clouds. *Geophys. Res. Lett.* **1997,** *24*, 3033-3036.

74. Atkinson, R.; Arey, J., Gas-phase tropospheric chemistry of biogenic volatile organic compounds: a review. *Atmospheric Environment* **2003,** *37*, (Supplement 2), 197-219.

75. Betterton, E. A.; Hoffmann, M. R., Henry's Law Constants of some environmentally important aldehydes. *Environmental Science and Technology* **1988,** *22*, (12), 1415-1418.

76. Zhou, X.; Mopper, K., Apparent partition coefficients of 15 carbonyl compounds between air and seawater and between air and freshwater; implications for air-sea exchange. *Environmental Science & Technology* **1990,** *24*, (12), 1864-1869.

77. Limbeck, A.; Puxbaum, H.; Otter, L.; Scholes, M. C., Semivolatile behavior of dicarboxylic acids and other polar organic species at a rural background site (Nylsvley, RSA) *Atmos. Environ.* **2001,** *35*, 1853-1862.

78. Hennigan, C. J.; Bergin, M. H.; Weber, R. J., Correlations between Water-Soluble Organic Aerosol and Water Vapor: A Synergistic Effect from Biogenic Emissions? *Environmental Science & Technology* **2008,** *42*, (24), 9079-9085.

79. Hennigan, C. J.; Bergin, M. H.; Dibb, J. E.; Weber, R. J., Enhanced secondary organic aerosol formation due to water uptake by fine particles. *Geophys. Res. Lett.* **2008,** *35*, (18), L18801, doi:10.1029/2008GL035046.

80. Hennigan, C. J.; Bergin, M. H.; Russell, A. G.; Nenes, A.; Weber, R. J., Gas/particle partitioning of water-soluble organic aerosol in Atlanta. *Atmos. Chem. Phys.* **2009,** *9*, (11), 3613-3628.

81. Warneck, P., In-cloud chemistry opens pathway to the formation of oxalic acid in the marine atmosphere. *Atmospheric Environment* **2003,** *37*, (17), 2423-2427.

82. Warneck, P., Multi-phase chemistry of C2 and C3 organic compounds in the marine atmosphere. *J. Atmos. Chem.* **2005,** *51*, 119-159.

83. Ervens, B.; Feingold, G.; Frost, G. J.; Kreidenweis, S. M., A modeling study of aqueous production of dicarboxylic acids: 1. Chemical pathways and speciated organic mass production. *Journal of Geophysical Research* **2004,** *109*, (D15205), doi:10.1029/2003JD004387.

84. Lim, H.-J.; Carlton, A. G.; Turpin, B. J., Isoprene Forms Secondary Organic Aerosol through Cloud Processing: Model Simulations. *Environmental Science & Technology* **2005,** *39*, (12), 4441-4446.

85. Ervens, B.; Carlton, A. G.; Turpin, B. J.; Altieri, K. E.; Kreidenweis, S. M.; Feingold, G., Secondary organic aerosol yields from cloud-processing of isoprene oxidation products. *Geophys. Res. Lett.* **2008,** *35*, L02816, doi:10.1029/2007GL031828.

86. Heald, C. L.; Jacob, D. J.; Turquety, S.; Hudman, R. C.; Weber, R. J.; Sullivan, A. P.; Peltier, R. E.; Atlas, E. L.; de Gouw, J. A.; Warneke, C.; Holloway, J. S.; Neuman, J. A.; Flocke, F. M.; Seinfeld, J. H., Concentrations and sources of organic carbon aerosols in the free troposphere over North America. *J. Geophys. Res.* **2006,** *111*, D23s47, doi:10.1029/2006JD007705.

87. Carlton, A. G.; Turpin, B. J.; Altieri, K. E.; Seitzinger, S. P.; Mathur, R.; Roselle, S. J.; Weber, R. J., CMAQ Model Performance Enhanced When In-Cloud Secondary

Organic Aerosol is Included: Comparisons of Organic Carbon Predictions with Measurements. *Environ. Sci. Technol.* **2008,** *42*, (23), 8798-8802.

88. Fu, T.-M.; Jacob, D. J.; Heald, C. L., Aqueous-phase reactive uptake of dicarbonyls as a source of organic aerosol over eastern North America. *Atmospheric Environment* **2009,** *43*, (10), 1814-1822.

89. Fu, T.-M.; Jacob, D. J.; Wittrock, F.; Burrows, J. P.; Vrekoussis, M.; Henze, D. K., Global budgets of atmospheric glyoxal and methylglyoxal, and implications for formation of secondary organic aerosols. *J. Geophys. Res.* **2008,** *113*, D15303, doi:10.1029/2007JD009505.

90. Stefan, M. I.; Bolton, J. R., Reinvestigation of the acetone degradation mechanism in dilute aqueous solution by the UV/H2O2 process. *Environmental Science and Technology* **1999,** *30*, 870-873.

91. Ervens, B.; Gligorovski, S.; Herrmann, H., Temperature-dependent rate constants for hydroxyl radical reactions with organic compounds in aqueous solutions. *Physical Chemistry Chemical Physics* **2003,** *5*, (9), 1811-1824.

92. Monod, A.; Poulain, L.; Grubert, S.; Voisin, D.; Wortham, H., Kinetics of OH-initiated oxidation of oxygenated organic compounds in the aqueous phase: new rate constants, structure-activity relationships and atmospheric implications. *Atmospheric Environment* **2005,** *39*, (40), 7667-7688.

93. Kawamura, K.; Kasukabe, H.; Barrie, L. A., Source and reaction pathways of dicarboxylic acids, ketoacids and dicarbonyls in arctic aerosols: One year of observations. *Atmospheric Environment* **1996,** *30*, (10-11), 1709-1722.

94. Kawamura, K.; Semere, R.; Imai, Y.; Fujii, Y.; Hayashi, M., Water soluble dicarboxylic acids and related compounds in Antarctic aerosols. *Journal of Geophysical Research-Atmospheres* **1996,** *101*, (D13), 18721-18728.

95. Kerminen, V.-M.; Ojanen, C.; Pakkanen, T.; Hillamo, R.; Aurela, M.; Merilainen, J., Low-molecular-weight dicarboxylic acids in an urban and rural atmosphere. *Journal of Aerosol Science* **2000,** *31*, (3), 349-362.

96. Rohrl, A.; Lammel, G., Low-molecular weight dicarboxylic acids: seasonal and air mass chracteristics. *Environmental Science and Technology* **2001,** *35*, 95-101.

97. Miyazaki, Y.; Aggarwal, S. G.; Singh, K.; Gupta, P. K.; Kawamura, K., Dicarboxylic acids and water-soluble organic carbon in aerosols in New Delhi, India, in winter: Characteristics and formation processes. *J. Geophys. Res.* **2009,** *114*, D19206, doi:10.1029/2009JD011790.

98. Hsieh, L.-Y.; Kuo, S.-C.; Chen, C.-L.; Tsai, Y. I., Origin of low-molecular-weight dicarboxylic acids and their concentration and size distribution variation in suburban aerosol. *Atmospheric Environment* **2007,** *41*, (31), 6648-6661.

99. Collett, J. L.; Hoag, K. J.; Rao, X.; Pandis, S. N., Internal acid buffering in San Joaquin Valley fog drops and its influence on aerosol processing. *Atmospheric Environment* **1999,** *33*, (29), 4833-4847.

100. Crahan, K. K.; Hegg, D.; Covert, D. S.; Jonsson, H., An exploration of aqueous oxalic acid production in the coastal marine atmosphere. *Atmospheric Environment* **2004,** *23*, 3757-3764.

101. Fuzzi, S.; Facchini, M. C.; Decesari, S.; Matta, E.; Mircea, M., Soluble organic compounds in fog and cloud droplets: what have we learned over the past few years? *Atmospheric Research* **2002,** *64*, 89-98.

102. Loflund, M.; Kasper-Giebl, A.; Schuster, B.; Giebl, H.; Hitzenberger, R.; Puxbaum, H., Formic, acetic, oxalic, malonic and succinic acid concentrations and their contribution to organic carbon in cloud water. *Atmospheric Environment* **2002,** *36*, (9), 1553-1558.

103. Collett Jr, J. L.; Herckes, P.; Youngster, S.; Lee, T., Processing of atmospheric organic matter by California radiation fogs. *Atmospheric Research* **2008,** *87*, (3-4), 232-241.

104. Legrand, M.; DeAngelis, M., Origin of light carboxylic acids in polar precipitation. *J. Geophys. Res.* **1995,** *100*, 1445-1462.

105. Maupetit, F.; Delmas, J. D., Carboxylic acids in high-elevation glacier snow. *J. Geophys. Res.* **1994,** *99*, 16481-16500.

106. Saxena, P.; Hildemann, L. M.; McMurry, P. H.; Seinfeld, J. H., Organics alter hygroscopic behavior of atmospheric particles. *J. Geophys. Res.* **1995,** *100*, (D9), 18755-18770.

107. Facchini, M. C.; Mircea, M.; Fuzzi, S.; Charlson, R. J., Cloud albedo enhancement by surface-active organic solutes in growing droplets. *Nature* **1999,** *401*, (6750), 257-259.

108. Kawamura, K.; Ikushima, K., Seasonal changes in the distribution of dicarboxylic acids in the urban atmosphere. *Environ. Sci. Technol.* **1993,** *27*, 2227-2235.

109. Chebbi, A.; Carlier, P., Carboxylic Acids in the Troposphere, Occurrence, Sources, and Sinks: a Review. *Atmospheric Environment* **1996,** *30*, (24), 4233-4249.

110. Kawamura, K.; Kaplan, I. R., Motor exhaust emissions as a primary source for dicarboxylic acids in Los Angeles ambient air. *Environmental Science & Technology* **1987,** *21*, (1), 105-110.

111. Huang, X.-F.; Yu, J. Z., Is vehicle exhaust a significant primary source of oxalic acid in ambient aerosols? *Geophys. Res. Lett.* **2007,** *34*, L02808, doi:10.1029/2006GL028457.

112. Kawamura, K.; Yasui, O., Diurnal changes in the distribution of dicarboxylic acids, ketocarboxylic acids and dicarbonyls in the urban Tokyo atmosphere. *Atmospheric Environment* **2005,** *39*, (10), 1945-1960.

113. Kawamura, K.; Imai, Y.; Barrie, L. A., Photochemical production and loss of organic acids in high Arctic aerosols during long-range transport and polar sunrise ozone depletion events. *Atmospheric Environment* **2005,** *39*, (4), 599-614.

114. Sullivan, R. C.; Prather, K. A., Investigations of the Diurnal Cycle and Mixing State of Oxalic Acid in Individual Particles in Asian Aerosol Outflow. *Environmental Science & Technology* **2007,** *41*, (23), 8062-8069.

115. Yu, J. Z.; Huang, X.-F.; Xu, J.; Hu, M., When Aerosol Sulfate Goes Up, So Does Oxalate: Implication for the Formation Mechanisms of Oxalate. *Environmental Science & Technology* **2005,** *39*, (1), 128-133.

116. Sorooshian, A.; Varutbangkul, V.; Brechtel, F. J.; Ervens, B.; Feingold, G.; Bahreini, R.; Murphy, S. M.; Holloway, J. S.; Atlas, E. L.; Buzorius, G.; Jonsson, H.; Flagan, R. C.; Seinfeld, J. H., Oxalic acid in clear and cloudy atmospheres: Analysis of data from International Consortium for Atmospheric Research on Transport and Transformation 2004. *J. Geophys. Res.* **2006,** *111*, D23S45, doi:10.1029/2005JD006880.

117. Kerminen, V.-M.; Wexler, A. S., Growth laws for atmospheric aerosol particles: An examination of the bimodality of the accumulation mode. *Atmospheric Environment* **1995,** *29*, (22), 3263-3275.

118. Meng, Z.; Seinfeld, J. H., On the Source of the Submicrometer Droplet Mode of Urban and Regional Aerosols. *Aerosol Science and Technology* **1994,** *20*, (3), 253 - 265.

119. Sorooshian, A.; Lu, M.-L.; Brechtel, F. J.; Jonsson, H.; Feingold, G.; Flagan, R. C.; Seinfeld, J. H., On the Source of Organic Acid Aerosol Layers above Clouds. *Environmental Science & Technology* **2007,** *41*, (13), 4647-4654.

120. Sorooshian, A.; Ng, N. L.; Chan, A. W. H.; Feingold, G.; Flagan, R. C.; Seinfeld, J. H., Particulate organic acids and overall water-soluble aerosol composition measurements from the 2006 Gulf of Mexico Atmospheric Composition and Climate Study (GoMACCS). *J. Geophys. Res.* **2007,** *112*, D13201, doi:10.1029/2007JD008537.

121. Carlton, A. G.; Turpin, B. J.; Lim, H.-J.; Altieri, K. E.; Seitzinger, S., Link between isoprene and secondary organic aerosol (SOA): Pyruvic acid oxidation yields low volatility organic acids in clouds. *Geophys. Res. Lett.* **2006,** *33*, L06822, doi:10.1029/2005GL025374.

122. Carlton, A. G.; Turpin, B. J.; Altieri, K. E.; Seitzinger, S.; Reff, A.; Lim, H.-J.; Ervens, B., Atmospheric oxalic acid and SOA production from glyoxal: Results of aqueous photooxidation experiments. *Atmos. Environ.* **2007,** *41*, (35), 7588-7602.

123. Liu, Y.; El Haddad, I.; Scarfogliero, M.; Nieto-Gligorovski, L.; Temime-Roussel, B.; Quivet, E.; Marchand, N.; Picquet-Varrault, B.; Monod, A., In-cloud processes of methacrolein under simulated conditions – Part 1: Aqueous phase photooxidation. *Atmos. Chem. Phys.* **2009,** *9*, (14), 5093-5105.

124. Carlton, A. G.; Turpin, B. J.; Altieri, K. E.; Seitzinger, S.; Reff, A.; Lim, H.-J.; Ervens, B., Atmospheric oxalic acid and SOA production from glyoxal: Results of aqueous photooxidation experiments. *Atmospheric Environment* **2007,** *41*, (35), 7588-7602.

125. Surratt, J. D.; Kroll, J. H.; Kleindienst, T. E.; Edney, E. O.; Claeys, M.; Sorooshian, A.; Ng, N. L.; Offenberg, J. H.; Lewandowski, M.; Jaoui, M.; Flagan, R. C.; Seinfeld, J. H., Evidence for Organosulfates in Secondary Organic Aerosol. *Environmental Science & Technology* **2007,** *41*, (2), 517-527.

126. Havers, N.; Burba, P.; Lambert, J.; Klockow, D., Spectroscopic Characterization of Humic-Like Substances in Airborne Particulate Matter. *Journal of Atmospheric Chemistry* **1998,** *29*, (1), 45-54.

127. Zappoli, S.; Andracchio, A.; Fuzzi, S.; Facchini, M. C.; Gelencser, A.; Kiss, G.; Krivacsy, Z.; Molnar, A.; Meszaros, E.; Hansson, H.-C.; Rosman, K.; Zebuhr, Y., Inorganic, organic, and Macromolecular Components of Fine Aerosol in Different Areas of Europe in Relation to their Water Solubility. *Atmospheric Environment* **1999,** *33*, 2733-2743.

128. Altieri, K. E.; Turpin, B. J.; Seitzinger, S. P., Oligomers, organosulfates, and nitrooxy organosulfates in rainwater identified by ultra-high resolution electrospray ionization FT-ICR mass spectrometry. *Atmos. Chem. Phys.* **2009,** *9*, (7), 2533-2542.

129. Kiss, G.; Varga, B.; Galambos, I.; Ganszky, I., Characterization of water-soluble organic matter isolated from atmospheric fine aerosol. *Journal of Geophysical Research-Atmospheres* **2002,** *107*, (D21), 8339, doi:10.1029/2001JD000603.

130. Dinar, E.; Taraniuk, I.; Graber, E. R.; Katsman, S.; Moise, T.; Anttila, T.; Mentel, T. F.; Rudich, Y., Cloud Condensation Nuclei properties of model and atmospheric HULIS. *Atmos. Chem. Phys.* **2006,** *6*, (9), 2465-2482.

131. Dinar, E.; Taraniuk, I.; Graber, E. R.; Anttila, T.; Mentel, T. F.; Rudich, Y., Hygroscopic growth of atmospheric and model humic-like substances. *J. Geophys. Res.* **2007,** *112*, (D5), D05211, doi:10.1029/2006JD007442.

132. Asa-Awuku, A.; Nenes, A., Effect of solute dissolution kinetics on cloud droplet formation: Extended Köhler theory. *J. Geophys. Res.* **2007,** *112*, (D22), D22201, doi:10.1029/2005JD006934.

133. Taraniuk, I.; Graber, E. R.; Kostinski, A.; Rudich, Y., Surfactant properties of atmospheric and model humic-like substances (HULIS). *Geophys. Res. Lett.* **2007,** *34*, (16), L16807, doi:10.1029/2007GL029576.

134. Wex, H.; Hennig, T.; Salma, I.; Ocskay, R.; Kiselev, A.; Henning, S.; Massling, A.; Wiedensohler, A.; Stratmann, F., Hygroscopic growth and measured and modeled critical super-saturations of an atmospheric HULIS sample. *Geophys. Res. Lett.* **2007,** *34*, (2), L02818, doi:10.1029/2006GL028260.

135. Guzman, M. I.; Colussi, A. J.; Hoffmann, M. R., Photoinduced Oligomerization of Aqueous Pyruvic Acid. *The Journal of Physical Chemistry A* **2006,** *110*, (10), 3619-3626.

136. Altieri, K. E.; Carlton, A. G.; Lim, H.-J.; Turpin, B. J.; Seitzinger, S. P., Evidence for Oligomer Formation in Clouds: Reactions of Isoprene Oxidation Products. *Environmental Science & Technology* **2006,** *40*, (16), 4956-4960.

137. Altieri, K. E.; Seitzinger, S. P.; Carlton, A. G.; Turpin, B. J.; Klein, G. C.; Marshall, A. G., Oligomers formed through in-cloud methylglyoxal reactions: Chemical composition, properties, and mechanisms investigated by ultra-high resolution FT-ICR mass spectrometry. *Atmospheric Environment* **2008,** *42*, (7), 1476-1490.

138. Perri, M. J.; Seitzinger, S.; Turpin, B. J., Secondary organic aerosol production from aqueous photooxidation of glycolaldehyde: Laboratory experiments. *Atmospheric Environment* **2009,** *43*, (8), 1487-1497.

139. Poulain, L.; Monod, A.; Wortham, H., Development of a new on-line mass spectrometer to study the reactivity of soluble organic compounds in the aqueous phase under tropospheric conditions: Application to OH-oxidation of N-methylpyrrolidone. *Journal of Photochemistry and Photobiology A: Chemistry* **2007,** *187*, (1), 10-23.

140. El Haddad, I.; Liu, Y.; Nieto-Gligorovski, L.; Michaud, V.; Temime-Roussel, B.; Quivet, E.; Marchand, N.; Sellegri, K.; Monod, A., In-cloud processes of methacrolein under simulated conditions – Part 2: Formation of secondary organic aerosol. *Atmos. Chem. Phys.* **2009,** *9*, (14), 5107-5117.

141. Holmes, B. J.; Petrucci, G. A., Water-Soluble Oligomer Formation from Acid-Catalyzed Reactions of Levoglucosan in Proxies of Atmospheric Aqueous Aerosols. *Environmental Science & Technology* **2006,** *40*, (16), 4983-4989.

142. Blando, J. D.; Turpin, B. J., Secondary organic aerosol formation in cloud and fog droplets: A literature evaluation of plausibility. *Atmos. Environ.* **2000,** *34*, 1623-1632.

143. Herrmann, H.; Tilgner, A.; Barzaghi, P.; Majdik, Z.; Gligorovski, S.; Poulain, L.; Monod, A., Towards a more detailed description of tropospheric aqueous phase organic chemistry: CAPRAM 3.0. *Atmospheric Environment* **2005,** *39*, (23-24), 4351-4363.

144. Saunders, S. M.; Jenkin, M. E.; Derwent, R. G.; Pilling, M. J., Protocol for the development of the Master Chemical Mechanism, MCM v3 (Part A): tropospheric

degradation of non-aromatic volatile organic compounds. *Atmos. Chem. Phys.* **2003,** *3*, (1), 161-180.

145. Jenkin, M. E.; Saunders, S. M.; Wagner, V.; Pilling, M. J., Protocol for the development of the Master Chemical Mechanism, MCM v3 (Part B): tropospheric degradation of aromatic volatile organic compounds. *Atmos. Chem. Phys.* **2003,** *3*, (1), 181-193.

146. Hays, M. D.; Geron, C. D.; Linna, K. J.; Smith, N. D.; Schauer, J. J., Speciation of Gas-Phase and Fine Particle Emissions from Burning of Foliar Fuels. *Environmental Science & Technology* **2002,** *36*, (11), 2281-2295.

147. McDonald, J. D.; Zielinska, B.; Fujita, E. M.; Sagebiel, J. C.; Chow, J. C.; Watson, J. G., Fine Particle and Gaseous Emission Rates from Residential Wood Combustion. *Environmental Science & Technology* **2000,** *34*, (11), 2080-2091.

148. Koch, S.; Moortgat, G. K., Photochemistry of Methylglyoxal in the Vapor Phase. *The Journal of Physical Chemistry A* **1998,** *102*, (46), 9142-9153.

149. Feierabend, K. J.; Zhu, L.; Talukdar, R. K.; Burkholder, J. B., Rate Coefficients for the OH + HC(O)C(O)H (Glyoxal) Reaction between 210 and 390 K. *The Journal of Physical Chemistry A* **2008,** *112*, (1), 73-82.

150. Volkamer, R.; San Martini, F.; Molina, L. T.; Salcedo, D.; Jimenez, J. L.; Molina, M. J., A missing sink for gas-phase glyoxal in Mexico City: Formation of secondary organic aerosol. *Geophys. Res. Lett.* **2007,** *34*, L19807, doi:10.1029/2007GL030752.

151. Ip, H. S. S.; Huang, X. H. H.; Yu, J. Z., Effective Henry's law constants of glyoxal, glyoxylic acid, and glycolic acid. *Geophys. Res. Lett.* **2009,** *36*, (1), L01802, doi:10.1029/2008GL036212.

152. Liggio, J.; Li, S.-M.; McLaren, R., Reactive uptake of glyoxal by particulate matter. *J. Geophys. Res.* **2005,** *110*, (D10), D10304, doi:10.1029/2004JD005113.

153. Schweitzer, F.; Magi, L.; Mirabel, P.; George, C., Uptake Rate Measurements of Methanesulfonic Acid and Glyoxal by Aqueous Droplets. *The Journal of Physical Chemistry A* **1998,** *102*, (3), 593-600.

154. Zhao, J.; Levitt, N. P.; Zhang, R.; Chen, J., Heterogeneous Reactions of Methylglyoxal in Acidic Media: Implications for Secondary Organic Aerosol Formation. *Environmental Science & Technology* **2006,** *40*, (24), 7682-7687.

155. Munger, J. W.; Jacob, D. J.; Daube, B. C.; Horowitz, L. W.; Keene, W. C.; Heikes, B. G., Formaldehyde, glyoxal, and methylglyoxal in air and cloudwater at a rural mountain site in central Virginia. *J. Geophys. Res.* **1995,** *100*, (D5), 9325-9333.

156. Nemet, I.; Vikic-Topic, D.; Varga-Defterdarovic, L., Spectroscopic studies of methylglyoxal in water and dimethylsulfoxide. *Bioorganic Chemistry* **2004,** *32*, (6), 560-570.

157. Whipple, E. B., Structure of glyoxal in water. *Journal of the American Chemical Society* **1970,** *92*, (24), 7183-7186.

158. De Haan, D. O.; Corrigan, A. L.; Tolbert, M. A.; Jimenez, J. L.; Wood, S. E.; Turley, J. J., Secondary Organic Aerosol Formation by Self-Reactions of Methylglyoxal and Glyoxal in Evaporating Droplets. *Environmental Science & Technology* **2009,** *43*, (21), 8184-8190.

159. Faust, B. C., Photochemistry of Clouds, Fogs, and Aerosols. *Environmental Science & Technology* **1994,** *28*, (5), 216A-222A.

160. Seinfeld, J. H.; Pandis, S. N., *Atmospheric Chemistry and Physics - From Air Pollution to Climate Change (2nd Edition)*. John Wiley and Sons, Inc.: New York, 2006.

161. Herrmann, H., Kinetics of Aqueous Phase Reactions Relevant for Atmospheric Chemistry. *Chemical Reviews* **2003,** *103*, (12), 4691-4716.

162. Arakaki, T.; Faust, B. C., Sources, sinks, and mechanisms of hydroxyl radical (OH) photoproduction and consumption in authentic acidic continental cloud waters from Whiteface Mountain, New York: The role of the Fe(r) (r = II, III) photochemical cycle. *J. Geophys. Res.* **1998,** *103*, (D3), 3487-3504.

163. Kelly, T. J.; Daum, P. H.; Schwartz, S. E., Measurements of Peroxides in Cloudwater and Rain. *J. Geophys. Res.* **1985,** *90*, (D5), 7861-7871.

164. Claiborn, C. S.; Aneja, V. P., Measurements of Atmospheric Hydrogen Peroxide in the Gas Phase and in Cloud Water at Mt. Mitchell, North Carolina. *J. Geophys. Res.* **1991,** *96*, (D10), 18771-18787.

165. Hua, W.; Chen, Z. M.; Jie, C. Y.; Kondo, Y.; Hofzumahaus, A.; Takegawa, N.; Chang, C. C.; Lu, K. D.; Miyazaki, Y.; Kita, K.; Wang, H. L.; Zhang, Y. H.; Hu, M., Atmospheric hydrogen peroxide and organic hydroperoxides during PRIDE-PRD'06, China: their concentration, formation mechanism and contribution to secondary aerosols. *Atmos. Chem. Phys.* **2008,** *8*, (22), 6755-6773.

166. Olszyna, K. J.; Meagher, J. F.; Bailey, E. M., Gas-phase, cloud and rain-water measurements of hydrogen peroxide at a high-elevation site. *Atmospheric Environment (1967)* **1988,** *22*, (8), 1699-1706.

167. Jacob, D. J., Chemistry of OH in Remote Clouds and Its Role in the Production of Formic Acid and Peroxymonosulfate. *J. Geophys. Res.* **1986,** *91*, (D9), 9807-9826.

168. Warneck, P., The relative importance of various pathways for the oxidation of sulfur dioxide and nitrogen dioxide in sunlit continental fair weather clouds. *Physical Chemistry Chemical Physics* **1999,** *1*, (24), 5471-5483.

169. Monod, A.; Carlier, P., Impact of clouds on the tropospheric ozone budget: Direct effect of multiphase photochemistry of soluble organic compounds. *Atmospheric Environment* **1999,** *33*, (27), 4431-4446.

170. Faust, B. C.; Allen, J. M., Aqueous-phase photochemical formation of hydroxyl radical in authentic cloudwaters and fogwaters. *Environmental Science & Technology* **1993,** *27*, (6), 1221-1224.

171. Anastasio, C.; McGregor, K. G., Chemistry of fog waters in California's Central Valley: 1. In situ photoformation of hydroxyl radical and singlet molecular oxygen. *Atmospheric Environment* **2001,** *35*, (6), 1079-1089.

172. Arakaki, T.; Kuroki, Y.; Okada, K.; Nakama, Y.; Ikota, H.; Kinjo, M.; Higuchi, T.; Uehara, M.; Tanahara, A., Chemical composition and photochemical formation of hydroxyl radicals in aqueous extracts of aerosol particles collected in Okinawa, Japan. *Atmospheric Environment* **2006,** *40*, (25), 4764-4774.

173. Collett, J. L.; Bator, A.; Sherman, D. E.; Moore, K. F.; Hoag, K. J.; Demoz, B. B.; Rao, X.; Reilly, J. E., The chemical composition of fogs and intercepted clouds in the United States. *Atmospheric Research* **2002,** *64*, (1-4), 29-40.

174. Cao, G.; Jang, M., Effects of particle acidity and UV light on secondary organic aerosol formation from oxidation of aromatics in the absence of NOx. *Atmospheric Environment* **2007,** *41*, (35), 7603-7613.

175. Ng, N. L.; Kroll, J. H.; Chan, A. W. H.; Chhabra, P. S.; Flagan, R. C.; Seinfeld, J. H., Secondary organic aerosol formation from m-xylene, toluene, and benzene. *Atmos. Chem. Phys.* **2007,** *7*, (14), 3909-3922.

176. Liggio, J.; Li, S.-M., Organosulfate formation during the uptake of pinonaldehyde on acidic sulfate aerosols. *Geophys. Res. Lett.* **2006,** *33*, (13), L13808, doi:10.1029/2006GL026079.

177. Perri, M. J.; Lim, Y. B.; Seitzinger, S. P.; Turpin, B. J., Organosulfates from glycolaldehyde in aqueous aerosols and clouds: Laboratory studies. *Atmospheric Environment* **2010,** *44*, (21-22), 2658-2664.

178. Grgic, I.; Nieto-Gligorovski, L. I.; Net, S.; Temime-Roussel, B.; Gligorovski, S.; Wortham, H., Light induced multiphase chemistry of gas-phase ozone on aqueous pyruvic and oxalic acids. *Physical Chemistry Chemical Physics* **2010,** *12*, (3), 698-707.

179. Gelencsér, A.; Hoffer, A.; Kiss, G.; Tombácz, E.; Kurdi, R.; Bencze, L., In-situ Formation of Light-Absorbing Organic Matter in Cloud Water. *Journal of Atmospheric Chemistry* **2003,** *45*, (1), 25-33.

180. Hoffer, A.; Kiss, G.; Blazso, M.; Gelencser, A., Chemical characterization of humic-like substances (HULIS) formed from a lignin-type precursor in model cloud water. *Geophys. Res. Lett.* **2004,** *31*, (6), L06115, doi:10.1029/2003GL018962.

181. Sun, Y. L.; Zhang, Q.; Anastasio, C.; Sun, J., Insights into secondary organic aerosol formed via aqueous-phase reactions of phenolic compounds based on high resolution mass spectrometry. *Atmos. Chem. Phys.* **2010,** *10*, (10), 4809-4822.

182. Aiken, A. C.; DeCarlo, P. F.; Kroll, J. H.; Worsnop, D. R.; Huffman, J. A.; Docherty, K. S.; Ulbrich, I. M.; Mohr, C.; Kimmel, J. R.; Sueper, D.; Sun, Y.; Zhang, Q.; Trimborn, A.; Northway, M.; Ziemann, P. J.; Canagaratna, M. R.; Onasch, T. B.; Alfarra, M. R.; Prevot, A. S. H.; Dommen, J.; Duplissy, J.; Metzger, A.; Baltensperger, U.;

Jimenez, J. L., O/C and OM/OC Ratios of Primary, Secondary, and Ambient Organic Aerosols with High-Resolution Time-of-Flight Aerosol Mass Spectrometry. *Environmental Science & Technology* **2008,** *42*, (12), 4478-4485.

183. Tan, Y.; Perri, M. J.; Seitzinger, S. P.; Turpin, B. J., Effects of Precursor Concentration and Acidic Sulfate in Aqueous Glyoxal-OH Radical Oxidation and Implications for Secondary Organic Aerosol. *Environmental Science & Technology* **2009,** *43*, (21), 8105-8112.

184. Tan, Y.; Carlton, A. G.; Seitzinger, S. P.; Turpin, B. J., SOA from Methylglyoxal in Clouds and Wet Aerosols: Measurement and Prediction of Key Products. *Atmospheric Environment In Press, Accepted Manuscript*.

Table 1-1. Summary of previous laboratory studies of aqueous phase oxidation of potential SOA precursors.

Reaction	**Conditions**			**Analytical methods**	**Products**		**Reference**
	Precursor conc. (mM)	**Radical source**	**pH**		**Primary products**	**Higher MW Products**	
Pyruvic acid + OH	5 and 10	H_2O_2 + UV	2.7 – 3.1	HPLC-UV, ESI-MS	Acetic, formic, glyoxylic, and oxalic acids	Oligomers (up to 500 amu)	[121, 136]
Pyruvic acid + UV	5 and 10	N/A	2.7 – 3.1	HPLC-UV, ESI-MS	Acetic and formic acids	Some (< 300 amu)	[121, 136]
Pyruvic acid + UV	5 – 100	N/A	1.0	HPLC-ESI-MS, UV/Vis, ^{13}C NMR	Not reported	Dimers and trimers (177 amu)	[135]
Pyruvic acid + O_3	5 and 10	O_3 + UV/Vis	2.2 – 2.5	HOLC-UV, ESI-MS, ESI-MS^2	Oxalic acid	Oligomers (< 440 amu)	[178]
Glyoxal + OH	2	H_2O_2 + UV	4.1 – 4.8	HPLC-UV/Vis, ESI-MS	Glyoxylic, formic, and oxalic acids	Oligomers (< 400 amu)	[122]
Methylglyoxal + OH	2	H_2O_2 + UV	4.2 – 4.5	ESI-MS, FT-ICR-MS, ESI-MS^2	Pyruvic, acetic, formic, glyoxylic, and oxalic acids	Oligomers (up to 500 amu)	[137]
Glycoaldehyde + OH	1	H_2O_2 + UV	4.0 – 5.6	IC, ESI-MS, FT-ICR-MS,	Glyoxal, glycolic, glyoxylic, formic, and oxalic acids	Oligomers (up to 500 amu)	[138]

Methacrolein + OH	2 – 5	H_2O_2 + UV	4.5 – 5.6	HPLC-UV, ESI-MS, GC-FID, $ESI\text{-}MS^2$	Methylglyoxal, formaldehyde, hydroxyacetone, acetic, methacrylic, oxalic, glyoxylic, and pyruvic acids	Polyfunctional compounds, oligomers (up to 400 amu),	[123, 140]
Phenol, guaiacol, and syringol + OH	0.1	H_2O_2 + UV	5 or 7	HPLC-UV, IC, HR-AMS	Oxalic, formic and acetic acids	Phenolic dimers and higher oligomers (up to 500 amu)	[181]
N-methyl-pyrrolidone + OH	0.5	H_2O_2 + UV	Free	HPLC-UV, ESI-MS, $ESI\text{-}MS^2$	succinimide, Nmethylsuccinimide, formyl-pyrrolidone, N-hydroxymethylpyrrolidone, 5-hydroxy-N-methylpyrrolidone, 2-pyrrolidone, methylamine, formamide, acetamide, N-methylformamide, N-ethylacetamide and dimethylacetamide	Oligomers (up to 300 amu)	[139]
Levoglucosan + OH	1	H_2O_2 + $FeCl_3$	4.5	MALDI-TOF-MS, ATR-FTIR	D-glucose	Oligomers (up to 1458 amu)	[141]
3,5-dihydroxy-benzoic acid + OH	0.02	H_2O_2 + $FeCl_3$	4.5	UV/Vis, ESI-MS, THM-GC/MS	Not reported	Oligomers (up to 600 amu)	[179-180]

Chapter 2. Effects of Precursor Concentration and Acidic Sulfate in Aqueous Glyoxal-OH Radical Oxidation and Implications for Secondary Organic Aerosol

Material in this chapter has been published previously as:

Tan, Y.; Perri, M. J.; Seitzinger, S. P.; Turpin, B. J., Effects of Precursor Concentration and Acidic Sulfate in Aqueous Glyoxal-OH Radical Oxidation and Implications for Secondary Organic Aerosol. *Environmental Science & Technology* **2009,** *43*, (21), 8105-8112.

2.1 Abstract

Previous experiments demonstrated that aqueous OH radical oxidation of glyoxal yields low-volatility compounds. When this chemistry takes place in clouds/fogs followed by droplet evaporation (or if it occurs in aerosol water) then products are expected to remain, in part, in the particle phase, forming secondary organic aerosol (SOA). Acidic sulfate exists ubiquitously in atmospheric water and has been shown to enhance SOA formation through aerosol phase reactions. In this work we investigate how starting concentrations of glyoxal (30 – 3000 μM) and the presence of acidic sulfate (0 – 840 μM) affect product formation in the aqueous reaction between glyoxal and OH radical. The oxalic acid yield decreased with increasing precursor concentrations, and the presence of sulfuric acid did not alter oxalic acid concentrations significantly. A dilute aqueous chemistry model successfully reproduced oxalic acid concentrations when the experiment was performed at cloud relevant concentrations (glyoxal < 300 μM), but predictions deviated from measurements at increasing concentrations. Results elucidate similarities and differences in aqueous glyoxal chemistry in clouds and in wet aerosols. They validate for the first time the accuracy of model predictions at cloud relevant

concentrations. These results suggest that the cloud processing of glyoxal could be an important source of SOA.

2.2 Introduction

Organic aerosols affect visibility, health and global climate [1-2]. Current models underestimate organic aerosol concentrations in the free troposphere, suggesting there is a missing secondary organic aerosol (SOA) formation mechanism [3-4]. There is ample evidence suggesting that fog/cloud processing contributes to global SOA budget [5-8], however, our knowledge about the overall importance of fog/cloud processing to SOA formation is quite limited.

Fog/cloud processing, which is the dominant source of atmospheric sulfate, has been hypothesized to be a substantial source of SOA globally [9-10]. Briefly, reactive organic precursors are oxidized in the gas phase to form water soluble products. These products readily partition into cloud droplets and react further with aqueous oxidants to form low volatility compounds. Some reactions occur only in the aqueous phase (e.g., Russell mechanism of peroxyl radicals), and these reactions may lead to products not seen in gas phase chemistry. Upon cloud droplet evaporation these low volatility organics remain at least in part in the particle phase (e.g., 90% for oxalic acid), forming SOA [11]. SOA could form through similar aqueous reactions in aerosol water as well.

Glyoxal is a common α-dicarbonyl formed in the atmospheric oxidation of both biogenic and anthropogenic precursors, with a global source of 45 Tg a^{-1} [12]. UV photolysis and reaction with hydroxyl radical (·OH) are primary gas phase loss processes for glyoxal [13]. Glyoxal concentrations in the Mexico City atmosphere are found significantly below model predictions, suggesting existence of missing sinks [14].

Reactive uptake of glyoxal by clouds and wet aerosols could plausibly explain this observation [12]. Glyoxal can enter droplets readily due to a high effective Henry's law constant ($H_{eff} > 3\times10^5$ M atm^{-1} at 25°C) and fast uptake rate [15-16]. Typical aqueous glyoxal concentrations vary from a few μM in rain water to 276 μM in fog water [17]. Concentrations in wet aerosols could be several orders of magnitude higher. Aqueous oxidation of glyoxal forms low volatility compounds including oxalic acid and larger multifunctional products [18]. In fact, aqueous formation from glyoxal and other carbonyl compounds helps to explain the atmospheric abundance of oxalic acid and the presence of oligomers in aerosols and clouds. Recent modeling suggests SOA through aqueous reaction pathway is comparable in magnitude to other SOA formation pathways, though uncertainties are large [12, 19].

Sulfur (VI) contributes to the acidity of cloud droplets. Several studies suggest that sulfuric acid may participate in aerosol phase oligomerization reactions including aldol condensation and hemiacetal/acetal formation [20-21]. However, the effect of acidic sulfate on SOA production through cloud processing has not been examined.

The kinetics of aqueous glyoxal OH radical oxidation have been studied by Carlton et al., but glyoxal concentrations in those experiments were 1 – 3 orders of magnitude higher than typical cloud/fog conditions [18]. In this work, we investigate how the presence of acidic sulfate and starting concentrations of glyoxal affect product formation in bulk aqueous glyoxal OH radical experiments conducted at cloud-relevant pH. Some organic acids not previously identified in glyoxal oxidation were observed in these experiments as a result of improved analytical resolution. Reaction vessel kinetic modeling captured well product formation at cloud relevant concentrations. Further

chemical mechanism development is needed to improve SOA predictions from glyoxal in wet aerosols.

2.3 Experimental Section

2.3.1 Batch reactions

Batch aqueous reactions of glyoxal and OH radical with and without sulfuric acid were conducted in a 1 L glass reaction vessel, as described in detail elsewhere [22]. The effect of two factors – glyoxal concentration and sulfuric acid concentration – on the production of low volatility compounds was studied. Experimental conditions are provided in Appendix A4. Initial glyoxal concentrations were 30, 300, and 3000 μM, and H_2SO_4 concentrations were 0, 280, and 840 μM. Hydroxyl radical (3×10^{-12} M – 6×10^{-12} M, estimated) was formed continuously by photolysis of H_2O_2, using a monochromatic (254 nm) mercury lamp (Heraeus Noblelight, Inc. Duluth, GA). Thus the OH radical concentration remained relatively constant while the concentration of glyoxal decreased to 0 during experiments. All experiments were conducted at 25 ± 2°C in duplicate. The pH varied from 5.2 to 2.1, decreasing with increasing H_2SO_4 and with increasing reaction time. Samples (10 mL) were taken at similar time points in each experiment with 10% duplicates. A 20 μL aliquot of a 1% catalase solution was added to each sample immediately to destroy H_2O_2. Batch reaction samples were analyzed within 12 hours of collection by ion chromatography. Selected samples were also analyzed by mass spectral methods. One glyoxal experiment was performed with real-time mass spectral analysis, as described in analytical methods.

The following control experiments were also conducted: glyoxal + UV, glyoxal + H_2SO_4, glyoxal + H_2O_2 ± H_2SO_4, H_2O_2 ± H_2SO_4 + UV, mixed standard + H_2O_2, and

mixed standard + UV. The mixed standard contained oxalic, glyoxylic, malonic, succinic, formic and glycolic acids. Pure water was also sampled from the reaction vessel and analyzed like samples.

The 30 μM glyoxal experiments are cloud relevant, and 300 μM experiments could represent some heavily polluted fogs. Glyoxal concentrations could reach extremely high values (~1 – 10 M) during cloud evaporation and in aerosol water. Examination of the chemistry with increasing glyoxal concentration provides some insights into differences between the aqueous photochemistry of glyoxal in cloud and aerosol water.

2.3.2 Online Experiments

ESI-MS online experiment (1000 μM glyoxal + 5 mM H_2O_2 + UV) was run as described by Perri et al. [23]. The isocratic pump continuously delivered reaction solution from reaction vessel into ESI-MS at 0.11 mL/min, and the binary pump delivered mobile phase at 0.11 mL/min. Samples were analyzed in the negative ionization mode. Discrete samples were frozen for IC analysis.

2.3.3 Analytical Methods

Carboxylic acids were quantified by ion chromatography (IC) (ICS-3000, Dionex, Sunnyvale, CA) with an IonPac AS11-HC column (30˚C), AG11-HC guard column (Dionex, Synnyvale, CA), and conductivity detector (35˚C). A photodiode array detector provided additional product validation. Monovalent anions such as glycolate (5.9 min), formate (6.8 min) and glyoxylate (9.7 min) are only weakly retained, bivalent ions such as succinate (20.4 min), malonate (21.5 min) and oxalate (24.6 min) elute after monovalent ions, and trivalent ions such as citrate are strongly retained and elute even

later. Acetate and glycolate (5.9 min), succinate and malate (20.4 min), as well as malonate and tartrate (21.5 min) coelute.

Fresh samples from batch experiments were analyzed by electrospray ionization mass spectrometry (ESI-MS) (HP-Agilent 1100) as described previously [24]. ESI-MS is a soft ionization method that does not fragment ions. Carboxylic acids are detected in the negative ionization mode as molecular weight minus one ion because of the loss of an acidic proton. Aldehydes and alcohols are detected in the positive mode. Glyoxal is detected as m/z^+ 117 and 131 as previously reported. The ion m/z^+ 117 was used to qualitatively represent glyoxal in this work. A frozen sample (-20 °C) taken 30 minutes into the experiment (3000 μM glyoxal + OH radical; experiment #13 Appendix A4) was analyzed by Fourier transform ion cyclotron resonance (FT-ICR) ESI-MS (Thermo-Finnigan LTQ-XL, Woods Hole Oceanographic Institute Mass Spectrometer Facility) to determine the elemental formulas of products from 95 – 500 amu (mass resolution 100 k – 750 k) as described by Perri et al. [23].

Selected samples were analyzed for total organic carbon, and hydrogen peroxide was measured in organic control experiments (H_2O_2 ± H_2SO_4 + UV). Analytical details are provided in Appendix A.

2.3.4 Kinetic modeling

Aqueous glyoxal photooxidation was modeled using a mechanism based on Lim et al. [25] (Table 2-1) and the differential solver, FACSIMILE (AEA technology, Oxford shire, UK). The H_2O_2 photolysis rate (k = 1.1e-4 s^{-1}, Reaction 1, Table 2-1) was fitted by simulating the H_2O_2 concentration in H_2O_2 + UV control experiments with reactions 1 –

5 (Table 2-1; Appendix A1). Modeled OH radical concentrations during the experiments were on average $3 \times 10^{-12} – 6 \times 10^{-12}$ M (Appendix A4).

2.3.5 Quality Assurance / Quality Control (QA/QC)

The expected products of glyoxal + OH radical are glyoxylic and oxalic acids. Neither glyoxal nor oxalic acid degraded in the presence of H_2O_2 alone (mixed standard + H_2O_2 control experiment). However, glyoxylic acid + H_2O_2 formed formic acid. To evaluate the effectiveness of catalase in destroying H_2O_2 in samples, some samples from the mixed standard (pH = 3.2) + H_2O_2 control experiment (10 mL) were treated with 20 μL of a 1% catalase solution. Some H_2O_2 was still present in these samples after 5 minutes of contact with catalase. We believe the sample acidity inhibited catalase performance. The reaction of glyoxylic acid + H_2O_2 is slow compared to glyoxylic acid + OH radical (Table 2-1) *in the reaction vessel*. However, *in samples* OH radicals are instantly depleted. The destruction of H_2O_2 by catalase in these samples was not fast enough to prevent conversion of glyoxylic acid to formic acid prior to sample analysis in batch experiments. This explains the low glyoxylic acid concentrations measured by Carlton et al. [18] and suggests that formic and glyoxylic acid concentrations measured in batch experiments described here do not accurately reflect concentrations in the reaction vessel.

Data quality for organic acids is presented in detail in Appendix A. Recoveries are near 100% except for glyoxylic acid (86.5%). With the addition of H_2O_2, recoveries were unchanged for glycolic acid, malonic acid, succinic acid and oxalic acid. However, glyoxylic acid disappeared and the formic acid concentration increased. Precision is better than 5% for all quantified organic acids.

2.4 Results and Discussion

2.4.1 Online Results

ESI-MS online analysis (Figure 2-1) demonstrates qualitative agreement with predictions [25-26] and batch aqueous glyoxal + OH radical experiments conducted previously [18]. Specifically, glyoxylic acid (m/z^- 73) is the first generation product. Oxalic acid (m/z^- 89) increased rapidly as glyoxylic acid decayed. The time profile of oxalic acid, quantified by IC, matches the abundance of m/z^- 89 (ESI-MS) very well. In agreement with previous batch experiments [18] a large number of additional ions were observed, including m/z^- 103, 117, 133, and 149, which will be discussed later. In previous batch experiments the rapid appearance of formic acid (measured by IC) was taken to suggest that glyoxal + OH radical forms formic acid directly. As discussed in the previous section, we now know that glyoxylic acid reacts with residual H_2O_2 to form formic acid in collected samples from batch experiments. Because the ESI-MS cannot measure formic acid, this on-line experiment cannot be used to verify/refute the possibility that formic acid is formed directly from glyoxal.

2.4.2. Effect of sulfuric acid addition

The addition of sulfuric acid had little effect on the oxalic acid production (Figure 2-2). Sulfuric acid appears to enhance oxalic acid decay slightly in the late stage of 30 μM experiments and a slight suppression of oxalic acid production might occur at the beginning of 3000 μM experiments. Formation of organo-sulfur compounds is possible but is beyond the scope of this work.

2.4.3. Effect of precursor concentration

Increasing precursor concentrations resulted in a non-linear decrease in the mass of oxalic acid (at maximum) per mass of glyoxal reacted, from 136% in 30 μM experiments to 94% and 38% in 300 and 3000 μM experiments, respectively (Figure 2-2, Appendix A4). Also, the oxalic acid production was slower in 3000 μM experiments compared to lower concentration experiments. Most but not all of the decrease in the yield of oxalic acid with increasing precursor concentration is captured by the model results and reflects the fact that H_2O_2 concentrations are also much higher in the higher concentration experiments, whereas OH radical concentrations are only slightly larger. At the higher H_2O_2 concentrations, the formation of formic acid from glyoxylic acid and H_2O_2 competes with the formation of oxalic acid from glyoxylic acid and OH radical in the reaction vessel, reducing oxalic acid production. Oxalic acid did not form in control experiments (glyoxal + UV; glyoxal + H_2O_2). In glyoxal + OH radical experiments, glyoxal was completely consumed after 40 minutes, as indicated by ESI-MS positive mode analysis (Appendix A2) and oxalic acid increased to a maximum concentration 40 – 70 minutes into the reaction. Peak oxalic acid concentrations were higher than reported previously [18]. We believe that is because large differences in the void volume between samples and standards in the previous analysis (conducted by HPLC-UV-Vis, not IC) altered the baseline near the oxalic acid peak.

The dilute aqueous chemistry model (Table 2-1) successfully reproduced oxalic acid time profiles in 30 μM experiments conducted without H_2SO_4 (Figure 2-2). Total organic carbon (TOC) analysis (Figure 2-3) shows that the model is capable of predicting the organic carbon content of the reaction vessel in 30 and 300 μM experiments. This

suggests that oxalic acid production from glyoxal can be predicted at cloud relevant concentrations without considering the formation of higher molecular weight products.

At higher concentrations (3000 μM), measured oxalic acid concentrations were lower and peaked later than the model predicted and expected organic carbon accounted for less than 60% of the measured TOC in 40 and 60 min samples. A similar observation has been made for glycoaldehyde and OH radical [23]. The ESI-MS negative mode spectrum of the 3000 μM glyoxal + OH radical products (20 min) is more complex and contains higher molecular weight compounds than the spectrum obtained 20 minutes into the 30 μM experiment (Figure 2-4). In the mass range from 50 to 500 amu, m/z^- 188, 271 and 279 were the median ions present in the 30, 300, and 3000 μM experiments, respectively. A total of 76, 161, and 204 ions were detected, respectively, in the 30, 300, and 3000 μM experiments. The negative mode spectrum of a mixed standard that included all expected products and precursors was quite simple, suggesting that the complexity seen in samples was not an artifact of the electrospray ionization process (Figure 2-4 insert; glyoxal, H_2O_2, glyoxylic acid, oxalic acid, formic acid, and glycolic acid, each at 200 μM; these products are 20-300 μM in 3000 μM glyoxal experiments at 20 min). This complexity was not seen in control experiments, indicating that the higher molecular weight products are only formed in the presence of OH radical. The larger number and complexity of higher molecular weight products with increasing precursor concentration could explain the gap between measured TOC and carbon in predicted products, and is consistent with the possibility that formation of higher molecular weight products/oligomers play an increasingly important role as concentrations increase. The formation of higher molecular weight products could explain the lower measured oxalic

acid concentrations and the slower production rate relative to predictions in the 3000 μM experiments. The trends exhibited in Figures 2-4 suggest that it will be necessary to account for the formation of higher molecular weight products in order to accurately predict oxalic acid formation (and aqueous-phase SOA formation) from glyoxal + OH radical in aerosol water, where glyoxal concentrations can be 3 orders of magnitude greater than those in our highest experiments.

2.4.4. Additional carboxylic acids and oligomer formation

IC chromatograms of 30 and 300 μM experiments are relatively simple, just showing organic acids predicted by the explicit dilute aqueous chemistry model. In contrast, several additional peaks not found in control experiments showed clear growth and decay in IC analysis of 3000 μM experiments (Appendix A3). Specifically, small peaks with the same retention time as malonic/tartaric acid and succinic/malic acid standards were observed. A peak with the retention time expected for mesoxalic acid was also found. Several small peaks that eluted after 30 minutes are consistent with the presence of tricarboxylic acids based on the separation mechanism of the column. Additionally, the presence of compounds with the exact elemental formulas as succinic acid (m/z^- 117.0193; $C_4H_5O_4^-$), malonic acid (m/z^- 103.0036; $C_3H_3O_4^-$), malic acid (m/z^- 133.01422; $C_4H_5O_5^-$), tartaric acid (149.00907; $C_4H_5O_6^-$), and mesoxalic acid (m/z^- 116.98294; $C_3H_1O_5^-$) in the FT-ICR mass spectra provides strong support for the formation of these compounds in 3000 μM experiments. These ions were not found in analyses of mixed standards or in control experiments. Figure 2-5 shows time profiles for malonic/tartaric acids (quantified as malonic acid) and succinic/malic acid (quantified as succinic acid). The relatively high concentrations of these compounds in 3000 μM

experiments suggest that compounds with more than two carbon atoms could be important products in glyoxal oxidation at the considerably higher concentrations observed in aerosol water. The carbon balance for 3000 μM experiments is improved by including malonic acid and succinic acid, but the carbon in the sum of quantified species is still ~25% less than measured TOC in 40 and 60 min samples (Figure 2-3).

Succinic acid is a key intermediate in the oligomer formation mechanism proposed for aqueous OH radical oxidation of methylglyoxal and glycoaldehyde [23, 27]. As previously reported for methylglyoxal [24], pyruvic acid [22] and glycolaldehyde [23], the mass spectra of 3000 μM glyoxal + OH radical samples exhibit a "haystack" pattern with mass differences of 12, 14 and 16 amu (Figure 2-4). Similar to methylglyoxal and glycolaldehyde, repeated addition of a subunit (s_1) with the elemental formula $C_3H_4O_2$ and molecular weight 72.0211 to organic acids was found (Table 2-2). These products did not form in the absence of OH radicals. The formation of oligoesters by repeated addition of s_1 was verified by MS-MS in methylglyoxal experiments [27]. Oligoesters might form through esterification (condensation) reactions or radical – radical reactions, suggesting that s_1 could be a radical or a compound with alcohol and acid functionalities. Unlike glyoxal oligomers formed through hemiacetal formation, we expect that oligomers from OH radical reactions will be irreversibly formed. In addition, in this work, the repeated addition of subunit with molecular formula $C_4H_4O_4$ (s_2) and $C_4H_4O_5$ (s_3) (molecular weight 116.0110 and 132.0058, respectively) to parent compounds could also be seen in the FT-ICR-MS analysis of 3000 μM glyoxal + OH radical samples (Table 2-2). For example, oxalic acid ($C_2H_2O_4$) was found to add 1 to 4 different or the same subunits, forming $C_2H_2O_4$-$C_3H_4O_2$, $C_2H_2O_4$-$(C_3H_4O_2)_2$, $C_2H_2O_4$-

$(C_3H_4O_2)_3$, etc. It should be noted that oligomeric products from these two subunits account for only a portion of the FT-ICR-MS signal. About 45% of the ion abundance in the 30 min sample is accounted for by the products listed in Table 2-2. The higher molecular weight carboxylic acids and oligomers identified by IC and/or FT-ICR-MS could partially account for the missing carbon in the 3000 μM experiment. This work suggests that product complexity and oligomer formation becomes increasingly important as precursor concentrations increase, from those typically seen in clouds to those typically seen in aerosol water.

This work provides insights pertaining to the aqueous OH radical oxidation of glyoxal at cloud and aerosol-relevant concentrations. At cloud relevant concentrations the Lim et al. [25] dilute aqueous chemistry model successfully predicts oxalic acid formation and total carbon. As precursor concentrations increase SOA prediction is complicated by the increasing formation of higher molecular weight products. Oxalic acid production decreases; peak oxalic acid concentrations occur later in the reaction sequence; higher molecular weight products, including >C2 organic acids and oligomers, form, and these products are also expected to contribute SOA. In wet aerosols were glyoxal reacts with species other than OH radical, glyoxal chemistry could be even more complex [28-31]. Thus, more research is needed to build a chemical model capable of accurately predicting SOA formation from glyoxal in wet aerosols. This work suggests acidic sulfate has only a small effect on oxalic acid production at cloud/fog relevant conditions; its effect on aqueous oligomers and organosulfur species formation was not explored nor was its effect at aerosol relevant concentrations. In some smog chamber experiments, reactive uptake of glyoxal seems to be enhanced by acidic sulfate [32-33].

This does not necessarily conflict with our findings because the sulfate and H^+ concentrations in wet aerosols are orders of magnitudes higher than in our experiments.

2.5 References

1. Kanakidou, M.; Seinfeld, J. H.; Pandis, S. N.; Barnes, I.; Dentener, F. J.; Facchini, M. C.; Van Dingenen, R.; Ervens, B.; Nenes, A.; Nielsen, C. J.; Swietlicki, E.; Putaud, J. P.; Balkanski, Y.; Fuzzi, S.; Horth, J.; Moortgat, G. K.; Winterhalter, R.; Myhre, C. E. L.; Tsigaridis, K.; Vignati, E.; Stephanou, E. G.; Wilson, J., Organic aerosol and global climate modelling: a review. *Atmos. Chem. Phys.* **2005,** *5*, 1053-1123.

2. Poschl, U., Atmospheric aerosols: Composition, transformation, climate and health effects. *Angew. Chem. Int. Ed.* **2005,** *44*, (46), 7520-7540.

3. Volkamer, R.; Jimenez, J. L.; San Martini, F.; Dzepina, K.; Zhang, Q.; Salcedo, D.; Molina, L. T.; Worsnop, D. R.; Molina, M. J., Secondary organic aerosol formation from anthropogenic air pollution: Rapid and higher than expected. *Geophys. Res. Lett.* **2006,** *33*, L17811, doi:10.1029/2006GL026899.

4. Heald, C. L.; Jacob, D. J.; Park, R. J.; Russell, L. M.; Huebert, B. J.; Seinfeld, J. H.; Liao, H.; Weber, R. J., A large organic aerosol source in the free troposphere missing from current models. *Geophys. Res. Lett.* **2005,** *32*, L18809, doi:10.1029/2005GL023831.

5. Chebbi, A.; Carlier, P., Carboxylic Acids in the Troposphere, Occurrence, Sources, and Sinks: a Review. *Atmos. Environ.* **1996,** *30*, (24), 4233-4249.

6. Heald, C. L.; Jacob, D. J.; Turquety, S.; Hudman, R. C.; Weber, R. J.; Sullivan, A. P.; Peltier, R. E.; Atlas, E. L.; de Gouw, J. A.; Warneke, C.; Holloway, J. S.; Neuman, J. A.; Flocke, F. M.; Seinfeld, J. H., Concentrations and sources of organic carbon aerosols in the free troposphere over North America. *J. Geophys. Res.* **2006,** *111*, D23s47, doi:10.1029/2006JD007705.

7. Sorooshian, A.; Lu, M.-L.; Brechtel, F. J.; Jonsson, H.; Feingold, G.; Flagan, R. C.; Seinfeld, J. H., On the Source of Organic Acid Aerosol Layers above Clouds. *Environ. Sci. Technol.* **2007,** *41*, (13), 4647-4654.

8. Sorooshian, A.; Ng, N. L.; Chan, A. W. H.; Feingold, G.; Flagan, R. C.; Seinfeld, J. H., Particulate organic acids and overall water-soluble aerosol composition measurements from the 2006 Gulf of Mexico Atmospheric Composition and Climate Study (GoMACCS). *J. Geophys. Res.* **2007,** *112*, D13201, doi:10.1029/2007JD008537.

9. Blando, J. D.; Turpin, B. J., Secondary organic aerosol formation in cloud and fog droplets: A literature evaluation of plausibility. *Atmos. Environ.* **2000,** *34*, 1623-1632.

10. Gelencser, A.; Varga, Z., Evaluation of the atmospheric significance of multiphase reactions in atmospheric secondary organic aerosol formation. *Atmos. Chem. Phys.* **2005,** *5*, 2823-2831.

11. Limbeck, A.; Puxbaum, H.; Otter, L.; Scholes, M. C., Semivolatile behavior of dicarboxylic acids and other polar organic species at a rural background site (Nylsvley, RSA) *Atmos. Environ.* **2001,** *35*, 1853-1862.

12. Fu, T.-M.; Jacob, D. J.; Wittrock, F.; Burrows, J. P.; Vrekoussis, M.; Henze, D. K., Global budgets of atmospheric glyoxal and methylglyoxal, and implications for formation of secondary organic aerosols. *J. Geophys. Res.* **2008,** *113*, D15303, doi:10.1029/2007JD009505.

13. Feierabend, K. J.; Zhu, L.; Talukdar, R. K.; Burkholder, J. B., Rate Coefficients for the OH + HC(O)C(O)H (Glyoxal) Reaction between 210 and 390 K. *J. Phys. Chem. A* **2008,** *112*, (1), 73-82.

14. Volkamer, R.; San Martini, F.; Molina, L. T.; Salcedo, D.; Jimenez, J. L.; Molina, M. J., A missing sink for gas-phase glyoxal in Mexico City: Formation of secondary organic aerosol. *Geophys. Res. Lett.* **2007,** *34*, L19807, doi:10.1029/2007GL030752.

15. Schweitzer, F.; L. Magi; P. Mirabel; George, C., Uptake rate measurements of methanesulfonic acid and glyoxal by aqueous droplets. *J. of Phys. Chem. A* **1998,** *102*, (3), 593-600.

16. Ip, H. S. S.; Huang, X. H. H.; Yu, J. Z., Effective Henry's law constants of glyoxal, glyoxylic acid, and glycolic acid. *Geophys. Res. Lett.* **2009,** *36*, L01802, doi:10.1029/2008GL036212.

17. Munger, J. W.; Jacob, D. J.; Daube, B. C.; Horowitz, L. W., Formaldehyde, glyoxal and methylglyoxal in air and cloudwater at a rural mountain site in central Virginia. *J. Geophys. Res.* **1995,** *100*, (D5), 9325-9333.

18. Carlton, A. G.; Turpin, B. J.; Altieri, K. E.; Seitzinger, S.; Reff, A.; Lim, H.-J.; Ervens, B., Atmospheric oxalic acid and SOA production from glyoxal: Results of aqueous photooxidation experiments. *Atmos. Environ.* **2007,** *41*, (35), 7588-7602.

19. Carlton, A. G.; Turpin, B. J.; Altieri, K. E.; Seitzinger, S. P.; Mathur, R.; Roselle, S. J.; Weber, R. J., CMAQ Model Performance Enhanced When In-Cloud Secondary Organic Aerosol is Included: Comparisons of Organic Carbon Predictions with Measurements. *Environ. Sci. Technol.* **2008,** *42*, (23), 8798-8802.

20. Jang, M.; Czoschke, N. M.; Lee, S.; Kamens, R. M., Heterogeneous atmospheric aerosol production by acid-catalyzed particle-phase reactions. *Science* **2002,** *298*, 814-817.

21. Iinuma, Y.; Müller, C.; Böge, O.; Gnauk, T.; Herrmann, H., The formation of organic sulfate esters in the limonene ozonolysis secondary organic aerosol (SOA) under acidic conditions. *Atmos. Environ.* **2007,** *41*, (27), 5571-5583.

22. Carlton, A. G.; Turpin, B. J.; Lim, H.-J.; Altieri, K. E.; Seitzinger, S., Link between isoprene and secondary organic aerosol (SOA): Pyruvic acid oxidation yields low volatility organic acids in clouds. *Geophys. Res. Lett.* **2006,** *33*, L06822, doi:10.1029/2005GL025374.

23. Perri, M. J.; Seitzinger, S.; Turpin, B. J., Secondary organic aerosol production from aqueous photooxidation of glycolaldehyde: Laboratory experiments. *Atmos. Environ.* **2009,** *43*, (8), 1487-1497.

24. Altieri, K. E.; Carlton, A. G.; Lim, H.-J.; Turpin, B. J.; Seitzinger, S. P., Evidence for Oligomer Formation in Clouds: Reactions of Isoprene Oxidation Products. *Environ. Sci. Technol.* **2006,** *40*, (16), 4956-4960.

25. Lim, H. J.; Carlton, A. G.; Turpin, B. J., Isoprene forms secondary organic aerosol through cloud processing: Model simulations. *Environ. Sci. Technol.* **2005,** *39*, 4441-4446.

26. Ervens, B.; Feingold, G.; Frost, G. J.; Kreidenweis, S. M., A modeling study of aqueous production of dicarboxylic acids: 1. Chemical pathways and speciated organic mass production. *J. Geophys. Res.* **2004,** *109*, D15205, doi:10.1029/2003JD004387.

27. Altieri, K. E.; Seitzinger, S. P.; Carlton, A. G.; Turpin, B. J.; Klein, G. C.; Marshall, A. G., Oligomers formed through in-cloud methylglyoxal reactions: Chemical composition, properties, and mechanisms investigated by ultra-high resolution FT-ICR mass spectrometry. *Atmos. Environ.* **2008,** *42*, (7), 1476-1490.

28. Noziere, B.; Dziedzic, P.; Cordova, A., Products and Kinetics of the Liquid-Phase Reaction of Glyoxal Catalyzed by Ammonium Ions (NH_4^+). *J. Phys. Chem. A* **2008,** *113*, (1), 231-237.

29. Shapiro, E. L.; Szprengiel, J.; Sareen, N.; Jen, C. N.; Giordano, M. R.; McNeill, V. F., Light-absorbing secondary organic material formed by glyoxal in aqueous aerosol mimics. *Atmos. Chem. Phys.* **2009,** *9*, (7), 2289-2300.

30. De Haan, D. O.; Tolbert, M. A.; Jimenez, J. L., Atmospheric condensed-phase reactions of glyoxal with methylamine. *Geophys. Res. Lett.* **2009,** *36*.

31. Galloway, M. M.; Chhabra, P. S.; Chan, A. W. H.; Surratt, J. D.; Flagan, R. C.; Seinfeld, J. H.; Keutsch, F. N., Glyoxal uptake on ammonium sulphate seed aerosol: reaction products and reversibility of uptake under dark and irradiated conditions. *Atmos. Chem. Phys.* **2009,** *9*, (10), 3331-3345.

32. Corrigan, A. L.; Hanley, S. W.; De Haan, D. O., Uptake of Glyoxal by Organic and Inorganic Aerosol. *Environ. Sci. Technol.* **2008,** *42*, (12), 4428-4433.

33. Liggio, J.; Li, S.-M.; McLaren, R., Heterogeneous Reactions of Glyoxal on Particulate Matter: Identification of Acetals and Sulfate Esters. *Environ. Sci. Technol.* **2005,** *39*, (6), 1532-1541.

34. Leitzke, A.; Reisz, E.; Flyunt, R.; von Sonntag, C., The reactions of ozone with cinnamic acids: formation and decay of 2-hydroxyperoxy-2-hydroxyacetic acid. *J. Chem. Soc., Perkin Trans. 2* **2001**, (5), 793 - 797.

Table 2-1. Aqueous reactions and rate constants in glyoxal + OH radical model. Reactions are taken from Lim et al. [25] and references therein except where footnoted. GLY = glyoxal, GLYAC = glyoxylic acid, OXLAC = oxalic acid, OH = OH radical. Dissociation rate constants (k_d, s^{-1}) are calculated from the equilibrium constant (K_{eq}, M) and association rate constants (k_a, M^{-1} s^{-1}) by $k_d = K_{eq} \times k_a$. [a], Hydrogen peroxide photolysis rate (k_1, s^{-1}) is estimated by fitting H_2O_2 loss in H_2O_2 + UV control experiments. [b], The reaction between oxalic acid and dissolved oxygen was removed from the initial mechanism as no reaction was observed in control experiments. [c], This reaction was measured by Leitzke et al. [34] and was not included by Lim et al.

Reaction	Rate constant (M^{-1} s^{-1})	Note
1 $H_2O_2 + h\nu \rightarrow 2OH$	1.1E-4 (s^{-1})	a
2 $OH + H_2O_2 \rightarrow HO_2 + H_2O$	2.7E+07	
3 $HO_2 + H_2O_2 \rightarrow OH + H_2O + O_2$	3.7	
4 $HO_2 + HO_2 \rightarrow H_2O_2 + O_2$	8.3E+05	
5 $OH + HO_2 \rightarrow H_2O + O_2$	7.1E+09	
6 $GLY + OH (+ O_2) \rightarrow GLYAC + HO_2$	1.1E+09	
7 $GLYAC + OH \rightarrow OXLAC + HO_2 + H_2O$	3.62E+08	
8 $GLYAC^- + OH \rightarrow OXLAC^- + HO_2 + H_2O$	2.9E+09	
9 $OXLAC + OH \rightarrow 2CO_2 + 2H_2O$	1.4E+06	b
10 $OXLAC^- + OH \rightarrow CO_2 + CO_2^- + H_2O$	4.7E+07	
11 $OXLAC^{2-} + OH \rightarrow CO_2 + CO_2^- + OH^-$	7.7E+06	
12 $H_2O \leftrightarrow H^+ + OH^-$	K_{eq} = 1.0E-14, k_a = 1.4E11	
13 $HO_2 \leftrightarrow H^+ + O_2^-$	K_{eq} = 1.6E-5, k_a = 5.0E10	
14 $GLYAC \leftrightarrow H^+ + GLYAC^-$	K_{eq} = 3.47E-4, k_a = 2.0E10	
15 $OXLAC \leftrightarrow H^+ + OXLAC^-$	K_{eq} = 5.67E-2, k_a = 5.0E10	
16 $OXLAC^- \leftrightarrow H^+ + OXLAC^{2-}$	K_{eq} = 5.42E-5, k_a = 5.0E10	
17 $CO_2^- + O_2 \rightarrow O_2^- + CO_2$	2.4E+09	
18 $GLYAC + H_2O_2 \rightarrow HCO_2H + CO_2 + H_2O$	0.3	c
19 $HCO_2H + OH \rightarrow CO_2 + HO_2 + H_2O$	1.0E+08	
20 $HCO_2^- + OH \rightarrow CO_2^- + H_2O$	2.4E+09	
21 $HCO_2H \leftrightarrow H^+ + HCO_2^-$	K_{eq} = 1.77E-4, k_a = 5.0E10	
22 $OH + O_2^- \rightarrow OH^- + O_2$	1E+10	
23 $HCO_3^- + OH \rightarrow CO_3^- + H_2O$	1E+07	
24 $CO_3^- + O_2^- \rightarrow CO_3^{2-} + O_2$	6.5E+08	
25 $CO_3^- + HCO_2^- \rightarrow HCO_3^- + CO_2^-$	1.5E+05	
26 $CO_3^- + H_2O_2 \rightarrow HCO_3^- + HO_2$	8E+05	
27 $CO_2 (+ H_2O) \leftrightarrow H^+ + HCO_3^-$	K_{eq} = 4.3E-7, k_a = 5.6E4	
28 $HCO_3^- \leftrightarrow H^+ + CO_3^{2-}$	K_{eq} = 4.69E-11, k_a = 5E10	

Table 2-2a. Oligomer series found by FT-ICR-MS negative ionization mode in a sample taken at 30 minutes reaction time (Experiment 13).

Parent acid	**Glyoxylic acid**		**Oxalic acid**		**Malonic acid**	
Subunit	Chemical Formula	m/z^-	Chemical Formula	m/z^-	Chemical Formula	m/z^-
	$C_2H_1O_3$	72.99297	$C_2H_1O_4$	88.98803	$C_3H_3O_4$	103.0037
s_1	$C_5H_5O_5$	145.0142	$C_5H_5O_6$	161.0091	$C_6H_7O_6$	175.0248
s_2	$C_6H_5O_7$	189.0041	$C_6H_5O_8$	204.9990	$C_7H_7O_8$	219.0146
s_3	$C_6H_5O_8$	204.9990	$C_6H_5O_9$	220.9939	$C_7H_7O_9$	235.0095
$2s_1$	$C_8H_9O_7$	217.0354	$C_8H_9O_8$	233.0303	$C_9H_{11}O_8$	247.046
s_1+s_2	$C_9H_9O_9$	261.0252	$C_9H_9O_{10}$	277.0201	$C_{10}H_{11}O_{10}$	291.0357
s_1+s_3	$C_9H_9O_{10}$	277.0201	$C_9H_9O_{11}$	293.0149	$C_{10}H_{11}O_{11}$	307.0305
$3s_1$	$C_{11}H_{13}O_9$	289.0564	$C_{11}H_{13}O_{10}$	305.0512		
$2s_2$	$C_{10}H_9O_{11}$	305.0149	$C_{10}H_9O_{12}$	321.0097	$C_{11}H_{11}O_{12}$	335.0254
s_2+s_3	$C_{10}H_9O_{12}$	321.0097	$C_{10}H_9O_{13}$	337.0049	$C_{11}H_{11}O_{13}$	351.0204
$2s_1+s_2$	$C_{12}H_{13}O_{11}$	333.0464	$C_{12}H_{13}O_{12}$	349.0412	$C_{13}H_{15}O_{12}$	363.0568
$2s_3$	$C_{10}H_9O_{13}$	337.0049	$C_{10}H_9O_{14}$	352.9997	$C_{11}H_{11}O_{14}$	367.0153
$2s_1+s_3$	$C_{12}H_{13}O_{12}$	349.0412	$C_{12}H_{13}O_{13}$	365.0360	$C_{13}H_{15}O_{13}$	379.0517
$4s_1$	$C_{14}H_{17}O_{11}$	361.0775	$C_{14}H_{17}O_{12}$	377.0724		
s_1+2s_2	$C_{13}H_{13}O_{13}$	377.0361	$C_{13}H_{13}O_{14}$	393.0310	$C_{14}H_{15}O_{14}$	407.0466
$s_1+s_2+s_3$	$C_{13}H_{13}O_{14}$	393.0310	$C_{13}H_{13}O_{15}$	409.026	$C_{14}H_{14}O_{15}$	423.0418
$3s_1+s_2$	$C_{15}H_{17}O_{13}$	405.0674	$C_{15}H_{17}O_{14}$	421.0624		
$2s_3+s_1$	$C_{13}H_{13}O_{15}$	409.026				
$3s_2$	$C_{14}H_{13}O_{15}$	421.0267				
$3s_1+s_3$	$C_{15}H_{17}O_{14}$	421.0624	$C_{15}H_{17}O_{15}$	437.0573		
$2s_1+2s_2$	$C_{16}H_{17}O_{15}$	449.0575				

Table 2-2b. Oligomer series found by FT-ICR-MS negative ionization mode in a sample taken at 30 minutes reaction time (Experiment 13). Products formed from parent acids are categorized by addition of subunits: s_1 denotes $C_3H_4O_2$, s_2 denotes $C_4H_4O_4$, and s_3 denotes $C_4H_4O_5$. All compounds are shown as anion with one negative charge via losing a proton during the ionization process. (Around 45% of the ion abundance in this sample is accounted for by products in this table.)

Parent acid	**Succinic acid**		**Malic acid**		**Tartaric acid**	
Subunit	Chemical Formula	m/z^-	Chemical Formula	m/z^-	Chemical Formula	m/z^-
	$C_4H_5O_4$	117.01929	$C_4H_5O_5$	133.01422	$C_4H_5O_6$	149.00907
s_1	$C_7H_9O_6$	189.04051	$C_7H_9O_7$	205.0354	$C_7H_9O_8$	221.03029
s_2	$C_8H_9O_8$	233.0303	$C_8H_9O_9$	249.0252	$C_8H_9O_{10}$	265.02011
s_3	$C_8H_9O_9$	249.0252	$C_8H_9O_{10}$	265.02011	$C_8H_9O_{11}$	281.01495
$2s_1$			$C_{10}H_{13}O_9$	277.05649	$C_{10}H_{13}O_{10}$	293.05128
s_1+s_2	$C_{11}H_{13}O_{10}$	305.05123	$C_{11}H_{13}O_{11}$	321.04609	$C_{11}H_{13}O_{12}$	337.04124
s_1+s_3	$C_{11}H_{13}O_{11}$	321.04609	$C_{11}H_{13}O_{12}$	337.04124	$C_{11}H_{13}O_{13}$	353.03607
$3s_1$			$C_{13}H_{17}O_{11}$	349.07748	$C_{13}H_{17}O_{12}$	365.07235
$2s_2$	$C_{12}H_{13}O_{12}$	349.0412	$C_{12}H_{13}O_{13}$	365.03604	$C_{12}H_{13}O_{14}$	381.03092
s_2+s_3	$C_{12}H_{13}O_{13}$	365.03604	$C_{12}H_{13}O_{14}$	381.03092	$C_{12}H_{13}O_{15}$	397.02577
$2s_1+s_2$	$C_{14}H_{17}O_{12}$	377.07244	$C_{14}H_{17}O_{13}$	393.06719	$C_{14}H_{17}O_{14}$	409.06211
$2s_3$	$C_{12}H_{13}O_{14}$	381.03092	$C_{12}H_{13}O_{15}$	397.02577		
$2s_1+s_3$	$C_{14}H_{17}O_{13}$	393.06719	$C_{14}H_{17}O_{14}$	409.06211	$C_{14}H_{17}O_{15}$	425.05733
$4s_1$						
s_1+2s_2	$C_{15}H_{17}O_{14}$	421.06241	$C_{15}H_{17}O_{15}$	437.05727		
$s_1+s_2+s_3$	$C_{15}H_{17}O_{15}$	437.05727				

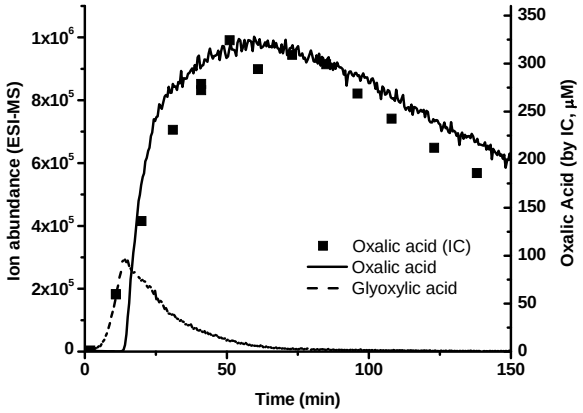

Figure 2-1. ESI-MS online analysis in negative scan mode of glyoxal (1 mM) + OH radical (5mM H_2O_2 + UV) experiment. Oxalic acid (m/z^- 89) and glyoxylic acid (m/z^- 73) are displayed in raw ion abundance from ESI-MS. Oxalic acid concentration quantified by IC is overlaid (squares).

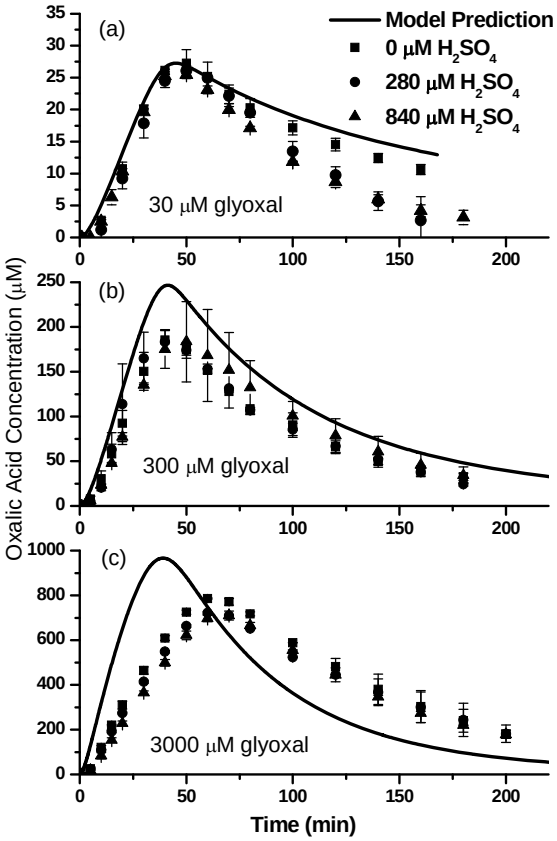

Figure 2-2. Oxalic acid time profiles from batch glyoxal ± H_2SO_4 + OH radical experiments and model predictions. Solid lines are modeled oxalic acid concentration and data points are quantified concentrations from IC analysis. H_2SO_4 concentration in μM is given in legend. Experimental oxalic acid yields are listed in Appendix A4.

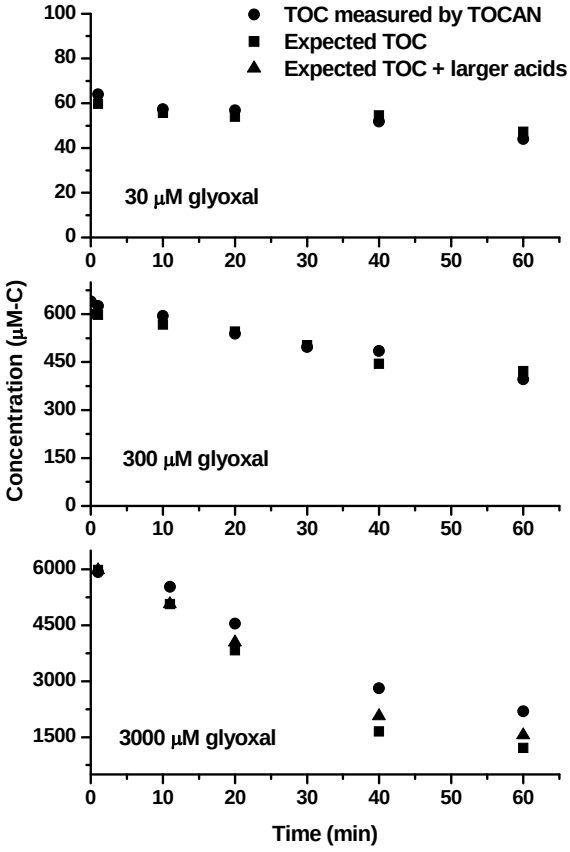

Figure 2-3. Measured total organic carbon (TOC) and reconstructed TOC. Circles are total TOC measured by the TOC-5000A analyzer. Reconstructed TOC is calculated by compound concentration × number of carbon in compound. Squares are the expected organic carbon (sum of carbon in oxalic acid measured by IC and modeled glyoxal and glyoxylic acid). Triangles indicate the sum of expected organic carbon and carbon from quantified malonic and succinic acids in 3000 μM experiments.

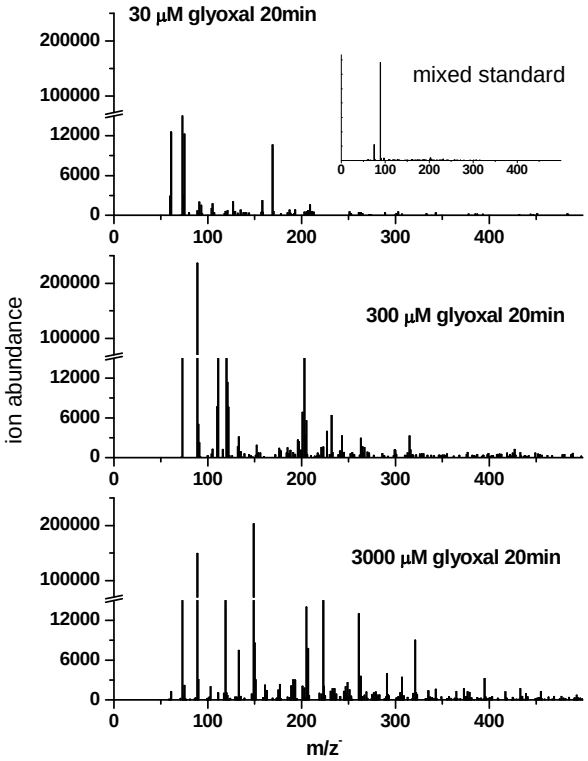

Figure 2-4. ESI-MS negative ionization mode spectra of samples taken from glyoxal + OH radical batch reactions (20 minutes reaction time). From top to bottom: 30 μM glyoxal + OH radical (0.15 mM H_2O_2 + UV), 300 μM glyoxal + OH radical (1.5 mM H_2O_2 + UV), and 3000 μM glyoxal + OH radical (15 mM H_2O_2 + UV). A mass spectrum of mixed standard is shown in the inset (hydrogen peroxide, glyoxal, formic acid, glycolic acid, glyoxylic acid, and oxalic acid each 200 μM, a similar concentration as observed for oxalic acid at 20 min, 3000 μM experiment).

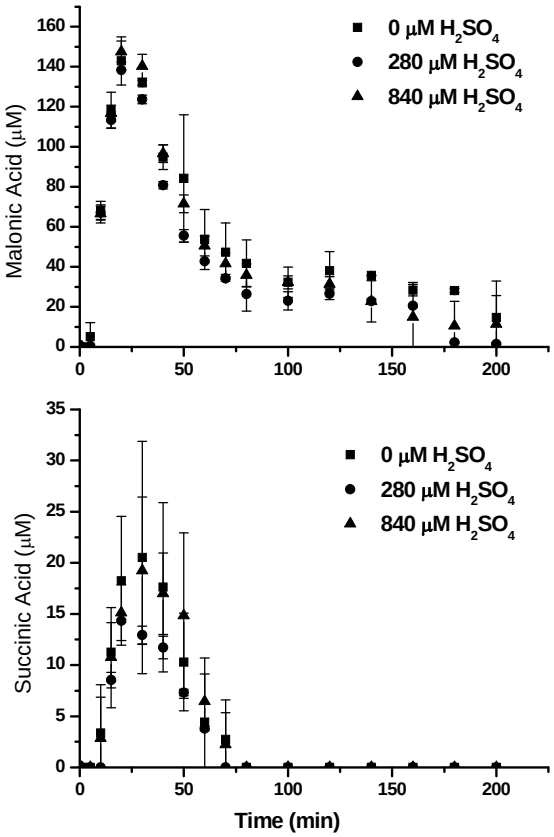

Figure 2-5. Malonic/tartaric acid and succinic/malic acid in 3000 μM glyoxal + OH radical experiments with and without H_2SO_4. Note malonic acid coelutes with tartaric acid and succinic acid coelutes with malic acid. Peaks were quantified based on malonic acid and succinic acid standards.

Chapter 3. SOA from Methylglyoxal in Clouds and Wet Aerosols: Measurement and Prediction of Key Products

Material in this chapter has been published previously as:

Tan, Y.; Carlton, A. G.; Seitzinger, S. P.; Turpin, B. J., SOA from Methylglyoxal in Clouds and Wet Aerosols: Measurement and Prediction of Key Products. *Atmospheric Environment In Press, Accepted Manuscript*.

3.1 Abstract

Aqueous OH radical oxidation of methylglyoxal in clouds and wet aerosols is a potentially important global and regional source of secondary organic aerosol (SOA). We quantify organic acid products of the aqueous reaction of methylglyoxal (30 – 3000 μM) and OH radical (approx. 4×10^{-12} M), model their formation in the reaction vessel and investigate how the starting concentrations of precursors and the presence of acidic sulfate (0 – 840 μM) affect product formation. Predicted products were observed. The predicted temporal evolution of oxalic acid, pyruvic acid and total organic carbon matched observations at cloud relevant concentrations (30 μM), validating this methylglyoxal cloud chemistry, which is currently being implemented in some atmospheric models of SOA formation. The addition of sulfuric acid at cloud relevant concentrations had little effect on oxalic acid yields. At higher concentrations (3000 μM), predictions deviate from observations. Larger carboxylic acids ($\geq C_4$) and other high molecular weight products become increasingly important as concentration increases, suggesting that small carboxylic acids are the major products in clouds while larger carboxylic acids and oligomers are important products in wet aerosols.

3.2 Introduction

Fog and cloud processing, a major source of atmospheric sulfate, has been hypothesized to be a substantial source of secondary organic aerosol (SOA) [1-3]. Observations provide support for in-cloud SOA production [4-7]. Modeling studies estimate that SOA formed through aqueous reactions in clouds and wet aerosols is comparable in magnitude to "traditional SOA" [8-11]. However, the uncertainties in these estimates are quite large, in part because the aqueous chemical mechanisms are largely unvalidated.

Methylglyoxal is a common α-dicarbonyl formed in atmospheric oxidation of both biogenic and anthropogenic precursors, including isoprene, acetone, and xylenes (Fu et al., 2008 and reference therein). Methylglyoxal has a global source of 140 Tg a^{-1} [8]. UV photolysis and reaction with hydroxyl radical are the main gas phase loss processes for methylglyoxal [12] and yield carbon monoxide, acetaldehyde, and formaldehyde. Methylglyoxal enters droplets readily due to its high effective Henry's law constant (H_{eff} = 3.71×10^3 M atm^{-1} at 25°C) and fast uptake rate [13-14]. Reactive uptake of methylglyoxal on sulfuric acid (55 – 85 wt%) has an effective Henry's law constant of 4.0×10^3 – 5.9×10^3 M atm^{-1} at 10°C, decreasing with increasing acidity [15]. Typical aqueous methylglyoxal concentrations vary from a few μM in rain water to >100 μM in fog water [16]. Methylglyoxal could reach very high concentrations in aerosol water (0.7 – 7 mM [17]) and during cloud evaporation. Aqueous methylglyoxal oxidation leads to the formation of oxalic acid and high molecular weight products [18-20]. When this chemistry takes place in clouds and fogs followed by droplet evaporation (or if this chemistry occurs in aerosol water) then the lower volatility products will remain in part in the particle phase, forming SOA. In addition, evaporation of droplets containing

methylglyoxal induces formation of methylglyoxal oligomers, which could contribute to SOA [21-22].

Several laboratory studies provide insights into the aqueous OH radical chemistry of methylglyoxal, illustrated in part by Fig. 3-1. In the aqueous phase, methylglyoxal hydrates [23]. Rate constants for reaction between OH radical and methylglyoxal have been measured [24-25]. The aqueous OH radical oxidation product of methylglyoxal is pyruvic acid [26]. Acetic, formic, glyoxylic, and oxalic acids were measured in aqueous pyruvic acid (5 – 10 mM) plus OH radical oxidation experiments [18-19]. These experiments verified that glyoxylic and oxalic acids formed from the OH radical oxidation of pyruvic acid (they did not form in control experiments), whereas acetic and formic acids could have been formed via OH radical and/or H_2O_2 oxidation. Formation of methylglyoxal, pyruvic and oxalic acids from methacrolein (0.4 – 5 mM) has also been documented [27]. Ambient measurements suggest that a majority of pyruvate, oxalate, and glyoxylate exist in the particle phase under typical atmospheric conditions [28]. Formation of additional carboxylic acids (i.e., glycolic, succinic and hydracrylic acids) and oligomers from aqueous methylglyoxal (2 mM) photooxidation has also been reported [20]. Moreover, oligomer production has been observed in OH radical oxidation, O_3 oxidation and direct photolysis of pyruvic acid (5 – 100 mM) [18, 29-30]. Methylglyoxal also interacts with inorganic aerosol constituents (e.g., sulfate, nitrate), forming oligomers via acetal/hemiacetal and aldol condensation in aqueous aerosol mimics (16 mM – 2.0 M methylglyoxal [17]) and simulated cloud water (1 mM methylglyoxal [31]). The formation of low volatility acids and oligomers from methylglyoxal suggests that aqueous methylglyoxal chemistry is a source of SOA.

However, none of these experiments were performed at cloud-relevant concentrations (1 - 100 μM).

This paper provides the first measurements of the products of aqueous OH radical oxidation of methylglyoxal at cloud relevant concentrations and the first quantitative validation of dilute aqueous chemistry model predictions against measured product concentrations. The effect of sulfuric acid on cloud processing of methylglyoxal is also reported. Batch aqueous methylglyoxal + OH radical oxidation experiments were performed at three concentrations. Products were measured by on-line (real-time) mass spectroscopy and by ion chromatography-mass spectrometry. The 30 μM experiments are cloud relevant; 300 μM experiments could represent some heavily polluted fogs, and 3000 μM experiments shed light on chemistry in aerosol water. (Methylglyoxal concentrations in aerosols are ~mM, whereas total organic concentrations in aerosol water are considerably higher.) Examination of the chemistry with increasing precursor concentration provides insights into differences between the aqueous photochemistry of dicarbonyls in clouds and in aerosol water.

3.3 Approach

3.3.1 Experiments with Real-Time ESI-MS

Electrospray ionization mass spectrometry (ESI-MS; HP-Agilent 1100) does not fragment ions. Carboxylic acids are detected in the negative ionization mode as molecular weight minus one. Aldehydes and alcohols are detected in the positive mode.

Experiments with real-time ESI-MS (online experiments, Fig. 3-2a,b) were performed as previously described [32-33]. Solution and mobile phase (40% of 0.05% formic acid in water and 60% methanol) were both continuously delivered from the

reaction vessel into the ESI-MS at 0.11 mL/min. Experiments were analyzed in negative or positive ionization mode from 50 – 1000 amu with a fragmentor voltage of 40 V and capillary voltage of 3000 V. Nitrogen was the drying gas (10 L/min, 350 °C). Discrete samples were taken for ion chromatography and total organic carbon analysis.

3.3.2 Batch Reactions

Batch aqueous reactions of methylglyoxal (30, 300, 3000 μM) and OH radical (~4 × 10^{-12} M, estimated) with and without sulfuric acid were conducted in a 1 L glass reaction vessel at 25 ± 2°C, as described previously [18, 33]. Experimental conditions are provided in Appendix B1. OH radicals were continuously generated by the photolysis of H_2O_2 by UV (254 nm) light from a monochromatic mercury lamp (Heraeus Noblelight, Inc. Duluth, GA). The pH varied from 6.7 to 2.1, decreasing with increasing H_2SO_4 and increasing reaction time. At least two experiments were conducted for each of the nine treatment combinations. Reaction samples and duplicates (10% of samples) were analyzed within 12 hours of collection for organic acids by ion chromatography (IC; ICS-3000, Dionex, Sunnyvale, CA; IonPac AS11-HC column with AG11-HC guard column, 30˚C), as described in detail by Tan et al. (2009). Pyruvic, acetic, formic, glyoxylic, glycolic, malonic, succinic and oxalic acids were identified and quantified with mixed standards and Chromeleon software (version 6.80 SP2, Dionex). Single standards of mesoxalate (prepared from sodium mesoxalate monohydrate, 98.7%, Sigma-Aldrich) were run separately. Selected samples and control samples were also analyzed by ESI-MS after preseparation in the IC (IC-ESI-MS), as shown in Fig. 3-3 and discussed in detail below. The conductivity detector effluent (0.4 mL/min) was directed into the ESI-MS which was operated as described above. Total organic carbon analysis was performed

on batch reaction samples as described previously [32] using a Shimadzu TOC-5000A Total Carbon Analyzer (TOCAN).

3.3.3 Control Experiments

The following control experiments were also conducted: methylglyoxal + UV, methylglyoxal + H_2O_2 + H_2SO_4, H_2O_2 ± H_2SO_4 + UV, and mixed standard + H_2O_2. The mixed standard contained pyruvic, acetic, formic, glyoxylic, glycolic, succinic, malonic, and oxalic acids. The interactions between UV and carboxylic acids were also investigated. Note that 254 nm UV light was used in these experiments to photolyze H_2O_2 and form OH radical. The control experiments are not intended to simulate photolysis in the atmosphere. Small amounts of pyruvic, acetic and formic acids formed in the methylglyoxal + H_2O_2 and methylglyoxal + UV control experiments, but dicarboxylic acids did not form in either control experiment.

Some higher molecular weight compounds were found in the methylglyoxal + UV (Appendix B5, B6) and methylglyoxal + H_2O_2 control samples (Appendix B7, B8). These spectra were distinctly different from the spectra of methylglyoxal + OH radical experiment samples (Fig. 3-3, 3-4).

Pure water was also sampled from the reaction vessel and analyzed like samples. Hydrogen peroxide in organic control experiments (H_2O_2 ± H_2SO_4 + UV) was quantified using the triiodide method and a UV-visible spectrometer [34].

Acetic, glycolic, succinic, malonic, and oxalic acids did not degrade either in presence of H_2O_2 alone or with UV irradiation only. Photolysis of pyruvic acid was observed in agreement with previous studies [18, 29-30]. Photolysis of mesoxalic acid produced glyoxylic acid. As discussed in Section 2.5, H_2O_2 is the principle absorber of

light in these experiments; in the presence of H_2O_2, methylglyoxal, pyruvic acid, and mesoxalic acid photolysis is negligible. Glyoxylic acid plus H_2O_2 formed formic acid, pyruvic acid with H_2O_2 formed acetic acid, and mesoxalic acid with H_2O_2 formed oxalic acid. Quality control measurements for organic acids in IC analysis are presented in Supplemental Information (Appendix B2, B7). Reactions of acids with H_2O_2 are slow compared to corresponding free radical reactions, thus dark reactions have little impact on concentrations in the reaction vessel and online experiments. Good agreement between online ESI-MS signals and IC measurements in collected samples and good agreement between duplicate samples analyzed immediately and after 7 hours suggest that H_2O_2 reactions in samples awaiting IC analysis have little effect on measured concentrations with the exception of glyoxylic and formic acids (Fig. 3-2b, Appendix B3, B9, B10).

3.3.4 IC-ESI-MS analysis

A new feature of this paper is the application of IC-ESI-MS to the analysis of reaction products. IC separation before ESI-MS helps ensure that detected products were not formed during electrospray ionization. The IC-ESI-MS negative mode spectra of the mixed standard are shown in Fig. 3-3a. The mixed standard contained glycolic acid (peak A, 5.1 min, m/z^- 75), acetic acid (peak A, 5.1 min, not detectable by ESI-MS), formic acid (peak B, 5.7 min, not detectable by ESI-MS), pyruvic acid (peak C, 6.4 min, m/z^- 87), glyoxylic acid (peak D, 8.2 min, m/z^- 73), succinic acid (peak E, 18.0 min, m/z^- 117), malonic acid (peak F, 19.1 min, m/z^- 103), and oxalic acid (peak I, 22.1 min, m/z^- 89). Some additional peaks can be seen in the ion chromatogram (G, H, and K) and in the mass spectra (e.g. peak B, m/z^- 75 and 141). In some cases these could be due to

incomplete compound separation by IC (e.g., m/z^- 75 is likely to be glycolic acid from the tail of peak A). In other cases they could be contaminants, products formed in the mixed standard, or dimers formed during electrospray ionization of compounds with the same IC retention time.

3.3.5 Kinetic modeling

Aqueous methylglyoxal oxidation was modeled using the dilute cloud chemistry provided in Table 3-1 and the differential solver, FACSIMILE (AEA technology, Oxfordshire, UK). The H_2O_2 photolysis rate (k_1 = (1.1±0.3) × 10^{-4} s^{-1}) was fitted by simulating the H_2O_2 concentration in H_2O_2 (15 mM) ± H_2SO_4 (280 μM) + UV control experiments. Identical control experiments conducted at 0.15, 1.5 and 20 mM H_2O_2 demonstrated that k_1 was independent of concentration. At λ = 254 nm, the molar absorption coefficients for H_2O_2 and methylglyoxal are 18.4 M^{-1} cm^{-1} and 12.7 M^{-1} cm^{-1}, respectively. Since the total absorbance of 3000 μM methylglyoxal + 15 mM H_2O_2 is less than that of 20 mM H_2O_2, we conclude that photon limiting conditions did not occur in experiments. As done in similar situations by others [26, 35-36], we neglected photolysis of methylglyoxal and pyruvic acid in kinetic modeling because it is 5 times slower than OH radical oxidation (e.g., photolysis rate of methylglyoxal is ~6 x 10^{-4} s^{-1} in UV control experiment). The average OH radical concentration during methylglyoxal + OH radical experiments, estimated using the chemistry of Table 3-1, was ~ 4 × 10^{-12} M (Appendix B11).

3.4 Results and Discussion

3.4.1 Chemical Mechanism at Cloud Relevant Concentrations

Online ESI-MS analysis of the aqueous OH radical oxidation of 30 μM methylglyoxal (Fig. 3-2a, 3-2b) is consistent with the mechanism used for kinetic modeling (Table 3-1, Fig. 3-1, Fig. 3-2c). The ion abundance of m/z^+ 131 decayed rapidly after the experiment started and matches the model prediction for methylglyoxal (m/z^+ 131) loss by OH very well for the first 10 minutes (Fig. 3-2a). A shoulder in the m/z^+ 131 ion abundance is evident at ~10 minutes, suggesting that at this point a product also contributes to this unit mass-to-charge ratio. Modeled and measured pyruvic acid and m/z^- 87 increased dramatically as methylglyoxal decayed, consistent with the expectation that pyruvic acid is the first generation product (Fig. 3-2b). Pyruvic acid formation was further verified by IC-ESI-MS (peak C, m/z^- 87, Fig. 3-3b). Acetic acid, the expected oxidation product of pyruvic acid, cannot be ionized or detected by ESI-MS and co-elutes with glycolic acid in the IC. Nevertheless, a peak with the same retention time as the acetic acid standard was observed in the IC (peak A, Fig. 3-3b). Carlton et al. (2006) previously reported that pyruvic acid is oxidized to acetic acid. Since acetic acid formed in OH radical experiments and in pyruvic acid + H_2O_2 control experiments, the evidence for acetic acid formation from OH radical oxidation is less definitive (Appendix B12). The growth of m/z^- 73 in the on-line ESI-MS analyses of methyglyoxal + OH radical experiments but not control experiments is consistent with the formation of glyoxylic acid from acetic acid, as shown previously by Stefan and Bolton (1999). As mentioned above, glyoxylic acid can be seen in the on-line experiment, but cannot be seen in collected samples because of dark reaction with H_2O_2 between sample collection and analysis, despite same day analysis.

Evidence for oxalic acid formation (m/z^- 89) in the presence but not in the absence of OH radical is quite strong. As glyoxylic acid decayed, the oxalic acid concentration measured by IC and the modeled concentration matched the temporal evolution of m/z^- 89 in the on-line experiment (ESI-MS; Fig. 3-2b). Moreover, the formation of oxalic acid was further verified by IC-ESI-MS (peak I, m/z^- 89, Fig. 3-3b). Oxalic acid was the only product with an IC retention time of 22.1 min, providing additional confidence in the quantitation of oxalic acid by IC.

Mesoxalic acid ($C_2H_2O_5$, peak J, m/z^- 117, Fig. 3-3b) was the most prominent unpredicted product in 30 μM experiments. Mesoxalic acid formation from pyruvic acid was proposed by [37] and its decarboxylation by OH radical is expected to produce oxalic acid with a molar yield of 1. Time profiles of mesoxalic acid are presented in Appendix B13.

3.4.2 Model Performance at Cloud Relevant Concentrations

Oxalic acid (Fig. 3-5), pyruvic acid (Appendix B14) and total organic carbon (TOC, Fig. 3-6) time profiles were reproduced by the simple dilute aqueous chemistry model (Table 3-1) when the experiment was conducted at a cloud relevant (30 μM) methylglyoxal concentration (χ^2 goodness of fit test, 5% significance level), despite the fact that the photolysis of reactants and the formation of mesoxalic acid were not included in model. Ten minutes into the reaction, a time representative of one cloud cycle, the mass of pyruvic acid per mass of methylglyoxal reacted (mass yield) was 108% for conditions in the reaction vessel (average OH radical and H_2O_2 concentrations were ~ 4×10^{-12} M and 50 μM during experiments, respectively). At this time oxalic acid mass yield was 7%. At the peak oxalic acid concentration (210 minutes) the mass yield was

35%. Note that formation of oxalic acid continues long after methylglyoxal is depleted. In the case of methylglyoxal, yields are sensitive to OH radical concentrations and much less sensitive to H_2O_2 concentrations as shown in Appendix B4. In the atmosphere, production of methylglyoxal in the interstitial spaces of clouds could provide a continuous source of precursor, and a variety of additional reactions could occur during droplet evaporation and in the resulting wet particle. Estimates of daytime OH radical concentrations in cloud droplets vary over two orders of magnitude as a result of different assumptions [38-40]. Jacob (1986) suggested that OH radicals are poorly mixed within droplets and that surface concentrations (~ 2×10^{-12} M) are much higher than bulk concentrations (~ 2×10^{-13} M). Warneck (1999) predicted steady state aqueous OH radical concentrations of $3 - 5 \times 10^{-14}$ M in a box model of a sunlit small cumulus cloud. Monod and Carlier (1999) predicted an aqueous OH radical concentration of ~ $10^{-13} - 10^{-12}$ M one hour after cloud onset. Hydrogen peroxide concentrations in cloud water of < 1 μM to over 200 μM have been measured in field studies [41-43]. Thus, while, reaction vessel conditions are reasonably representative of atmospheric conditions, it is preferable to use the aqueous chemistry rather than product yields in atmospheric models. An important finding of this paper is that the dilute aqueous chemistry model works well at cloud relevant conditions and is appropriate for use in chemical transport models.

3.4.3 Effect of Sulfuric Acid Addition

The addition of sulfuric acid had little effect on the production of pyruvic and oxalic acids from methylglyoxal (Fig. 3-5 and Appendix B14). The average pH of clouds, fog and rainwater measured in southern California varied from 2.9 to 4.9, and the average sulfate concentration varied from 9.4 to 475 μM [44]. Therefore, the pH and sulfuric acid

concentrations in these batch experiments are representative of those in cloud and fog water. While differences in oxalic acid concentrations with and without sulfuric acid were statistically significant (t-test at 95% confidence level) from 120 – 210 minutes in 3000 μM experiments and after 210 minutes in 30 μM experiments, differences were modest. Formation of organosulfur compounds is possible but is beyond the scope of this work.

3.4.4 Mechanism and Model Performance at Higher Concentrations

On-line ESI-MS (Appendix B9) and IC-ESI-MS spectra of samples (Fig. 3-3c, 3-3d) provide strong evidence for pyruvic and oxalic acid formation in 300 and 3000 μM experiments. Again, a peak with the IC retention time of acetic acid is also seen, consistent with the modeled mechanism. The 300 μM IC-ESI mass spectra (Fig. 3-3c) are only slightly different from the 30 μM spectra (Fig. 3-3b), whereas additional products were evident in the 3000 μM spectra (Fig. 3-3d). In all experiments but not controls (Appendix B5 and Appendix B7) m/z^- 89 was the predominant ion in peak I, confirming that oxalic acid forms from the aqueous OH radical oxidation of methylglyoxal.

The kinetic model does not capture oxalic acid production very well in 300 and 3000 μM experiments (Fig. 3-5). The maximum oxalic acid concentration is underestimated by ~40% in 300 μM experiments, while it is overestimated by ~40% in 3000 μM experiments. In addition, oxalic acid production was much slower than predicted in the 3000 μM experiments. The model reproduces TOC in 300 μM experiments up to 60 minutes into reaction, and slightly underestimates TOC at longer times (Fig. 3-6). In 3000 μM experiments, predicted TOC agrees with measurements late in the reaction (after ~130 min), but the model underestimates TOC from 30 to 120

minutes. Reconstructed TOC was only 63% of measured TOC at 60 minutes. The disagreements between the model and measurements suggests that there are pathways missing from the model that become important at higher concentrations.

3.4.5 Formation of Glycolic and Succinic Acids at Higher Concentrations

The discrepancy between model predictions and observations in 3000 μM experiments must be explained by products not included in the dilute aqueous chemistry model. Increasing methylglyoxal concentrations resulted in increasing complexity of products (Fig. 3-4), as seen previously for glyoxal [33]. In higher concentration experiments, many prominent ions in the ESI-MS and IC-ESI-MS samples were not predicted by the chemical mechanism or found in the mixed standard, or formed in the control experiments.

Glycolic and succinic acids were not included in the dilute aqueous chemistry model. However, glycolic acid (m/z^- 75) is proposed to form from OH radical oxidation of acetic acid [26], and m/z^- 75 (unit mass) was measured by ESI-MS in 2 mM methylglyoxal + OH radical experiments [20]. The formation of a product with the same IC retention time and unit mass as glycolic acid in the IC-ESI-MS spectra of 300 and 3000 μM experiment samples (180 min sample, peak A, m/z^- 75, Fig. 3-3c, 3-3d) but not in controls (Appendix B5, B7) provides strong evidence that glycolic acid does form, at least in the higher concentration experiments. Glycolic acid was not seen in the 180 minute 30 μM IC-ESI-MS sample, although m/z^- 75 formation could be seen in the 30 μM online experiment (Fig. 3-2b). A possible explanation is that glycolic acid formation was minimal at 30 μM and this compound was largely depleted 180 minutes into the reaction.

The formation of succinic acid (C_4, m/z^- 117) from γ-radiolysis of acetic acid (C_2) solution (2mM) was previously reported [45]. Likewise, the formation of m/z^- 117 from OH radical oxidation of methylglyoxal (1 mM), which is consistent with the formation of succinic acid, has been previously demonstrated [20]. Note that succinic acid has a larger carbon number (C_4) than the precursor, methylglyoxal (C_3). In this work we verified by IC-ESI-MS that succinic acid did in fact form from methylglyoxal + OH radical in 3000 μM experiments. Specifically, peak E in Fig. 3-3d has the retention time of succinic acid and this peak contains a high absolute abundance of m/z^- 117 ($> 6 \times 10^4$). However, it should be noted that the ion abundance of m/z^- 177 in peak E was even more substantial. Peak E is clearly a mixture of succinic acid (m/z^- 117) and another carboxylic acid (m/z^- 177) with the same retention time. These compounds were not found in 30 and 300 μM experiments. The evidence for succinic acid is more definitive in this study than in the work by Altieri et al. (2008), because mesoxalic acid, which was also detected as m/z^- 117 in ESI-MS, was separated by IC. Malonic acid (m/z^- 103) is a major product of OH radical oxidation of succinic acid [37]. In 3000 μM experiments, malonic acid was the most abundant compound (abundance $> 1.2 \times 10^5$) in peak F (Fig. 3-3d); other acids (m/z^- 133 and 177) contribute to peak F as well.

Peaks E and F were quantified based on malonic and succinic acid standards for demonstration purposes (Fig. 3-7). The concentration of organic acids in peak E (succinic acid + m/z^- 177) increased rapidly after experiments began and reached around 300 μM within 60 minutes. Because of their fast production rate, the production of peak E acids could explain the suppression of oxalic acid production observed in the 3000 μM experiments (Fig. 3-5). The concentration of organic acids in peak F (malonic acid + m/z^-

133 and 177) did not increase until compounds in peak E started to decay, and the concentration of these acids remained relatively constant (around 160 μM) after 180 minutes. We speculate that the production of peak F acids might help to explain the modest underestimation of oxalic acid by the model late in the 3000 μM experiments (Fig. 3-5).

3.4.6 Oligomers and Other Higher Molecular Weight Products

A number of products with larger carbon numbers than the precursor, methylglyoxal, were identified by IC-ESI-MS in the 3000 μM experiments (Fig. 3-3d). For example, the peak labeled "unknown 2" in Fig. 3-3d (IC retention time of 16.7 min) was dominated by m/z^- 177. This peak was not seen in control experiments or in the mixed standard, and its temporal behavior suggests that it is a reaction product. In fact, peaks E, F and H also include organic acids with a unit mass (m/z^-) of 177. We conclude based on the IC column properties (Tan et al., 2009) that the OH radical oxidation of methylglyoxal (3000 μM) produces several structurally different dicarboxylic acids with a unit mass (m/z^-) of 177. Note that Altieri et al. (2008) also observed the formation of m/z^- 177 from (2 mM) methylglyoxal + OH radical. Because carboxylic acids with ≤ 3 carbons are unlikely to have such a high unit mass, we suspect that these diacid products have higher carbon numbers than methylglyoxal (> C_3). Also interesting are several small peaks with retention times of 28 - 30 minutes, labeled "unknown 3" in Fig. 3-3d. The most abundant ions are m/z^- 221, 235, 249 and 263. Minor ions differing ±2 amu from major species (e.g. m/z^- 219, 233, 247, 251 and 265) were also detected. Many compounds that eluted in this peak (unknown 3) were identified previously as oligomers

by ultra-high resolution mass spectroscopy of samples from 2 mM methylglyoxal + OH radical experiments [20].

Nine series of oligomers with differences of $C_3H_4O_2$ between compounds within a series were identified previously [20]. ESI-MS analyses of samples (Fig. 3-4), but not control samples (Appendix B6, B8) contain unit mass ions corresponding to all compounds in the Altieri et al. oligomer series. Formation of oligomers does not explain the discrepancy between measured and modeled oxalic acid early in the 3000 μM experiments because oligomers seem to be more important at later reaction times. The acids eluding in Peak E (succinic acid and m/z^- 177) are the best candidates for that. Formation of oligomers and other high molecular weight products appears to increase with increasing methylglyoxal concentration. This suggests that, while oligomers do not account for a large portion of the product mass at cloud-relevant concentrations, they might be substantial products at the high organic concentrations found in wet aerosols.

3.5 Conclusions and Atmospheric Implications

This work confirms that low volatility products (oxalic acid and higher carbon number products) form from the aqueous phase OH radical oxidation of methylglyoxal at cloud-relevant concentrations, as has been previously confirmed for glyoxal [33]. In addition, we show that the dilute aqueous chemistry model for methylglyoxal + OH radical (Table 3-1) provides accurate pyruvic acid, oxalic acid, and TOC predictions at cloud relevant concentrations. Thus, this body of work shows strong laboratory-based evidence suggesting that SOA will form from cloud processing of glyoxal and methylglyoxal and provides validated chemistry for use in larger-scale modeling.

Incorporation of aqueous chemistry into chemical transport models is needed to evaluate the magnitude of this process regionally and globally.

The model of Table 3-1 does not adequately represent the aqueous chemistry leading to SOA formation in wet aerosols. At higher methylglyoxal concentrations compounds with carbon numbers higher than methylglyoxal (> C_3) form, such as succinic acid and oligomers. This chemistry is not included in the model. Altieri et al. (2008) concluded based on MS-MS of several oligomeric products of methylglyoxal + OH radical that these products are oligoesters. They proposed that these oligoesters form from repeated addition of hydroxy acids to parent diacids via condensation reactions. In this scheme, hydroxy acids are formed from the oxidation of succinic acid. Interestingly, these oligoesters formed only in the presence of OH radical and did not form in the mixed standard when lactic acid was added but OH radical was not. The IC-ESI-MS analyses of this work confirm that succinic acid does in fact form from methylglyoxal + OH radical in 3000 μM experiments. Another possible explanation for the production of higher carbon number (> C_3) products is radical-radical chemistry. Guzman et al. (2006) showed that the recombination of organic radicals could produce C_6 and C_7 carboxylic acids in the aqueous photolysis of oxygen-saturated pyruvic acid solutions (5 – 100 mM). A radical-radical mechanism has been proposed to explain the aqueous formation of organosulfates [46], and has been proposed for the formation of higher carbon number products from glyoxal + OH radical [47], and oligomers from aqueous photooxidation of phenols [48]. Note that methylglyoxal oligomers have been observed to form in concentrated aqueous solutions in the dark via acetal/hemiacetal formation and aldol condensation (Sareen et al., 2010; Yasmeen et al., 2010). While this aerosol-phase

chemistry might be important at night, these reactions are slow relative to radical-radical reactions and produce oligomers that are structurally different than observed in our experiment.

3.6 References

1. Gelencser, A.; Varga, Z., Evaluation of the atmospheric significance of multiphase reactions in atmospheric secondary organic aerosol formation. *Atmospheric Chemistry and Physics* **2005,** *5*, 2823-2831.

2. Blando, J. D.; Turpin, B. J., Secondary organic aerosol formation in cloud and fog droplets: A literature evaluation of plausibility. *Atmospheric Environment* **2000,** *34*, 1623-1632.

3. Carlton, A. G.; Wiedinmyer, C.; Kroll, J. H., A review of Secondary Organic Aerosol (SOA) formation from isoprene. *Atmospheric Chemistry and Physics* **2009,** *9*, (14), 4987-5005.

4. Sorooshian, A.; Ng, N. L.; Chan, A. W. H.; Feingold, G.; Flagan, R. C.; Seinfeld, J. H., Particulate organic acids and overall water-soluble aerosol composition measurements from the 2006 Gulf of Mexico Atmospheric Composition and Climate Study (GoMACCS). *Journal of Geophysical Research* **2007,** *112*, D13201, doi:10.1029/2007JD008537.

5. Heald, C. L.; Jacob, D. J.; Turquety, S.; Hudman, R. C.; Weber, R. J.; Sullivan, A. P.; Peltier, R. E.; Atlas, E. L.; de Gouw, J. A.; Warneke, C.; Holloway, J. S.; Neuman, J. A.; Flocke, F. M.; Seinfeld, J. H., Concentrations and sources of organic carbon aerosols in the free troposphere over North America. *Journal of Geophysical Research* **2006,** *111*, D23s47, doi:10.1029/2006JD007705.

6. Yu, J. Z.; Huang, X.-F.; Xu, J.; Hu, M., When Aerosol Sulfate Goes Up, So Does Oxalate: Implication for the Formation Mechanisms of Oxalate. *Environmental Science & Technology* **2005,** *39*, (1), 128-133.

7. Sorooshian, A.; Lu, M.-L.; Brechtel, F. J.; Jonsson, H.; Feingold, G.; Flagan, R. C.; Seinfeld, J. H., On the Source of Organic Acid Aerosol Layers above Clouds. *Environmental Science & Technology* **2007,** *41*, (13), 4647-4654.

8. Fu, T.-M.; Jacob, D. J.; Wittrock, F.; Burrows, J. P.; Vrekoussis, M.; Henze, D. K., Global budgets of atmospheric glyoxal and methylglyoxal, and implications for formation of secondary organic aerosols. *Journal of Geophysical Research* **2008,** *113*, D15303, doi:10.1029/2007JD009505.

9. Chen, J.; Griffin, R. J.; Grini, A.; Tulet, P., Modeling secondary organic aerosol formation through cloud processing of organic compounds. *Atmospheric Chemistry and Physics* **2007,** *7*, (20), 5343-5355.

10. Carlton, A. G.; Turpin, B. J.; Altieri, K. E.; Seitzinger, S. P.; Mathur, R.; Roselle, S. J.; Weber, R. J., CMAQ Model Performance Enhanced When In-Cloud Secondary Organic Aerosol is Included: Comparisons of Organic Carbon Predictions with Measurements. *Environmental Science & Technology* **2008,** *42*, (23), 8798-8802.

11. Fu, T.-M.; Jacob, D. J.; Heald, C. L., Aqueous-phase reactive uptake of dicarbonyls as a source of organic aerosol over eastern North America. *Atmospheric Environment* **2009,** *43*, (10), 1814-1822.

12. Koch, S.; Moortgat, G. K., Photochemistry of Methylglyoxal in the Vapor Phase. *The Journal of Physical Chemistry A* **1998,** *102*, (46), 9142-9153.

13. Zhou, X.; Mopper, K., Apparent partition coefficients of 15 carbonyl compounds between air and seawater and between air and freshwater; Implications for air-sea exchange. *Environmental Science & Technology* **1990,** *24*, 1864-1869.

14. Betterton, E. A.; Hoffmann, M. R., Henry's Law Constants of some environmentally important aldehydes. *Environmental Science and Technology* **1988,** *22*, (12), 1415-1418.

15. Zhao, J.; Levitt, N. P.; Zhang, R.; Chen, J., Heterogeneous Reactions of Methylglyoxal in Acidic Media: Implications for Secondary Organic Aerosol Formation. *Environmental Science & Technology* **2006,** *40*, (24), 7682-7687.

16. Munger, J. W.; Jacob, D. J.; Daube, B. C.; Horowitz, L. W., Formaldehyde, glyoxal and methylglyoxal in air and cloudwater at a rural mountain site in central Virginia. *Journal of Geophysical Research* **1995,** *100*, (D5), 9325-9333.

17. Sareen, N.; Schwier, A. N.; Shapiro, E. L.; Mitroo, D.; McNeill, V. F., Secondary organic material formed by methylglyoxal in aqueous aerosol mimics. *Atmospheric Chemistry and Physics* **2010,** *10*, (3), 997-1016.

18. Carlton, A. G.; Turpin, B. J.; Lim, H.-J.; Altieri, K. E.; Seitzinger, S., Link between isoprene and secondary organic aerosol (SOA): Pyruvic acid oxidation yields low volatility organic acids in clouds. *Geophysical Research Letters* **2006,** *33*, L06822, doi:10.1029/2005GL025374.

19. Altieri, K. E.; Carlton, A. G.; Lim, H.-J.; Turpin, B. J.; Seitzinger, S. P., Evidence for Oligomer Formation in Clouds: Reactions of Isoprene Oxidation Products. *Environmental Science & Technology* **2006,** *40*, (16), 4956-4960.

20. Altieri, K. E.; Seitzinger, S. P.; Carlton, A. G.; Turpin, B. J.; Klein, G. C.; Marshall, A. G., Oligomers formed through in-cloud methylglyoxal reactions: Chemical composition, properties, and mechanisms investigated by ultra-high resolution FT-ICR mass spectrometry. *Atmospheric Environment* **2008,** *42*, (7), 1476-1490.

21. Loeffler, K. W.; Koehler, C. A.; Paul, N. M.; De Haan, D. O., Oligomer Formation in Evaporating Aqueous Glyoxal and Methyl Glyoxal Solutions. *Environmental Science & Technology* **2006,** *40*, (20), 6318-6323.

22. De Haan, D. O.; Corrigan, A. L.; Tolbert, M. A.; Jimenez, J. L.; Wood, S. E.; Turley, J. J., Secondary Organic Aerosol Formation by Self-Reactions of Methylglyoxal and Glyoxal in Evaporating Droplets. *Environmental Science & Technology* **2009,** *43*, (21), 8184-8190.

23. Nemet, I.; Vikic-Topic, D.; Varga-Defterdarovic, L., Spectroscopic studies of methylglyoxal in water and dimethylsulfoxide. *Bioorganic Chemistry* **2004,** *32*, (6), 560-570.

24. Ervens, B.; Gligorovski, S.; Herrmann, H., Temperature-dependent rate constants for hydroxyl radical reactions with organic compounds in aqueous solutions. *Physical Chemistry Chemical Physics* **2003,** *5*, (9), 1811-1824.

25. Monod, A.; Poulain, L.; Grubert, S.; Voisin, D.; Wortham, H., Kinetics of OH-initiated oxidation of oxygenated organic compounds in the aqueous phase: new rate constants, structure-activity relationships and atmospheric implications. *Atmospheric Environment* **2005,** *39*, (40), 7667-7688.

26. Stefan, M. I.; Bolton, J. R., Reinvestigation of the Acetone Degradation Mechanism in Dilute Aqueous Solution by the UV/H2O2 Process. *Environmental Science & Technology* **1999,** *33*, (6), 870-873.

27. Liu, Y.; El Haddad, I.; Scarfogliero, M.; Nieto-Gligorovski, L.; Temime-Roussel, B.; Quivet, E.; Marchand, N.; Picquet-Varrault, B.; Monod, A., In-cloud processes of methacrolein under simulated conditions – Part 1: Aqueous phase photooxidation. *Atmospheric Chemistry and Physics* **2009,** *9*, (14), 5093-5105.

28. Limbeck, A.; Puxbaum, H.; Otter, L.; Scholes, M. C., Semivolatile behavior of dicarboxylic acids and other polar organic species at a rural background site (Nylsvley, RSA). *Atmospheric Environment* **2001,** *35*, (10), 1853-1862.

29. Guzman, M. I.; Colussi, A. J.; Hoffmann, M. R., Photoinduced Oligomerization of Aqueous Pyruvic Acid. *The Journal of Physical Chemistry A* **2006,** *110*, (10), 3619-3626.

30. Grgic, I.; Nieto-Gligorovski, L. I.; Net, S.; Temime-Roussel, B.; Gligorovski, S.; Wortham, H., Light induced multiphase chemistry of gas-phase ozone on aqueous pyruvic and oxalic acids. *Physical Chemistry Chemical Physics* **2010,** *12*, (3), 698-707.

31. Yasmeen, F.; Sauret, N.; Gal, J. F.; Maria, P. C.; Massi, L.; Maenhaut, W.; Claeys, M., Characterization of oligomers from methylglyoxal under dark conditions: a pathway to produce secondary organic aerosol through cloud processing during nighttime. *Atmospheric Chemistry and Physics* **2010,** *10*, (8), 3803-3812.

32. Perri, M. J.; Seitzinger, S.; Turpin, B. J., Secondary organic aerosol production from aqueous photooxidation of glycolaldehyde: Laboratory experiments. *Atmospheric Environment* **2009,** *43*, (8), 1487-1497.

33. Tan, Y.; Perri, M. J.; Seitzinger, S. P.; Turpin, B. J., Effects of Precursor Concentration and Acidic Sulfate in Aqueous Glyoxal-OH Radical Oxidation and Implications for Secondary Organic Aerosol. *Environmental Science & Technology* **2009,** *43*, (21), 8105-8112.

34. Allen, A. O.; Hochanadel, C. J.; Ghormley, J. A.; Davis, T. W., Decomposition of Water and Aqueous Solutions under Mixed Fast Neutron and γ-Radiation. *The Journal of Physical Chemistry* **1952,** *56*, (5), 575-586.

35. Stefan, M. I.; Hoy, A. R.; Bolton, J. R., Kinetics and Mechanism of the Degradation and Mineralization of Acetone in Dilute Aqueous Solution Sensitized by the UV Photolysis of Hydrogen Peroxide. *Environmental Science & Technology* **1996,** *30*, (7), 2382-2390.

36. Ervens, B.; Feingold, G.; Frost, G. J.; Kreidenweis, S. M., A modeling study of aqueous production of dicarboxylic acids: 1. Chemical pathways and speciated organic mass production. *Journal of Geophysical Research* **2004,** *109*, D15205, doi:10.1029/2003JD004387.

37. Herrmann, H.; Tilgner, A.; Barzaghi, P.; Majdik, Z.; Gligorovski, S.; Poulain, L.; Monod, A., Towards a more detailed description of tropospheric aqueous phase organic chemistry: CAPRAM 3.0. *Atmospheric Environment* **2005,** *39*, (23-24), 4351-4363.

38. Jacob, D. J., Chemistry of OH in Remote Clouds and Its Role in the Production of Formic Acid and Peroxymonosulfate. *Journal of Geophysical Research* **1986,** *91*, (D9), 9807-9826.

39. Warneck, P., The relative importance of various pathways for the oxidation of sulfur dioxide and nitrogen dioxide in sunlit continental fair weather clouds. *Physical Chemistry Chemical Physics* **1999,** *1*, (24), 5471-5483.

40. Monod, A.; Carlier, P., Impact of clouds on the tropospheric ozone budget: Direct effect of multiphase photochemistry of soluble organic compounds. *Atmospheric Environment* **1999,** *33*, (27), 4431-4446.

41. Kelly, T. J.; Daum, P. H.; Schwartz, S. E., Measurements of Peroxides in Cloudwater and Rain. *Journal of Geophysical Research* **1985,** *90*, (D5), 7861-7871.

42. Olszyna, K. J.; Meagher, J. F.; Bailey, E. M., Gas-phase, cloud and rain-water measurements of hydrogen peroxide at a high-elevation site. *Atmospheric Environment (1967)* **1988,** *22*, (8), 1699-1706.

43. Claiborn, C. S.; Aneja, V. P., Measurements of Atmospheric Hydrogen Peroxide in the Gas Phase and in Cloud Water at Mt. Mitchell, North Carolina. *Journal of Geophysical Research* **1991,** *96*, (D10), 18771-18787.

44. Seinfeld, J. H.; Pandis, S. N., *Atmospheric Chemistry and Physics - From Air Pollution to Climate Change (2nd Edition)*. John Wiley and Sons, Inc.: New York, 2006.

45. Wang, W.-F.; Schuchmann, M. N.; Schuchmann, H.-P.; Sonntag, C. v., The Importance of Mesomerism in the Termination of α-Carboxymethyl Radicals from Aqueous Malonic and Acetic Acids. *Chemistry - A European Journal* **2001,** *7*, (4), 791-795.

46. Perri, M. J.; Lim, Y. B.; Seitzinger, S. P.; Turpin, B. J., Organosulfates from Glycolaldehyde in Aqueous Aerosols and Clouds: Laboratory Studies. *Atmospheric Environment* **2010,** *In Press, Accepted Manuscript*.

47. Lim, Y. B.; Tan, Y.; Perri, M. J.; Seitzinger, S. P.; Turpin, B. J., Secondary Organic Aerosol Formation through Reactions in Atmospheric Water: Chemical Insights. *In preparation* **2010**.

48. Sun, Y.; Zhang, Q.; Anastasio, C.; Sun, J., Insights into secondary organic aerosol formed via aqueous-phase reactions of phenolic compounds based on high resolution mass spectrometry. *Atmospheric Chemistry and Physics Discussions* **2010,** *10*, (2), 2915-2943.

49. Leitzke, A.; Reisz, E.; Flyunt, R.; von Sonntag, C., The reactions of ozone with cinnamic acids: formation and decay of 2-hydroperoxy-2-hydroxyacetic acid. *J. Chem. Soc.-Perkin Trans. 2* **2001**, (5), 793-797.

50. Lim, H. J.; Carlton, A. G.; Turpin, B. J., Isoprene forms secondary organic aerosol through cloud processing: Model simulations. *Environmental Science & Technology* **2005,** *39*, 4441-4446.

Table 3-1. Aqueous reactions and rate constants in methylglyoxal + OH radical model. Reactions are taken from Lim et al. (2005) and references therein except where footnoted. MGLY = methylglyoxal, GLYAC = glyoxylic acid, OXLAC = oxalic acid, OH = OH radical. Dissociation rate constants (k_d) are calculated from the equilibrium constant (K_{eq}) and association rate constants (k_a) by $k_d = K_{eq} \times k_a$. [a]Hydrogen peroxide photolysis rate (k_1) is estimated by fitting H_2O_2 loss in H_2O_2 + UV control experiments (Appendix B15). [b]Measured by Ervens et al. (2003) and Monod et al. (2005). This work uses the value from Ervens et al. (2003). [c]Measured by Leitzke et al. [49] and not included by Lim et al.

Reaction	Rate constant (M^{-1} s^{-1})	Note
$H_2O_2 + h\nu \rightarrow 2OH$	$(1.1\pm0.3)\times10^{-4}$ (s^{-1})	a
$OH + H_2O_2 \rightarrow HO_2 + H_2O$	2.7×10^{7}	
$HO_2 + H_2O_2 \rightarrow OH + H_2O + O_2$	3.7	
$HO_2 + HO_2 \rightarrow H_2O_2 + O_2$	8.3×10^{5}	
$OH + HO_2 \rightarrow H_2O + O_2$	7.1×10^{9}	
$OH + O_2^- \rightarrow OH^- + O_2$	1×10^{10}	
$HO_2 + O_2^- \rightarrow H_2O_2 + O_2$	1×10^{8}	
$OH + OH \rightarrow H_2O_2$	5.5×10^{9}	
$HCO_3^- + OH \rightarrow CO_3^- + H_2O$	1×10^{7}	
$CO_3^- + O_2^- \rightarrow CO_3^{2-} + O_2$	6.5×10^{8}	
$CO_3^- + HCO_2^- \rightarrow HCO_3^- + CO_2^-$	1.5×10^{5}	
$CO_3^- + H_2O_2 \rightarrow HCO_3^- + HO_2$	4.3×10^{5}	
$H_2O \leftrightarrow H^+ + OH^-$	$K_{eq} = 1.0\times10^{-14}$, $k_a = 1.4\times10^{11}$	
$HO_2 \leftrightarrow H^+ + O_2^-$	$K_{eq} = 1.6\times10^{-5}$, $k_a = 5.0\times10^{10}$	
$CO_2 (+ H_2O) \leftrightarrow H^+ + HCO_3^-$	$K_{eq} = 4.3\times10^{-7}$, $k_a = 5.6\times10^{4}$	
$HCO_3^- \leftrightarrow H^+ + CO_3^{2-}$	$K_{eq} = 4.69\times10^{-11}$, $k_a = 5\times10^{10}$	
$HCO_2H \leftrightarrow H^+ + HCO_2^-$	$K_{eq} = 1.77\times10^{-4}$, $k_a = 5\times10^{10}$	
$PYRAC \leftrightarrow H^+ + PYRAC^-$	$K_{eq} = 3.2\times10^{-3}$, $k_a = 2\times10^{10}$	
$CH_3CO_2H \leftrightarrow H^+ + CH_3CO_2^-$	$K_{eq} = 1.75\times10^{-5}$, $k_a = 5\times10^{10}$	
$GLYAC \leftrightarrow H^+ + GLYAC^-$	$K_{eq} = 3.47\times10^{-4}$, $k_a = 2\times10^{10}$	
$OXLAC \leftrightarrow H^+ + OXLAC^-$	$K_{eq} = 5.67\times10^{-2}$, $k_a = 5\times10^{10}$	
$OXLAC^- \leftrightarrow H^+ + OXLAC^{2-}$	$K_{eq} = 5.42\times10^{-5}$, $k_a = 5\times10^{10}$	
$MGLY + OH \rightarrow PYRAC^- + HO_2 + H_2O$	6.44×10^{8}	b
$MGLY + OH \rightarrow GLYAC^- + HO_2 + H_2O$	5.6×10^{7}	
$PYRAC + OH \rightarrow CH_3CO_2H + HO_2 + CO_2$	6.0×10^{7}	
$PYRAC^- + OH \rightarrow CH_3CO_2^- + HO_2 + CO_2$	6.0×10^{7}	
$CH_3CO_2H + OH \rightarrow GLYAC + HO_2 + H_2O$	1.36×10^{7}	
$CH_3CO_2H + OH \rightarrow HCHO + HO_2 + CO_2$	2.4×10^{6}	
$CH_3CO_2^- + OH \rightarrow GLYAC^- + HO_2 + H_2O$	7.23×10^{7}	
$CH_3CO_2^- + OH \rightarrow HCHO + O_2^- + CO_2$	1.28×10^{7}	
$GLYAC + OH \rightarrow OXLAC + HO_2 + H_2O$	3.62×10^{8}	
$GLYAC^- + OH \rightarrow OXLAC^- + HO_2 + H_2O$	2.9×10^{9}	
$OXLAC + OH \rightarrow 2CO_2 + 2H_2O$	1.4×10^{6}	
$OXLAC^- + OH \rightarrow CO_2 + CO_2^- + 2H_2O$	4.7×10^{7}	
$OXLAC^{2-} + OH \rightarrow CO_2 + CO_2^- + OH^-$	7.7×10^{6}	

$CO_2^- + O_2 \rightarrow O_2^- + CO_2$	2.4×10^9	
$GLYAC + H_2O_2 \rightarrow HCO_2H + CO_2 + H_2O$	0.3	c
$HCO_2H + OH \rightarrow CO_2 + HO_2 + H_2O$	1.0×10^8	
$HCO_2^- + OH \rightarrow CO_2^- + H_2O$	2.4×10^9	
$HCHO + OH \rightarrow HCO_2H + HO_2$	1.1×10^9	
$PYRAC^- + H_2O_2 \rightarrow CH_3CO_2^- + CO_2 + H_2O$	0.11	

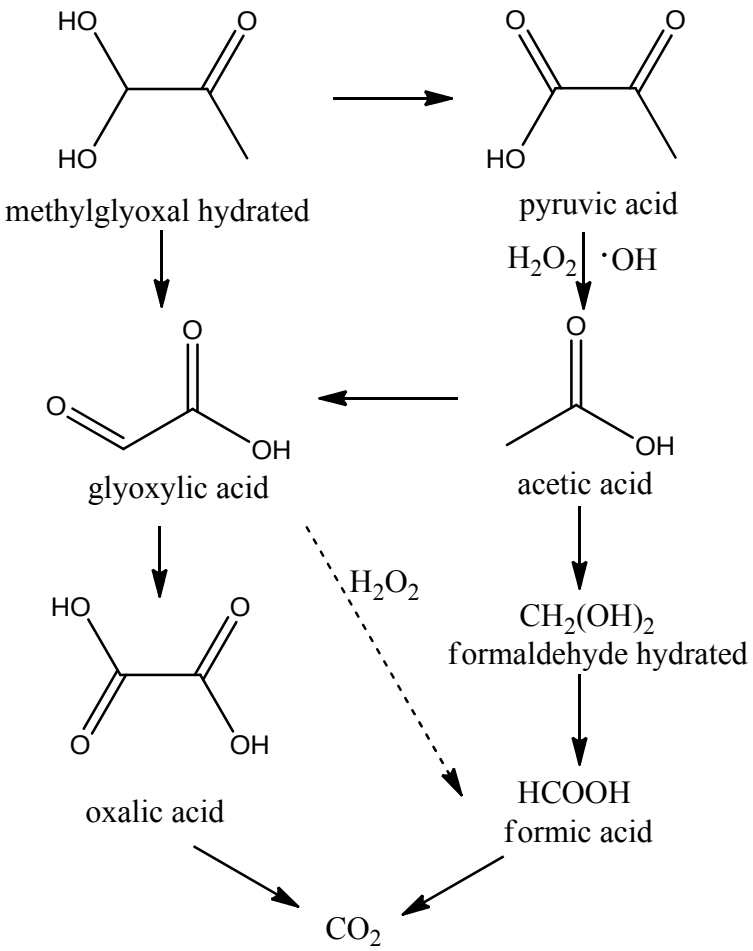

Fig. 3-1. Reactions included in kinetic modeling (Table 3-1) for aqueous OH radical oxidation of methyglyoxal [50].

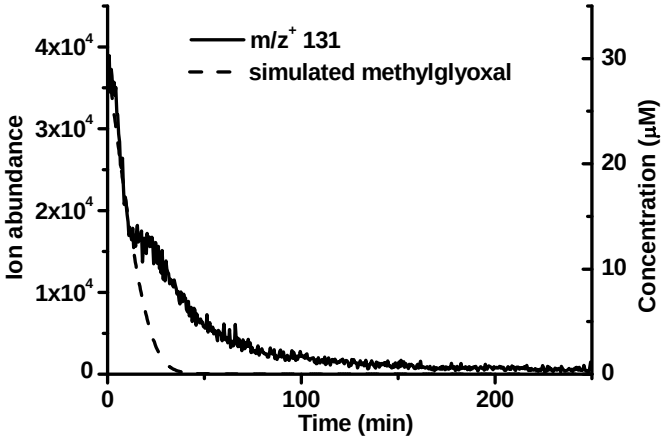

Fig. 3-2a. Ion abundance of methylglyoxal (m/z^+ 131) in the positive mode ESI-MS online analysis of methylglyoxal (30 μM) + OH radical (0.15 mM H_2O_2 + UV) experiment (solid line) and model predicted methylglyoxal concentration (μM; dashed line).

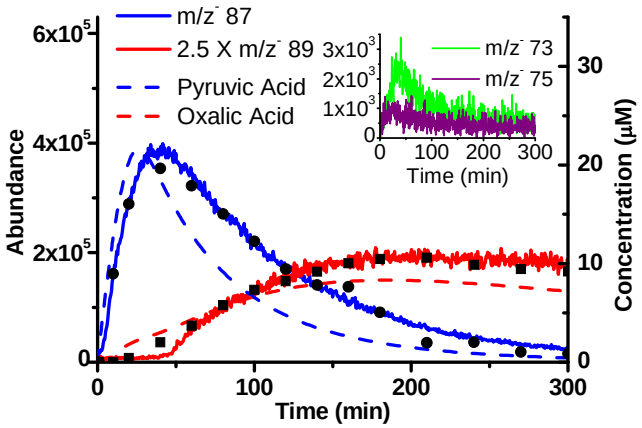

Fig. 3-2b. Ion abundance of pyruvic acid (m/z⁻ 87) and oxalic acid (m/z⁻ 89) (multiplied by 2.5 for m/z⁻ 89) in the negative mode ESI-MS online analysis of methylglyoxal (30 μM) + OH radical (0.15 mM H_2O_2 + UV) experiment. Pyruvic acid (circles) and oxalic acid (squares) concentrations quantified by IC; modeled pyruvic acid and oxalic acid concentrations (dashed lines); glyoxylic acid (m/z⁻ 73) and glycolic acid (m/z⁻ 75) are shown in the inset.

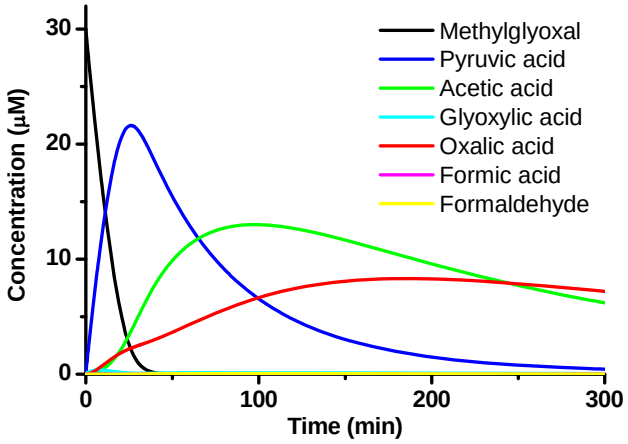

Fig. 3-2c. model simulated evolution of methylglyoxal and organic acids in methylglyoxal (30 μM) + OH radical (0.15 mM H_2O_2 + UV) experiment.

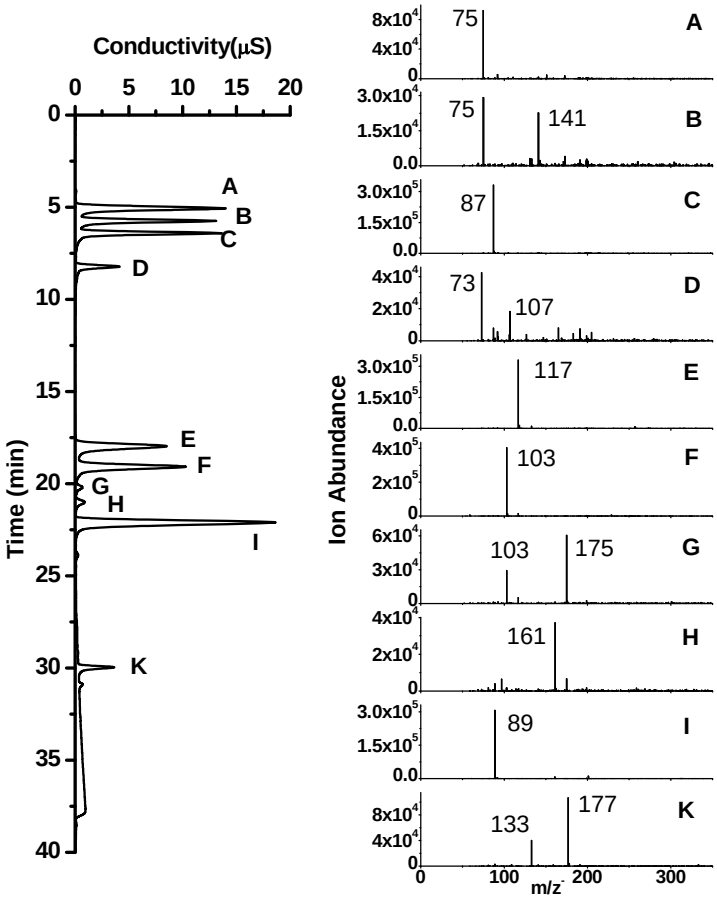

Fig. 3-3a. IC-ESI mass spectra of a mixed standard. (A) acetic acid (not detected in ESI-MS) and glycolic acid (m/z$^-$ 75), (B) formic acid (not detected in ESI-MS), (C) pyruvic acid (m/z$^-$ 87), (D) glyoxylic acid (m/z$^-$ 73), (E) succinic acid (m/z$^-$ 117), (F) malonic acid (m/z$^-$ 103), (I) oxalic acid (m/z$^-$ 89).

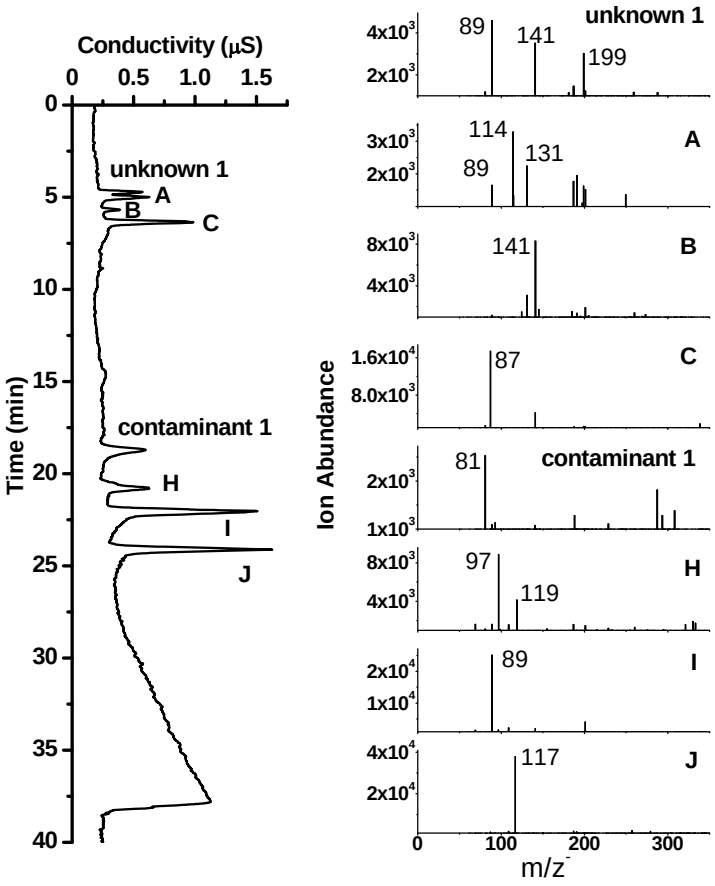

Fig. 3-3b. IC-ESI-MS spectra of a sample taken from 30 μM methylglyoxal + OH radical batch reactions (180 minutes reaction time). (A) peak with the retention time of acetic/glycolic acids, (B) peak with the retention time of formic acid, (C) pyruvic acid (m/z^- 87), (I) oxalic acid (m/z^- 89), (J) mesoxalic acid (m/z^- 117).

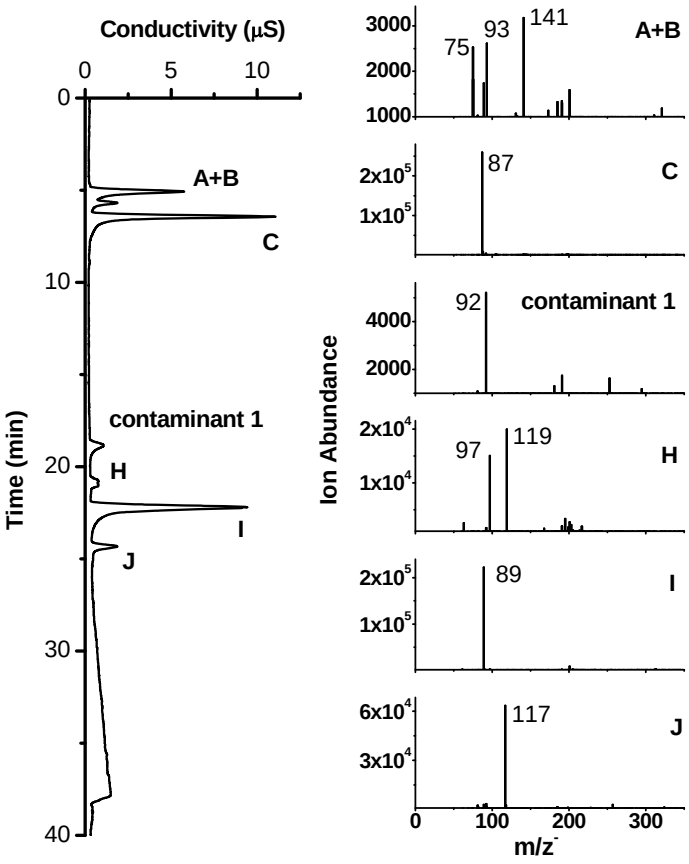

Fig. 3-3c. IC-ESI-MS spectra of a sample taken from 300 μM methylglyoxal + OH radical batch reactions (180 minutes reaction time). (A+B) peak with the retention time of acetic/glycolic acids + formic acid, (C) pyruvic acid (m/z^- 177), (I) oxalic acid (m/z^- 89), (J) mesoxalic acid (m/z^- 117).

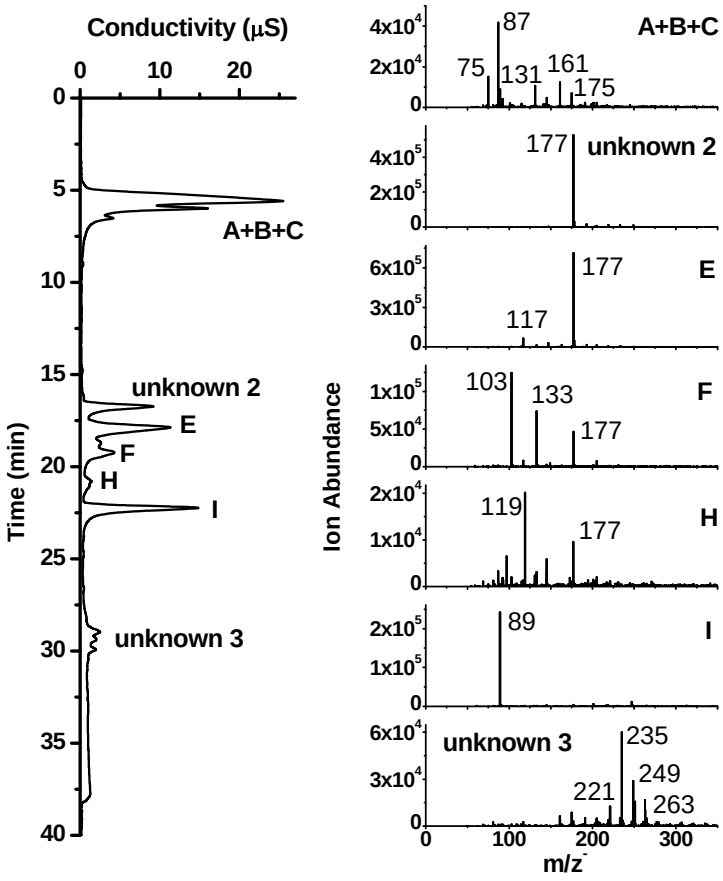

Fig. 3-3d. IC-ESI-MS spectra of a sample taken from 3000 μM methylglyoxal + OH radical batch reactions (180 minutes reaction time). (A+B+C) peak with the retention time of acetic/glycolic acids + formic acid + pyruvic acid, (E) peak with the retention time of succinic acid (m/z^- 117), (F) peak with the retention time of malonic acid (m/z^- 103), (I) oxalic acid (m/z^- 89).

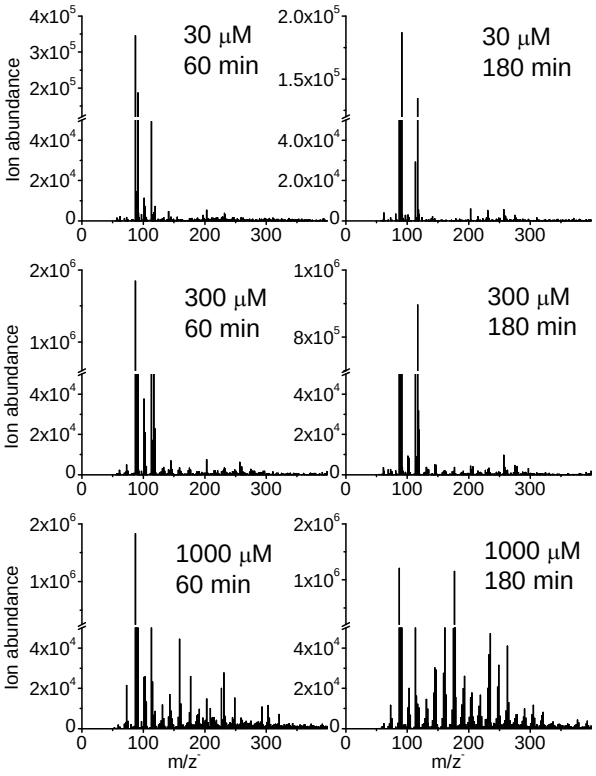

Fig. 3-4. ESI-MS negative ionization mode spectra of time points taken from methylglyoxal + OH radical online experiments: 60 minutes reaction time (top left) and 180 minutes reaction time (top right) from 30 μM methylglyoxal + OH radical (0.15 mM H_2O_2 + UV), 60 minutes reaction time (middle left) and 180 minutes reaction time (middle right) from 300 μM methylglyoxal + OH radical (1.5 mM H_2O_2 + UV), and 60 minutes reaction time (bottom left) and 180 minutes reaction time (bottom right) from 1 mM methylglyoxal + OH radical (5 mM H_2O_2 + UV).

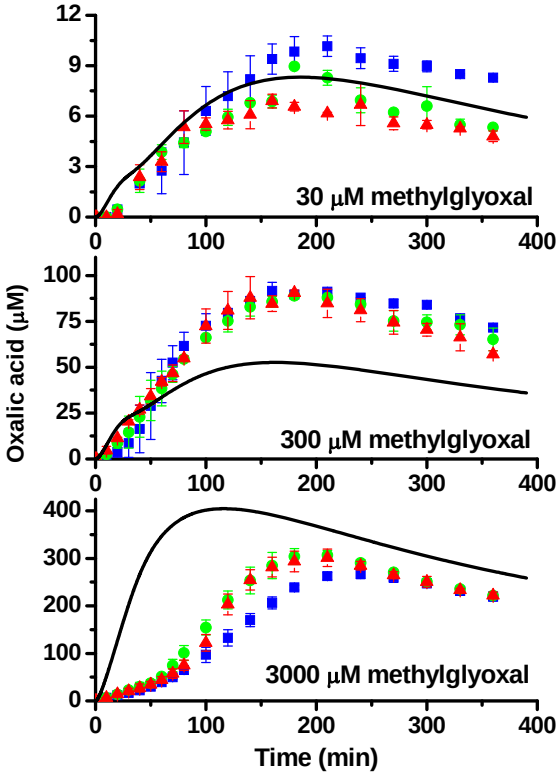

Fig. 3-5. Oxalic acid time profiles from batch methylglyoxal ± H_2SO_4 + OH radical experiments and model predictions. Initial model pH is 5.6. The effect of initial pH on simulated results is small. Solid lines are modeled oxalic acid concentration and data points are quantified concentrations from IC analysis. Squares (blue) represent oxalic acid in experiments without H_2SO_4, circles (green) represent oxalic acid in experiments with 280 μM H_2SO_4, and triangles (red) represent oxalic acid in experiments with 840 μM H_2SO_4. Experimental oxalic acid yields are listed in Appendix B4.

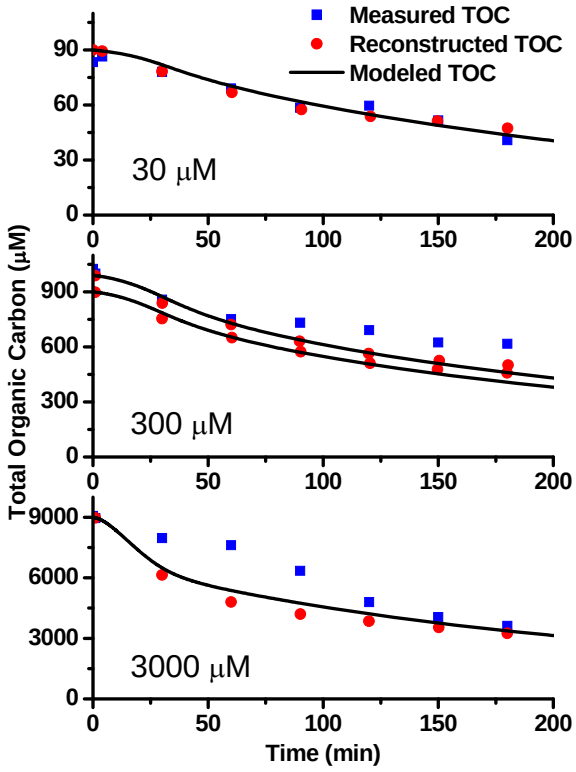

Fig. 3-6. Measured, modeled and reconstructed total organic carbon (TOC). Squares (blue) are total TOC measured by the TOC-5000A analyzer. Circles (red) indicate reconstructed TOC calculated as the sum of carbon in oxalic acid measured by IC and predicted carbon in all other compounds (predicted concentration × number of carbon). Model predicted TOC are presented as black lines. Uncertainties in TOC are ~ 5% for 30 μM experiments. Because samples from 300 and 3000 μM experiments had to be diluted before carbon analysis, TOC uncertainties are ~ 15%. The modeled TOC in the 300 μM experiment is shown with methylglyoxal initialized at 900 and 990 μM.

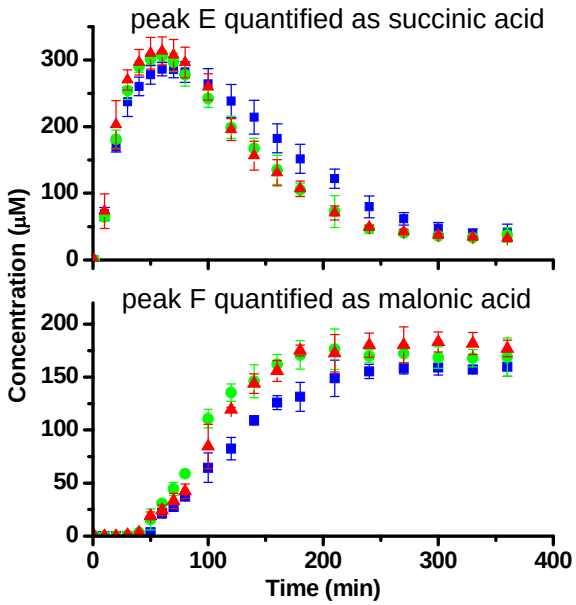

Fig. 3-7. Larger dicarboxylic acids in 3000 μM methylglyoxal + OH radical experiments with and without H_2SO_4. Top panel shows the peak at the retention time of succinic acid, and the bottom panel shows the peak at the retention time of malonic acid. Theses peaks were quantified based on succinic and malonic acid standards. Squares (blue) are experiments without H_2SO_4, circles (green) are experiments with 280 μM H_2SO_4, and triangles (red) are experiments with 840 μM H_2SO_4.

Chapter 4. Mechanisms Leading to Oligomers and SOA through aqueous photooxidation: Insights from OH Radical Oxidation of Acetic Acid

Material in this chapter will be submitted for publication as:

Tan, Y.; Turpin, B. J.; Altieri, K. E.; Seitzinger, S. P.; Lim, Y. B., Mechanisms Leading to Oligomers and SOA through aqueous photooxidation: Insights from OH Radical Oxidation of Acetic Acid. *Atmospheric Chemistry and Physics Discussions* **2010**.

4.1 Abstract

Previous experiments have demonstrated that the aqueous OH radical oxidation of methylglyoxal produces low volatility products including oxalic acid and oligomers. We expect these products to partially remain in the particle phase upon droplet evaporation, forming secondary organic aerosol (SOA). Acetic acid is an important intermediate in aqueous methylglyoxal oxidation and a ubiquitous product of gas phase photochemistry, making it a potential "aqueous" SOA precursor in its own right. Altieri et al. [1] proposed that acetic acid was the precursor of oligoesters observed in methylglyoxal oxidation. However, there is a discrepancy in the literature regarding the fate of acetic acid during aqueous-phase oxidation. In this research, acetic acid at concentrations relevant to atmospheric waters (20 μM – 10 mM) was oxidized by OH radical. Products were analyzed by ion chromatography (IC), electrospray ionization mass spectrometry (ESI-MS), and IC-ESI-MS. The formation of glyoxylic, glycolic, and oxalic acids were observed. In contrast to methylglyoxal oxidation, succinic acid and oligomers were not detected. Using results from these and methylglyoxal + OH radical experiments, radical mechanisms responsible for oligomer formation from methylglyoxal oxidation in clouds and wet aerosols are proposed. The importance of acetic acid as an SOA precursor is also

discussed. We hypothesize that this and similar chemistry is central to the daytime formation of oligomers in wet aerosols.

4.2 Introduction

Large uncertainties remain in the predicted impact of secondary organic aerosol (SOA) on air quality, climate and human health [2]. Field studies suggest that SOA formation is underestimated by current chemical transport models [2-3]. The properties of ambient SOA are also not reproduced in laboratory studies. Specifically, the oxygen-to-carbon (O/C) ratio of aged ambient oxygenated organic aerosol (OA) is higher than that formed in traditional smog chamber experiments [4]. Longer reaction times, alternate formation mechanisms, and SOA precursors not included in models are considered as the most likely explanations [2]. Laboratory and modeling experiments demonstrate that aqueous oxidation of small volatile organic compounds leads to high O/C ratios and can effectively contribute to SOA mass [5-11]. However, aqueous reaction mechanisms leading to the formation of higher-molecular-weight (higher-MW) compounds, including oligomers, are not fully understood.

Organic acids and higher-MW compounds are identified products in the aqueous OH radical oxidation of methylglyoxal [1]. A number of these products (e.g. oxalic, pyruvic and succinic acids) are found predominantly in the particle phase in the atmosphere [12]. Thus the oxidation of methylglyoxal in atmospheric waters is a source of SOA. The formation of simple carboxylic acids is generally well understood. Pyruvic acid is the major first generation product in the aqueous OH radical oxidation of methylglyoxal [13], and the subsequent oxidation of pyruvic acid yields acetic acid [14]. Aqueous OH radicals are expected to react with acetic acid primarily by H abstraction at

the methyl group to produce $\cdot CH_2CO_2H$ radicals, and by H abstraction at the carboxyl group to a minor extent to form the $CH_3CO_2\cdot$ radicals (Scheme 4-1) [15]. The $CH_3CO_2\cdot$ radicals decompose rapidly to form $\cdot CH_3$ radicals and are not expected to participate in bimolecular reactions. Dissolved oxygen adds rapidly to the $\cdot CH_2CO_2H$ radicals to yield the corresponding peroxyl radicals ($\cdot O_2CH_2CO_2H$). Products from the decay of $\cdot O_2CH_2CO_2H$ include glyoxylic and glycolic acids, formaldehyde and CO_2 [15]. The oxidation of glycolic acid produces glyoxylic acid and the oxidation of glyoxylic acid produces oxalic acid. In contrast, mechanisms leading to the formation of higher-MW compounds remain ambiguous.

The experiments of Chapter 3 suggest that higher-MW products including oligomers become increasingly important as organic concentrations increase from those typically observed in clouds to the higher concentrations found in aerosol water. Acid catalyzed esterification was previously proposed to explain the observed oligomer formation from the methylglyoxal and OH radical reaction, and it was proposed that products of acetic acid and OH radicals initiated the esterification process [1]. Specifically, Altieri et al. [1] suggested that succinic acid was produced via the recombination of $\cdot CH_2CO_2H$ radicals from acetic acid, based on the work of Wang et al. (2001) who observed succinic acid formation from γ-radiolysis of aqueous acetic acid (2mM, saturated with N_2O) [16]. Altieri et al. [1] further proposed that succinic acid was oxidized by OH radicals to give hydroxy acids (e.g. lactic or hydracrylic acid), and that repeated addition of monomers from hydroxy acids (e.g. $C_3H_4O_2$ from hydracrylic acid) to parent carboxylic acids (e.g. pyruvic, oxalic, and glyoxylic acids) via esterification formed nine series of oligomers. Elemental composition and ion fragmentation patterns

of a large number of higher-MW compounds in methylglyoxal + OH radical experiments are consistent with this proposed mechanism. Note that these oligoesters did not form in a mixed standard containing predicted reaction components and lactic acid. They only formed in the presence of OH radical. Higher molecular weight compounds were also observed in the OH radical oxidation of pyruvic acid (10 mM) and were quite similar to oligomers from methylglyoxal oxidation (230 of 296 ions in the mass range 50 – 500 amu are the same in the electrospray ionization mass spectrometry analysis) [17]. Altieri et al. [1] implied that oligomer formation in OH radical oxidation of pyruvic acid could be explained by esterfification as well. Calculations indeed suggested that esterification is thermodynamically favorable for carboxylic acids under atmospheric conditions [18], and the formation of succinic acid in methylglyoxal (3 mM) + OH radical experiments has now been confirmed by IC-ESI-MS (Chapter 3).

Higher-MW compounds including oligomers have also been hypothesized to form in atmospheric waters via radical-radical reactions (e.g. methacrolein, glycoaldehyde, glyoxal, pyruvic acid and phenols) [9, 19-22]. For example, C_6 and C_7 carboxylic acid formation was observed during the photolysis (320 nm UV) of oxygen-saturated pyruvic acid solutions [22]. The formation of these products was explained by radical-radical chemistry [22]. Ketyl ($CH_3\dot{C}(OH)C(O)OH$) and acetyl (CH3C(O)·) radicals are produced when pyruvic acid solution is irradiated by UV light. Guzman et al. (2006) argued that the reactivity of these radicals towards O_2 must be lower than previously believed, making radical recombination and the formation of the observed C_6 and C_7 carboxylic acids possible [22]. Similarly, radical-radical reactions could play an important role in the formation of higher carbon number products from methylglyoxal and pyruvic acid.

The fate of acetic acid needs further investigation to understand the origin of oligomers in the aqueous phase oxidation of methylglyoxal. The OH radical oxidation of methylglyoxal was modeled in Chapter 3 with acetic acid only forming glyoxylic acid and formaldehyde, even though additional products (e.g. glycolic and succinic acids) have been proposed [23]. Succinic acid and oligomers should be observed in acetic acid + OH radical experiments if the acid catalyzed esterification pathway proposed by Altieri et al. [1] is accurate. This chapter reports the result of batch aqueous acetic acid + OH radical experiments conducted at four concentrations. The products were analyzed by on-line (real-time) mass spectroscopy and by electrospary ionization-mass spectrometry with preseparation by IC (IC-ESI-MS). Interestingly, formation of succinic acid and oligomers was not observed. Below we explain how these and previous results suggest that radical-radical chemistry rather than acid catalyzed condensation reactions (esterficiation) is the likely oligomer formation mechanism and propose how this happens. In addition, we demonstrate that acetic acid can effectively form oxalic acid through aqueous phase reactions under atmospherically relevant conditions. Oxalate is largely found in the particle phase in the atmosphere. Thus acetic acid is an SOA precursor. Acetic acid/acetate is ubiquitous in atmospheric precipitation, cloud water, fog water and dew (Henry's law constant = 8.8×10^3 M atm^{-1}) [24]. Concentrations of acetate in cloud water, fog water and dew range from 0.4 – 245 μM in various field studies [25]. However, to our knowledge, the contribution of acetic acid to SOA was not previously considered.

4.3 Methods

Batch experiments were conducted in a 1 L glass reaction vessel at 25 ± 2°C, as described previously [7, 14]. Commercially available acetic acid (Sigma-Aldrich,

99.999% purity) was diluted to 20 and 100 μM, 1 and 10 mM for experiments. OH radicals were generated by the photolysis of H_2O_2 by UV (254 nm) light from a mercury lamp (Heraeus Noblelight, Inc. Duluth, GA). The concentration of OH radicals was approximately $3–4\times10^{-12}$ M, as simulated by a dilute aqueous chemistry model (Table 3-1). Dissolved oxygen was measured at the beginning and the end of experiments (YSI ProODO, YSI Inc., Yellow Springs, OH). Solutions remained saturated with oxygen and pH varied from 6.6 – 3.3 during experiments. The following control experiments were also conducted: acetic acid + UV, acetic acid + H_2O_2, H_2O_2 + UV, mixed standard (250 μM each acetic, formic, glyoxylic, glycolic, succinic, malonic, and oxalic acids) + UV, and mixed standard + H_2O_2. Experiments were also performed with pyruvic acid (1 mM) + 5 mM H_2O_2 + UV and 1 mM pyruvic acid + UV. While H_2O_2 reacts with glyoxylic and pyruvic acids and pyruvic acid photolyzes in control experiments (in the absence of OH radical), dark reactions with H_2O_2 and photolysis are too slow to compete in the presence of OH radical, as explained in Chapter 3.

Batch aqueous reactions were monitored in real-time by electrospray ionization mass spectrometry (ESI-MS; HP-Agilent 1100), as described by Perri et al. (2009) and in Chapter 2 and 3. Discrete samples were collected for analysis by ion chromatography (IC; ICS-3000, Dionex, Sunnyvale, CA; IonPac AS11-HC column with AG11-HC guard column, 30˚C), as described in Chapters 2 and 3. Acetic, formic, glyoxylic, glycolic, oxalic and mesoxalic acids were identified and quantified with authentic standards and Chromeleon software (version 6.80 SP2, Dionex). Acetic and glycolic acids were not quantified due to coelution. Whether or not it is present, glyoxylic acid cannot be detected in discrete samples because it reacts with residual H_2O_2 while awaiting analysis.

This reaction is not expected to affect concentrations and chemistry in the reaction vessel as it is slow compared to OH radical reactions [7]. Selected samples were analyzed by ESI-MS after pre-separation in the IC (IC-ESI-MS), as described in detail in Chapter 3. A 1000 μM methylglyoxal + 5 mM H_2O_2 + UV experimental sample that was taken at 76 minutes was analyzed by ultra high resolution Fourier transform ion cyclotron resonance electrospray ionization mass spectrometry (ESI FT-ICR MS; Thermo-Finnigan LTQ-XL, Woods Hole Oceanographic Institute Mass Spectrometer Facility; negative ionization mode, described by Perri et al. [10]) to determine the elemental formulas of products from 50 – 500 amu. MS/MS analysis was performed with ESI FT-ICR MS on selected ions to obtain further structural information about selected compounds.

4.4 Results and Discussion

4.4.1 Aqueous Phase Oxidation of Acetic Acid by OH Radical

The formation of glyoxylic, glycolic and oxalic acid is supported by the existence of products with m/z^- of 73, 75 and 89 in the online ESI-MS analysis of the aqueous OH radical oxidation of acetic acid (Fig. 4-1), and was further verified by IC-ESI-MS analysis (Fig. 4-2). Glyoxylic acid (m/z^- 73) and glycolic acid (m/z^- 75) both increased rapidly when the experiment started, in agreement with the bimolecular decay of $\cdot O_2CH_2CO_2H$ radical. Glyoxylic and glycolic acids can be effectively oxidized to oxalic acid (m/z^- 89) [7, 10]. At the cloud relevant concentration of 20 μM acetic acid, the maximum oxalic acid concentration was ~27% of the acetic acid reacted (Fig. 4-3). This finding and the high abundance of acetic acid in atmospheric waters suggest that OH radical oxidation of acetic acid could contribute considerably to SOA mass. Interestingly, unlike the oxidation of pyruvic acid and methylglyoxal, neither succinic acid (m/z^- 117)

nor higher-MW compounds consistent with oligomer series were detected in any acetic acid experiment (Fig. 4-4). Acetic acid oxidation does not seem to explain the formation of oligomers and other higher carbon number products ($\geq C_4$) from methylglyoxal.

4.4.2 Higher-MW Products from Methylglyoxal + OH Radical Experiments

The absence of succinic acid and higher-MW compounds in acetic acid + OH radical experiments challenges the acid catalyzed esterification mechanism for oligomer formation from methylglyoxal and OH radical proposed previously [1]. Also oligomers were not observed when lactic acid is added to the mixed standard containing proposed parent acids, suggesting that acid catalyzed esterification might not be fast enough to produce noticeable amounts of oligomers at these concentrations. Interestingly, one of the proposed parent compounds is m/z^- 177, which is a prominent peak in 3 mM methylglyoxal + OH radical experiments. Altieri et al. [1] noted that the ESI-MS/MS analysis of m/z^- 177 is consistent with an oxalic acid–pyruvic acid dimer ($C_5H_5O_7^-$), although $C_6H_9O_6^-$ also corresponds to m/z^- 177. The m/z^- 177 does form when oxalic and pyruvic acids are simply mixed together (Fig. 3-3a, Chapter 3). However, the IC retention time of m/z^- 177 from mixed standard was different from that of m/z^- 177 formed in 3 mM methylglyoxal + OH radical experiments (Fig. 3-3d, Chapter 3), suggesting that the oxalic acid–pyruvic acid dimer was negligible in methylglyoxal + OH radical experiments (Fig. 3-3a,3d). To resolve these discrepancies, radical-radical reactions are proposed below.

In the FT-ICR MS analysis, the m/z^- 177 formed in methylglyoxal + OH radical experiments only corresponded to a molecular formula of $C_6H_9O_6^-$ (177.04029). FT-ICR MS/MS analysis of m/z^- 177 showed major negatively charged fragments of $C_4H_7O^-$

(71.05024), $C_3H_3O_3^-$ (87.00881), $C_4H_7O_2^-$ (87.04520), $C_5H_5O_2^-$ (97.02956), $C_5H_7O_3^-$ (115.04013), $C_5H_7O_4^-$ (131.03507), and $C_6H_7O_5^-$ (159.03007) (Fig. 4-5). Possible structures of $C_6H_9O_6^-$ and hypothesized fragment ions are proposed based on these results (Scheme 4-2). The proposed structure of $C_6H_9O_6^-$ is the same as that of a C_6 dicarboxylic acid observed in the photolysis of aqueous pyruvic acid [22]. In fact, similar IC peaks with m/z^- 177 were found when comparing the IC-ESI-MS spectrum of a 1 mM pyruvic acid + UV experiment sample (Appendix C2) with that of a 3 mM methylglyoxal + OH radical experiment sample in the study of Chapter 3, suggesting that the same $C_6H_9O_6^-$ might form in both experiments. (These peaks were not observed in either 1 mM pyruvic acid + OH radical experiment (Appendix C3) nor 3 mM methylglyoxal + UV experiment.) Guzman et al. (2006) proposed that the recombination of ketyl radicals ($CH_3\dot{C}(OH)C(O)OH$, denoted as ·K) from pyruvic acid photolysis leads to the formation of $C_6H_9O_6^-$. We expect that similar chemistry leads to the formation of $C_6H_9O_6^-$ in the OH radical oxidation of methylglyoxal, except that the ketyl radicals form differently (Scheme 4-3). Experimental observations [26] and theoretical calculations [27] indicate that methylglyoxal immediately transforms to monohydrate (~60%) and dihydrate (~40%) forms in aqueous solutions. The enol form of methylglyoxal should be negligible (< 0.01%) based on thermodynamic calculations. OH radicals react with mono- and dihydrated methylglyoxal via H-abstraction to give corresponding radicals. The proton coupled electron transfer in monohydrated methylglyoxal radical [28] and the dehydration of dihydrated methylglyoxal radical [29] readily produce the ketyl radical (·K) proposed by Guzman et al. (2006) which forms $C_6H_9O_6^-$ via recombination. Note that the $C_6H_9O_6^-$ in methylglyoxal + OH radical experiments may have other structures

yet to be understood, because $C_6H_9O_6^-$ was observed in four distinct IC peaks and chiral isomers are not separated by the IC column.

The structures of previously observed oligomers can also be explained by radical-radical reactions. For example, Altieri et al. [1] proposed that $C_9H_{13}O_8^-$ (m/z$^-$ 249.061591) is an oligoester formed via condensation between m/z$^-$ 177 and hydracrylic acid, adding $C_3H_4O_2$. Here I propose an alternative structure for $C_9H_{13}O_8^-$ based on FT-ICR MS/MS analysis (Scheme 4-4, Fig. 4-6, Appendix C1). Radical-radical reactions are can produce this structure of $C_9H_{13}O_8^-$ (Scheme 4-5). This involves the addition of the ketyl radical (·K) to the carbonyl group of monohydrated methylglyoxal, subsequent radical rearrangement and combination with the ketyl radical (·K). Radical addition to the carbonyl group is endothermic but was suggested by Guzman et al. (2006). Similar radical rearrangements were proposed in the radiolysis of glyceraldehyde [30]. Another oligoester, $C_9H_{12}O_7^-$ (m/z$^-$ 231), was proposed to form from pyruvic acid via repeated esterification with hydracrylic acid ($C_3H_6O_3$). Major negatively charged fragments of $C_9H_{12}O_7^-$ in previous ESI-MS/MS analysis included m/z$^-$ 159, 143, 87 and 71; this is also in agreement with the structure proposed in Scheme 4-6. The formation of $C_9H_{12}O_7^-$ could be similar to that of $C_9H_{13}O_8^-$ except that the rearranged radical (A) associates with the methylglyoxal radical rather than the ketyl radical (·K) in the last step (Scheme 4-7).

4.5 Conclusions and Atmospheric Implications

Rapid oxalic acid production from aqueous acetic acid oxidation, suggested by Warneck et al. (2005) [31], is confirmed by this work. If SOA production from aqueous acetic acid oxidation is incorporated in chemical transport models, the predicted SOA

distribution is expected to change because of the large amount of acetic acid in the atmosphere.

We found that radical-radical chemistry is capable of explaining higher molecular weight products observed in methylglyoxal oxidation experiments (e.g. $C_6H_9O_6^-$, $C_9H_{13}O_8^-$ and $C_9H_{12}O_7^-$). Because the oligoesters formed by acid catalyzed condensation reactions were not indentified in mixed standard with lactic acid, it appears that these reactions are slower than radical-radical reactions and radical chemistry is the major mechanism leading to oligomer formation. The apparent oligomer series identified as such through the existence of series of compounds differing by "$C_3H_4O_2$" do not necessarily form from acid catalyzed condensation reactions. It appears that having the hydroxyl group on the same carbon (as the case for ketyl radical in Scheme 3) might stabilize the radical, making the radical is less reactive towards dissolved oxygen. This explains why succinic acid and oligomers were not observed in acetic acid oxidation because acetic acid only forms primary radicals (e.g. $\cdot CH_2CO_2H$) which are not stabilized by hydroxyl groups (as shown in Scheme 4-1). Aldehydes usually hydrate in aqueous solutions, and their oxidation by OH radical produces potentially stable tertiary radicals with hydroxyl groups, except the case of formaldehyde. It is likely that $\geq C_2$ aldehydes could also form higher molecular weight products through aqueous radical-radical reactions and contribute to SOA. More experimental studies are needed to fully understand the formation of higher molecular weight compounds in atmospheric waters.

4.6 References

1. Altieri, K. E.; Seitzinger, S. P.; Carlton, A. G.; Turpin, B. J.; Klein, G. C.; Marshall, A. G., Oligomers formed through in-cloud methylglyoxal reactions: Chemical composition, properties, and mechanisms investigated by ultra-high resolution FT-ICR mass spectrometry. *Atmospheric Environment* **2008,** *42*, (7), 1476-1490.

2. Hallquist, M.; Wenger, J. C.; Baltensperger, U.; Rudich, Y.; Simpson, D.; Claeys, M.; Dommen, J.; Donahue, N. M.; George, C.; Goldstein, A. H.; Hamilton, J. F.; Herrmann, H.; Hoffmann, T.; Iinuma, Y.; Jang, M.; Jenkin, M. E.; Jimenez, J. L.; Kiendler-Scharr, A.; Maenhaut, W.; McFiggans, G.; Mentel, T. F.; Monod, A.; Prévôt, A. S. H.; Seinfeld, J. H.; Surratt, J. D.; Szmigielski, R.; Wildt, J., The formation, properties and impact of secondary organic aerosol: current and emerging issues. *Atmospheric Chemistry and Physics* **2009,** *9*, (14), 5155-5236.

3. Kanakidou, M.; Seinfeld, J. H.; Pandis, S. N.; Barnes, I.; Dentener, F. J.; Facchini, M. C.; Van Dingenen, R.; Ervens, B.; Nenes, A.; Nielsen, C. J.; Swietlicki, E.; Putaud, J. P.; Balkanski, Y.; Fuzzi, S.; Horth, J.; Moortgat, G. K.; Winterhalter, R.; Myhre, C. E. L.; Tsigaridis, K.; Vignati, E.; Stephanou, E. G.; Wilson, J., Organic aerosol and global climate modelling: a review. *Atmospheric Chemistry and Physics* **2005,** *5*, 1053-1123.

4. Aiken, A. C.; DeCarlo, P. F.; Kroll, J. H.; Worsnop, D. R.; Huffman, J. A.; Docherty, K. S.; Ulbrich, I. M.; Mohr, C.; Kimmel, J. R.; Sueper, D.; Sun, Y.; Zhang, Q.; Trimborn, A.; Northway, M.; Ziemann, P. J.; Canagaratna, M. R.; Onasch, T. B.; Alfarra, M. R.; Prevot, A. S. H.; Dommen, J.; Duplissy, J.; Metzger, A.; Baltensperger, U.; Jimenez, J. L., O/C and OM/OC Ratios of Primary, Secondary, and Ambient Organic Aerosols with High-Resolution Time-of-Flight Aerosol Mass Spectrometry. *Environmental Science & Technology* **2008,** *42*, (12), 4478-4485.

5. Ervens, B.; Carlton, A. G.; Turpin, B. J.; Altieri, K. E.; Kreidenweis, S. M.; Feingold, G., Secondary organic aerosol yields from cloud-processing of isoprene oxidation products. *Geophysical Research Letters* **2008,** *35*.

6. Carlton, A. G.; Turpin, B. J.; Altieri, K. E.; Seitzinger, S. P.; Mathur, R.; Roselle, S. J.; Weber, R. J., CMAQ Model Performance Enhanced When In-Cloud Secondary Organic Aerosol is Included: Comparisons of Organic Carbon Predictions with Measurements. *Environmental Science & Technology* **2008,** *42*, (23), 8798-8802.

7. Tan, Y.; Perri, M. J.; Seitzinger, S. P.; Turpin, B. J., Effects of Precursor Concentration and Acidic Sulfate in Aqueous Glyoxal-OH Radical Oxidation and Implications for Secondary Organic Aerosol. *Environmental Science & Technology* **2009,** *43*, (21), 8105-8112.

8. Lim, H. J.; Carlton, A. G.; Turpin, B. J., Isoprene forms secondary organic aerosol through cloud processing: Model simulations. *Environmental Science & Technology* **2005,** *39*, 4441-4446.

9. Liu, Y.; El Haddad, I.; Scarfogliero, M.; Nieto-Gligorovski, L.; Temime-Roussel, B.; Quivet, E.; Marchand, N.; Picquet-Varrault, B.; Monod, A., In-cloud processes of methacrolein under simulated conditions – Part 1: Aqueous phase photooxidation. *Atmospheric Chemistry and Physics* **2009,** *9*, (14), 5093-5105.

10. Perri, M. J.; Seitzinger, S.; Turpin, B. J., Secondary organic aerosol production from aqueous photooxidation of glycolaldehyde: Laboratory experiments. *Atmospheric Environment* **2009,** *43*, (8), 1487-1497.

11. El Haddad, I.; Liu, Y.; Nieto-Gligorovski, L.; Michaud, V.; Temime-Roussel, B.; Quivet, E.; Marchand, N.; Sellegri, K.; Monod, A., In-cloud processes of methacrolein under simulated conditions – Part 2: Formation of secondary organic aerosol. *Atmospheric Chemistry and Physics* **2009,** *9*, (14), 5107-5117.

12. Limbeck, A.; Puxbaum, H.; Otter, L.; Scholes, M. C., Semivolatile behavior of dicarboxylic acids and other polar organic species at a rural background site (Nylsvley, RSA). *Atmospheric Environment* **2001,** *35*, (10), 1853-1862.

13. Stefan, M. I.; Bolton, J. R., Reinvestigation of the Acetone Degradation Mechanism in Dilute Aqueous Solution by the UV/H2O2 Process. *Environmental Science & Technology* **1999,** *33*, (6), 870-873.

14. Carlton, A. G.; Turpin, B. J.; Lim, H.-J.; Altieri, K. E.; Seitzinger, S., Link between isoprene and secondary organic aerosol (SOA): Pyruvic acid oxidation yields low volatility organic acids in clouds. *Geophysical Research Letters* **2006,** *33*, L06822, doi:10.1029/2005GL025374.

15. Schuchmann, M. N.; Zegota, H.; Vonsonntag, C., Acetate Peroxyl Radicals, O2CH2CO2(-) - a Study on the γ-Radiolysis and Pulse-Radiolysis of Acetate in Oxygenated Aqueous-Solutions. *Z.Naturforsch.(B)* **1985,** *40*, (2), 215-221.

16. Wang, W.-F.; Schuchmann, M. N.; Schuchmann, H.-P.; Sonntag, C. v., The Importance of Mesomerism in the Termination of α-Carboxymethyl Radicals from Aqueous Malonic and Acetic Acids. *Chemistry - A European Journal* **2001,** *7*, (4), 791-795.

17. Altieri, K. E.; Carlton, A. G.; Lim, H.-J.; Turpin, B. J.; Seitzinger, S. P., Evidence for Oligomer Formation in Clouds: Reactions of Isoprene Oxidation Products. *Environmental Science & Technology* **2006,** *40*, (16), 4956-4960.

18. Barsanti, K. C.; Pankow, J. F., Thermodynamics of the formation of atmospheric organic particulate matter by accretion reactions--Part 3: Carboxylic and dicarboxylic acids. *Atmospheric Environment* **2006,** *40*, (34), 6676-6686.

19. Perri, M. J.; Lim, Y. B.; Seitzinger, S. P.; Turpin, B. J., Organosulfates from Glycolaldehyde in Aqueous Aerosols and Clouds: Laboratory Studies. *Atmospheric Environment* **2010,** *In Press, Accepted Manuscript*.

20. Lim, Y. B.; Tan, Y.; Perri, M. J.; Seitzinger, S. P.; Turpin, B. J., Aqueous chemistry and its role in secondary organic aerosol (SOA) formation. *Atmos. Chem. Phys. Discuss.* **2010,** *10*, (6), 14161-14207.

21. Sun, Y.; Zhang, Q.; Anastasio, C.; Sun, J., Insights into secondary organic aerosol formed via aqueous-phase reactions of phenolic compounds based on high resolution mass spectrometry. *Atmospheric Chemistry and Physics Discussions* **2010,** *10*, (2), 2915-2943.

22. Guzman, M. I.; Colussi, A. J.; Hoffmann, M. R., Photoinduced Oligomerization of Aqueous Pyruvic Acid. *The Journal of Physical Chemistry A* **2006,** *110*, (10), 3619-3626.

23. Tan, Y.; Carlton, A. G.; Seitzinger, S. P.; Turpin, B. J., SOA from Methylglyoxal in Clouds and Wet Aerosols: Measurement and Prediction of Key Products. *Atmospheric Environment In Press, Accepted Manuscript*.

24. Seinfeld, J. H.; Pandis, S. N., *Atmospheric Chemistry and Physics - From Air Pollution to Climate Change (2nd Edition)*. John Wiley and Sons, Inc.: New York, 2006.

25. Khare, P.; Kumar, N.; Kumari, K. M.; Srivastava, S. S., Atmospheric formic and acetic acids: An overview. *Reviews of Geophysics* **1999,** *37*, (2), 227-248.

26. Nemet, I.; Vikic-Topic, D.; Varga-Defterdarovic, L., Spectroscopic studies of methylglyoxal in water and dimethylsulfoxide. *Bioorganic Chemistry* **2004,** *32*, (6), 560-570.

27. Krizner, H. E.; De Haan, D. O.; Kua, J., Thermodynamics and Kinetics of Methylglyoxal Dimer Formation: A Computational Study. *The Journal of Physical Chemistry A* **2009,** *113*, (25), 6994-7001.

28. Livingston, R.; Zeldes, H., Paramagnetic Resonance Study of Liquids during Photolysis. III. Aqueous Solutions of Alcohols with Hydrogen Peroxide1. *Journal of the American Chemical Society* **1966,** *88*, (19), 4333-4336.

29. Buley, A. L.; Norman, R. O. C.; Pritchett, R. J., Electron spin resonance studies of oxidation. Part VIII. Elimination reactions of some hydroxyalkyl radicals. *Journal of the Chemical Society B: Physical Organic* **1966**, 849-852.

30. Fuchs, E.; Heusinger, H., Sonolysis and radiolysis of glyceraldehyde in deaerated aqueous solution. *Ultrason. Sonochem.* **1995,** *2*, (2), S105-S109.

31. Warneck, P., Multi-Phase Chemistry of C2 and C3 Organic Compounds in the Marine Atmosphere. *Journal of Atmospheric Chemistry* **2005,** *51*, (2), 119-159.

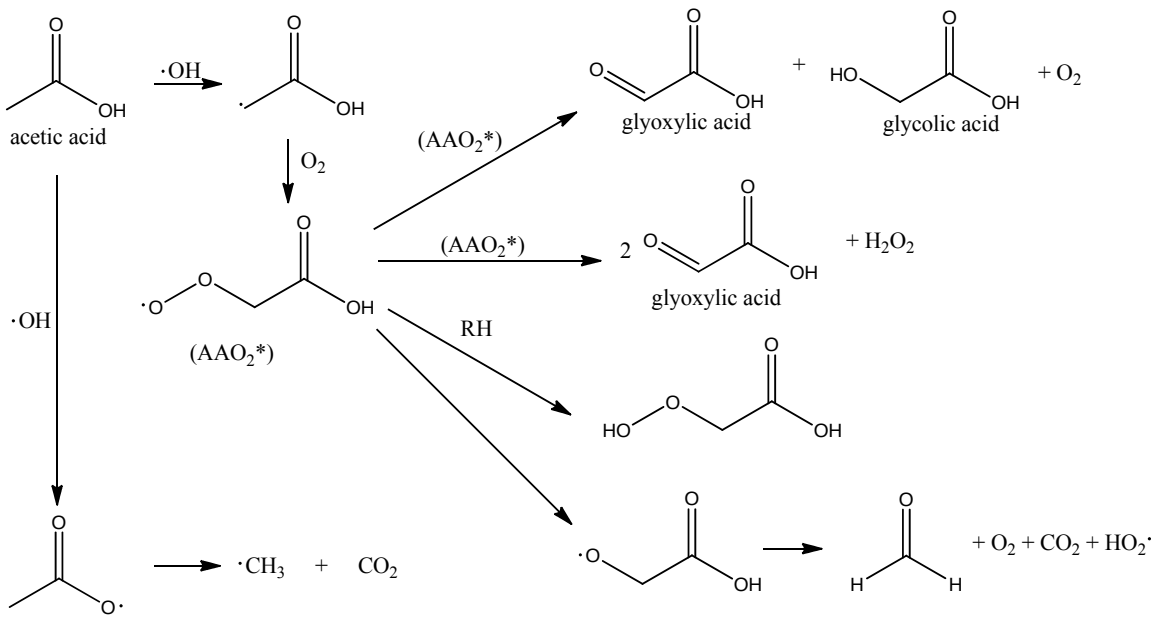

Scheme 4-1. Oxidation of acetic acid by OH radical.

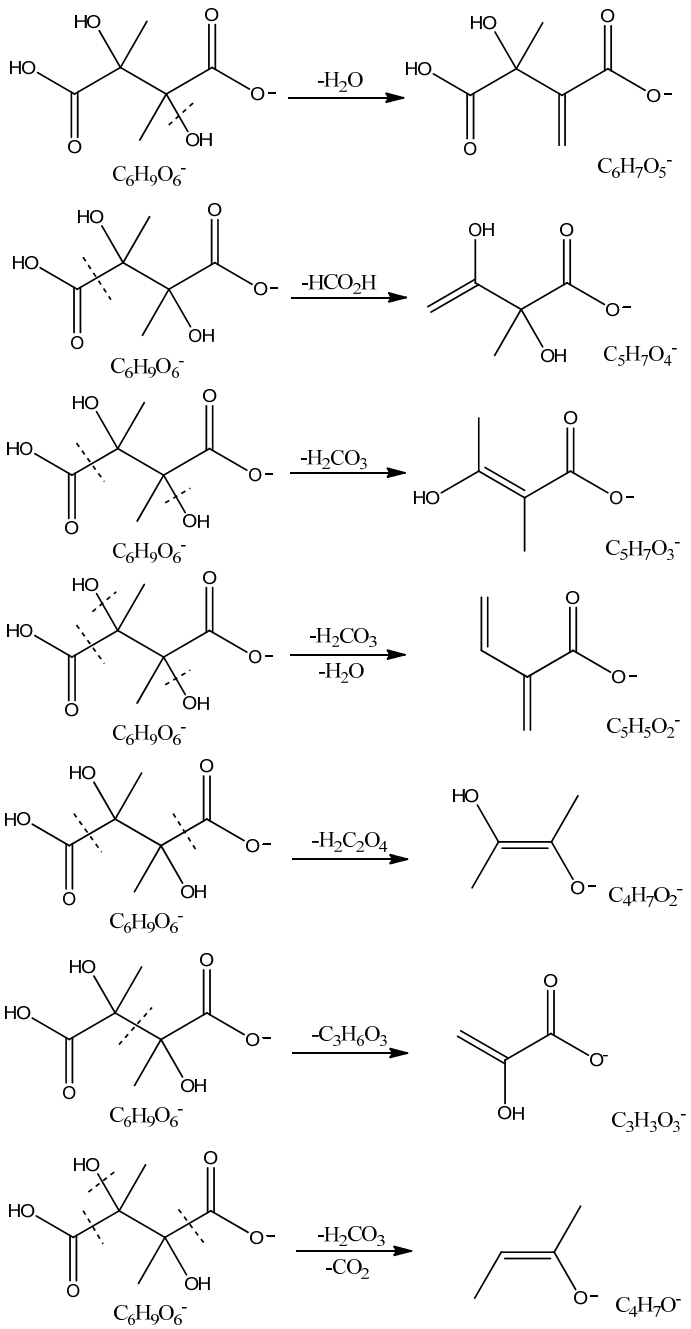

Scheme 4-2. Proposed structures of $C_6H_9O_6^-$ and fragment ions of $C_6H_9O_6^-$ in FT-ICR MS/MS.

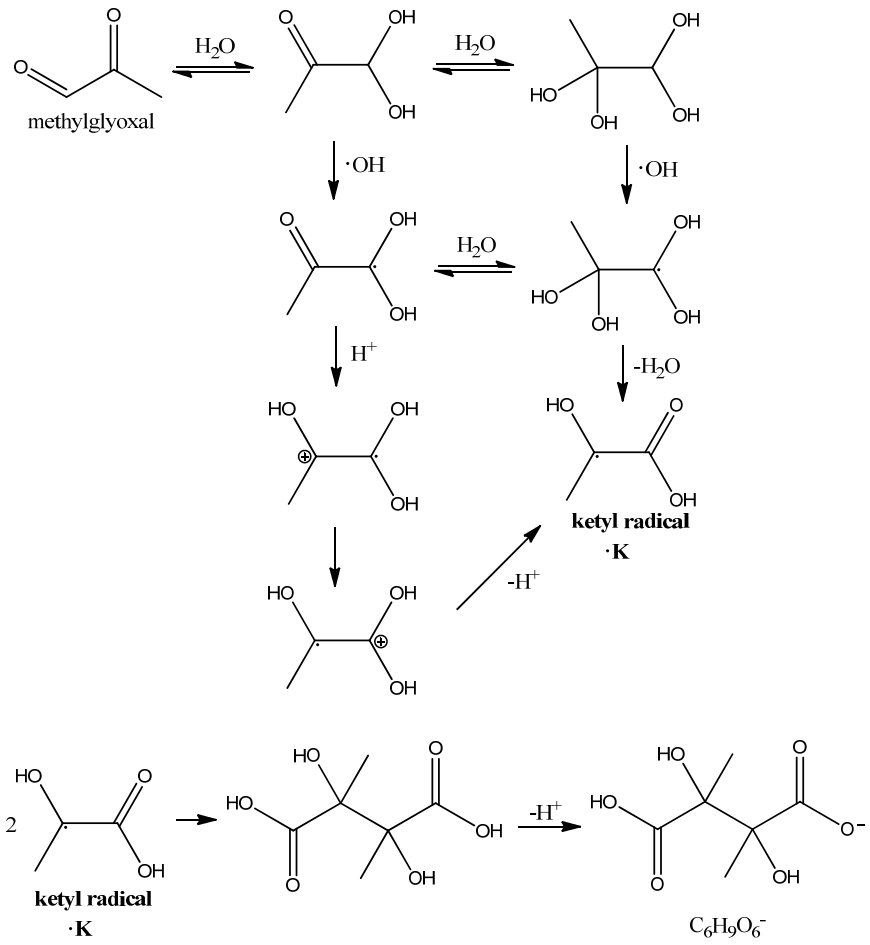

Scheme 4-3. The formation of ketyl radical (·K) and $C_6H_9O_6^-$ from OH radical oxidation of hydrated methylglyoxal.

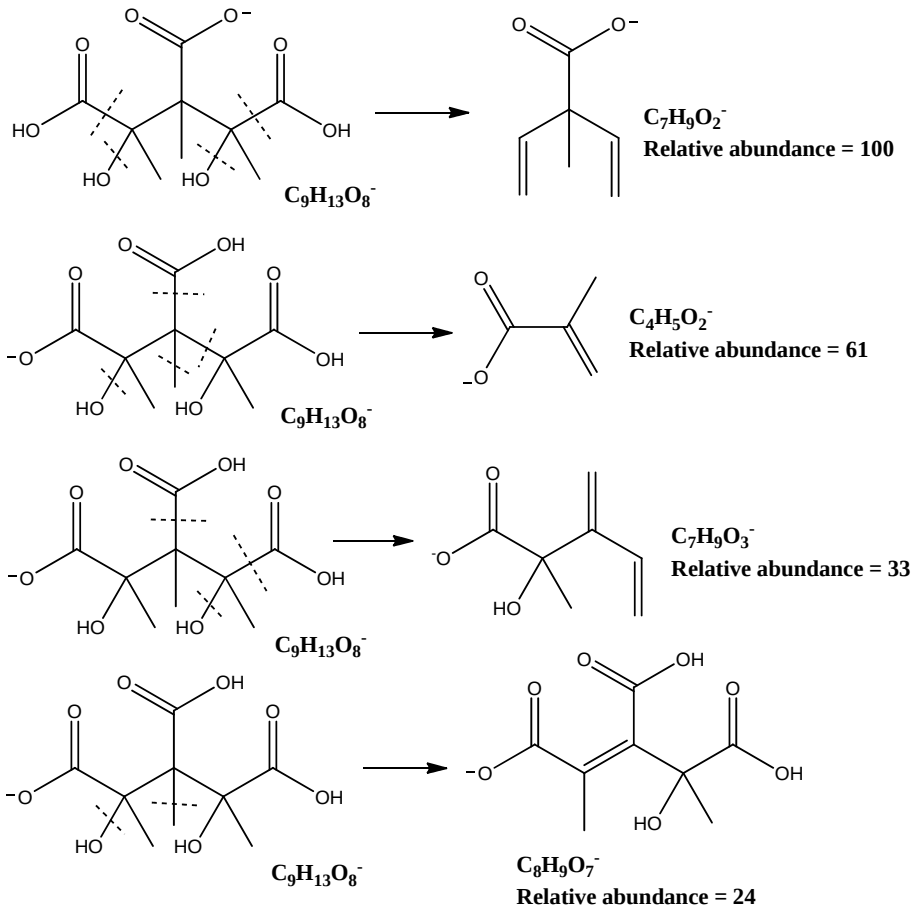

Scheme 4-4. Proposed structures of $C_9H_{13}O_8^-$ (m/z$^-$ 249 in ESI-MS) and some fragment ions of $C_9H_{13}O_8^-$ in FT-ICR MS/MS.

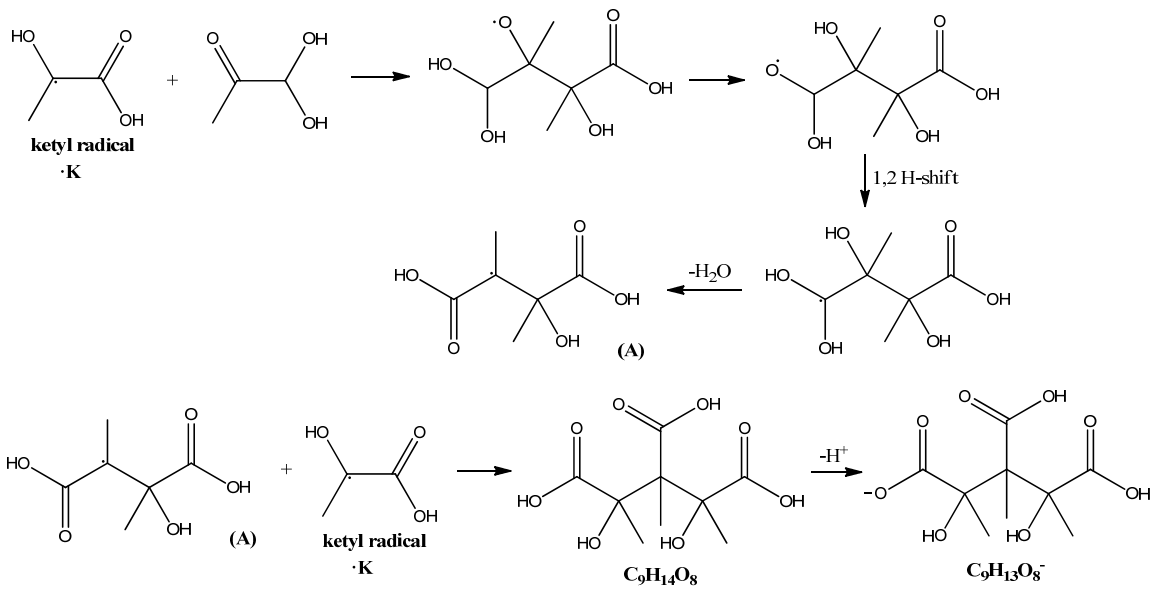

Scheme 4-5. The formation of $C_9H_{13}O_8^-$ from radical-radical reactions.

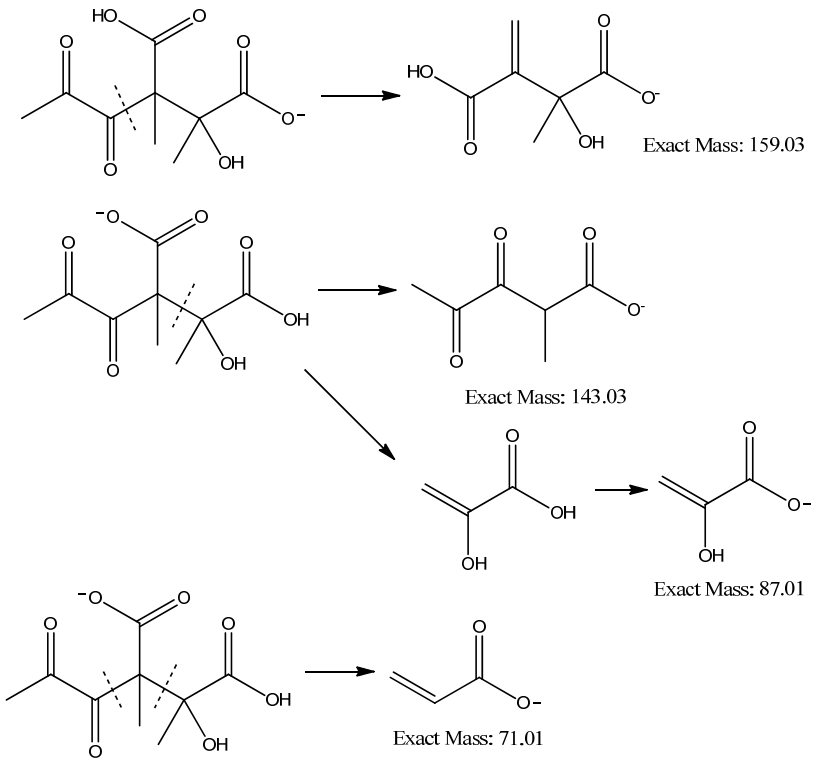

Scheme 4-6. The structure of $C_9H_{12}O_7^-$ (m/z$^-$ 231 in ESI-MS) and major fragment ions of m/z$^-$ 231 in ESI-MS/MS. Note that chemical formulas of fragment ions were not determined by ESI-MS/MS.

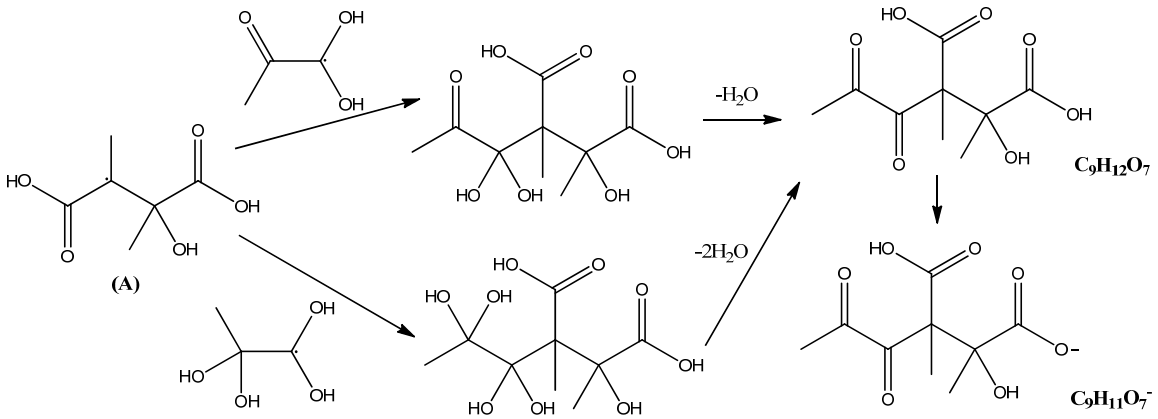

Scheme 4-7. The formation of $C_9H_{12}O_7^-$ from radical-radical reactions. Formation of (A) is shown in Scheme 5.

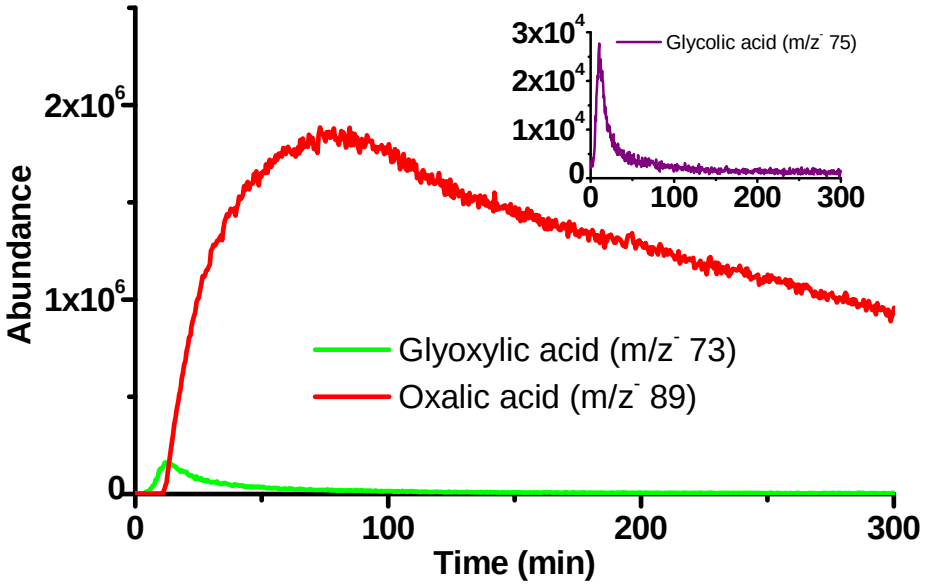

Figure 4-1. ESI-MS online analysis of 1 mM acetic acid + OH radical experiment.

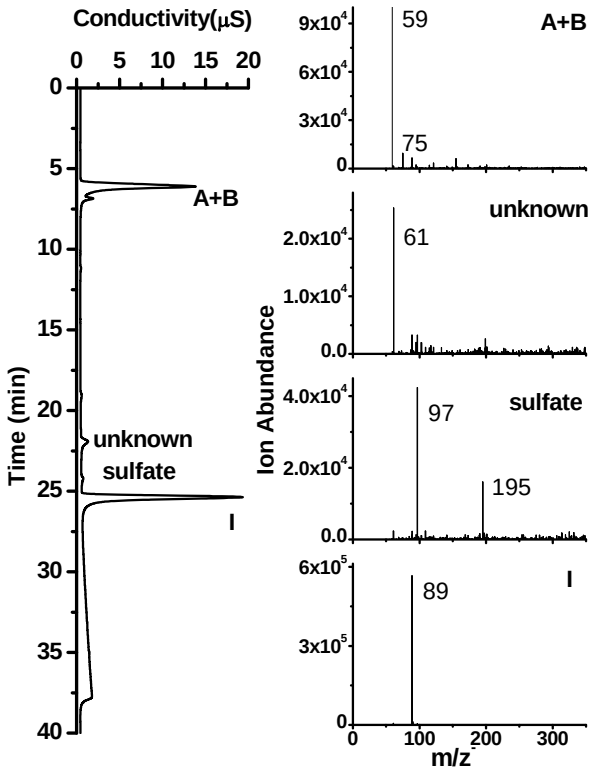

Fig. 4-2. IC-ESI-MS spectra of a sample taken from 1 mM acetic acid + OH radical batch reactions (120 minutes reaction time). (A+B) peak with the retention time of acetic acid (m/z$^-$ 59), glycolic acid (m/z$^-$ 75) and formic acid (not detected in ESI-MS), (sulfate) peak with the retention time of sulfate (As the peak area did not change with reaction time, sulfate present here could be contaminant), (I) oxalic acid (m/z$^-$ 89).

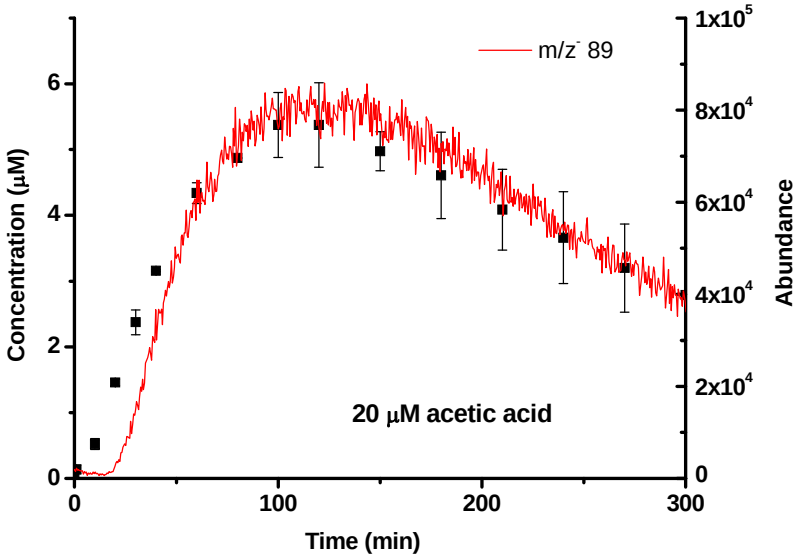

Fig. 4-3. Oxalic acid production from acetic acid (20 μM) + OH experiments. Ion abundance of oxalic acid (m/z⁻ 89) in the negative mode ESI-MS online experiment (red line), oxalic acid concentrations quantified by IC (black squares) are shown.

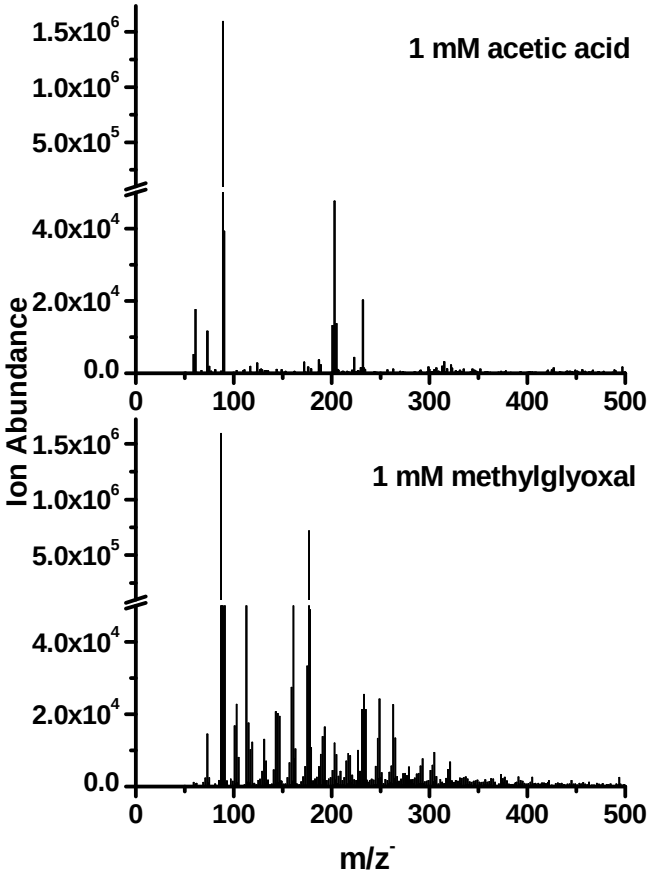

Fig. 4-4. ESI-MS spectra of a sample taken from 1 mM acetic acid + OH radical batch reactions (120 minutes reaction time) and a sample taken from 1 mM methylglyoxal + OH radical batch reactions (120 minutes reaction time).

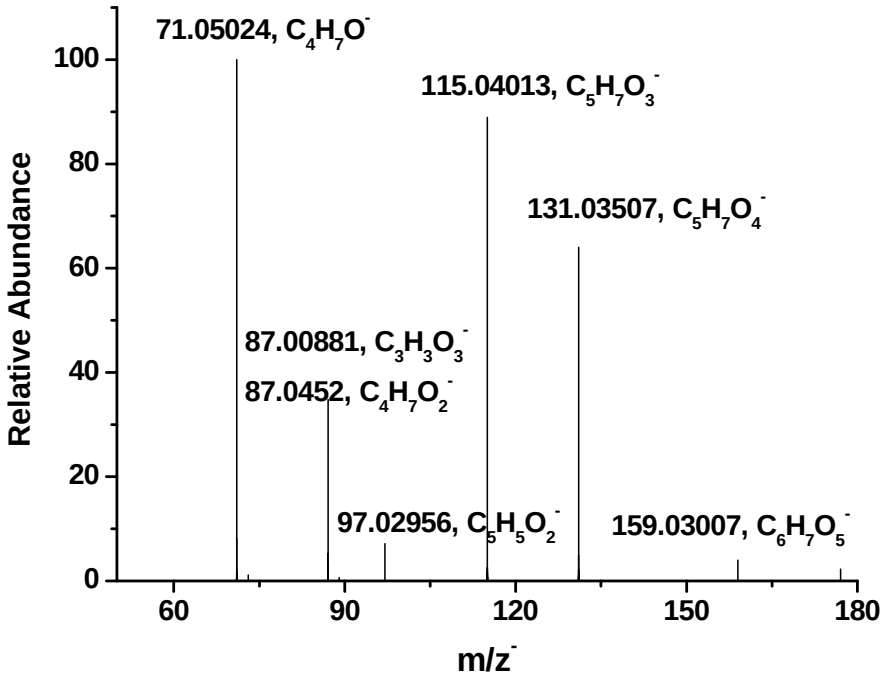

Fig. 4-5. FT-ICR MS-MS spectra of m/z$^-$ 177 from a sample taken from 1 mM methylglyoxal + OH radical batch reactions (76 minutes reaction time).

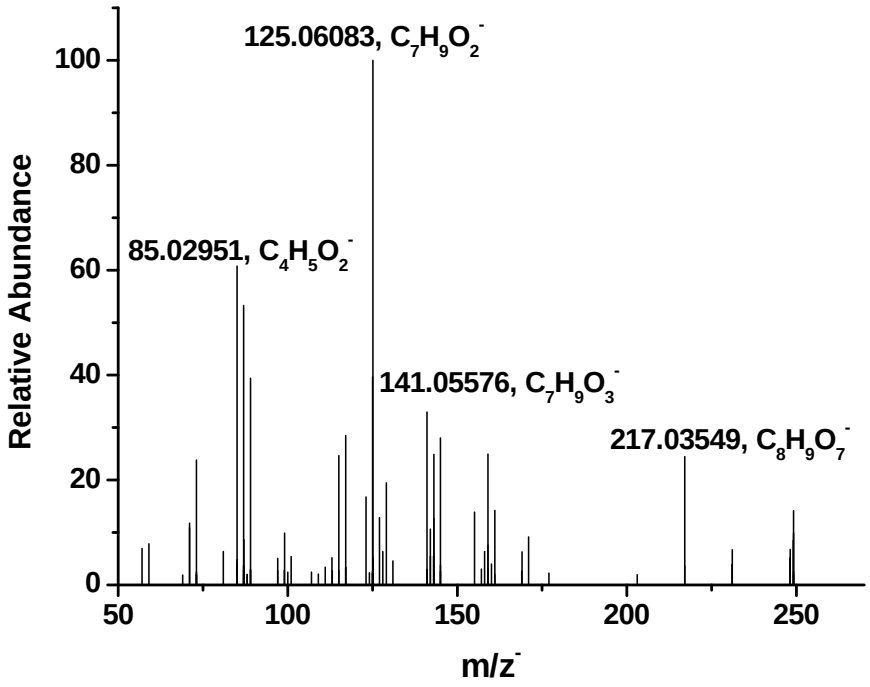

Fig. 4-6. FT-ICR MS-MS spectra of m/z$^-$ 249 from a sample taken from 1 mM methylglyoxal + OH radical batch reactions (76 minutes reaction time). A few major fragments are labeled here.

Chapter 5. Future Directions and Implications

5.1 Future Directions

This dissertation documents advancements in the understanding of SOA formation through aqueous phase reactions of dicarbonyls. However, large uncertainties about photochemical processes in the atmospheric aqueous phase remain. Many organic compounds measured in cloud and fog water are potential "aqueous" SOA precursors [1]. However, current laboratory studies have only examined a very limited number of precursors [2-14]. Many of these studies reveal that precursors are transformed by OH radicals more or less directly into carboxylic acids [2-4, 7-12]. Oxalic acid appears to be an often encountered end product apart from volatile CO_2, formic and acetic acids. Most studies also observe the formation of higher molecular weight compounds through photochemical reactions [2-14]. Oxalic acid and higher molecular weight compounds remain mostly in the particle phase after water evaporation [15-18]. Below I review the SOA forming potential of several of the most abundant organic compounds found in atmospheric waters.

5.1.1 Formaldehyde

Formaldehyde (HCHO) is one of the most abundant carbonyl compounds in the atmosphere [19-20]. It is directly emitted from biomass burning, incomplete combustion, industrial processes, and vegetation [21]. Formaldehyde also forms in the atmosphere from the reaction of most anthropogenic and biogenic hydrocarbons with the hydroxyl (OH) radical and ozone (O_3) [22]. Typical gas phase mixing ratios of formaldehyde vary from less than 100 pptv in the remote background atmosphere to several 10s of ppbv in polluted urban areas [20] and in air influenced by industrial emissions during summer

months [23]. Removal of formaldehyde occurs via reaction with OH radicals, photolysis, wet/dry deposition, and vapor exchange across the air–water interface [19]. Formaldehyde effectively partitions into water (Henry's law constant, $H^* = \sim 10^4$ M atm^{-1}[24]) and is one of the most abundant organic compounds found in cloud/fog water. Concentrations of HCHO measured in cloud/fog water samples vary from less than 0.1 μM to more than 200 μM [25].

Formaldehyde is immediately converted to methylene glycol ($CH_2(OH)_2$) with >99.9% efficiency in water [19]. The reaction between $CH_2(OH)_2$ and OH radicals proceeds via H atom abstraction to yield $\cdot CH(OH)_2$ radicals (Reaction 71, Table 5-1) [26]. At low concentrations, $\cdot CH(OH)_2$ radicals react with dissolved O_2 (saturated, ~270 μM) to give formic acid (Reaction 10, Table 5-1) and subsequently CO_2. I expect that this is the fate of formaldehyde in cloud water. However, concentrations of water soluble organic compounds (WSOCs) are high in aerosol water. Thus, in aerosol water, radical-radical reactions (Reaction 11, 19, 20, 28, 63, 64, Table 5-1) might be faster enough to compete with radical-O_2 reactions. Thus $\cdot CH(OH)_2$ radicals from hydrated formaldehyde could potentially contribute to "aqueous" SOA formation via radical-radical reactions in wet aerosols. Measurements in summer in Atlanta, Georgia indicated that the mass of dissolved formic acid in aerosol water (35 μg/m^3) was 5 μg/m^3 at a relative humidity (RH) of 90%, suggesting a concentration of 3 M if subsequent aqueous phase reactions are not considered [27]. Interestingly, hydrogen peroxide has also been measured in aerosol liquid water in much higher concentrations than expected from Henry's Law [28]. The same study found that the mean concentration of particle-phase WSOCs was 2.74 μg C/m^3 while the mean liquid water content was ~14 μg/m^3 (mean RH = 74.4%) during an

event. Assuming complete dissolution of WSOCs, this measurement corresponds to a concentration of 16 M. This is consistent with the fact that the solubilities of dicarboxylic acids in water are ~1 – 20 M [29]. Because organic solutes could form highly concentrated solutions (> 1M) in aerosol water, OH radical reactions and photolysis are expected to produce high organic radical concentrations. When organic radical concentrations reach ~5×10^{-7} M, the half life of $\cdot CH(OH)_2$ radical against radical-radical reactions (~1×10^{-3} s) becomes comparable with that against the reaction with dissolved oxygen (~5×10^{-4} s), suggesting that radical-radical reactions can be important in aerosol water even the solution is saturated with oxygen.

To investigate the fate of formaldehyde in atmospheric waters in the presence of OH radical, I performed the following simulations making use of the radical chemistry of Lim et al. [30], with the formation of $\cdot CH(OH)_2$ radical from hydrated formaldehyde added (reaction 71, Table 5-1). C3D denotes dimeric compounds with 3 carbons (e.g. tartronic and mesoxalic acids) in these reactions. C3D, together with glyoxylic and oxalic acids, are less volatile and contribute to SOA mass. The simulation starts with (a) 30 μM formaldehyde + 150 μM H_2O_2 + UV, (b) 3 M formaldehyde + 15 M H_2O_2 + UV, (c) 30 μM formaldehyde + 3 M glyoxal + 15 M H_2O_2 + UV and (d) 3 M glyoxal + 15 M H_2O_2 + UV. The UV photolysis of H_2O_2 is used to form OH radical. Simulation (a) represents cloud relevant conditions and assumes formaldehyde partitions according to Henry's law, simulation (b) considers the possibility that formaldehyde concentrations in wet aerosols might be much higher than expected from Henry's law, simulation (c) represents all WSOCs as if they are glyoxal and examines the effect of added formaldehyde, and simulation (d) is the control run for simulation (c). Simulation (c) uses glyoxal as a

surrogate for WSOCs in aerosols; which is reasonable because formaldehyde is usually found along with glyoxal, methylglyoxal and many other water soluble organic compounds in atmospheric waters [25], and glyoxal was detected in ambient aerosol samples [31-32]. OH radical concentrations in these simulations are 7×10^{-13} – 1×10^{-11} M. The total organic radical concentrations are always lower than 1×10^{-10} M in simulation (a) but can be higher than 1×10^{-6} M in other simulations, suggesting that radical-radical reactions are important in all simulations except simulation (a).

At cloud relevant conditions, formic acid is the major product and compounds with ≥2 carbons (e.g. glyoxal, oxalic and malonic acids) only form at trace concentrations (Fig. 5-1). Simulation (a) suggests that formaldehyde oxidation in clouds and fogs will not contribute to the global SOA burden significantly even considering its high abundance. At the elevated concentration (3 M), formic acid is still the most abundant oxidation product from formaldehyde, while the formation of compounds with ≥2 carbons becomes important (Fig. 5-2). The maximum concentrations of malonic (C_3) and oxalic (C_2) acids are ~0.1 M and ~0.04 M, respectively. If formaldehyde does in fact form a highly concentrated solution in aerosol water, aqueous oxidation of formaldehyde could effectively produce SOA. While particulate measurements of formaldehyde are quite uncertain, it is well accepted that the total aqueous concentration of organics in aerosol water is quite high. The addition of 30 μM formaldehyde to the WSOC surrogate (glyoxal) had little effect on product formation compared to the glyoxal only simulation (Fig. 5-3). The differences in concentrations are minimal (<0.01%) between simulation (c) and (d) for all simulated species and are not explained by formaldehyde chemistry alone. Due to the uncertainty associated with formaldehyde concentrations in aerosol

water, the role of formaldehyde in aqueous SOA formation is still unclear and needs further investigation.

5.1.2 Acetaldehyde

The largest source of acetaldehyde is atmospheric oxidation of alkanes, alkenes, and ethanol (128 Tg a^{-1}) [33]. Ocean emission is the second largest global acetaldehyde source (57 Tg a^{-1}) [33]. Other minor sources include emissions from decaying plants (23 Tg a^{-1}), biomass burning (3 Tg a^{-1}) and direct anthropogenic emissions (2 Tg a^{-1}). In the gas phase, acetaldehyde is mainly destroyed by reaction with OH radicals and to a lesser content by photolysis [34]. Acetaldehyde is also widely found in cloud/fog water and in rainwater, but is less frequently quantified than formaldehyde. During the 2004 ICARTT intensive campaign, acetaldehyde was the most abundant carbonyl found in bulk cloud water samples after formaldehyde; it had an average concentration of 4.3 μM [35]. At cloud relevant conditions, previous results with other dicarbonyls have shown that radical-radical reactions are negligible and dilute aqueous chemistry models are capable of reproducing the oxidation of dicarbonyls [30, 36]. The OH radical oxidation of acetaldehyde will mainly produce acetic acid at low precursor concentrations [37-38]. Subsequent oxidation steps produce glyoxylic and oxalic acids. The following reaction from Warneck [38] is incorporated to the aqueous chemistry model used in Chapter 3 (Table 3-1):

$$CH_3CHO_{(aq)} + \cdot OH_{(aq)} (+ O_2) = CH_3COOH + HO_2 + H_2O \ (k_1 = 2.6\times10^9\ M^{-1}\ s^{-1}) \quad (A)$$

To simulate the oxidation of 4 μM acetaldehyde by OH radicals at an OH radical concentration concentration of 1×10^{-12} M. After a typical cloud cycle (~ 10 min), acetaldehyde has been depleted and the concentration of oxalic acid has reached 0.4 μM

(~1% molar yield) (Fig. 5-4). Because oxalic acid continues to form after acetaldehyde is depleted, the oxalic acid yield will be considerably higher after more cloud cycles (e.g. ~20% after 80 minutes of reaction). Since oxalate is largely found in the particle phase, acetaldehyde is a potential SOA precursor through cloud and fog processing.

5.1.3 Ethanol

Ethanol is another potential precursor to SOA formation through cloud processing [1]. Ethanol has been widely measured in urban (0.4 – 240 ppbv) [39-41], rural (0.04 – 0.4 ppbv) [42-44], and remote (0.02 – 0.2 ppbv) [34, 45] atmospheres. Important ethanol sources include industrial emissions, biofuel combustion, biogenic emissions, biomass burning and atmospheric oxidation of ethane by the OH radical [46-47]. The National Energy Policy Act of 2005 requires that nation-wide use of biofuels (mainly ethanol) must increase to 7.5 billion gallons or about 5% of total gasoline volume by 2012 [48]. Further increases in ethanol usage may substantially affect its global budget. Atmospheric sinks for ethanol include gas phase oxidation by OH radical (33.5 Tg a^{-1}, 77%), dry deposition (5 Tg a^{-1}, 11%), and wet deposition (5.2 Tg a^{-1}, 12%) [46]. The Henry's law coefficient of ethanol is ~194 M atm^{-1} at 298K [49]. Ethanol concentrations in 12 rainwater samples collected near Paris (France) ranged from <1 to 5 μM [50]. The major product in aqueous phase oxidation of ethanol by the OH radical is acetaldehyde [38, 51]:

$$C_2H_5OH_{(aq)} + \cdot OH_{(aq)} (+ O_2) = CH_3CHO + HO_2 + H_2O \ (k_2 = 2.1\times10^9\ M^{-1}\ s^{-1}) \quad (B)$$

Reaction (B) was added to the dilute aqueous chemistry model used in Section 5.1.2 to evaluate the SOA forming potential of ethanol at cloud-relevant conditions. For reasons explained previously, radical-radical reactions were neglected in the simulation of the dilute aqueous chemistry of ethanol. I simulated oxalic acid formation from the

oxidation of 4 μM ethanol by OH radicals at 1×10^{-12} M (Fig. 5-5). The oxalic acid molar yield is approximately 0.3% after 10 minutes of reaction and reaches ~17% after 80 minutes. Considering the large amount of ethanol removed by wet deposition, aqueous phase oxidation of ethanol may substantially contribute to the global oxalic acid and SOA budgets.

5.2 Summary and Implications

Due to the lack of knowledge about the chemical and physical processes associated with SOA formation, a quantitative and predictive evaluation of the impact of SOA on the environment, climate and human health is a major research challenge in atmospheric science [52-53]. Discoveries in this dissertation lead to an improved understanding of SOA formation through aqueous-phase reactions in the atmosphere. Although the formation of lower volatility products (e.g., oxalic acid and oligomers) formed from aqueous OH radical oxidation of glyoxal and methylglyoxal was previously demonstrated, this is the first study of product formation from these dicarbonyls at cloud relevant conditions. This dissertation demonstrates that carboxylic acids are major oxidation products; sulfuric acid shows little effect on product formation, and a dilute aqueous chemistry model can successfully reproduce product formation for both glyoxal and methylglyoxal at cloud relevant concentrations. The validation of dilute aqueous chemistry mechanisms for use in chemical transport models is an important outcome of this research.

Experiments conducted at increasing concentrations have provided insights into aqueous chemistry in aerosol water where organic concentrations are quite high (potentially > 1M, [27, 54-55]). Measurements deviated from predictions at elevated

concentrations. As the starting concentration of the dicarbonyl precursor increases, products with higher carbon numbers than the precursor form increasingly; suggesting that radical-radical reactions become increasingly important. This work also suggest that radical-radical reactions could be more important than non-radical reactions during the daytime (e.g. esterification, aldol condensation and acetal/hemicacetal formation) because they are faster [30, 56-57]. Making use of the findings in Chapter 2, Lim et al. [30] concluded that aqueous phase SOA formation in wet aerosols is better described by detailed radical chemistry that includes both radical-O_2 and radical-radical reactions; they predict that higher molecular weight compounds will be the predominant products from OH radical oxidation of glyoxal in wet aerosols, while traditional cloud processing of glyoxal would mostly yield oxalic acid [30]. An independent yet concurrent modeling study concluded that glyoxal processing in wet aerosols could produce SOA more effectively than traditional cloud processing [58].

This dissertation has made important contributions to the growing recognition that condensed phase radical-radical chemistry is important to SOA formation [30, 36, 58-61]. Higher molecular weight compounds, called humic like substances (HULIS), are often detected in ambient atmospheric aerosols, cloud and fog water [16-18, 62-64]. 9-30% of the total organic carbon in aerosol samples collected at downtown Zurich, Switzerland is HULIS [65]. It is now widely anticipated that atmospheric HULIS are predominantly associated with secondary formation in the particle phase, although primary emissions (e.g. wood combustion and soil) clearly also contribute [53, 66]. Aqueous radical-radical reactions at the high organic concentrations found in aerosol water provide a satisfactory explanation for the observation that HULIS are a major component of organic aerosols.

To the best of my knowledge, this work provides the first direct laboratory evidence of oxalic acid formation from acetic acid at atmospherically relevant conditions. Acetic acid has not previously been identified as an SOA precursor. Acetic acid is one of the most abundant non-methane organic compounds found in the atmosphere and is ubiquitously found in cloud water [19, 67]. Though oxalic acid yields from acetic acid are low compared to those from glyoxal, the higher abundance of acetic acid makes it a potentially important SOA source. Formaldehyde is unlikely to be an important SOA precursor unless its concentrations in aerosol water are much higher than predicted by Henry's Law. Ethanol and acetaldehyde could be increasingly important precursors because cloud processing of these compounds may effectively produce oxalic acid and their atmospheric abundances are expected to rise (Table 5-2). These predictions warrant further laboratory investigation including in aerosol water. In order to evaluate the regional and global magnitude of "aqueous" SOA, this chemistry must be incorporated into chemical transport models. This process has already begun [58, 68-70]. This dissertation plays an important role in validating and refining the chemistry underlying these modeling activities.

The aqueous phase reactions investigated here produce products with high O/C ratios. The O/C ratios of simple dicarboxylic acids identified in this work range from 1.0 – 2.0; the higher molecular weight products also have O/C ratios ~1.0 [36]. Aiken et al. (2008) observed O/C ratios of 0.83 – 1.02 and 0.52 – 0.64 for aged regional OA and freshly produced ambient SOA, respectively; whereas the O/C ratio of SOA produced from "traditional" precursors (α-pinene, aromatics, isoprene) in high concentration smog chamber experiments was in the range 0.27–0.43 [71]. Lim et al. (2010) note that

aqueous phase oxidation in wet aerosols is a potential explanation for the high O/C ratios observed in aged aerosols [30].

5.3 Reference

1. Blando, J. D.; Turpin, B. J., Secondary organic aerosol formation in cloud and fog droplets: A literature evaluation of plausibility. *Atmos. Environ.* **2000,** *34*, 1623-1632.

2. Carlton, A. G.; Turpin, B. J.; Altieri, K. E.; Seitzinger, S.; Reff, A.; Lim, H.-J.; Ervens, B., Atmospheric oxalic acid and SOA production from glyoxal: Results of aqueous photooxidation experiments. *Atmospheric Environment* **2007,** *41*, (35), 7588-7602.

3. Altieri, K. E.; Carlton, A. G.; Lim, H.-J.; Turpin, B. J.; Seitzinger, S. P., Evidence for Oligomer Formation in Clouds: Reactions of Isoprene Oxidation Products. *Environmental Science & Technology* **2006,** *40*, (16), 4956-4960.

4. Carlton, A. G.; Turpin, B. J.; Lim, H.-J.; Altieri, K. E.; Seitzinger, S., Link between isoprene and secondary organic aerosol (SOA): Pyruvic acid oxidation yields low volatility organic acids in clouds. *Geophys. Res. Lett.* **2006,** *33*, L06822, doi:10.1029/2005GL025374.

5. Guzman, M. I.; Colussi, A. J.; Hoffmann, M. R., Photoinduced Oligomerization of Aqueous Pyruvic Acid. *The Journal of Physical Chemistry A* **2006,** *110*, (10), 3619-3626.

6. Grgic, I.; Nieto-Gligorovski, L. I.; Net, S.; Temime-Roussel, B.; Gligorovski, S.; Wortham, H., Light induced multiphase chemistry of gas-phase ozone on aqueous pyruvic and oxalic acids. *Physical Chemistry Chemical Physics* **2010,** *12*, (3), 698-707.

7. Liu, Y.; El Haddad, I.; Scarfogliero, M.; Nieto-Gligorovski, L.; Temime-Roussel, B.; Quivet, E.; Marchand, N.; Picquet-Varrault, B.; Monod, A., In-cloud processes of methacrolein under simulated conditions – Part 1: Aqueous phase photooxidation. *Atmos. Chem. Phys.* **2009,** *9*, (14), 5093-5105.

8. Altieri, K. E.; Seitzinger, S. P.; Carlton, A. G.; Turpin, B. J.; Klein, G. C.; Marshall, A. G., Oligomers formed through in-cloud methylglyoxal reactions: Chemical composition, properties, and mechanisms investigated by ultra-high resolution FT-ICR mass spectrometry. *Atmospheric Environment* **2008,** *42*, (7), 1476-1490.

9. Perri, M. J.; Seitzinger, S.; Turpin, B. J., Secondary organic aerosol production from aqueous photooxidation of glycolaldehyde: Laboratory experiments. *Atmospheric Environment* **2009,** *43*, (8), 1487-1497.

10. Poulain, L.; Monod, A.; Wortham, H., Development of a new on-line mass spectrometer to study the reactivity of soluble organic compounds in the aqueous phase under tropospheric conditions: Application to OH-oxidation of N-methylpyrrolidone. *Journal of Photochemistry and Photobiology A: Chemistry* **2007,** *187*, (1), 10-23.

11. El Haddad, I.; Liu, Y.; Nieto-Gligorovski, L.; Michaud, V.; Temime-Roussel, B.; Quivet, E.; Marchand, N.; Sellegri, K.; Monod, A., In-cloud processes of methacrolein under simulated conditions – Part 2: Formation of secondary organic aerosol. *Atmos. Chem. Phys.* **2009,** *9*, (14), 5107-5117.

12. Gelencsér, A.; Hoffer, A.; Kiss, G.; Tombácz, E.; Kurdi, R.; Bencze, L., In-situ Formation of Light-Absorbing Organic Matter in Cloud Water. *Journal of Atmospheric Chemistry* **2003,** *45*, (1), 25-33.

13. Hoffer, A.; Kiss, G.; Blazso, M.; Gelencser, A., Chemical characterization of humic-like substances (HULIS) formed from a lignin-type precursor in model cloud water. *Geophys. Res. Lett.* **2004,** *31*, (6), L06115, doi:10.1029/2003GL018962.

14. Holmes, B. J.; Petrucci, G. A., Water-Soluble Oligomer Formation from Acid-Catalyzed Reactions of Levoglucosan in Proxies of Atmospheric Aqueous Aerosols. *Environmental Science & Technology* **2006,** *40*, (16), 4983-4989.

15. Limbeck, A.; Puxbaum, H.; Otter, L.; Scholes, M. C., Semivolatile behavior of dicarboxylic acids and other polar organic species at a rural background site (Nylsvley, RSA) *Atmos. Environ.* **2001,** *35*, 1853-1862.

16. Havers, N.; Burba, P.; Lambert, J.; Klockow, D., Spectroscopic Characterization of Humic-Like Substances in Airborne Particulate Matter. *Journal of Atmospheric Chemistry* **1998,** *29*, (1), 45-54.

17. Zappoli, S.; Andracchio, A.; Fuzzi, S.; Facchini, M. C.; Gelencser, A.; Kiss, G.; Krivacsy, Z.; Molnar, A.; Meszaros, E.; Hansson, H.-C.; Rosman, K.; Zebuhr, Y., Inorganic, organic, and Macromolecular Components of Fine Aerosol in Different Areas of Europe in Relation to their Water Solubility. *Atmospheric Environment* **1999,** *33*, 2733-2743.

18. Kiss, G.; Varga, B.; Galambos, I.; Ganszky, I., Characterization of water-soluble organic matter isolated from atmospheric fine aerosol. *Journal of Geophysical Research-Atmospheres* **2002,** *107*, (D21), 8339, doi:10.1029/2001JD000603.

19. Seinfeld, J. H.; Pandis, S. N., *Atmospheric Chemistry and Physics - From Air Pollution to Climate Change (2nd Edition)*. John Wiley and Sons, Inc.: New York, 2006.

20. Dasgupta, P. K.; Li, J.; Zhang, G.; Luke, W. T.; McClenny, W. A.; Stutz, J.; Fried, A., Summertime Ambient Formaldehyde in Five U.S. Metropolitan Areas: Nashville, Atlanta, Houston, Philadelphia, and Tampa. *Environmental Science & Technology* **2005,** *39*, (13), 4767-4783.

21. Carlier, P.; Hannachi, H.; Mouvier, G., The chemistry of carbonyl compounds in the atmosphere--A review. *Atmospheric Environment (1967)* **1986,** *20*, (11), 2079-2099.

22. Stavrakou, T.; Müller, J. F.; De Smedt, I.; Van Roozendael, M.; van der Werf, G. R.; Giglio, L.; Guenther, A., Global emissions of non-methane hydrocarbons deduced from SCIAMACHY formaldehyde columns through 2003–2006. *Atmos. Chem. Phys.* **2009,** *9*, (11), 3663-3679.

23. Wert, B. P.; Trainer, M.; Fried, A.; Ryerson, T. B.; Henry, B.; Potter, W.; Angevine, W. M.; Atlas, E.; Donnelly, S. G.; Fehsenfeld, F. C.; Frost, G. J.; Goldan, P. D.; Hansel, A.; Holloway, J. S.; Hubler, G.; Kuster, W. C.; Nicks, D. K., Jr.; Neuman, J. A.; Parrish, D. D.; Schauffler, S.; Stutz, J.; Sueper, D. T.; Wiedinmyer, C.; Wisthaler, A., Signatures of terminal alkene oxidation in airborne formaldehyde measurements during TexAQS 2000. *J. Geophys. Res.* **2003,** *108*, (D3), 4104.

24. Zhou, X.; Mopper, K., Apparent partition coefficients of 15 carbonyl compounds between air and seawater and between air and freshwater; implications for air-sea exchange. *Environmental Science & Technology* **1990,** *24*, (12), 1864-1869.

25. Munger, J. W.; Jacob, D. J.; Daube, B. C.; Horowitz, L. W.; Keene, W. C.; Heikes, B. G., Formaldehyde, glyoxal, and methylglyoxal in air and cloudwater at a rural mountain site in central Virginia. *J. Geophys. Res.* **1995,** *100*, (D5), 9325-9333.

26. Warneck, P., The relative importance of various pathways for the oxidation of sulfur dioxide and nitrogen dioxide in sunlit continental fair weather clouds. *Physical Chemistry Chemical Physics* **1999,** *1*, (24), 5471-5483.

27. Hennigan, C. J.; Bergin, M. H.; Dibb, J. E.; Weber, R. J., Enhanced secondary organic aerosol formation due to water uptake by fine particles. *Geophys. Res. Lett.* **2008,** *35*, (18), L18801, doi:10.1029/2008GL035046.

28. Arellanes, C.; Paulson, S. E.; Fine, P. M.; Sioutas, C., Exceeding of Henry's Law by Hydrogen Peroxide Associated with Urban Aerosols. *Environmental Science & Technology* **2006,** *40*, (16), 4859-4866.

29. Clegg, S. L.; Seinfeld, J. H., Thermodynamic Models of Aqueous Solutions Containing Inorganic Electrolytes and Dicarboxylic Acids at 298.15 K. 1. The Acids as Nondissociating Components. *The Journal of Physical Chemistry A* **2006,** *110*, (17), 5692-5717.

30. Lim, Y. B.; Tan, Y.; Perri, M. J.; Seitzinger, S. P.; Turpin, B. J., Aqueous chemistry and its role in secondary organic aerosol (SOA) formation. *Atmos. Chem. Phys. Discuss.* **2010,** *10*, (6), 14161-14207.

31. Kawamura, K.; Yasui, O., Diurnal changes in the distribution of dicarboxylic acids, ketocarboxylic acids and dicarbonyls in the urban Tokyo atmosphere. *Atmospheric Environment* **2005,** *39*, (10), 1945-1960.

32. Ho, K. F.; Cao, J. J.; Lee, S. C.; Kawamura, K.; Zhang, R. J.; Chow, J. C.; Watson, J. G., Dicarboxylic acids, ketocarboxylic acids, and dicarbonyls in the urban atmosphere of China. *J. Geophys. Res.* **2007,** *112*, (D22), D22S27.

33. Millet, D. B.; Guenther, A.; Siegel, D. A.; Nelson, N. B.; Singh, H. B.; de Gouw, J. A.; Warneke, C.; Williams, J.; Eerdekens, G.; Sinha, V.; Karl, T.; Flocke, F.; Apel, E.; Riemer, D. D.; Palmer, P. I.; Barkley, M., Global atmospheric budget of acetaldehyde: 3-D model analysis and constraints from in-situ and satellite observations. *Atmos. Chem. Phys.* **2010,** *10*, (7), 3405-3425.

34. Singh, H. B.; Salas, L. J.; Chatfield, R. B.; Czech, E.; Fried, A.; Walega, J.; Evans, M. J.; Field, B. D.; Jacob, D. J.; Blake, D.; Heikes, B.; Talbot, R.; Sachse, G.; Crawford, J. H.; Avery, M. A.; Sandholm, S.; Fuelberg, H., Analysis of the atmospheric distribution, sources, and sinks of oxygenated volatile organic chemicals based on measurements over the Pacific during TRACE-P. *J. Geophys. Res.* **2004,** *109*, (D15), D15S07.

35. Li, S.-M.; Macdonald, A. M.; Leithead, A.; Leaitch, W. R.; Gong, W.; Anlauf, K. G.; Toom-Sauntry, D.; Hayden, K.; Bottenheim, J.; Wang, D., Investigation of carbonyls in cloudwater during ICARTT. *J. Geophys. Res.* **2008,** *113*, (D17), D17206.

36. Tan, Y.; Perri, M. J.; Seitzinger, S. P.; Turpin, B. J., Effects of Precursor Concentration and Acidic Sulfate in Aqueous Glyoxal-OH Radical Oxidation and Implications for Secondary Organic Aerosol. *Environmental Science & Technology* **2009,** *43*, (21), 8105-8112.

37. Schuchmann, M. N.; Von Sonntag, C., The rapid hydration of the acetyl radical. A pulse radiolysis study of acetaldehyde in aqueous solution. *Journal of the American Chemical Society* **1988,** *110*, (17), 5698-5701.

38. Warneck, P., Multi-phase chemistry of C2 and C3 organic compounds in the marine atmosphere. *J. Atmos. Chem.* **2005,** *51*, 119-159.

39. Grosjean, E.; Grosjean, D.; Gunawardena, R.; Rasmussen, R. A., Ambient Concentrations of Ethanol and Methyl tert-Butyl Ether in Porto Alegre, Brazil, March 1996−April 1997. *Environmental Science & Technology* **1998,** *32*, (6), 736-742.

40. Nguyen, H. T.-H.; Takenaka, N.; Bandow, H.; Maeda, Y.; de Oliva, S. T.; Botelho, M. M. f.; Tavares, T. M., Atmospheric alcohols and aldehydes concentrations measured in Osaka, Japan and in Sao Paulo, Brazil. *Atmospheric Environment* **2001,** *35*, (18), 3075-3083.

41. Millet, D. B.; Donahue, N. M.; Pandis, S. N.; Polidori, A.; Stanier, C. O.; Turpin, B. J.; Goldstein, A. H., Atmospheric volatile organic compound measurements during the Pittsburgh Air Quality Study: Results, interpretation, and quantification of primary and secondary contributions. *J. Geophys. Res.* **2005,** *110*, (D7), D07S07.

42. Millet, D. B.; Goldstein, A. H.; Allan, J. D.; Bates, T. S.; Boudries, H.; Bower, K. N.; Coe, H.; Ma, Y.; McKay, M.; Quinn, P. K.; Sullivan, A.; Weber, R. J.; Worsnop, D. R., Volatile organic compound measurements at Trinidad Head, California, during ITCT 2K2: Analysis of sources, atmospheric composition, and aerosol residence times. *J. Geophys. Res.* **2004,** *109*, (D23), D23S16.

43. Millet, D. B.; Goldstein, A. H.; Holzinger, R.; Williams, B. J.; Allan, J. D.; Jimenez, J. L.; Worsnop, D. R.; Roberts, J. M.; White, A. B.; Hudman, R. C.; Bertschi, I. T.; Stohl, A., Chemical characteristics of North American surface layer outflow: Insights from Chebogue Point, Nova Scotia. *J. Geophys. Res.* **2006,** *111*, (D23), D23S53.

44. Balzani Lööv, J. M.; Henne, S.; Legreid, G.; Staehelin, J.; Reimann, S.; Prévôt, A. S. H.; Steinbacher, M.; Vollmer, M. K., Estimation of background concentrations of trace gases at the Swiss Alpine site Jungfraujoch (3580 m asl). *J. Geophys. Res.* **2008,** *113*, (D22), D22305.

45. Singh, H.; Chen, Y.; Staudt, A.; Jacob, D.; Blake, D.; Heikes, B.; Snow, J., Evidence from the Pacific troposphere for large global sources of oxygenated organic compounds. *Nature* **2001,** *410*, (6832), 1078-1081.

46. Naik, V.; Fiore, A. M.; Horowitz, L. W.; Singh, H. B.; Wiedinmyer, C.; Guenther, A.; de Gouw, J. A.; Millet, D. B.; Goldan, P. D.; Kuster, W. C.; Goldstein, A., Observational constraints on the global atmospheric budget of ethanol. *Atmos. Chem. Phys.* **2010,** *10*, (12), 5361-5370.

47. Ban-Weiss, G. A.; McLaughlin, J. P.; Harley, R. A.; Kean, A. J.; Grosjean, E.; Grosjean, D., Carbonyl and Nitrogen Dioxide Emissions From Gasoline- and Diesel-Powered Motor Vehicles. *Environmental Science & Technology* **2008,** *42*, (11), 3944-3950.

48. Farrell, A. E.; Plevin, R. J.; Turner, B. T.; Jones, A. D.; O'Hare, M.; Kammen, D. M., Ethanol Can Contribute to Energy and Environmental Goals. *Science* **2006,** *311*, (5760), 506-508.

49. Warneck, P., A note on the temperature dependence of Henry's Law coefficients for methanol and ethanol. *Atmospheric Environment* **2006,** *40*, (37), 7146-7151.

50. Monod, A.; Bonnefoy, N.; Kaluzny, P.; Denis, I.; Foster, P.; Carlier, P., Methods for sampling and analysis of tropospheric ethanol in gaseous and aqueous phases. *Chemosphere* **2003,** *52*, (8), 1307-1319.

51. Monod, A.; Poulain, L.; Grubert, S.; Voisin, D.; Wortham, H., Kinetics of OH-initiated oxidation of oxygenated organic compounds in the aqueous phase: new rate constants, structure-activity relationships and atmospheric implications. *Atmospheric Environment* **2005,** *39*, (40), 7667-7688.

52. Kanakidou, M.; Seinfeld, J. H.; Pandis, S. N.; Barnes, I.; Dentener, F. J.; Facchini, M. C.; Van Dingenen, R.; Ervens, B.; Nenes, A.; Nielsen, C. J.; Swietlicki, E.; Putaud, J. P.; Balkanski, Y.; Fuzzi, S.; Horth, J.; Moortgat, G. K.; Winterhalter, R.; Myhre, C. E. L.; Tsigaridis, K.; Vignati, E.; Stephanou, E. G.; Wilson, J., Organic aerosol and global climate modelling: a review. *Atmos. Chem. Phys.* **2005,** *5*, 1053-1123.

53. Hallquist, M.; Wenger, J. C.; Baltensperger, U.; Rudich, Y.; Simpson, D.; Claeys, M.; Dommen, J.; Donahue, N. M.; George, C.; Goldstein, A. H.; Hamilton, J. F.; Herrmann, H.; Hoffmann, T.; Iinuma, Y.; Jang, M.; Jenkin, M. E.; Jimenez, J. L.; Kiendler-Scharr, A.; Maenhaut, W.; McFiggans, G.; Mentel, T. F.; Monod, A.; Prévôt, A. S. H.; Seinfeld, J. H.; Surratt, J. D.; Szmigielski, R.; Wildt, J., The formation, properties

and impact of secondary organic aerosol: current and emerging issues. *Atmos. Chem. Phys.* **2009,** *9*, (14), 5155-5236.

54. Hennigan, C. J.; Bergin, M. H.; Russell, A. G.; Nenes, A.; Weber, R. J., Gas/particle partitioning of water-soluble organic aerosol in Atlanta. *Atmos. Chem. Phys.* **2009,** *9*, (11), 3613-3628.

55. Hennigan, C. J.; Bergin, M. H.; Weber, R. J., Correlations between Water-Soluble Organic Aerosol and Water Vapor: A Synergistic Effect from Biogenic Emissions? *Environmental Science & Technology* **2008,** *42*, (24), 9079-9085.

56. Yasmeen, F.; Sauret, N.; Gal, J. F.; Maria, P. C.; Massi, L.; Maenhaut, W.; Claeys, M., Characterization of oligomers from methylglyoxal under dark conditions: a pathway to produce secondary organic aerosol through cloud processing during nighttime. *Atmos. Chem. Phys.* **2010,** *10*, (8), 3803-3812.

57. Volkamer, R.; Ziemann, P. J.; Molina, M. J., Secondary Organic Aerosol Formation from Acetylene (C2H2): seed effect on SOA yields due to organic photochemistry in the aerosol aqueous phase. *Atmos. Chem. Phys.* **2009,** *9*, (6), 1907-1928.

58. Ervens, B.; Volkamer, R., Glyoxal processing outside clouds: towards a kinetic modeling framework of secondary organic aerosol formation in aqueous particles. *Atmos. Chem. Phys. Discuss.* **2010,** *10*, (5), 12371-12431.

59. Sun, Y. L.; Zhang, Q.; Anastasio, C.; Sun, J., Insights into secondary organic aerosol formed via aqueous-phase reactions of phenolic compounds based on high resolution mass spectrometry. *Atmos. Chem. Phys.* **2010,** *10*, (10), 4809-4822.

60. Perri, M. J.; Lim, Y. B.; Seitzinger, S. P.; Turpin, B. J., Organosulfates from glycolaldehyde in aqueous aerosols and clouds: Laboratory studies. *Atmospheric Environment* **2010,** *44*, (21-22), 2658-2664.

61. Nozière, B.; Ekström, S.; Alsberg, T.; Holmström, S., Radical-initiated formation of organosulfates and surfactants in atmospheric aerosols. *Geophys. Res. Lett.* **2010,** *37*, (5), L05806.

62. Surratt, J. D.; Kroll, J. H.; Kleindienst, T. E.; Edney, E. O.; Claeys, M.; Sorooshian, A.; Ng, N. L.; Offenberg, J. H.; Lewandowski, M.; Jaoui, M.; Flagan, R. C.;

Seinfeld, J. H., Evidence for Organosulfates in Secondary Organic Aerosol. *Environmental Science & Technology* **2007,** *41*, (2), 517-527.

63. Altieri, K. E.; Turpin, B. J.; Seitzinger, S. P., Oligomers, organosulfates, and nitrooxy organosulfates in rainwater identified by ultra-high resolution electrospray ionization FT-ICR mass spectrometry. *Atmos. Chem. Phys.* **2009,** *9*, (7), 2533-2542.

64. Surratt, J. D.; Gómez-González, Y.; Chan, A. W. H.; Vermeylen, R.; Shahgholi, M.; Kleindienst, T. E.; Edney, E. O.; Offenberg, J. H.; Lewandowski, M.; Jaoui, M.; Maenhaut, W.; Claeys, M.; Flagan, R. C.; Seinfeld, J. H., Organosulfate Formation in Biogenic Secondary Organic Aerosol. *The Journal of Physical Chemistry A* **2008,** *112*, (36), 8345-8378.

65. Samburova, V.; Zenobi, R.; Kalberer, M., Characterization of high molecular weight compounds in urban atmospheric particles. *Atmos. Chem. Phys.* **2005,** *5*, (8), 2163-2170.

66. Gelencser, A.; Hoffer, A.; Krivacsy, Z.; Kiss, G.; Molnar, A.; Meszaros, E., On the possible origin of humic matter in fine continental aerosol. *J. Geophys. Res.* **2002,** *107*, 4137, doi:10.1029/2001JD001299.

67. Collett Jr, J. L.; Herckes, P.; Youngster, S.; Lee, T., Processing of atmospheric organic matter by California radiation fogs. *Atmospheric Research* **2008,** *87*, (3-4), 232-241.

68. Carlton, A. G.; Turpin, B. J.; Altieri, K. E.; Seitzinger, S. P.; Mathur, R.; Roselle, S. J.; Weber, R. J., CMAQ Model Performance Enhanced When In-Cloud Secondary Organic Aerosol is Included: Comparisons of Organic Carbon Predictions with Measurements. *Environ. Sci. Technol.* **2008,** *42*, (23), 8798-8802.

69. Fu, T.-M.; Jacob, D. J.; Wittrock, F.; Burrows, J. P.; Vrekoussis, M.; Henze, D. K., Global budgets of atmospheric glyoxal and methylglyoxal, and implications for formation of secondary organic aerosols. *J. Geophys. Res.* **2008,** *113*, D15303, doi:10.1029/2007JD009505.

70. Fu, T.-M.; Jacob, D. J.; Heald, C. L., Aqueous-phase reactive uptake of dicarbonyls as a source of organic aerosol over eastern North America. *Atmospheric Environment* **2009,** *43*, (10), 1814-1822.

71. Aiken, A. C.; DeCarlo, P. F.; Kroll, J. H.; Worsnop, D. R.; Huffman, J. A.; Docherty, K. S.; Ulbrich, I. M.; Mohr, C.; Kimmel, J. R.; Sueper, D.; Sun, Y.; Zhang, Q.; Trimborn, A.; Northway, M.; Ziemann, P. J.; Canagaratna, M. R.; Onasch, T. B.; Alfarra, M. R.; Prevot, A. S. H.; Dommen, J.; Duplissy, J.; Metzger, A.; Baltensperger, U.; Jimenez, J. L., O/C and OM/OC Ratios of Primary, Secondary, and Ambient Organic Aerosols with High-Resolution Time-of-Flight Aerosol Mass Spectrometry. *Environmental Science & Technology* **2008,** *42*, (12), 4478-4485.

72. Stavrakou, T.; Müller, J. F.; De Smedt, I.; Van Roozendael, M.; van der Werf, G. R.; Giglio, L.; Guenther, A., Evaluating the performance of pyrogenic and biogenic emission inventories against one decade of space-based formaldehyde columns. *Atmos. Chem. Phys.* **2009,** *9*, (3), 1037-1060.

73. Khare, P.; Kumar, N.; Kumari, K. M.; Srivastava, S. S., Atmospheric formic and acetic acids: An overview. *Rev. Geophys.* **1999,** *37*, (2), 227-248.

Table 5-1. Reactions and rate/equilibrium constants used in the kinetic model of formaldehyde ± glyoxal + OH reactions. Reactions 1 – 70 are taken from Lim et al. (2010) and reference therein. Reaction 71 is taken from Warneck (1999) [26].

	Reactions	**Rate constants (M^{1-n} s^{-1})**
1	$H_2O_2 \rightarrow 2OH$	1.1e-4
2	$OH + H_2O_2 \rightarrow HO_2 + H_2O$	2.7e7
3	$HO_2 + H_2O_2 \rightarrow OH + H_2O + O_2$	3.7
4	$2HO_2 \rightarrow H_2O_2 + O_2$	8.3e5
5	$OH + HO_2 \rightarrow H_2O + O_2$	7.1e9
6	$GLY + OH \rightarrow GLY^* + H_2O$	1.1e9
7	$GLY^* + O_2 \rightarrow GLYOO^*$	1.0e6
8	$GLYOO^* \rightarrow GLYAC + HO_2$	5.0e1
9	$2GLYOO^* \rightarrow 2CHOHOH + 2CO_2 + O_2 + 2H_2O$	3.0e8
10	$CHOHOH + O_2 \rightarrow HCO_2H + HO_2$	5.0e6
11	$GLY^* + CHOHOH \rightarrow C3D$	1.3e9
12	$GLY^* + GLY^* \rightarrow TA$	1.3e9
13	$GLYAC + OH \rightarrow GLYAC^* + H_2O$	3.62e8
14	$GLYAC^* + O_2 \rightarrow GLYACOO^*$	1.0e6
15	$GLYACOO^* \rightarrow OXLAC + HO_2$	5.0e1
16	$2GLYACOO^* \rightarrow 2CO_2 + 2COOH$	3.0e8
17	$COOH + O_2 \rightarrow CO_2 + H_2$	5.0e6
18	$GLY^* + COOH \rightarrow C3D$	1.3e9
19	$GLYAC^* + CHOHOH \rightarrow C3D$	1.3e9
20	$GLYAC^* + CHOHOH \rightarrow C3D$	1.3e9
21	$2GLYAC^* \rightarrow C4D$	1.3e9
22	$GLYAC^- + OH \rightarrow GLYAC^{*-} + H_2O$	2.9e9
23	$GLYAC^* + GLY^* \rightarrow C4D$	1.3e9
24	$GLYAC^{*-} + GLY^* \rightarrow C4D$	1.3e9
25	$GLYAC^{*-} + GLYAC^* \rightarrow C4D$	1.3e9
26	$2GLYAC^{*-} \rightarrow C3D$	1.3e9
27	$GLYA^{*-} + COOH \rightarrow C3D$	1.3e9
28	$GLYAC^{*-} + CHOHOH \rightarrow C3D$	1.3e9
29	$GLYAC^{*-} + O_2 \rightarrow GLYACOO^{*-}$	1.0e6
30	$GLYACOO^{*-} \rightarrow OXLAC^- + HO_2$	1.0e2
31	$2GLYACOO^{*-} \rightarrow 2CO_2^- + 2COOH$	3.0e8
32	$OXLAC + OH \rightarrow COOH + CO_2 + 2H_2O$	1.4e6
33	$OXLAC^- + OH \rightarrow COOH + CO_2^- + 2H_2O$	2.0e7
34	$OXLAC^{2-} + OH \rightarrow COOH + CO_2^- + OH^-$	4.0e7
35	$H_2O \leftrightarrow H^+ + OH^-$	K_{eq} = 1.0e-14 k_r = 1.4e11
36	$HO_2 \leftrightarrow H^+ + O_2^-$	K_{eq} = 1.6e-5

		k_r = 5.0e10
37	$GLYAC \leftrightarrow H^+ + GLYAC^-$	K_{eq} = 3.47e-4 k_r = 2.0e10
38	$OXLAC \leftrightarrow H^+ + OXLAC^-$	K_{eq} = 5.67e-2 k_r = 5.0e10
39	$OXLAC^- \leftrightarrow H^+ + OXLAC^{2-}$	K_{eq} = 5.42e-5 k_r = 5.0e10
40	$CO_2^- + O_2 \rightarrow O_2^- + CO_2$	2.4e9
41	$GLYAC + H_2O_2 \rightarrow HCO_2H + CO_2 + H_2O$	0.3
42	$HCO_2H + OH \rightarrow COOH + H_2O$	1.0e8
43	$HCO_2^- + OH \rightarrow CO_2^- + H_2O$	2.4e9
44	$HCO_2H \leftrightarrow H^+ + HCO_2^-$	K_{eq} = 1.77e-4 k_r = 5.0e10
45	$GLY + H_2O_2 \rightarrow HCO_2H + HCO_2H$	0
46	$OH + O_2^- \rightarrow OH^- + O_2$	1.0e10
47	$HCO_2^- + OH \rightarrow CO_2^- + H_2O$	1.0e7
48	$CO_2^- + O_2^- \rightarrow CO_2^{-2} + O_2$	6.5e8
49	$CO_3^- + HCO_3^- \rightarrow HCO_3^- + CO_2^-$	1.5e5
50	$CO_3^- + H_2O_2 \rightarrow HCO_3^- + HO_2$	8.0e5
51	$CO_2 \leftrightarrow H^+ + HCO_3^-$	K_{eq} = 4.3e-7 k_r = 5.6e4
52	$HCO_3^- \leftrightarrow H^+ + CO_3^{2-}$	K_{eq} = 4.69e-11 k_r = 5.0e10
53	O_2 (g) $\leftrightarrow$ O2	K_{eq} = 1.3e-3 k_r = 5.3e2
54	CO_2 (g) $\leftrightarrow CO_2$	K_{eq} = 3.4e-2 k_r = 5.3e2
55	$C3D + OH \rightarrow C3D^* + H_2O$	3.0e8
56	$C3D^* + O_2 \rightarrow C3DOO^*$	1.0e6
57	$C3DOO^* \rightarrow X + HO_2$	5.0e1
58	$C3DOO^* \rightarrow 2COOH + 2GLYAC$	3.0e8
59	$C4D + OH \rightarrow C4D^* + H_2O$	1.1e8
60	$C4D^* + O_2 \rightarrow C4DOO^*$	1.0e6
61	$C4DOO^* \rightarrow Y + HO_2$	5.0e1
62	$2C4DOO^* \rightarrow 2GLYAC$	3.0e8
63	$2CHOHOH \rightarrow GLY$	1.3e9
64	$CHOHOH + COOH \rightarrow GLYAC$	1.3e9
65	$2COOH \rightarrow OXLAC$	1.3e9
66	$CO_2^- + COOH \rightarrow OXLAC^-$	1.3e9
67	$2CO_2^- \rightarrow OXLAC^{2-}$	1.3e9
68	$C3D \leftrightarrow MA + H_2O$	K_{eq} = 1e5 k_r = 1e-8
69	$MA + OH \rightarrow C3D^* + H_2O$	1.6e7
70	$TA + OH \rightarrow C4D^* + H_2O$	3.1e8

71	CH2OHOH + OH $\rightarrow$ CHOHOH + H_2O	1.1e9

* = radical For example, glyoxal* = glyoxal radical; OO* = peroxy radical, C4D = C_4 dimer, TA = tartaric acid, C3D = C_3 dimer; MA = malonic acid, GLY = glyoxal, GLYAC = glyoxylic acid, OXLAC = oxalic acid, n = n^{th} order; K_{eq} = the equilibrium constant (M), k_r = the reverse rate constant for corresponding K_{eq}., Thus, the forward rate constant can be calculated by $K_{eq} \times k_r$; (g) = in the gas phase; X, and Y = anonymous organic products.

Table 5-2. The SOA forming potential of formaldehyde, acetaldehyde, ethanol, glyoxal, methylglyoxal, and acetic acid.

	Global source (Tg/yr)	Conc. in cloud/fog (μM)	Conc. used in simulation (μM)	Average OH radical concentration (10^{-12} M)	Oxalic acid molar yield after 1 cloud cycle (10 min)	Oxalic acid molar yield after 8 cloud cycles (80 min)
Formaldehyde	1600, [72]	0.1 – 200, [25]	30	3.6	1.1×10^{-6}	6.3×10^{-6}
Acetaldehyde	213, [33]	0.8 – 16.1, [35]	4	1.0 (constant)	1.0%	20%
Ethanol	44, [46]	<1 – 5, [50]	4	1.0 (constant)	0.3%	17%
Glyoxal	45, [69]	<1 – 276, [25]	30	3.5	45%	72%
Methylglyoxal	140, [69]	<1 – >100, [25]	30	3.6	5.5%	19%
Acetic acid	n.a.	0.4 – 245, [73]	20	4.1	73%	62%

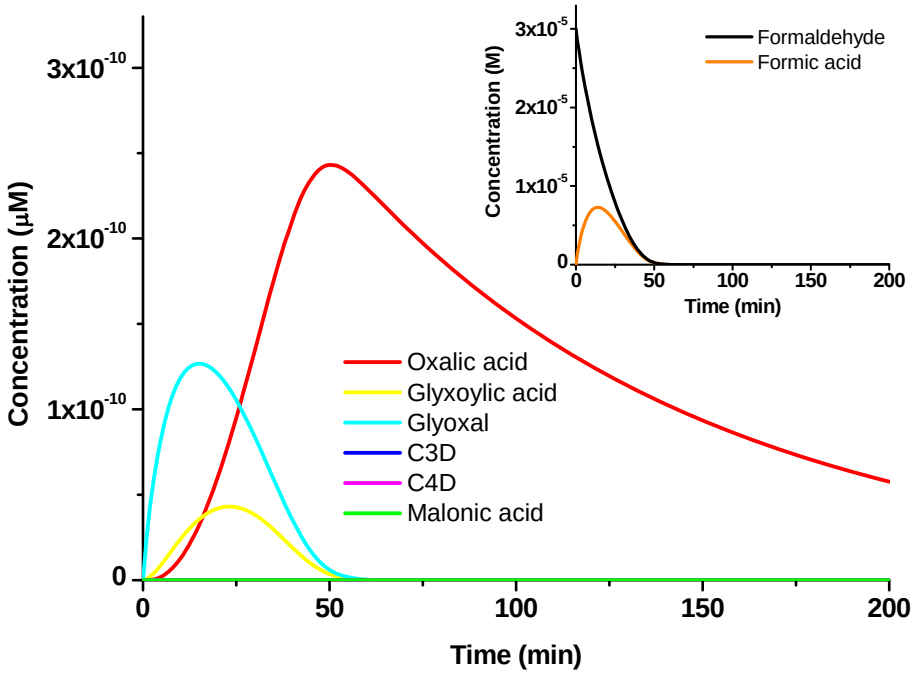

Fig. 5-1. Simulated product formation in formaldehyde (30 μM) + H_2O_2 (150 μM) + UV experiment. C3D represents dimeric compounds with 3 carbons (e.g. tartronic and mesoxalic acids), and C4D represents dimeric compounds with 4 carbons (e.g. malic acid).

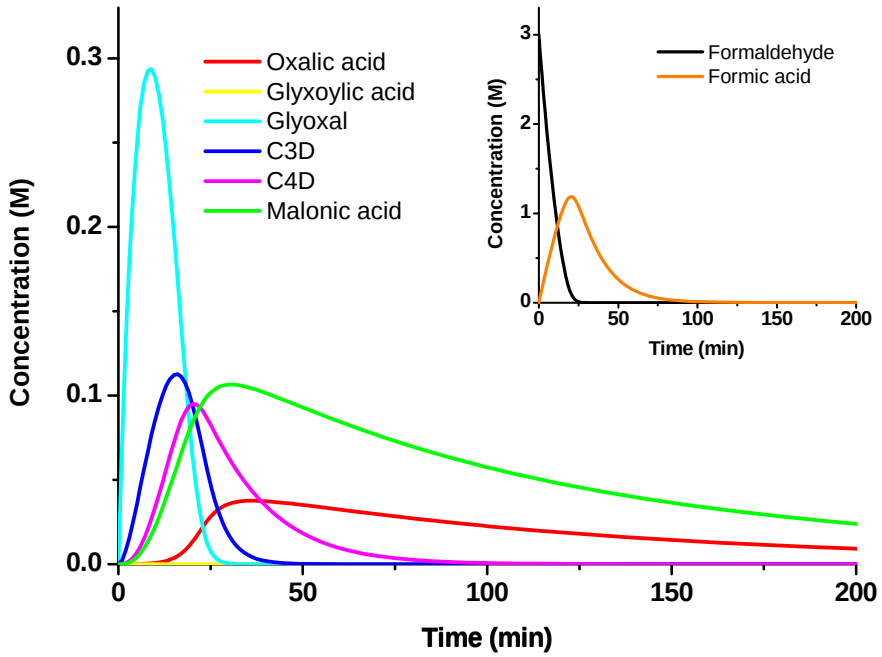

Fig. 5-2. Simulated product formation in formaldehyde (3 M) + H_2O_2 (15 M) + UV experiment. C3D represents dimeric compounds with 3 carbons (e.g. tartronic and mesoxalic acids), and C4D represents dimeric compounds with 4 carbons (e.g. malic acid).

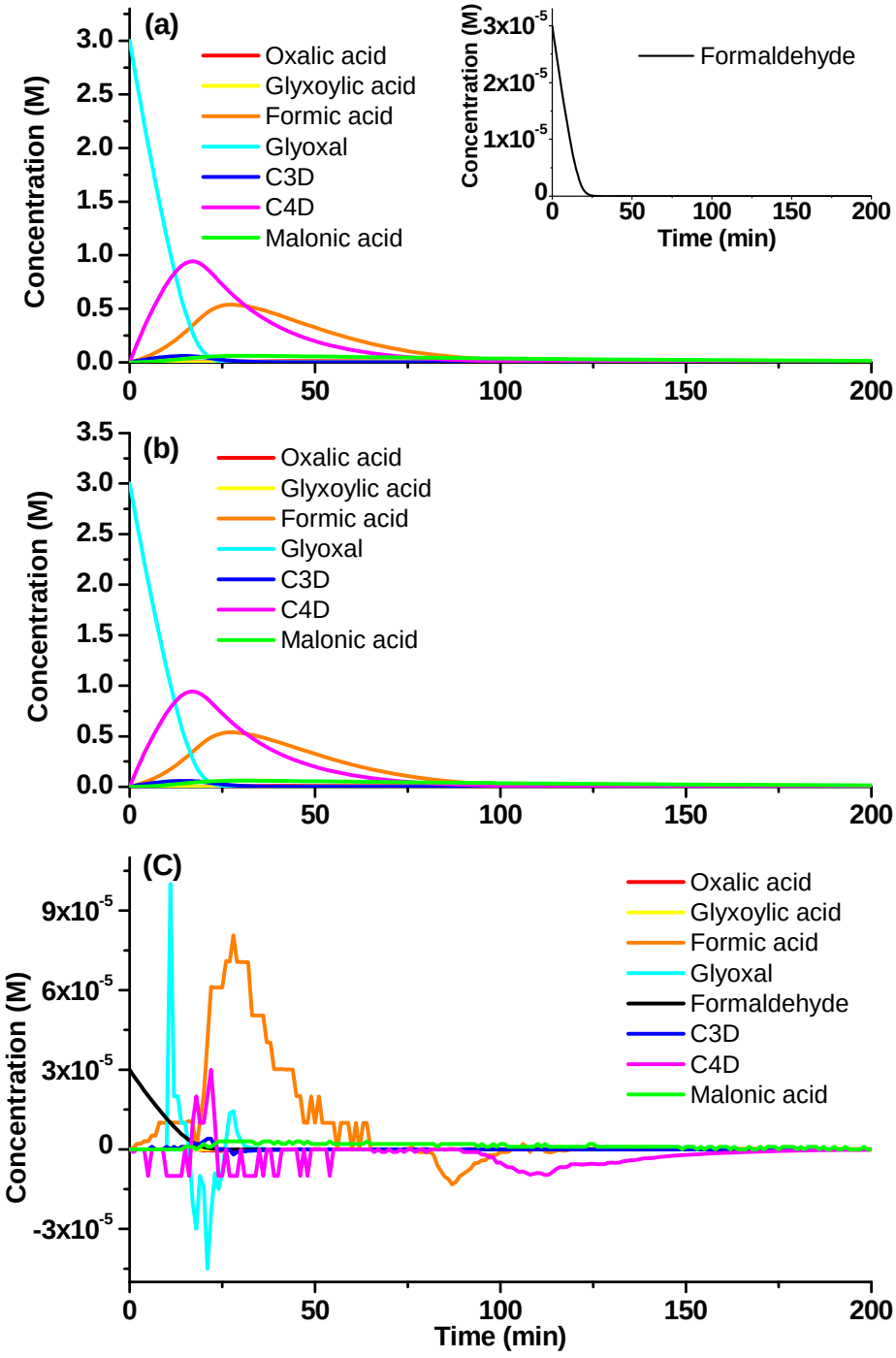

Fig. 5-3. Comparison between simulation (c) and (d). Panel (a) shows simulated product formation in simulation (c) (30 μM formaldehyde + 3 M glyoxal + 15 M H_2O_2 + UV). Panel (b) shows simulated product formation in simulation (d) (3 M glyoxal + 15 M H_2O_2 + UV). Panel (c) shows the difference of simulated product concentrations between simulation (c) and (d) (concentrations in simulation (c) - concentrations in simulation

(d)). C3D represents dimeric compounds with 3 carbons (e.g. tartronic and mesoxalic acids), and C4D represents dimeric compounds with 4 carbons (e.g. malic acid).

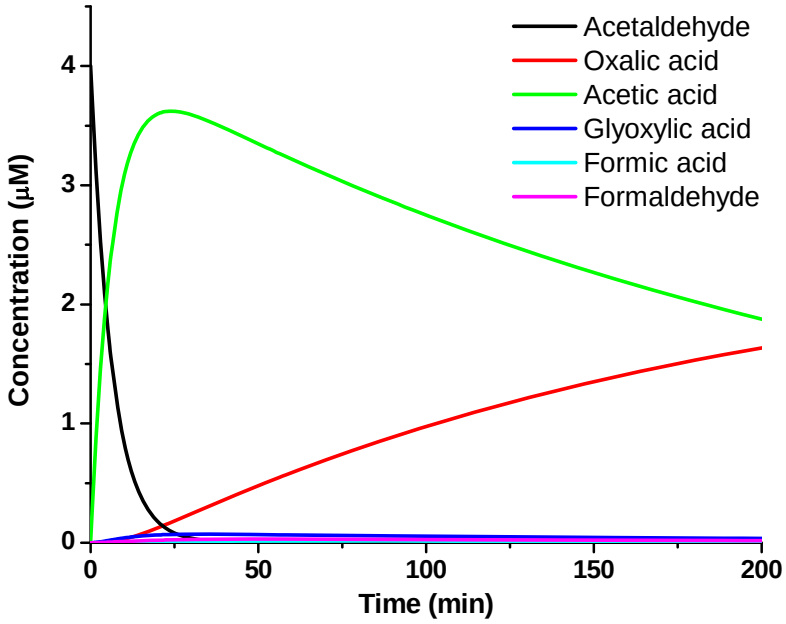

Fig. 5-4. Predicted oxidation of acetaldehyde (4 μM, blue line) by OH radicals (1×10^{-12} M, constant).

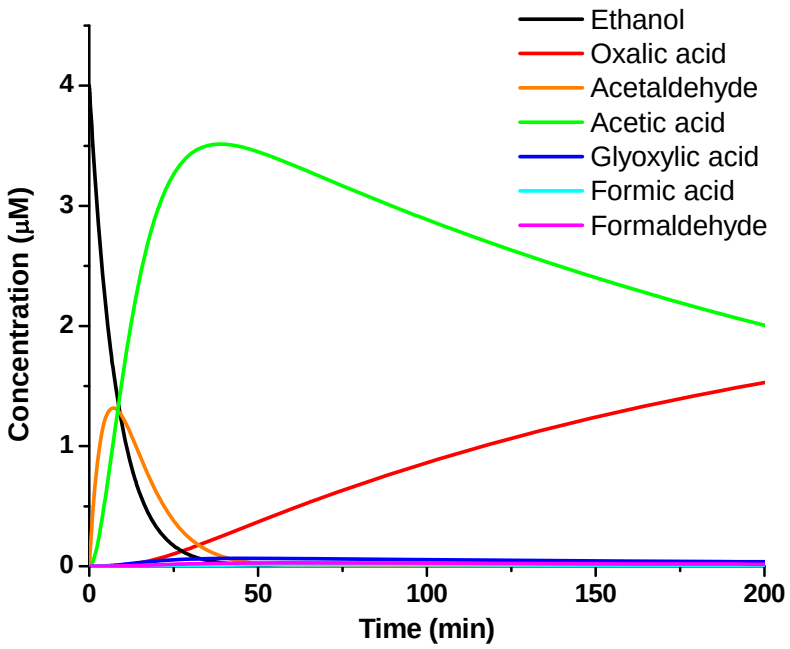

Fig. 5-5. Predicted oxidation of ethanol (4 μM, blue line) by OH radicals (1×10^{-12} M, constant).

Appendix A: Supporting Information for Chapter 2

Analytical Methods

Carboxylic acids were quantified by IC (ICS-3000, Dionex, Sunnyvale, CA) with a conductivity detector. A photodiode array detector provided additional product validation. The IC employed an IonPac AS11-HC column with AG11-HC guard column (Dionex, Synnyvale, CA). The column is specifically designed to separate a large number of inorganic anions and organic acid anions in gradient runs using hydroxide eluent systems. The system was operated in gradient mode (0.4 ml min^{-1}) programmed from 1 mM to 84 mM hydroxide in 35 min. The IC run time was about 40 min. The column temperature was maintained at 30˚C. An ASRS-ULTRA II (2-mm) anion self-regenerating suppressor after the column was used to remove potassium hydroxide and reduce background noise levels. The conductivity detector cell was maintained at 35˚C. Most organic acid anions are detected by both the conductivity detector and photodiode array (PDA) detector at 205 nm, while some inorganic anions, such as sulfate, are only detected in the conductivity detector. Monovalent anions such as glycolate (5.9 min), formate (6.8 min) and glyoxylate (9.7 min) are only weakly retained, bivalent ions such as succinate (20.4 min), malonate (21.5 min) and oxalate (24.6 min) elute after monovalent ions, and trivalent ions such as citrate are strongly retained and elute even later. Acetate and glycolate (5.9 min), succinate and malate (20.4 min), as well as malonate and tartrate (21.5 min) coelute. Glyoxal partially disproportionates in the alkaline mobile phase and is detected as glycolic acid. Disproportionation is suppressed by acids and therefore the glycolic acid signal cannot be used to quantify glyoxal. Unretained compounds elute at ~ 3.5 min. They are observed in the PDA detector, but not

the conductivity detector, since they do not form ions. Chromeleon software (version 6.80 SP2, Dionex) is used to quantify products.

Electrospray ionization mass spectrometry (ESI-MS) is a soft ionization method that does not fragment ions. Carboxylic acids are detected in the negative ionization mode as molecular weight minus one ion because of the loss of an acidic proton. Aldehydes and alcohols are detected in the positive mode. Glyoxal is detected as m/z^+ 117 and 131 as previously reported. The ion m/z^+ 117 was used to qualitatively represent glyoxal in this work.

Fresh samples from batch experiments were analyzed by electrospray ionization mass spectrometry (ESI-MS) (HP-Agilent 1100) as described previously (Altieri et al, 2006). Mobile phase (40% of 0.05% formic acid in water and 60% of pure methanol) was delivered at 0.22 mL/min. Samples (20 μL) were analyzed in both negative and positive ionization mode over the mass range 50 – 1000 amu with a fragmenter voltage of 40 V and capillary voltage of 3000 V. Nitrogen was the drying gas (10 L/min, 350 °C). Unit mass resolution spectra were recorded in Chemstation (version A.07.01) and exported to EXCEL (Microsoft, Inc.) for interpretation.

A frozen sample (-20 °C) taken 30 minutes into the experiment (3000 μM glyoxal + ·OH; experiment #13 Table S1) was analyzed by Fourier transform ion cyclotron resonance (FT-ICR) ESI-MS (Thermo-Finnigan LTQ-XL, Woods Hole Oceanographic Institute Mass Spectrometer Facility) to determine the elemental formulas of products from 95 – 500 amu (mass resolution 100 k – 750 k) as described by Perri et al. (2009). The instrument was mass calibrated with an external calibrant (Thermo Scientific LTQ-FT external calibration mix). Analyte was delivered to FT ICR ESI-MS at 5 μL/min, with

a source voltage between 2.5-3.5 kV, capillary temperature of 250 ˚C, and no sheath gas flow.

Total organic carbon analysis was performed on selected samples using a Shimadzu TOC-5000A Total Carbon Analyzer (Sharp et al., 1993). HCl (8μL, 6M) was added to 3.5 mL of sample (diluted 1/4 for 300 μM experiment and 1/40 for 3000 μM experiment) and sparged with zero-air to eliminate inorganic carbon (CO, H_2CO_3). Organic carbon was then combusted to CO_2 and measured using infrared absorption. Hydrogen peroxide in organic control experiments ($H_2O_2 \pm H_2SO_4$ + UV) was quantified using the triiodide method and UV-visible spectrometer (Allen et al., 1952). Quantification was based on 5-point calibration conducted just prior to sample analysis.

Quality Assurance / Quality Control (QA/QC)

Data quality for organic acids is presented in Table S2. Organic acids were quantified by quadratic regression of 5 points in IC with coefficients of determination, r^2, better than 99% for all acids. Mixed standards containing organic acids (oxalic, formic, glyoxylic, glycolic, malonic and succinic acids, all at 100 μM) were sampled from the reaction vessel to determine recoveries. Recoveries are around 100% except for glyoxylic acid (86.5%). With the addition of 15 mM H_2O_2 and 20 μL of a 1% catalase solution into 10 mL mixed standard, recoveries were unchanged for glycolic acid, malonic acid, succinic acid and oxalic acid. However, glyoxylic acid disappeared and the formic acid concentration increased. Method detection limits are from Perri et al. (2009) using the same analytical protocol. Method precision (4.1%) is the pooled standard deviation of replicate analysis of samples on the IC divided by the mean concentration for organic acids excluding glyoxylic acid and formic acid; replicates were analyzed at the beginning

and end of each run. Analytical precision (1.5%) was calculated as the pooled standard deviation divided by the mean of duplicate samples analyzed sequentially.

Supporting Information References

Allen, A. O.; Hochanadel, C. J.; Ghormley, J. A.; Davis, T. W., Decomposition of Water and Aqueous Solutions under Mixed Fast Neutron and γ-Radiation. *J. Phys. Chem.* **1952,** *56*, (5), 575-586.

Altieri, K. E.; Carlton, A. G.; Lim, H.-J.; Turpin, B. J.; Seitzinger, S. P., Evidence for Oligomer Formation in Clouds: Reactions of Isoprene Oxidation Products. *Environ. Sci. Technol.* **2006,** *40*, (16), 4956-4960.

Perri, M. J.; Seitzinger, S.; Turpin, B. J., Secondary organic aerosol production from aqueous photooxidation of glycolaldehyde: Laboratory experiments. *Atmos. Environ.* **2009,** *43*, (8), 1487-1497.

Sharp, J. H.; Benner, R.; Bennett, L.; Carlson, C. A.; Dow, R.; Fitzwater, S. E., Re-evaluation of High Temperature Combustion and Chemical Oxidation Measurements of Dissolved Organic Carbon in Seawater. *Limnol. Oceanogr.* **1993,** *38*, (8), 1774-1782.

Appendix A1

H_2O_2 + UV ± H_2SO_4 Control Experiments

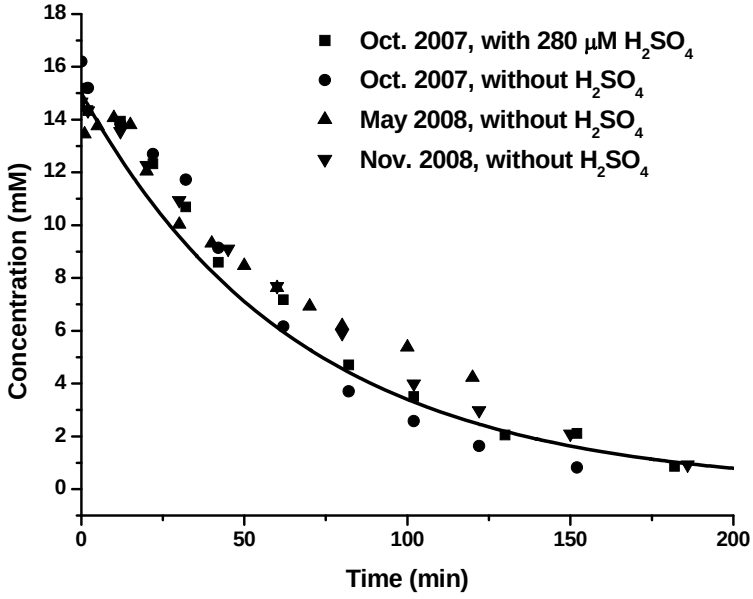

H_2O_2 concentration (mM) and time (min) in H_2O_2 + UV ± H_2SO_4 control experiments. Line is the model fit (Table 3, reactions 1 – 5), where the H_2O_2 photolysis rate (Table 3, k_1 = 1.1E-4 s^{-1}) is a fitted value.

Appendix A2

Decay of Glyoxal

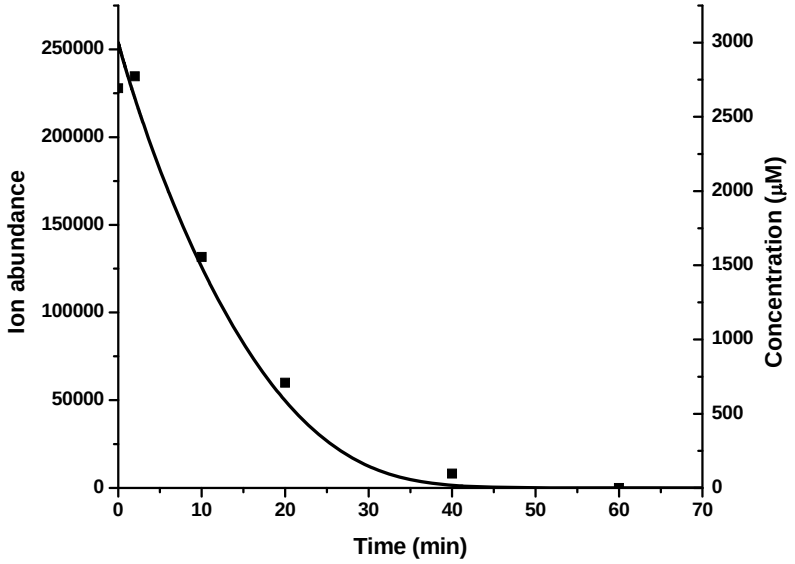

Decay of m/z$^+$ 117 (glyoxal) in ESI-MS positive mode analysis of 3000 μM experiment samples (squares) and kinetic model prediction on glyoxal (solid line)

Appendix A3

IC Chromatogram

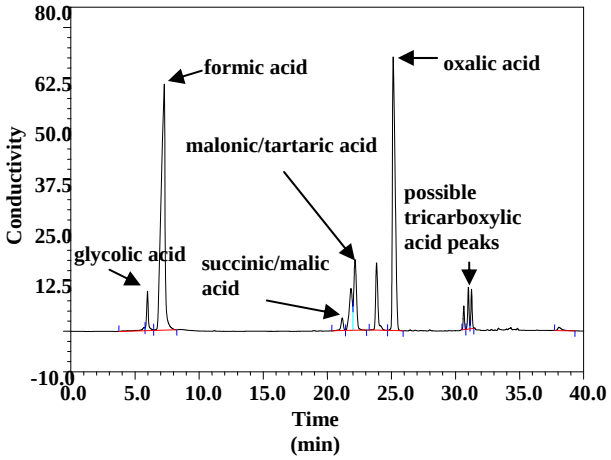

IC chromatogram of a sample from 3000 micromolar experiment 13, t = 20 minutes, analyzed on conductivity detector

Appendix A4

Aqueous Batch Reaction Experiments

Exp. #	Glyoxal (μM)	H_2O_2 (mM)	H_2SO_4 (μM)	Estimated ·OH (10^{-12} M)	Oxalic acid molar yield	Oxalic acid mass yield (%)
1	30	0.15	0	3.5	0.866	133%
2	30	0.15	0	3.5	0.959	149%
3	30	0.15	280	3.5	0.850	132%
4	30	0.15	280	3.5	0.888	138%
5	30	0.15	840	3.5	0.834	129%
6	30	0.15	840	3.5	0.864	134%
7	300	1.5	0	4.7	0.646	100%
8	300	1.5	0	4.7	0.590	92%
9	300	1.5	280	4.7	0.619	96%
10	300	1.5	280	4.7	0.613	95%
11	300	1.5	840	4.7	0.533	83%
12	300	1.5	840	4.7	0.718	111%
13	3000	15	0	5.8	0.261	41%
14	3000	15	0	5.8	0.263	41%
15	3000	15	280	5.8	0.242	38%
16	3000	15	280	5.8	0.239	37%
17	3000	15	840	5.8	0.241	37%
18	3000	15	840	5.8	0.232	36%

Glyoxal ± H_2SO_4 + OH radical aqueous batch reaction experiments. OH radical concentrations are modeled using the reactions in Table 1. Oxalic acid yield is defined as maximum oxalic acid mass (or moles) divided by mass (moles) of glyoxal reacted. Atmospheric yields will differ from experimental yields in part due to lower atmospheric concentrations of H_2O_2. Atmospheric yields can be determined using the kinetic model for glyoxal < 300 μM.

Appendix A5

Quality Control Measures for Organic Acids in IC Analysis

	Glycolic acid	**Formic acid**	**Glyoxylic acid**	**Succinic acid**	**Malonic acid**	**Oxalic acid**
Retention time (min)	5.9	6.8	9.7	20.4	21.5	24.6
Coefficient of determination	99.95%	99.53%	99.70%	99.87%	99.98%	99.90%
Recovery in mixed standard recovery	106.4%	103.0%	86.5%	104.6%	99.7%	102.7%
Recovery in mixed standard with H_2O_2 and catalase	101.8%	158.0%	<5%	102.3%	98.6%	102.5%
Method Detection Limit (μM)	0.6	0.7	0.2	4.3	0.03	0.1
Method Precision	pooled standard deviation for all replicate analyses = 4.1% (n=28)					
Analytical Precision	pooled standard deviation for all duplicate samples = 1.5% (n=36)					

Quality control measures for organic acids in IC analysis. Retention time in IC, Coefficient of determination (r^2) of 5-point calibration; recovery of standards containing glycolic, formic, glyoxylic, succinic, malonic, and oxalic acids sampled from the reaction vessel and analyzed as samples; pooled standard deviation divided by mean for samples analyzed twice (replicates) and samples taken at the same time and analyzed as independent samples (duplicates). Method detection limits were determined by Perri et al. (2009).

Appendix B: Supplemental Information for Chapter 3

Appendix B1

Methylglyoxal (MGLY) ± H_2SO_4 + OH Experiments and Controls

Exp. #	MGLY (μM)	H_2O_2 (mM)	H_2SO_4 (μM)	Estimated ·OH (10^{-12} M)
1	30	0.15	0	3.6
2	30	0.15	0	3.6
3	30	0.15	280	3.6
4	30	0.15	280	3.6
5	30	0.15	840	3.6
6	30	0.15	840	3.6
7	300	1.5	0	3.8
8	300	1.5	0	3.8
9	300	1.5	280	3.8
10	300	1.5	280	3.8
11	300	1.5	840	3.8
12	300	1.5	840	3.8
13	3000	15	0	3.9
14	3000	15	0	3.9
15	3000	15	0	3.9
16	3000	15	280	3.9
17	3000	15	280	3.9
18	3000	15	280	3.9
19	3000	15	840	3.9
20	3000	15	840	3.9
Online 1	30	0.15	0	3.6
Online 2	300	1.5	0	3.8
Online 3	1000	5	0	3.9
Control 1	3000	15	0	No UV
Control 2	300	1.5	0	No UV
Control 3	3000	0	0	UV
Control 4	3000	15	840	No UV
Control 5	0	15	280	UV

Methylglyoxal (MGLY) ± H_2SO_4 + OH radical aqueous batch reaction experiments and controls. OH radical concentrations are modeled using the reactions in Table 1.

Appendix B2

Quality Control Measurements

	Acetic+ Glycolic acid	Formic acid	Pyruvic acid	Glyoxylic acid	Succinic acid	Malonic acid	Oxalic acid	Mesoxalic acid
Coefficient of determination	99.945%	99.981%	99.967%	99.842%	99.858%	99.992%	99.986%	99.971%
MDL (μM)	0.2	0.1	0.2	0.5	0.4	0.1	0.1	0.2
Recovery (no H_2O_2 added)	95.5%	96.7%	95.3%	98.1%	98.5%	98.7%	99.0%	98.6%
Recovery (1 mM H_2O_2, 2.1 hrs)	106.8%	197.8%	85.1%	2.3%	97.9%	97.2%	122.0%	71.0%
Recovery (1 mM H_2O_2, 3.5 hrs)	107.8%	197.7%	82.9%	2.5%	100.1%	99.4%	124.2%	66.6%
Recovery (1 mM H_2O_2, 4.8 hrs)	109.5%	198.4%	79.4%	2.4%	99.1%	97.5%	128.2%	64.1%
Recovery (1 mM H_2O_2, 6.2 hrs)	110.3%	198.3%	77.6%	2.4%	99.7%	97.3%	130.6%	60.8%
Recovery (1 mM H_2O_2, 7.6 hrs)	111.4%	198.2%	73.7%	2.5%	99.9%	97.3%	133.2%	57.3%
Recovery (1 mM H_2O_2, 8.8 hrs)	112.1%	198.2%	72.7%	2.6%	100.4%	97.3%	135.1%	54.9%
Recovery (1 mM H_2O_2, 10.0 hrs)	113.5%	198.7%	69.2%	2.4%	101.3%	97.5%	138.1%	51.7%
Recovery (1 mM H_2O_2, 11.2 hrs)	113.8%	198.3%	68.5%	2.6%	101.5%	97.3%	139.3%	50.0%
Recovery (1 mM H_2O_2, 12.4 hrs)	114.9%	198.3%	65.1%	2.4%	101.9%	97.3%	141.7%	46.6%
Recovery (1 mM H_2O_2, 13.6 hrs)	115.9%	199.3%	65.1%	2.6%	102.4%	97.2%	143.9%	45.8%

Coefficients of determination for calibration, method detection limits (MDL), and recoveries of carboxylic acids (each at 250 μM, with/without 1 mM H_2O_2 added to mixed standard). Time given indicates the time between addition H_2O_2 and IC analysis of sample.

Analytical and method precision have been previously reported (Tan et al., 2009). Pyruvic acid + $H_2O_2 \rightarrow$ acetic acid; glyoxylic acid + $H_2O_2 \rightarrow$ formic acid; mesoxalic acid + $H_2O_2 \rightarrow$ oxalic acid.

Appendix B3

Examples of Duplicate samples

	Duplicate	Acetic/ Glycolic acid	Formic acid	Pyruvic acid	Glyoxylic acid	Succinic acid	Malonic acid	Oxalic acid	Mesoxalic acid
Experiment #7	1	63.6	N.D.	71.2	N.D.	N.D.	N.D.	86.0	54.4
	2	64.1	N.D.	68.9	N.D.	N.D.	N.D.	88.9	52.5
Experiment #15	1	1169.9	206.2	80.2	N.D.	185.0	105.5	186.0	N.D.
	2	1153.0	204.6	78.2	N.D.	179.7	95.8	183.3	N.D.

Examples of quantified organic acid concentrations (in μM) in duplicate samples (N.D. = not detected). The analyses of duplicate #1 and duplicate #2 were separated by approximately 7 hours. The differences of organic acid concentrations are modest, suggesting that H_2O_2 reactions in samples awaiting analysis are negligible, with the exception of glyoxylic acid + $H_2O_2 \rightarrow$ formic acid.

Appendix B4

Predicted Pyruvic and Oxalic acid Yields

Simulations	Yields at 10 minutes				Yields at maximum concentrations					
	Pyruvic acid		Oxalic acid		Pyruvic acid			Oxalic acid		
	Molar yield	Mass yield	Molar yield	Mass yield	Time (min)	Molar yield	Mass yield	Time (min)	Molar yield	Mass yield
(1)	84.9%	104%	7.3%	9.1%	18	78.5%	95.9%	218	33.4%	41.8%
(2)	88.8%	108%	5.5%	6.9%	18	77.7%	95.0%	212	27.8%	34.8%
(3)	84.9%	104%	7.4%	9.3%	18	78.3%	95.7%	248	54.8%	68.5%
(4)	91.8%	112%	0.7%	0.8%	641	78.4%	95.8%	8868	54.6%	68.2%
(5)	92.0%	112%	6.88×10^{-4}	8.60×10^{-4}	6428	78.3%	95.7%	89206	54.5%	68.2%

Model predicted pyruvic and oxalic acid yields ten minutes into the reaction and at the maximum pyruvic acid or oxalic acid concentration. The model simulated conditions: (1) 30 μM methylglyoxal with constant OH radical (3.6×10^{-12} M), no initial H_2O_2, (2) Reaction vessel conditions, 30 μM methylglyoxal and OH radical produced by photolysis of 0.15 mM H_2O_2, (3) 1 μM methylglyoxal with constant OH radical (3.6×10^{-12} M), no initial H_2O_2, (4) 1 μM methylglyoxal with constant OH radical (1×10^{-13} M), no initial H_2O_2, (5) 1 μM methylglyoxal with constant OH radical (1×10^{-14} M), no initial H_2O_2.

Appendix B5

IC-ESI-MS Spectra of 3000 μM MGLY + UV Control Experiment

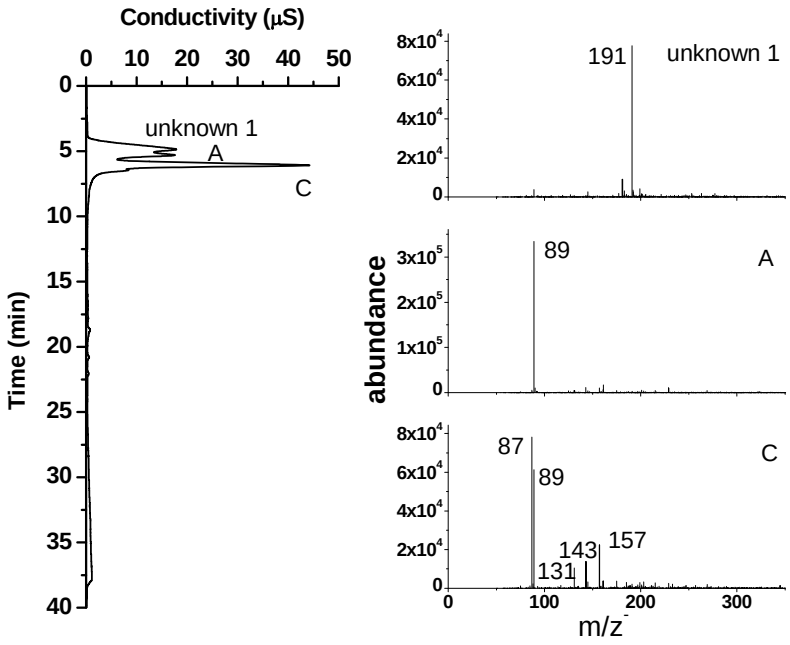

IC-ESI-MS spectra of 3000 μM MGLY + UV control experiment samples (180 min reaction time). (A) peak with the retention time of acetic/glycolic acids (m/z^- 89), (C) peak with the retention time of pyruvic acid (m/z^- 87).

Appendix B6

ESI-MS Spectra of 3000 μM MGLY + UV Control Experiment

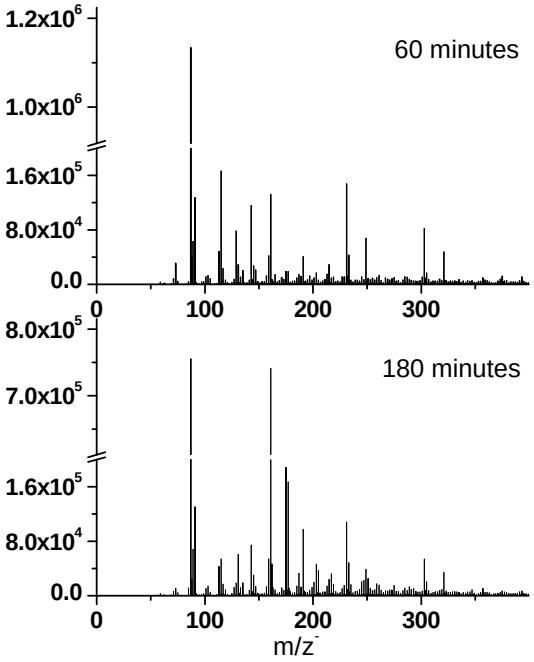

ESI-MS spectra of 3000 μM MGLY + UV control experiment samples (60 and 180 min reaction time).

Appendix B7

IC-ESI-MS Spectra of MGLY (3000 μM) + H_2O_2 (15 mM) Control Experiment

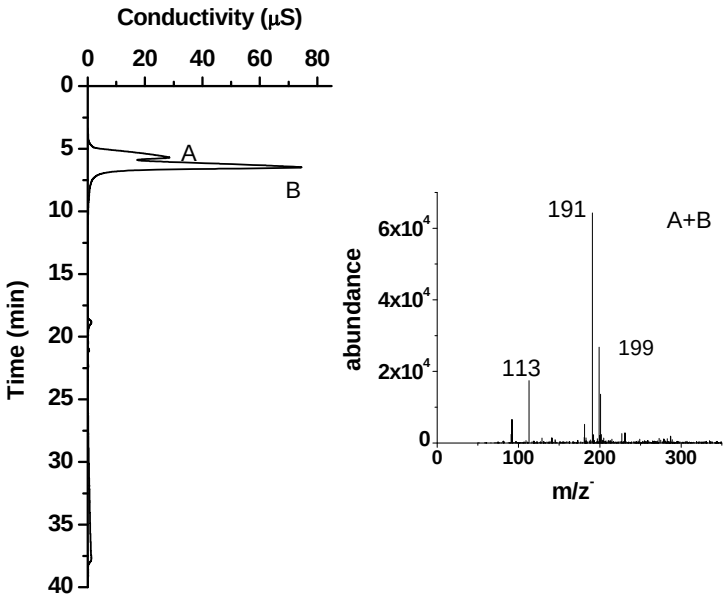

(A+B) peak at the retention time of acetic/glycolic acids and formic acid.

Appendix B8

ESI-MS Spectra of MGLY (3000 μM) + H_2O_2 (15 mM) Control Experiment

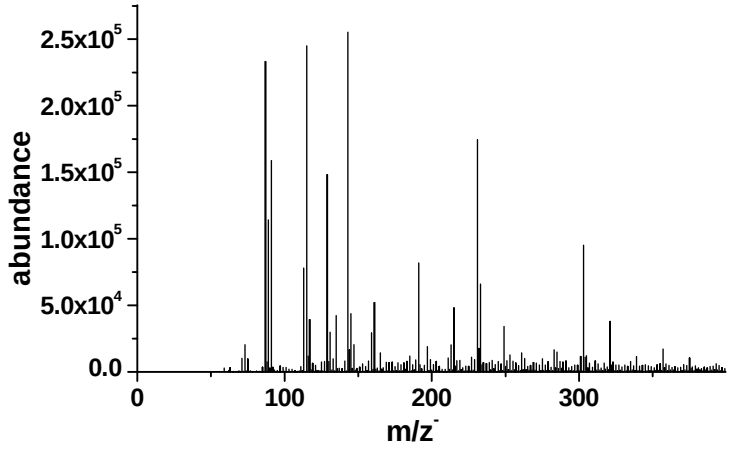

Appendix B9

ESI-MS Online Analysis of Methylglyoxal (300μM) + OH Radical Experiment

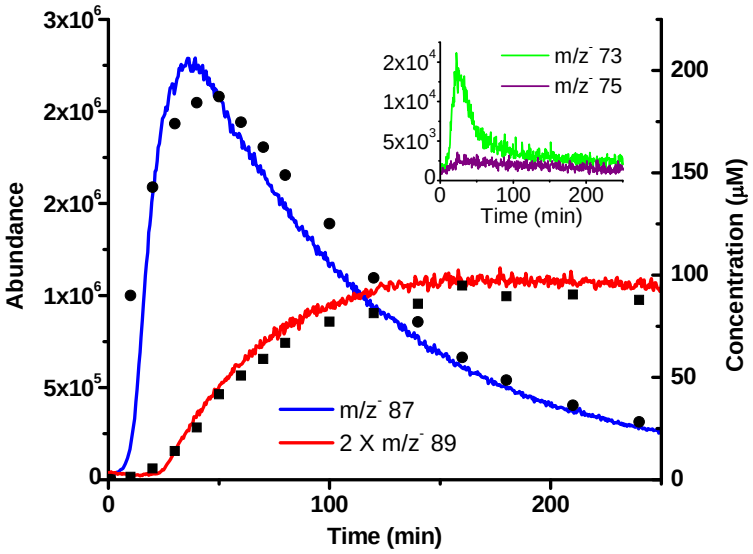

ESI-MS online analysis of methylglyoxal (300μM) + OH radical (1.5mM H_2O_2 + UV) experiment. Pyruvic acid (m/z^- 87) and oxalic acid (m/z^- 89) are displayed in ion abundance (multiplied by 2 for m/z^- 89) from ESI-MS negative scan mode. Pyruvic acid (circles) and oxalic acid (squares) concentrations quantified by IC are overlaid. Evolution of glyoxylic acid (m/z^- 73, green line) and glycolic acid (m/z^- 75, purple line) is shown in the inset.

Appendix B10

ESI-MS Online Analysis of Mesoxalic Acid in 30 and 300 μM Experiments

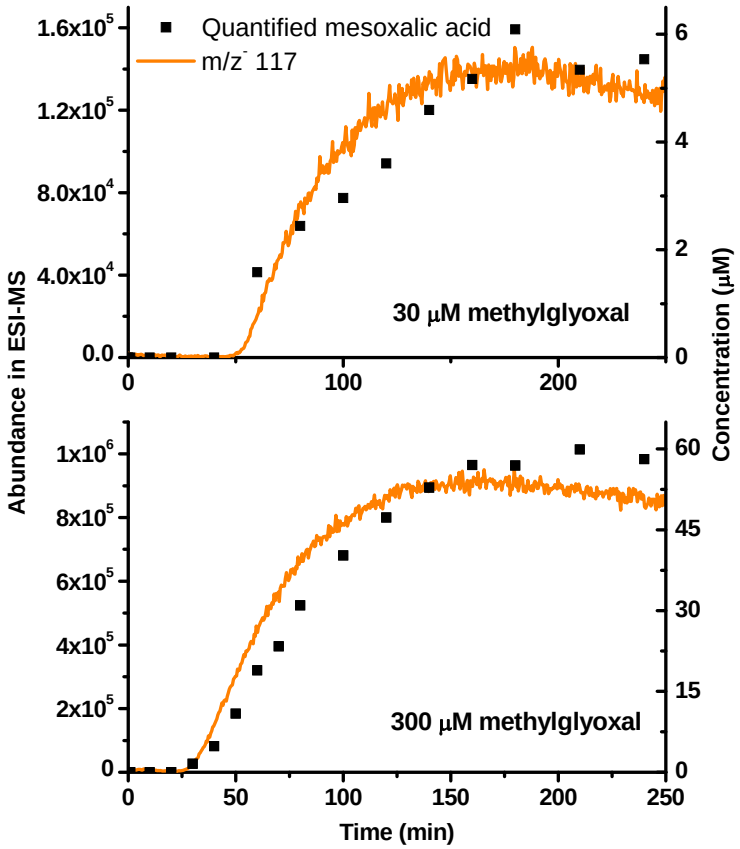

m/z⁻ 117 from ESI-MS online analysis (solid line) and quantified mesoxalic acid (squares) by IC in (a) 30 and (b) 300 μM experiments.

Appendix B11

Predicted OH Radical Concentrations in Batch Experiments

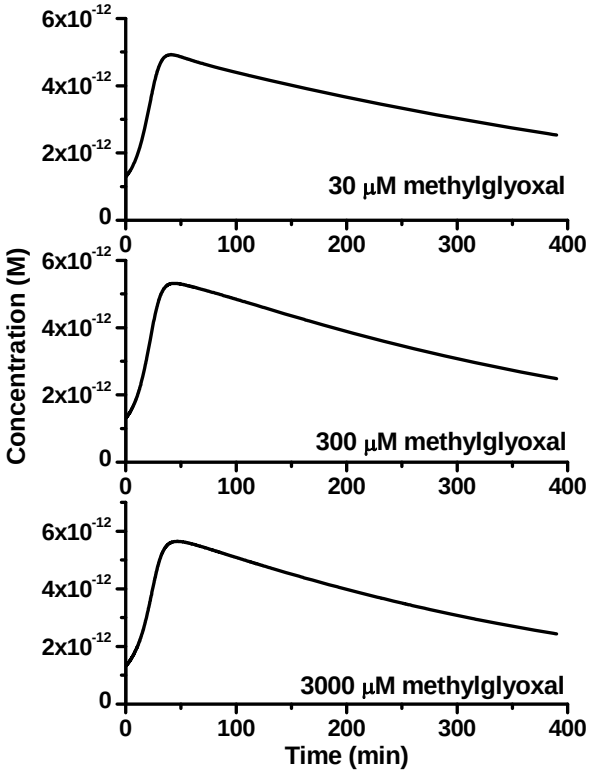

Appendix B12

Acetic Acid in HPLC Analysis

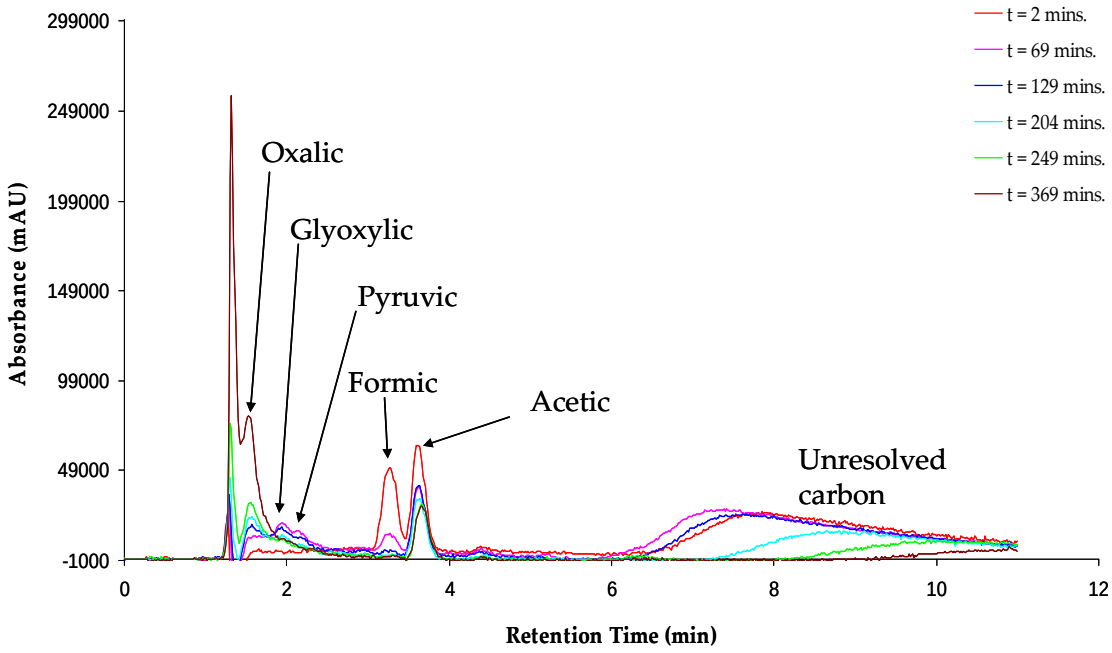

HPLC-UV/vis chromatograms of selected samples from methylglyoxal (2 mM) + H_2O_2 (10 mM) + UV experiment. This plot is provided by Annmarie Carlton.

Appendix B13

Quantified Mesoxalic Acid in 30 and 300 μM Experiments

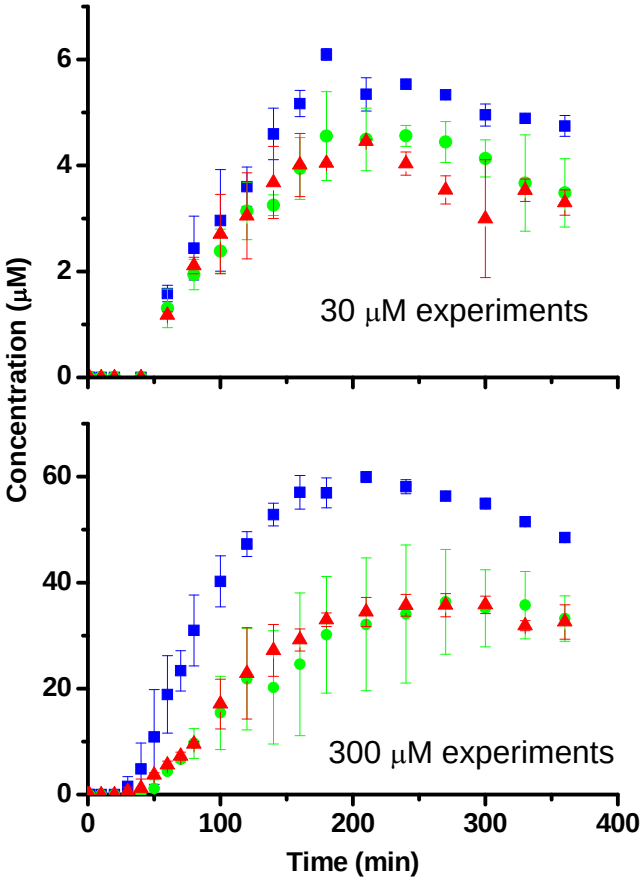

Time profiles of mesoxalic acid in (a) 30 and (b) 300 μM experiments. Blue squares are experiments without H_2SO_4, green dots are experiments with 280 μM H_2SO_4, and red triangles are experiments with 840 μM H_2SO_4.

Appendix B14

Quantified Pyruvic Acid

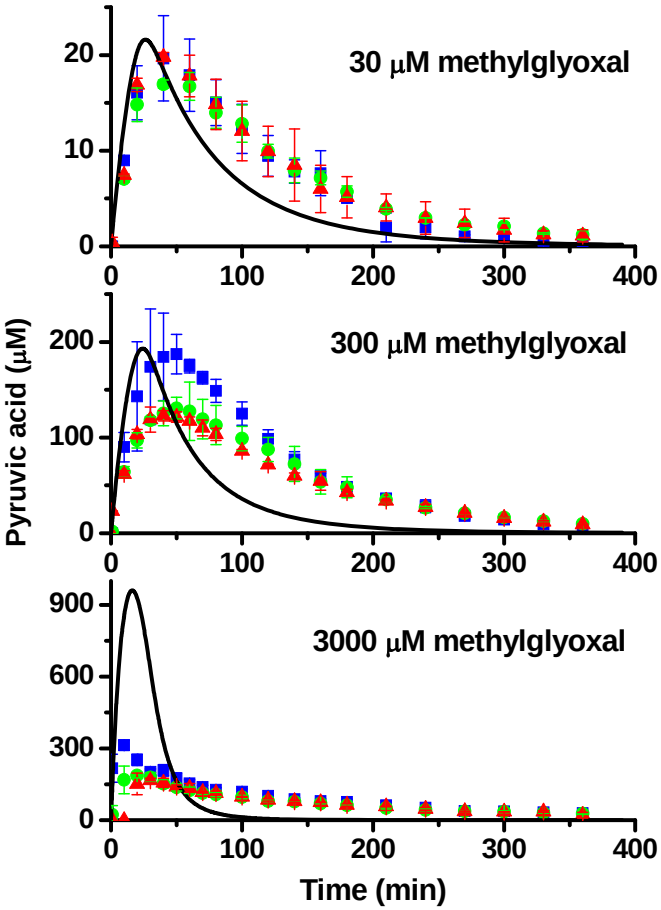

Pyruvic acid time profiles from batch methylglyoxal ± H_2SO_4 + OH radical experiments and model predictions. Initial model pH is 5.6. The effect of initial pH on simulated results is small. Solid lines are modeled pyruvic acid concentration and data points are quantified concentrations from IC analysis. Blue squares are experiments without H_2SO_4, green dots are experiments with 280 μM H_2SO_4, and red triangles are experiments with 840 μM H_2SO_4.

Appendix B15

Sensitivity of Oxalic Acid Prediction to the Photolysis Rate

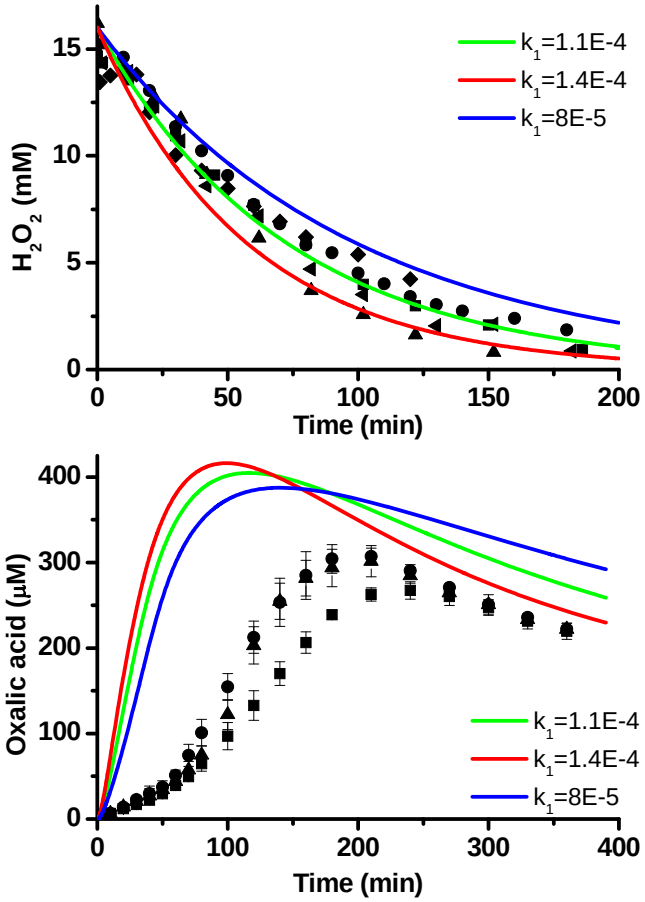

Sensitivity of oxalic acid prediction to the photolysis rate (k_1). (a) model predicted H_2O_2 concentrations for three values of k_1 (Table 1) and measured H_2O_2 concentrations. (b) model predicted oxalic acid concentrations using the same three values of k_1 and measured oxalic acid concentrations in 3000 μM experiments.

Appendix C: Supplemental Information for Chapter 4

Appendix C1

FT-ICR-MS/MS analysis of m/z$^-$ 249

Fragment ions from FT-ICR-MS/MS analysis of m/z$^-$ 249. Only fragments with 9 or less carbons are considered.

m/z	Intensity	Relative	Theo. Mass	Delta (ppm)	Composition
57.03458	255.4	6.94	57.03459	-0.1	C3 H5 O1
59.01385	288.7	7.85	59.01385	-0.08	C2 H3 O2
69.03459	70.6	1.92	69.03459	0	C4 H5 O1
71.01385	432.8	11.77	71.01385	-0.01	C3 H3 O2
71.05024	400.1	10.88	71.05024	-0.01	C4 H7 O1
73.02942	73	1.98	73.0295	-1.18	C3 H5 O2
73.02946	73.2	1.99	73.0295	-0.63	C3 H5 O2
73.0295	876.4	23.83	73.0295	-0.01	C3 H5 O2
73.02956	90.8	2.47	73.0295	0.77	C3 H5 O2
81.03459	235.2	6.39	81.03459	0.05	C5 H5 O1
85.02933	113.4	3.08			
85.02939	155.6	4.23	85.0295	-1.33	C4 H5 O2
85.02943	176.6	4.8	85.0295	-0.8	C4 H5 O2
85.02951	2236.5	60.8	85.0295	0.05	C4 H5 O2
85.02958	102.8	2.79	85.0295	0.95	C4 H5 O2
85.0297	115.3	3.13			
87.00865	135.3	3.68	87.00877	-1.33	C3 H3 O3
87.00871	137.4	3.74	87.00877	-0.71	C3 H3 O3
87.00877	1960.4	53.29	87.00877	0.05	C3 H3 O3
87.00885	105.4	2.86	87.00877	0.97	C3 H3 O3
87.00898	70.5	1.92			
87.04516	317.6	8.63	87.04515	0.09	C4 H7 O2
88.01213	74.1	2.01	88.01212	0.1	C2 [13]C1 H3 O3
88.0166	71.2	1.94	88.01659	0.1	C3 H4 O3
89.0243	105.5	2.87	89.02442	-1.35	C3 H5 O3
89.02435	111.5	3.03	89.02442	-0.71	C3 H5 O3
89.02442	1448.9	39.39	89.02442	0.07	C3 H5 O3
97.02952	185.1	5.03	97.0295	0.15	C5 H5 O2
97.0659	101	2.75	97.06589	0.16	C6 H9 O1
99.00878	104.1	2.83	99.00877	0.17	C4 H3 O3
99.04517	362.9	9.87	99.04515	0.16	C5 H7 O2
100.01661	90.1	2.45	100.0166	0.18	C4 H4 O3

101.02443	198.4	5.39	101.0244	0.17	C4 H5 O3
107.05026	90.8	2.47	107.0502	0.23	C7 H7 O1
109.02953	77.6	2.11	109.0295	0.23	C6 H5 O2
111.04518	124.7	3.39	111.0452	0.22	C6 H7 O2
113.02444	189.4	5.15	113.0244	0.23	C5 H5 O3
113.06083	98.7	2.68	113.0608	0.23	C6 H9 O2
115.03998	100.5	2.73	115.0401	-0.8	C5 H7 O3
115.04009	906.6	24.65	115.0401	0.2	C5 H7 O3
117.01925	120.1	3.27	117.0193	-0.74	C4 H5 O4
117.01936	1047.1	28.47	117.0193	0.21	C4 H5 O4
117.05575	123.6	3.36	117.0557	0.25	C5 H9 O3
123.04518	616.5	16.76	123.0452	0.25	C7 H7 O2
124.04854	86.6	2.35	124.0485	0.27	C6 [13]C1 H7 O2
125.02406	81.9	2.23			
125.02419	92.9	2.53	125.0244	-1.8	C6 H5 O3
125.02431	95.9	2.61	125.0244	-0.85	C6 H5 O3
125.02444	1459.1	39.67	125.0244	0.2	C6 H5 O3
125.02462	87.3	2.37	125.0244	1.64	C6 H5 O3
125.0601	96.7	2.63			
125.06042	168.9	4.59			
125.06058	187.5	5.1	125.0608	-1.8	C7 H9 O2
125.06068	178.3	4.85	125.0608	-0.99	C7 H9 O2
125.06083	3678.4	100	125.0608	0.18	C7 H9 O2
125.06099	72	1.96	125.0608	1.51	C7 H9 O2
125.06126	193.8	5.27			
125.06158	88.3	2.4			
127.0401	472.8	12.85	127.0401	0.26	C6 H7 O3
128.04793	233.1	6.34	128.0479	0.31	C6 H8 O3
129.05575	716.9	19.49	129.0557	0.26	C6 H9 O3
131.03502	169.4	4.6	131.035	0.3	C5 H7 O4
141.01938	99.5	2.7	141.0193	0.33	C6 H5 O4
141.05543	85.4	2.32			
141.0556	110.2	3	141.0557	-0.84	C7 H9 O3
141.05576	1213.6	32.99	141.0557	0.28	C7 H9 O3
142.05912	391.3	10.64	142.0591	0.33	C6 [13]C1 H9 O3
142.06359	200.4	5.45	142.0635	0.34	C7 H10 O3
142.99864	203.7	5.54	142.9986	0.33	C5 H3 O5
143.03487	108.8	2.96	143.035	-0.79	C6 H7 O4
143.03502	915.2	24.88	143.035	0.29	C6 H7 O4
143.07141	467.7	12.71	143.0714	0.33	C7 H11 O3
145.0143	137.1	3.73	145.0143	0.35	C5 H5 O5

145.0505	96.8	2.63	145.0506	-0.93	C6 H9 O4
145.05068	1030.3	28.01	145.0506	0.3	C6 H9 O4
155.03504	511	13.89	155.035	0.36	C7 H7 O4
157.05069	111.6	3.03	157.0506	0.4	C7 H9 O4
158.05405	234	6.36	158.054	0.4	C6 [13]C1 H9 O4
159.02996	281.1	7.64	159.0299	0.4	C6 H7 O5
159.06614	116.1	3.16	159.0663	-0.92	C7 H11 O4
159.06634	917.1	24.93	159.0663	0.35	C7 H11 O4
160.0697	147	4	160.0696	0.41	C6 [13]C1 H11 O4
161.0454	74.4	2.02	161.0456	-0.91	C6 H9 O5
161.04561	524	14.25	161.0456	0.38	C6 H9 O5
169.01431	95.2	2.59	169.0143	0.38	C7 H5 O5
169.05071	232.1	6.31	169.0506	0.44	C8 H9 O4
171.02997	337.7	9.18	171.0299	0.44	C7 H7 O5
177.04054	82.4	2.24	177.0405	0.47	C6 H9 O6
203.05622	72.3	1.97	203.0561	0.53	C8 H11 O6
217.03513	133.8	3.64	217.0354	-1.12	C8 H9 O7
217.03549	900.1	24.47	217.0354	0.53	C8 H9 O7
231.01479	145.3	3.95	231.0146	0.63	C8 H7 O8
			231.0151	-1.29	C17 [13]C2 H1
231.05117	246.7	6.71	231.051	0.64	C9 H11 O7
248.0802	188.1	5.11	248.0798	1.57	C16 [13]C1 H11 O2
248.17835	250.3	6.81	248.1782	0.69	C16 H24 O2
249.06176	312.8	8.5	249.0616	0.7	C9 H13 O8

Appendix C2

IC-ESI-MS Spectra of 1 mM Pyruvic Acid + UV Reactions

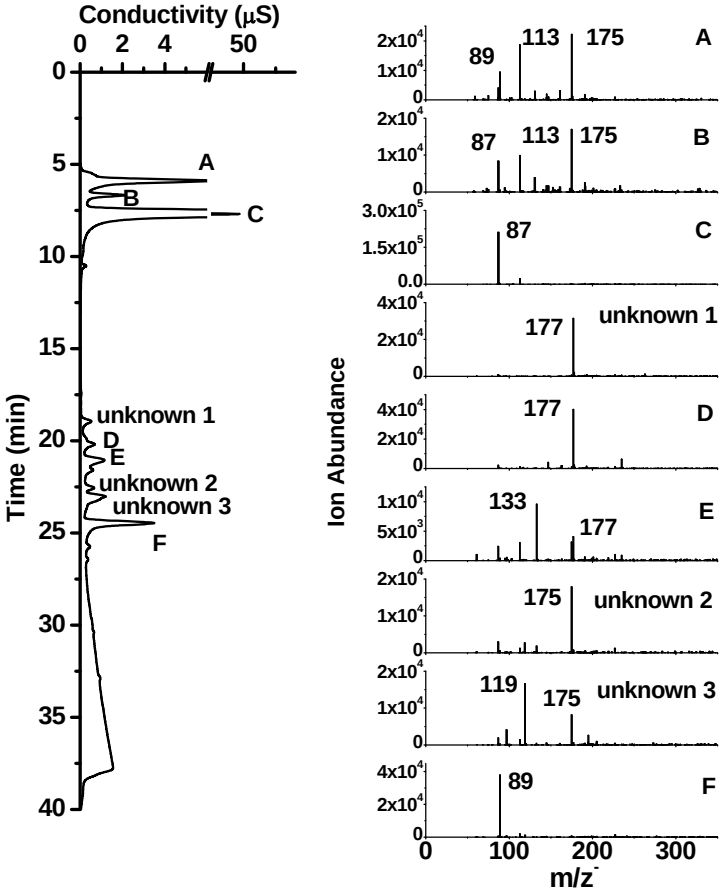

IC-ESI-MS spectra of a sample taken from 1 mM pyruvic acid + UV batch reactions (180 minutes reaction time). (A) peak with the retention time of acetic/glycolic acids, (B) peak with the retention time of formic acid, (C) peak with the retention time of pyruvic acid (m/z^- 87), (D) peak with the retention time of succinic acid (m/z^- 117), (E) peak with the retention time of malonic acid (m/z^- 103), (F) oxalic acid (m/z^- 89).

Appendix C3

IC-ESI-MS Spectra of 1 mM Pyruvic Acid + OH Radical Reactions

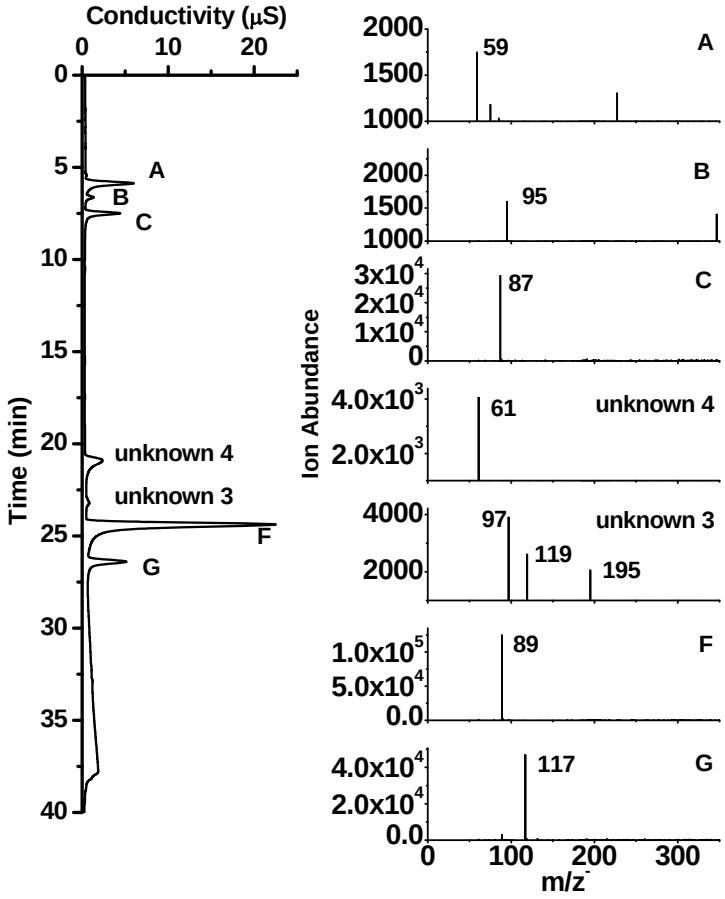

IC-ESI-MS spectra of a sample taken from 1 mM pyruvic acid + OH radical batch reactions (180 minutes reaction time). (A) peak with the retention time of acetic/glycolic acids, (B) peak with the retention time of formic acid, (C) peak with the retention time of pyruvic acid (m/z^- 87), (F) oxalic acid (m/z^- 89), (G) mesoxalic acid (m/z^- 117).

Appendix D: Aqueous Batch Reaction SOP

1) Plan experiment
    a. Calculate amount of compounds, determine sampling frequency and volume.
2) Clean all glassware, sampling lines, syringes, thermometers.
3) Place magnets inside vessels, attach sampling lines and syringes with appropriate adapters, then place the immersion well inside the vessel.
4) Wrap the reaction vessel with aluminum foil, to block ambient light from vessels.
5) Set up reaction vessel
    a. Place reaction vessels in stands on top of stirrer surfaces
    b. Attach tubes for water cooling
        i. Faucet to bottom of reaction vessel and top of reaction vessel to drain
        ii. Turn on water
    c. Attach cooling air tubes to lab vacuum, turn on vacuum
    d. Place thermometer and thermometer adapter in vessels if necessary
    e. Wrap top of immersion wells in aluminum foil
6) Place UV lamp inside the immersion well. Use the same lamp for each experiment. Turn on UV lamp and note time on lab logbook. Warm-up time should be at least 45 minutes.
7) Calibrate pH meter and DO meter if needed.
8) Make reaction and/or control solutions in 1L volumetric flask. Add organic compound and sulfuric acid first and then add H_2O_2. Note the time on logbook when the solution is made.
9) Experiment and controls

a. Take the first sample directly from volumetric flask.

b. Pour solution into reaction vessel and turn stirrer onto to setting4. Note the time on sample data sheet. This should be done within 3 minutes to avoid dark reactions becoming important.

a. Take samples and note the time on logbook.

i. 2nd sample is taken immediately after solution is placed in vessel. The process may take around 1-2 minutes.

ii. Take samples at similar time points in each experiment.

iii. Pump syringe 3 times before taking each sample.

10) Label all samples with the same experiment code and sample time. Put sample on autosampler and run. For IC and TOCAN analysis, never freeze batch experiment samples.

Appendix E: Online ESI-MS Analysis SOP and Checklist

This SOP and checklist is modified based on Dr. Mark Perri's work.

Time	Operation
_____	Lamp on in unused vessel
_____	Turn on ESI-MS (click the "On" button on the screen)
_____	Check Tune +, - mode if necessary.
_____	Check volumes in mobile phase bottles, fill if needed
_____	DI Blank 30 min (from mobile phase bottle) (0.11 mL/min each pump) (using 2pumpsN.m or 2pumpsP.m from 2009 folder)
_____	Clean reaction vessel / let dry upside down for a while if necessary
_____	Start tubing flush with rainin rabbit from DI water in beaker
_____	Makeup solution in 1L volumetric flask
_____	Setup reaction vessel by MS, cover the bottom 2/3 with foil
_____	Turn stir bar on at 300 RPM
_____	Check cooling water connections on vessel, turn on cooling water
_____	Insert Rainin Rabbit tubing
_____	Set Isocratic pump to 0 mL/min, take out the immersion well
_____	Take out the HPLC pump (isocratic pump) inlet tubing, take out the fritz, put the inlet tubing into reaction vessel, put the fritz back on
_____	Make sure rabbit tubing is above the HPLC inlet tubing
_____	Pour reaction solution into vessel

_____ Purge HPLC pump for 2 min at 5 mL/min

_____ Set isocratic pump to 0.11 mL/min; **Close waste valve**

_____ Setup sequence with n runs of 2Pumps(N/P), 60 min each

_____ Start analysis, start stopwatch timer, leave for at least 15 min

_____ Set Isocratic pump to 0 mL/min

_____ Pour H_2O_2 in, mix, put the lamp in (note time)

_____ Set Isocratic pump to 0.11 mL / min

_____ Turn on cooling air

_____ Cover the top portion with foil

Monitor cooling water for leaks! Make sure stir bar is stirring properly. Sample every now and then, run samples on IC ASAP. Don't forget to take duplicates!

Cleanup

_____ Turn lamp off, stored in its container

_____ Set isocratic pump to 0 mL/min (it'll probably already be on standby)

_____ Put isocratic pump inlet into a clean beaker with DI water

_____ Purge isocratic pump for 5-10 min at 5 mL/min

_____ Put isocratic pump inlet back into DI mobile phase bottle

_____ Purge isocratic pump for 5-10 min at 5 mL/min

_____ Switch to MS at 0.11 mL/min

_____ Run DI Blank for 30 min (from mobile phase bottle) (0.11 mL/min each pump) using 2pumpsN.m or 2pumpsP.m

_____ Empty reaction vessel, sampling waste into waste bottle

_____ Start tubing flush with rainin rabbit from DI water in beaker

_____ Clean reaction vessel and stir bar

Appendix F: SOP of Ion Chromatography Analysis

This SOP was originally written by Diana Ortiz and modified by Yi Tan.

Overview

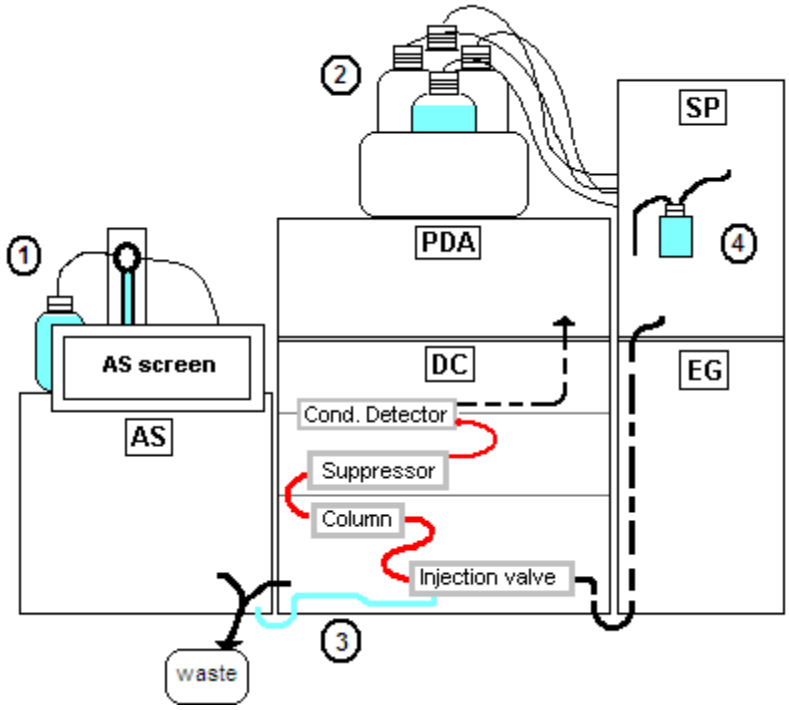

Appendix Fig. F-1

SP - Single Gradient Pump, with the waste bottle.

EG - Eluent Generator, generates high purity OH eluents in deionized water. Trap column is located below EG.

DC - Detector/Chromatography Module, with the following components:

Lower part: Injection valve, Guard column, Column,

Upper part: Suppressor, and Conductivity Detector

PDA - Photodiode Array Detector, measures absorbance spectrum (190-800 nm).

AS - Autosampler

Red tubing - contains sample plus eluent (KOH solution).

1. Deionized water in the 1L pressure bottle and the syringe are used to inject sample into the system. (NOTE: This water must be change WEEKLY)

2. Deionized water from bottles in the tray on the top of SP is used to generate the eluent. (NOTE: This water must be change WEEKLY)

3. Deionized water in the 1L pressure bottle is used to rinse pump seal.

Chromeleon Software:

1. Click the "Chromeleon" shortcut on the desktop.

2. On the left side of the window, create a subfolder with user's name in the "2_Data" folder.

3. Go to "File", then "New", and select "Sequence (using Wizard)" to create a new sequence from scratch, see section 5.6.1 of ICS-3000 Manual for more details (attached in SOP). Following screen prompts. Set up the number of samples, standards. Set up the quantification method to use. Set up the subfolder of sequence. Alternative method: Copy and paste any previous sequence.

4. NOTE: If using a copy of a previous sequence, be aware of deleting the finished samples that don't correspond to your experiment, or if writing on top of the information make sure to change the "Name", "Type", "Position", "Status", "Program", etc.

5. Go to “Default Panel Tabset” on the “Chromeleon” window if when panel tabset is open. Otherwise, Go to “Windows”, and then switch to the panel tabset (or use “ctrl” + “tab” to switch).

6. A new small window will pop out, click on “My Computer”, then click on the “Chromeleon Server”, and finally “Ok”.

7. The Chromeleon [Panel Tabset1] will open; this is the main Control panel.

Setup

(A) Prime Single Pump (SP)

1. Switch to Chromeleon’s control panel, go to the “Gradient Pump” tab. Make sure the “connect” box on the top left of the tab screen is checked.

2. Check the following parameters on the pump Control panel:

   Prime Control: Duration is 300 s, Prime rate is 6.0 ml/min

   Gradient Control: A = 100.0 and the rest = 0.0 if not using binary mobile phase.

3. Open the SP door, then open the priming valve by turning it one-half turn counterclockwise. See Figure 1. NOTE: If the priming valve is opened too much, air is drawn through the valve and air bubbles can be seen exiting the waste line.

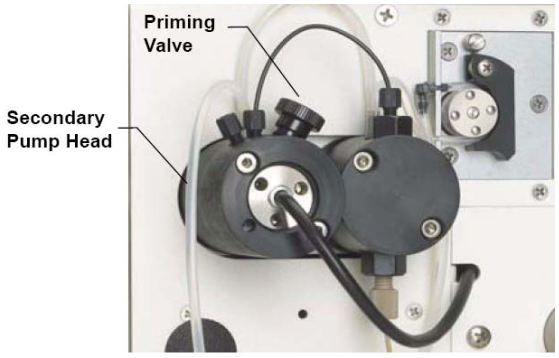

Appendix Fig. F-2 SP priming valve

4. To enable priming, click the “Prime” button to “On” on the pump Control panel.

5. Continue priming the pump until all air and previous eluents are purged and no air bubbles can be seen exiting the waste line.

6. When finished priming, make sure the “Prime” button is back to “Off”.

7. Close the priming valve by closing it clockwise. (DO NOT OVERTIGHTEN THE PRIMING VALVE.)

8. Set the following settings on the pump Control panel: Flow Control: Flow: 0.400 ml/min

9. Switch Motor “On”, wait until the system pressure become stable (2000-2500 psi)

(B) Autosampler (AS) Flush/Prime

1. On the Chromeleon Control panel, click on the “Autosampler” tab.

2. Make sure the “Connect” box is checked, so that the AS is connected to the software.

3. Check the prime volume: if daily use: 2000 μL; If non-daily use: 3000 μL

4. Click “Prime” button under the “syringe” area to make sure no bubbles exist in the syringe. If priming doesn’t get rid of bubbles, click “prime”, manually shutdown the autosampler (press the switch at the bottom left of the AS) when syringe stroke moves down, remove the syringe from the assembly, put Milli-Q water in a clean beaker, pump the syringe with Milli-Q water several times, put the syringe back on, turn on the AS, connect with the software.

(C) Eluent Generator

1. Make sure the “Connected” box is checked
2. EGC_1 Control: switch to “On”, EluGen-OH Target Concentration is usually 1 mM,
3. Switch CR-TC to On
4. Check the remaining ion count precentage: %.

(D) Detector Compartment (for regular IC setup)

1. Make sure the “Connected” box is checked
2. Suppressor1 Settings: Type: ASRS-2mm; Mode: On. When running at standby mode, the current is 24 mA. During the analysis, this current will be 70 mA. At the standby mode, the current can be set to 1 mA.
3. Set up Column_TC: Set Point: 30^{o}C, Mode: On
4. Make sure “Regen” option at lower right part is “closed”.

(E) Conductivity Detector

1. Cell Heater: Cell Heater Mode: On (at 35.00 C)

2. Conductivity Detector Settings: Verify the Total Signal is low (ideally < 1 μS) (Optional: Click on the blue dot on top of the tabs to check the stability of the baseline.)

Sample Run

(A) Loading Samples into the Autosampler. Filter samples with 0.45μm filter if they possibly contain solids (NOT necessary for batch experiment samples). Fill the 1.8 mL sample vials at least halfway through and place them in the autosampler tray. Place pre-slit septum before putting the caps. Each vial position has a corresponding number in the tray.

NOTE: Run 1-4 water blanks at the beginning of the sequence. Run the mixed standard after water blank. Run the mixed standard again after all the experimental samples. The last sample should switch the IC back to "standby" or "shutdown" using corresponding program. Check previous finished sequences if not sure about something.

(B) Setup Automatic (Batch) Sample Processing

1. Use Chromeleon to create a sequence to be processed automatically. On the sequence screen, name all samples. Make sure their statuses are "single".

2. For each sample, the sequence includes a program with commands and parameters for controlling ICS-3000 modules and acquiring sample data. To create a program, go to Chromeleon's Control Panel, open the "Sequence Control" tab and click "Create

Program". Usually, copy the desired programs from previous runs. Modify existing programs to meet specific objectives (e.g. not using the PDA detector). Check the software manual to understand the meaning to each command in the program. Chromeleon also provides dialog wizards in modifying programs.

3. Copy a previous quantification method or create a new one using the wizard. When use a new method, run at least 4-5 standards in the sequence. To create a quantification method, go to the File menu and select "New", then select "Method File" from the list. Follow the wizard and check the detailed SOP.

(C) Start batch processing

1. In the Chromeleon window, click on "Start/Stop Batch" button (on the top navigation bar, green, looks like "play").

2. A dialog box appears, check that the instrument is ready by clicking "Ready check", then click "OK".

(D) Note: Standby & Shutdown

1. Standby

Use this when the instrument will be running regularly, for example during the week. Copy the standby program (standby.pgm) from a previous sequence and paste it in your sequence.

2. Shutdown

Use this when the instrument isn't going to be used for some days, for example during the weekend. Copy the shutdown program (shutdown.pgm) from a previous sequence and paste it in your sequence. See previous figure (green).

Appendix G: FACSIMILE Code for Modeling Methylglyoxal + OH radical Reactions

```
* ModiFied by Yi Tan ;
* Wednesday, ApRil 01, 2009 ;
*=========================================================== ;
* Methylglyoxal ExpeRiments using k values FRom Lim et al., 2005
;
*  ;
*=========================================================== ;

EXECUTE OPEN 8 "MGLYExpTan.OUT";

PARAMETER
K1F   1.1E-4
K2F   8.3E5
K3F   1.0E8
K4F   7.1E9
K5F   1.0E10
K6F   5.5E9
K7F   2.7E7
K8F   1.0E7
K9F   6.5E8
K10F  1.5E5
K11F  4.3E5
K12F  0.0014
K12R  1.4E11
K13F  8.0E5
K13R  5.0E10
K14F  2.408E-2
K14R  5.6E4
K15F  2.345
K15R  5.0E10
K16F  6.94E6
K16R  2.0E10
K17F  2.8E9
K17R  5.0E10
K18F  2.71E6
K18R  5.0E10
K19F  8.85E6
K19R  5.0E10
K20F  8.75E5
K20R  5.0E10
K21F  6.4E7
K21R  2.0E10
K22F  6.44E8
K23F  6.0E7
K24F  6.0E7
K25F  1.36E7
K26F  7.225E7
```

```
K27F  3.62E8
K28F  2.9E9
K29F  1.4E6
K30F  4.7E7
K31F  7.7E6
K32F  2.4E9
K33F  0.3
K34F  1E8
K35F  2.4E9
K36F  1.1E9
K37F  5.6E7
K38F  2.4E6
K39F  1.275E7
K40F 0.11
K41F 3.7
;

VARIABLE
H2O2  OH    HO2   MGLY  PYRAC PYRACN
CH3COOH     CH3COON     GLYAC GLYACN      OXLAC OXLACN
OXLAC2N     HCOOH HCOON CO2N  HCHO  O2
O2N   Hp    OHN   CO2   HCO3N CO32N
CO3N  H2O
;

COMPILE INSTANT;
MGLY = 0.003 ;
H2O2 = 0.015 ;
Hp = 0.0000025 ;
H2O = 1;
**;

COMPILE EQUATIONS ;
% K1F : H2O2 = OH + OH;
% K2F : HO2 + HO2 = H2O2 + O2;
% K3F : HO2 + O2N = H2O2 + O2;
% K4F : OH + HO2 = O2 + H2O;
% K5F : OH + O2N = OHN + O2;
% K6F : OH + OH = H2O2;
% K7F : H2O2 + OH = HO2 + H2O;
% K8F : HCO3N + OH = CO3N +H2O;
% K9F : CO3N + O2N = CO32N + O2;
% K10F : CO3N + HCOON = HCO3N + CO2N;
% K11F : CO3N + H2O2 = HCO3N + HO2;
% K12F % K12R : H2O = Hp + OHN;
% K13F % K13R : HO2 = Hp + O2N;
% K14F % K14R : CO2 = Hp + HCO3N;
% K15F % K15R : HCO3N = Hp + CO32N;
% K16F % K16R : GLYAC = Hp + GLYACN;
% K17F % K17R : OXLAC = Hp + OXLACN;
% K18F % K18R : OXLACN = Hp + OXLAC2N;
% K19F % K19R : HCOOH = Hp + HCOON ;
```

```
% K20F % K20R : CH3COOH = Hp + CH3COON;
% K21F % K21R : PYRAC = Hp + PYRACN;
% K22F : MGLY + OH = PYRACN + HO2 + H2O;
% K23F : PYRAC + OH = CH3COOH + HO2 + CO2;
% K24F : PYRACN + OH = CH3COON + HO2 + CO2;
% K25F : CH3COOH + OH = GLYAC;
% K26F : CH3COON + OH = GLYACN;
% K27F : GLYAC + OH = OXLAC + HO2 + H2O;
% K28F : GLYACN + OH = OXLACN + HO2 + H2O;
% K29F : OXLAC + OH = CO2 + CO2 + HO2 + H2O;
% K30F : OXLACN + OH = CO2 + CO2N + H2O + H2O;
% K31F : OXLAC2N + OH = CO2 + CO2N + OHN;
% K32F : CO2N + O2 = O2N + CO2 ;
% K33F : GLYAC + H2O2 = HCOOH + CO2 + H2O;
% K34F : HCOOH + OH = CO2 + HO2 + H2O ;
% K35F : HCOON + OH = CO2N + H2O ;
% K36F : HCHO + OH = HCOOH + HO2;
% K37F : MGLY + OH = GLYACN + HO2 + H2O;
% K38F : CH3COOH + OH = HCHO;
% K39F : CH3COON + OH = HCHO;
% K40F : PYRACN + H2O2 = CH3COON + CO2;
% K41F : HO2 + H2O2 = OH + H2O + O2;

**;

SETPSTREAM 1 8 ;
TIME ;
H2O2  OH    HO2   MGLY  PYRAC PYRACN;
CH3COOH     CH3COON     GLYAC GLYACN      OXLAC OXLACN;
OXLAC2N     HCOOH HCOON CO2N  HCHO  O2;
O2N   Hp    OHN   CO2   HCO3N CO32N;
CO3N  H2O;
**;

COMPILE OUT ;
PSTREAM 1 ;
**;

WHENEVER TIME=
 5001 * (+25) 0  %
CALL OUT;
**;

BEGIN;
STOP;
```

Appendix H: MATLAB Code for Modeling Glyoxal + OH Radical Experiments

```
%% main function
function glyoxal(m,n,h)

%glyoxal reaction system
tspan = [0; 14400];
conc = zeros(20,1);
conc(1) = n; %H2O2
conc(4) = m; %Glyoxal
conc(12) = 2.8E-4; %dissolved oxygen
conc(14) = h; %H+, 1E-5

options = odeset('RelTol',1e-14,'AbsTol',1e-14,'NonNegative',1);
[t,y] = ode15s(@reaction,tspan,conc,options);
x = 1/60.*t;
oxalate = (y(:,7) + y(:,8) + y(:,9))*1000000;
OH = y(:,2);
organic = y(:,4)*2 + y(:,5)*2 + y(:,6)*2 + y(:,7)*2 + y(:,8)*2 +
y(:,9)*2 + y(:,10) + y(:,11);
glyoxal = y(:,4);
save ('D:\Research\Experiment\Matlab codes\organic3000.out', 'x',
'organic', '-ASCII', '-tabs');
save ('D:\Research\Experiment\Matlab codes\glyoxal3000.out', 'x',
'glyoxal', '-ascii', '-double', '-tabs');

%% Plot

% plot pH vs. time (w/ and w/o H2SO4)

% f1='D:\\Research\\Experiment\\Matlab codes\\';
% importHPLC([f1 '2008Result.txt']);

figure(1);
clf;
orient landscape;
set (gca,'FontSize',14);

plot(x,oxalate);

title('Oxalic Acid vs. Time');
xlabel ('Time (min)');
ylabel ('Conc. (mM)');
legend('Oxalic Acid');

%% reactions and rate constants, sub function
function dconc = reaction(time,conc)
% rate constants
% H2O2 experiment simulation
% Reactions:
% K1F : H2O2 = OH + OH;
```

```
% K2F : OH + H2O2 = HO2 + H2O
% K3F : HO2 + H2O2 = OH + H2O + O2
% K4F : HO2 + HO2 = H2O2 + O2
% K5F : OH + HO2 = H2O + O2
% K6F : GLY + OH (+ O2) = GLYAC + HO2;
% K7F : GLYAC + OH = OXLAC + HO2 + H2O;
% K8F : GLYACN1 + OH = OXLACN1 + HO2 + H2O;
% K9F : OXLAC + OH = 2CO2 + 2H2O; product mistake here...also
only one OH
% K10F : OXLACN1 + OH = CO2 + CO2N1 + H2O + H2O;
% K11F : OXLACN2 + OH = CO2 + CO2N1 + OHN1;
% K12F % K12R : H2O = HP1 + OHN1;
% K13F % K13R : HO2 = HP1 + O2N1;
% K14F % K14R : GLYAC = HP1 + GLYACN1;
% K15F % K15R : OXLAC = HP1 + OXLACN1;
% K16F % K16R : OXLACN1 = HP1 + OXLACN2;
% K17F : CO2N1 + O2 = O2N1 + CO2 ;
% K18F : GLYAC + H2O2 = HCO2H + CO2 + H2O;
% K19F : HCO2H + OH = CO2 + HO2 + H2O ;
% K20F : HCO2N1 + OH = CO2N1 + H2O ;
% K21F % K21R : HCO2H = HP1 + HCO2N1 ;

% Reaction rate constants:

K1F = 1.1E-4;
K2F = 2.7E7;
K3F = 3.7;
K4F = 8.3E5;
K5F = 7.1E9;
K6F = 1.1E9;
K7F = 3.62E8;
K8F = 2.9E9;
K9F = 1.4E6;
K10F = 4.7E7;
K11F = 7.7E6;
K12F = 0.0014;
K12R = 1.4E11;
K13F = 8.0E5;
K13R = 5.0E10;
K14F = 6.94E6;
K14R = 2.0E10;
K15F = 2.8E9;
K15R = 5.0E10;
K16F = 2.71E6;
K16R = 5.0E10;
K17F = 2.4E9;
K18F = 0.3;
K19F = 1E8;
K20F = 2.4E9;
K21F = 8.85E6;
K21R = 5.0E10;
```

```
% New reactions added;
% K22F : OH + O2- = OH- + O2;
% K23F : HCO3- + OH = CO3- + H2O;
% K24F : CO3- + O2- = CO32- + O2; %instead of HCO3-
% K25F : CO3- + HCO2- = HCO3- + CO2-;
% K26F : CO3- + H2O2 = HCO3- + HO2; (Seinfeld's book)
% K27F % K27R : CO2 (+ H2O) = H+ + HCO3-;
% K28F % K28R : HCO3- = H+ + CO32-

K22F = 1E10;
K23F = 1E7;
K24F = 6.5E8;
K25F = 1.5E5;
K26F = 8E5;
K27F = 5.6E4*4.3E-7;
K27R = 5.6E4;
K28F = 5.0E10*4.69E-11;
K28R = 5.0E10;

%% species and reactions
% conc(1)=H2O2; conc(2)=OH; conc(3)=HO2; conc(4)=GLY;
conc(5)=GLYAC; conc(6)=GLYACN1; conc(7)=oxalic;
% conc(8)=oxalic-1; conc(9)=oxalic-2; conc(10)=HCOOH;
conc(11)=HCOO-; conc(12)=O2; conc(13)=O2-;
% conc(14)=H+; conc(15)=OH-; conc(16)=CO2; conc(17)=CO2-;
% conc(18)=HCO3-; conc(19)=CO32-; conc(20)=CO3-;

% rxn1 = K1F*conc(1);
% rxn2 = K2F*conc(1)*conc(2);
% rxn3 = K3F*conc(3)*conc(1);
% rxn4 = K4F*conc(3)*conc(3);
% rxn5 = K5F*conc(2)*conc(3);
% rxn6 = K6F*conc(4)*conc(2);
% rxn7 = K7F*conc(5)*conc(2);
% rxn8 = K8F*conc(6)*conc(2);
% rxn9 = K9F*conc(7)*conc(2); big change here!!!
% rxn10 = K10F*conc(8)*conc(2);
% rxn11 = K11F*conc(9)*conc(2);
% rxn12 = K12F-K12R*conc(14)*conc(15);
% rxn13 = K13F*conc(3)-K13R*conc(14)*conc(13);
% rxn14 = K14F*conc(5)-K14R*conc(14)*conc(6);
% rxn15 = K15F*conc(7)-K15R*conc(14)*conc(8);
% rxn16 = K16F*conc(8)-K16R*conc(14)*conc(9);
% rxn17 = K17F*conc(17)*conc(12);
% rxn18 = K18F*conc(5)*conc(1);
% rxn19 = K19F*conc(10)*conc(2);
% rxn20 = K20F*conc(11)*conc(2);
% rxn21 = K21F*conc(10)-K21R*conc(14)*conc(11);

% rxn22 = K22F*conc(2)*conc(13);
% rxn23 = K23F*conc(18)*conc(2);
% rxn24 = K24F*conc(20)*conc(13);
```

```
% rxn25 = K25F*conc(20)*conc(11);
% rxn26 = K26F*conc(20)*conc(1);
% rxn27 = K27F*conc(16)-K27R*conc(14)*conc(18);
% rxn28 = K28F*conc(18)-K28R*conc(14)*conc(19);

%% differential equations

dconc = zeros(20,1);

dconc(1) = -K1F*conc(1) - K2F*conc(1)*conc(2) -
K3F*conc(3)*conc(1) + K4F*conc(3)*conc(3) -
K18F*conc(5)*conc(1)...
     - K26F*conc(20)*conc(1);

dconc(2) = 2*K1F*conc(1) - K2F*conc(1)*conc(2) +
K3F*conc(3)*conc(1) - K5F*conc(2)*conc(3) -
K5F*conc(2)*conc(3)...
    - K6F*conc(4)*conc(2) - K7F*conc(5)*conc(2) -
K8F*conc(6)*conc(2) - K9F*conc(7)*conc(2) -
K10F*conc(8)*conc(2)...
    - K11F*conc(9)*conc(2) - K19F*conc(10)*conc(2) -
K20F*conc(11)*conc(2) - K22F*conc(2)*conc(13) -
K23F*conc(18)*conc(2);

dconc(3) = K2F*conc(1)*conc(2) - K3F*conc(3)*conc(1) -
2*K4F*conc(3)*conc(3) - K5F*conc(2)*conc(3) +
K6F*conc(4)*conc(2)...
    + K7F*conc(5)*conc(2) + K8F*conc(6)*conc(2) - (K13F*conc(3)-
K13R*conc(14)*conc(13)) + K19F*conc(10)*conc(2)...
    + K26F*conc(20)*conc(1);

dconc(4) = -K6F*conc(4)*conc(2);

dconc(5) = K6F*conc(4)*conc(2) - K7F*conc(5)*conc(2) -
(K14F*conc(5)-K14R*conc(14)*conc(6)) - K18F*conc(5)*conc(1);

dconc(6) = -K8F*conc(6)*conc(2) + (K14F*conc(5)-
K14R*conc(14)*conc(6));

dconc(7) = K7F*conc(5)*conc(2) - K9F*conc(7)*conc(2) -
(K15F*conc(7)-K15R*conc(14)*conc(8));

dconc(8) = K8F*conc(6)*conc(2) - K10F*conc(8)*conc(2) +
(K15F*conc(7)-K15R*conc(14)*conc(8))...
    - (K16F*conc(8)-K16R*conc(14)*conc(9));

dconc(9) = -K11F*conc(9)*conc(2) + (K16F*conc(8)-
K16R*conc(14)*conc(9));

dconc(10) = K18F*conc(5)*conc(1) - K19F*conc(10)*conc(2) -
(K21F*conc(10)-K21R*conc(14)*conc(11));
```

```
dconc(11) = -K20F*conc(11)*conc(2) + (K21F*conc(10)-
K21R*conc(14)*conc(11)) - K25F*conc(20)*conc(11);

dconc(12) = K3F*conc(3)*conc(1) + K4F*conc(3)*conc(3) +
K5F*conc(2)*conc(3) - K17F*conc(17)*conc(12)...
    + K22F*conc(2)*conc(13) + K24F*conc(20)*conc(13);

dconc(13) = (K13F*conc(3)-K13R*conc(14)*conc(13)) +
K17F*conc(17)*conc(12) - K22F*conc(2)*conc(13) -
K24F*conc(20)*conc(13);

dconc(14) = (K12F-K12R*conc(14)*conc(15)) + (K13F*conc(3)-
K13R*conc(14)*conc(13)) + (K14F*conc(5)-K14R*conc(14)*conc(6))...
    + (K15F*conc(7)-K15R*conc(14)*conc(8)) + (K16F*conc(8)-
K16R*conc(14)*conc(9)) + (K21F*conc(10)-
K21R*conc(14)*conc(11))...
    + (K27F*conc(16)-K27R*conc(14)*conc(18)) + (K28F*conc(18)-
K28R*conc(14)*conc(19));

dconc(15) = K11F*conc(9)*conc(2) + (K12F-K12R*conc(14)*conc(15))
+ K22F*conc(2)*conc(13);

dconc(16) = 2*K9F*conc(7)*conc(2) + K10F*conc(8)*conc(2) +
K11F*conc(9)*conc(2) + K17F*conc(17)*conc(12)...
    + K18F*conc(5)*conc(1) + K19F*conc(10)*conc(2) -
(K27F*conc(16)-K27R*conc(14)*conc(18));

dconc(17) = K10F*conc(8)*conc(2) + K11F*conc(9)*conc(2) -
K17F*conc(17)*conc(12) + K20F*conc(11)*conc(2) +
K25F*conc(20)*conc(11);

dconc(18) = -K23F*conc(18)*conc(2) + K25F*conc(20)*conc(11) +
K26F*conc(20)*conc(1)...
    - (K28F*conc(18)-K28R*conc(14)*conc(19)) + (K27F*conc(16)-
K27R*conc(14)*conc(18));

dconc(19) = K28F*conc(18) + K24F*conc(20)*conc(13) -
K28R*conc(14)*conc(19);

dconc(20) = K23F*conc(18)*conc(2) - K24F*conc(20)*conc(13) -
K25F*conc(20)*conc(11) - K26F*conc(20)*conc(1);
```

Appendix I: MATLAB Code for Modeling Methylglyoxal + OH Radical Experiments

```
%%main function
function mgly(m,n,h)

tspan = [0; 23400];
conc = zeros(25,1);
conc(1) = n; %H2O2
conc(4) = m; %MGLY
conc(18) = 2.8E-4; %dissolved oxygen
conc(20) = h; %H+, 1E-5

options = odeset('RelTol',1e-14,'AbsTol',1e-14,'NonNegative',1);
[t,y] = ode15s(@reaction,tspan,conc,options);

%% plot figures

min = 1/60.*t;
oxalate = (y(:,11) + y(:,12) + y(:,13))*1E6;
pyruvate = (y(:,5)+y(:,6))*1E6;
acetate = (y(:,7)+y(:,8))*1E6;
glyoxylate = (y(:,9)+y(:,10))*1E6;
formate = (y(:,14)+y(:,15))*1E6;
formaldehyde = y(:,17)*1E6;
MGLY = y(:,4)*1E6;
OH = y(:,2);
TOC = oxalate*2 + pyruvate*3 + acetate*2 + glyoxylate*2 + formate
+ formaldehyde + MGLY*3;
H2O2 = y(:,1)*1E6;
%reacted = (m - y(:,4))*1E6;
%unmeasured = pyruvate*3 + acetate*2 + glyoxylate*2 + formate +
formaldehyde + MGLY*3;

xlswrite('C:\Research\Methylglyoxal Experiment\3mMOH.xls',
[min,OH]);
%xlswrite('C:\Research\Methylglyoxal
Experiment\30uM_MGLY_time.xls', t);
%'pyruvate','acetate','glyoxylate','formate','formaldehyde','oxal
ate','oxalate'

figure(1);
clf;
orient landscape;
set (gca,'FontSize',14);
%plot(min,[MGLY,oxalate,pyruvate,acetate,glyoxylate,formate,forma
ldehyde]);
%plot(min,oxalate);
plot (min,OH);
%title('Oxalic Acid vs. Time');
```

```
xlabel ('Time (min)');
ylabel ('Concentration');
%legend('Methylglyoxal','Oxalic Acid','Pyruvic acid','Acetic
Acid','Glyoxylic Acid','Formic Acid','Formaldehyde');

%% reactions and rate constants, sub function
function dconc = reaction(time,conc)

% inorganic reactions
% K1: H2O2 = 2 OH
% K2: HO2 + HO2 = H2O2 + O2
% K3: HO2 + O2- = H2O2 + O2
% K4: OH + HO2 = O2 + H2O
% K5: OH + O2- = OH- + O2
% K6: OH + OH = H2O2
% K7: H2O2 + OH = HO2 + H2O
% K8: HCO3- + OH = CO3- +H2O
% K9: CO3- + O2- = CO32- + O2
% K10: CO3- + HCOO- = HCO3- + CO2-
% K11: CO3- + H2O2 = HCO3- + HO2

K1 = 1.1E-4; %1.1E-4
K2 = 8.3E5;
K3 = 1.0E8;
K4 = 7.1E9;
K5 = 1.0E10;
K6 = 5.5E9;
K7 = 2.7E7;
K8 = 1.0E7;
K9 = 6.5E8;
K10 = 1.5E5;
K11 = 4.3E5;

% equilibriums
% K12F % K12R : H2O = H+ + OH-
% K13F % K13R : HO2 = H+ + O2-
% K14F % K14R : CO2 = H+ + HCO3-
% K15F % K15R : HCO3- = H+ + CO32-
% K16F % K16R : GLYAC = H+ + GLYAC-;
% K17F % K17R : OXLAC = H+ + OXLAC-
% K18F % K18R : OXLAC- = H+ + OXLAC2-;
% K19F % K19R : HCOOH = H+ + HCOO- ;
% K20F % K20R : CH3COOH = H+ + CH3COO-;
% K21F % K21R : PYRAC = H+ + PYRAC-;

K12F = 0.0014;
K12R = 1.4E11;
K13F = 8.0E5;
K13R = 5.0E10;
K14F = 5.6E4*4.3E-7;
K14R = 5.6E4;
K15F = 5.0E10*4.69E-11;
```

```
K15R = 5.0E10;
K16F = 6.94E6;
K16R = 2.0E10;
K17F = 2.8E9;
K17R = 5.0E10;
K18F = 2.71E6;
K18R = 5.0E10;
K19F = 8.85E6;
K19R = 5.0E10;
K20F = 8.75E5;
K20R = 5.0E10;
K21F = 6.4E7;
K21R = 2.0E10;

% organic reactions
% K22: MGLY + OH = 0.92 PYRAC- + 0.08 GLYAC- + HO2 + H2O
% K23: PYRAC + OH = CH3COOH + HO2 + CO2
% K24: PYRAC- + OH = CH3COO- + HO2 + CO2
% K25: CH3COOH + OH = 0.85 GLYAC + 0.15 HCHO
% K26: CH3COO- + OH = 0.85 GLYAC- + 0.15 HCHO
% K27: GLYAC + OH = OXLAC + HO2 + H2O
% K28: GLYAC- + OH = OXLAC- + HO2 + H2O
% K29: OXLAC + OH = CO2 + CO2 + HO2 + H2O; %Ervens
% K30: OXLAC- + OH = CO2 + CO2- + H2O + H2O;
% K31: OXLAC2- + OH = CO2 + CO2- + OH-;
% K32: CO2- + O2 = O2- + CO2 ;
% K33: GLYAC + H2O2 = HCOOH + CO2 + H2O;
% K34: HCOOH + OH = CO2 + HO2 + H2O ;
% K35: HCOO- + OH = CO2- + H2O ;
% K36: HCHO + OH = HCOOH + HO2;

K22 = 7.0E8; %5.0E8;
K23 = 6.0E7;
K24 = 6.0E7;
K25 = 1.6E7;
K26 = 8.5E7;
K27 = 3.62E8;
K28 = 2.9E9;
K29 = 1.4E6;
K30 = 4.7E7;
K31 = 7.7E6;
K32 = 2.4E9;
K33 = 0.3;
K34 = 1E8;
K35 = 2.4E9;
K36 = 1.1E9;

%additonal reaction
% K37: PYRAC- + H2O2 = CH3COO- + CO2;
K37 = 0.11;

% K38 : HO2 + H2O2 = OH + H2O + O2;
```

```
K38 = 3.7;

%% species and reactions
% conc(1)=H2O2;
% conc(2)=OH;
% conc(3)=HO2;
% conc(4)=MGLY;
% conc(5)=PYRAC;
% conc(6)=PYRAC-;
% conc(7)=CH3COOH;
% conc(8)=CH3COO-;
% conc(9)=GLYAC;
% conc(10)=GLYAC-;
% conc(11)=OXLAC;
% conc(12)=OXLAC-;
% conc(13)=OXLAC2-;
% conc(14)=HCOOH;
% conc(15)=HCOO-;
% conc(16)=CO2-;
% conc(17)=HCHO;
% conc(18)=O2;
% conc(19)=O2-;
% conc(20)=H+;
% conc(21)=OH-;
% conc(22)=CO2;
% conc(23)=HCO3-;
% conc(24)=CO32-;
% conc(25)=CO3-;

% rxn1 = K1*conc(1) = 2 conc(2)
% rxn2 = K2*conc(3)*conc(3) = conc(1) + conc(18)
% rxn3 = K3*conc(3)*conc(19) = conc(1) + conc(18)
% rxn4 = K4*conc(2)*conc(3) = conc(18) + H2O
% rxn5 = K5*conc(2)*conc(19) = conc(21) + conc(18)
% rxn6 = K6*conc(2)*conc(2) = conc(1)
% rxn7 = K7*conc(1)*conc(2) = conc(3) + H2O
% rxn8 = K8*conc(23)*conc(2) = conc(25) +H2O
% rxn9 = K9*conc(25)*conc(19) = conc(24) + conc(18)
% rxn10 = K10*conc(25)*conc(15) = conc(23) + conc(16)
% rxn11 = K11*conc(25)*conc(1) = conc(23) + conc(3)
% rxn12 = (K12F-K12R*conc(20)*conc(21));
% rxn13 = (K13F*conc(3)-K13R*conc(20)*conc(19));
% rxn14 = (K14F*conc(22)-K14R*conc(20)*conc(23));
% rxn15 = (K15F*conc(23)-K15R*conc(20)*conc(24));
% rxn16 = (K16F*conc(9)-K16R*conc(20)*conc(10));
% rxn17 = (K17F*conc(11)-K17R*conc(20)*conc(12));
% rxn18 = (K18F*conc(12)-K18R*conc(20)*conc(13));
% rxn19 = (K19F*conc(14)-K19R*conc(20)*conc(15));
% rxn20 = (K20F*conc(7)-K20R*conc(20)*conc(8));
% rxn21 = (K21F*conc(5)-K21R*conc(20)*conc(6));
% rxn22 = K22*conc(4)*conc(2) = 0.92 conc(6) + 0.08 conc(10) +
conc(3) + H2O
```

```
% rxn23 = K23*conc(5)*conc(2) = conc(7) + conc(3) + conc(22)
% rxn24 = K24*conc(6)*conc(2) = conc(8) + conc(3) + conc(22)
% rxn25 = K25*conc(7)*conc(2) = 0.85 conc(9) + 0.15 conc(17)
% rxn26 = K26*conc(8)*conc(2) = 0.85 conc(10) + 0.15 conc(17)
% rxn27 = K27*conc(9)*conc(2) = conc(11) + conc(3) + H2O
% rxn28 = K28*conc(10)*conc(2) = conc(12) + conc(3) + H2O
% rxn29 = K29*conc(11)*conc(2) = conc(22) + conc(22) + conc(3) +
H2O;
% rxn30 = K30*conc(12)*conc(2) = conc(22) + conc(16) + H2O + H2O;
% rxn31= K31*conc(13)*conc(2) = conc(22) + conc(16) + conc(21);
% rxn32= K32*conc(16)*conc(18) = conc(19) + conc(22) ;
% rxn33= K33*conc(9)*conc(1) = conc(14) + conc(22) + H2O;
% rxn34= K34*conc(14)*conc(2) = conc(22) + conc(3) + H2O ;
% rxn35= K35*conc(15)*conc(2) = conc(16) + H2O ;
% rxn36= K36*conc(17)*conc(2) = conc(14) + conc(3);
% rxn37= K37*conc(1)*conc(6) = conc(8) + conc(22);
% rxn38 = K38*conc(3)*conc(1) = conc(2) + conc(18);

%% differential equations

dconc = zeros(25,1);
dconc(1) = -
K1*conc(1)+K2*conc(3)*conc(3)+K3*conc(3)*conc(19)+K6*conc(2)*conc
(2)...
    -K7*conc(1)*conc(2)-K11*conc(25)*conc(1)-K33*conc(9)*conc(1)-
K37*conc(1)*conc(6)-K38*conc(3)*conc(1);
dconc(2) = 2*K1*conc(1)-K4*conc(2)*conc(3)-K5*conc(2)*conc(19)-
2*K6*conc(2)*conc(2)...
    -K7*conc(1)*conc(2)-K8*conc(23)*conc(2)-K22*conc(4)*conc(2)-
K23*conc(5)*conc(2)...
    -K24*conc(6)*conc(2)-K25*conc(7)*conc(2)-K26*conc(8)*conc(2)-
K27*conc(9)*conc(2)...
    -K28*conc(10)*conc(2)-K29*conc(11)*conc(2)-
K30*conc(12)*conc(2)-K31*conc(13)*conc(2)...
    -K34*conc(14)*conc(2)-K35*conc(15)*conc(2)-
K36*conc(17)*conc(2)+ K38*conc(3)*conc(1);
dconc(3) = -2*K2*conc(3)*conc(3)-K3*conc(3)*conc(19)-
K4*conc(2)*conc(3)...
    +K7*conc(1)*conc(2)+K11*conc(25)*conc(1)-(K13F*conc(3)-
K13R*conc(20)*conc(19))...

+K22*conc(4)*conc(2)+K23*conc(5)*conc(2)+K24*conc(6)*conc(2)+K27*
conc(9)*conc(2)...

+K28*conc(10)*conc(2)+K29*conc(11)*conc(2)+K34*conc(14)*conc(2)+K
36*conc(17)*conc(2)-K38*conc(3)*conc(1);
dconc(4) = -K22*conc(4)*conc(2);
dconc(5) = -(K21F*conc(5)-K21R*conc(20)*conc(6))-
K23*conc(5)*conc(2);
dconc(6) = (K21F*conc(5)-
K21R*conc(20)*conc(6))+0.92*K22*conc(4)*conc(2)-
K24*conc(6)*conc(2)-K37*conc(1)*conc(6);
```

```
dconc(7) = -(K20F*conc(7)-
K20R*conc(20)*conc(8))+K23*conc(5)*conc(2)-K25*conc(7)*conc(2);
dconc(8) = (K20F*conc(7)-
K20R*conc(20)*conc(8))+K24*conc(6)*conc(2)-
K26*conc(8)*conc(2)+K37*conc(1)*conc(6);
dconc(9) = -(K16F*conc(9)-
K16R*conc(20)*conc(10))+0.85*K25*conc(7)*conc(2)-
K27*conc(9)*conc(2)-K33*conc(9)*conc(1);
dconc(10) = (K16F*conc(9)-
K16R*conc(20)*conc(10))+0.08*K22*conc(4)*conc(2)+0.85*K26*conc(8)
*conc(2)-K28*conc(10)*conc(2);
dconc(11) = -(K17F*conc(11)-
K17R*conc(20)*conc(12))+K27*conc(9)*conc(2)-K29*conc(11)*conc(2);
dconc(12) = (K17F*conc(11)-K17R*conc(20)*conc(12))-
(K18F*conc(12)-K18R*conc(20)*conc(13))...
    +K28*conc(10)*conc(2)-K30*conc(12)*conc(2);
dconc(13) = (K18F*conc(12)-K18R*conc(20)*conc(13))-
K31*conc(13)*conc(2);
dconc(14) = -(K19F*conc(14)-
K19R*conc(20)*conc(15))+K33*conc(9)*conc(1)-
K34*conc(14)*conc(2)+K36*conc(17)*conc(2);
dconc(15) = -K10*conc(25)*conc(15)+(K19F*conc(14)-
K19R*conc(20)*conc(15))-K35*conc(15)*conc(2);
dconc(16) =
K10*conc(25)*conc(15)+K30*conc(12)*conc(2)+K31*conc(13)*conc(2)-
K32*conc(16)*conc(18)+K35*conc(15)*conc(2);
dconc(17) = 0.15*K25*conc(7)*conc(2)+0.15*K26*conc(8)*conc(2)-
K36*conc(17)*conc(2);
dconc(18) =
K2*conc(3)*conc(3)+K3*conc(3)*conc(19)+K4*conc(2)*conc(3)+K5*conc
(2)*conc(19)...
    +K9*conc(25)*conc(19)-
K32*conc(16)*conc(18)+K38*conc(3)*conc(1);
dconc(19) = -K3*conc(3)*conc(19)-K5*conc(2)*conc(19)-
K9*conc(25)*conc(19)+(K13F*conc(3)...
    -K13R*conc(20)*conc(19))+K32*conc(16)*conc(18);
dconc(20) = (K12F-K12R*conc(20)*conc(21))+(K13F*conc(3)-
K13R*conc(20)*conc(19))...
    +(K14F*conc(22)-K14R*conc(20)*conc(23))+(K15F*conc(23)-
K15R*conc(20)*conc(24))...
    +(K16F*conc(9)-K16R*conc(20)*conc(10))+(K17F*conc(11)-
K17R*conc(20)*conc(12))...
    +(K18F*conc(12)-K18R*conc(20)*conc(13))+(K19F*conc(14)-
K19R*conc(20)*conc(15))...
    +(K20F*conc(7)-K20R*conc(20)*conc(8))+(K21F*conc(5)-
K21R*conc(20)*conc(6));
dconc(21) = K5*conc(2)*conc(19)+(K12F-
K12R*conc(20)*conc(21))+K31*conc(13)*conc(2);
dconc(22) = -(K14F*conc(22)-
K14R*conc(20)*conc(23))+K23*conc(5)*conc(2)+K24*conc(6)*conc(2)..
.
```

```
+2*K29*conc(11)*conc(2)+K30*conc(12)*conc(2)+K31*conc(13)*conc(2)
+K32*conc(16)*conc(18)...

+K33*conc(9)*conc(1)+K34*conc(14)*conc(2)+K37*conc(1)*conc(6);
dconc(23) = -
K8*conc(23)*conc(2)+K10*conc(25)*conc(15)+K11*conc(25)*conc(1)...
    +(K14F*conc(22)-K14R*conc(20)*conc(23))-(K15F*conc(23)-
K15R*conc(20)*conc(24));
dconc(24) = K9*conc(25)*conc(19)+(K15F*conc(23)-
K15R*conc(20)*conc(24));
dconc(25) = K8*conc(23)*conc(2)-K9*conc(25)*conc(19)-
K10*conc(25)*conc(15)-K11*conc(25)*conc(1);
```

Curriculum Vitae
Yi Tan

EDUCATION

2010/10 **Ph.D. in Environmental Sciences,** Rutgers University, New Brunswick, NJ.
2005/07 **B.S. in Environmental Engineering**, Beijing University of Aeronautics and Astronautics (BUAA), Beijing, China.

PUBLICATIONS

Tan, Y, Perri, MJ, Seitzinger, SP, Turpin, BJ, Effects of Precursor Concentration and Acidic Sulfate in Aqueous Glyoxal-OH Radical Oxidation and Implications for Secondary Organic Aerosol, *Environmental Science & Technology* **43**(2009), pp. 8105-8112.

Tan, Y, Carlton, AG, Seitzinger, SP, Turpin, BJ, SOA from Methylglyoxal in Clouds and Wet Aerosols: Measurement and Prediction of Key Products, *Atmospheric Environment In Press, Accepted Manuscript*.

Lim, Y. B.; **Tan, Y.**; Perri, M. J.; Seitzinger, S. P.; Turpin, B. J., Aqueous chemistry and its role in secondary organic aerosol (SOA) formation. *Atmos. Chem. Phys. Discuss.* **2010,** *10*, (6), 14161-14207.

Tan, Y, Lim, YB, Altieri KE, Carlton, AG, Seitzinger, SP, Turpin, BJ, Mechanisms Leading to Oligomer Formation in Cloud Processing of Methylglyoxal: Insights from OH Radical Oxidation of Acetic Acid, *in preparation*.

TEACHING EXPERIENCE

Teaching assistant, Analytical Environmental Chemistry Laboratory, Fall 2006
Teaching assistant, Air Sampling and Analysis Techniques, Spring, 2007